Understanding of Li production and its evolution in evolved stars

A thesis

submitted for the degree of

Doctor of Philosophy

in

The Department of Physics,

Pondicherry University,

Puducherry - 605 014, India

by

Raghubar Singh

Indian Institute of Astrophysics,

Bangalore - 560 034, India

July 2021

Understanding of Li production and its evolution in evolved stars

Raghubar Singh
Indian Institute of Astrophysics

Indian Institute of Astrophysics
Bangalore - 560 034, India

Title of the thesis	:	**Understanding of Li production and its evolution in evolved stars**
Name of the author	:	**Raghubar Singh**
Address	:	Indian Institute of Astrophysics II Block, Koramangala Bangalore - 560 034, India
Email	:	raghubar.singh@iiap.res.in
Name of the supervisor	:	**Prof. B. Eswar Reddy**
Address	:	Indian Institute of Astrophysics II Block, Koramangala Bangalore - 560 034, India
Email	:	ereddy@iiap.res.in

Declaration of Authorship

I hereby declare that the matter contained in this thesis is the result of the investigations carried out by me at the Indian Institute of Astrophysics, Bangalore, under the supervision of Prof. B. Eswar Reddy. This work has not been submitted for the award of any other degree, diploma, associateship, fellowship, etc. of any other university or institute.

Signed: _____

Date: _____

Certificate

This is to certify that the thesis titled **'Understanding of Li production and its evolution in evolved stars'** submitted to the Pondicherry University by Mr. Raghubar Singh for the award of the degree of Doctor of Philosophy, is based on the results of the investigations carried out by him under my supervision and guidance, at the Indian Institute of Astrophysics. This thesis has not been submitted for the award of any other degree, diploma, associateship, fellowship, etc. of any other university or institute.

Signed: _____

Date: _____

List of Publications

1. Yerra Bharat Kumar, **Raghubar Singh**, Bacham E. Reddy, Gang Zhou, Two New Super Li-rich Core He-burning Giants: A New Twist to the Long Tale of Li Enhancement in K Giants, **ApJL, 858, L22, 2018**.

2. **Raghubar Singh**, Bacham E. Reddy., Yerra Bharat Kumar, Spectroscopic study of two new super Li-rich red clump K giants, **MNRAS, 482,3822–3830 (2019)**.

3. **Raghubar Singh**, Bacham E. Reddy, Yerra Bharat Kumar, H.M. Antia, Survey of Li-rich Giants among Keplerand LAMOST Fields: Determination of Li-richGiants'Evolutionary Phase, **ApJL, 878, L21, 2019**

4. **Raghubar Singh**, Yerra Bharat Kumar, Bacham E. Reddy., Wako Aoki, Concerning the Li-rich status of KIC 9821622: a Kepler field RGB star-reported as a Li-rich giant, **MNRAS, 491,3838–3843 (2020)**

5. **Raghubar Singh**, Bacham E. Reddy, Yerra Bharat Kumar, Simon W. Campbell, Mathieu Vrard, Tracking the evolution of lithium in giants using asteroseismology: Super-Li-rich stars are almost exclusively young red-clump stars, **ApJL, 913, L4, 2021**.

6. **Raghubar Singh**, Bacham E. Reddy, Understanding Li enhancement in K giants and role of accurate parallaxes, **Proceedings of the International Astronomical Union , Volume 12 , Symposium S330: Astrometry and Astrophysics in the Gaia sky , April 2017 , pp. 348 - 349**

Presentations at Conferences

1. **Name**: 37th, Astronomical society of India
   Venue: CHRIST (Deemed to be University), Bengaluru, India
   Nature of participation: Oral
   Title: Spectroscopic and asteroseismic study of Li-rich giants

2. **Name**: 38th, Astronomical society of India
   Venue: IISER, Tirupati, India
   Nature of participation: Poster
   Title: Survey of Li - rich giants among Kepler and LAMOST fields

3. **Name**: 39th, Astronomical society of India
   Venue: Online
   Nature of participation: Poster
   Title: Li evolution in low mass red giants stars

4. **Name**: Chemical evolution and nucleosynthesis across the galaxy
   Venue: MPI HOUSE, Heidelberg, Germany
   Nature of participation: Oral
   Title: Enhancement of Li in red giants

Acknowledgements

Firstly, I am extremely grateful to my thesis supervisor Prof. B. Eswar Reddy for his guidance, continuous support and patience. His immense knowledge and experience has always encouraged me in academic, research and daily life. He has always inspired me to do the hard work, discuss research papers time to time, be frank in research and to do the best in life. I would like to offer my special thanks to my collaborator Dr. Bharat Kumar Yerra for his unconditional assistance at every phase of research.

I express my gratitude to the Doctoral Committee members, Prof. Sivarani Thirupathi and Dr. Latha for their insightful comments and encouragement which helped me to explore my research. I would like to thank Prof. Annapurni Subramaniam, Director, IIA, Prof. G. C. Anupama, Dean of faculty of sciences, IIA and all the academic and administrative staff, including the Board of Graduate Studies, for their assistance and support in creating a research friendly atmosphere for me. I am very grateful to Ashok, Fayaz and other 'Data Center' staff for their time-to-time technical support in computer and internet related matters and the administration of the University of Pondicherry for their support and input during my various research phases. I thank IIA library team for helping me to access necessary books and journals. Many thanks to the Administrative Officer, the Personnel Officer, the Account Officers and all other administrative staff for their timely assistance in the administrative work. I thank the supervisors, cooks and other staff members of Bhaskara for taking care during my stay in Bhaskara.

I express my sincere gratitude to instructors of Ph.D. course work, Prof. Anuj Nandi, Prof. Arun Manglam, Prof. Avinash Despande, Prof. Biman Nath, Prof. Prateek Sharma, Prof. R. T. Gangadhara, Prof. S. Sridhar, Prof. Shiv K. Sethi, Prof. Subinoy Das, Prof. S. P. Rajaguru and Prof. U. S. Kamath for teaching me the basics of astrophysics which was instrumental in selecting Ph.D. research

topic and carrying out research. I express my sincere gratitude to Prof. H. M. Antia for facilitating visit to TIFR and helping me learn basics of asteroseismic data analysis which played a crucial part in my Ph.D. thesis work. I thank Simon W. Campbell, Mathieu Vrard for their collaborative work. I would also like to thank Prof. Gajendra Pandey for always being motivating.

I would like to thank my friends in IIA, Phanindra and Nirmal with whom I enjoyed my time here. I thank them for their scientific discussions, helping me learn programming and time we spent together in treks, sports and extra curricular activities. I also thank to Avrajit and Arun Surya for helping me learn spectroscopic data analysis tools.

I acknowledge my batchmates Amit, Chinthak, Deepak, Kshama, Maninder, Priya, Prolay for their support. I am obliged to thank my seniors, colleagues and juniors, Abhijit, Ambily, Anwesh, Aritra, Annu, Ashish, Ankit, Anirban Dutta, Avinash, Anirban, Bhoomika, Bibhuti, Bharat, Chayan, Dipanweeta, Dhanush, Honey, Hemanth, Joice, Jyoti, Kanhaiya, Megha, Manika, Manoj, Nagraju, Nancy, Mageshwaran, Panini, Pallavi, Pawan, Partha, Priyanka, Prasanta, Pavana, Rubinur, Ravi, Rishabh, Ramya, Samyaday, Sajal, Shubham, Sowmya, Supriya, Sangeetha, Sudip, Susmitha, Srijit, Sindhu, Srikant, Seerisha, Samrat, Snehlata, Ritesh, Sreenath, Sandeep, Shubhankar, Soumya, Satabdwa, Swastik, Suman Saha, Sonith, Shejeela, Sudhakar, Selvan, Tridib, Tanmoy, Vaibhav, Varun, Vishnu, Vikrant, Brajesh, Vema Reddy for a cherished time spent together. It is their kind help and support that made my study and life in Bangalore a wonderful time.

I express my gratitude to my family for their tremendous understanding and encouragement to complete my study. Finally, I would like to thanks kind staff of Vainu Bappu Observatory, for their support and help during this difficult time of Covid-19, where this thesis writing was made possible.

Data usage

The work presented in this thesis is the product of data collected from the various ground and space-based telescopes. I thank all the scientific institutions, agencies and the staff involved in providing the data, without which this thesis would not have happened.

We have collected high-resolution spectra using the Hanle Echelle Spectrograph (HESP) mounted on 2.0 m Himalayan Chandra Telescope (HCT) operated by the Indian Institute of Astrophysics, Bangalore.

Much of the low resolution spectroscopic data was taken from the LAMOST spectroscopic survey conducted by the National Astronomical Observatories of China (NAOC) of Chinese Academy of Sciences (CAS). High-resolution archival spectra from APOGEE, Gemini and Subaru supplemented the low-resolution spectroscopic data.

We extensively used astrometry data from the *Gaia* space mission operated by European Space Agency (ESA) and photometric data from the NASA's *Kepler* space mission for asteroseismic analysis of sample stars.

Dedicated to
My Family

Abstract

Lithium (Li) is susceptible to relatively low temperatures. Hence, Li abundances among red giants are expected to be depleted significantly, by a factor of 40-60, from its original value on the main sequence. Assuming A(Li)= 3.2 dex on the main sequence, it is predicted maximum of A(Li)=1.6 - 1.8 dex, depending on mass, for RGB giants. In literature, giants with A(Li) $\geq$ 1.6 dex, in general, termed as Li-rich. The Li excess anomaly has been a puzzle to stellar evolutionary models ever since its serendipitous discovery in the early 1980s. This thesis aims to understand the anomaly among a small group of low mass red giant branch (RGB) stars. Understanding of the Li excess phenomenon in stars has broader implications for our better understanding of Li evolution in the universe and in stars, which in turn would help to better constrain theoretical models of stellar evolution.

We used large scale surveys for data collection such as LAMOST spectroscopic survey, photometric survey of $Kepler$ space telescope, $Gaia$ astrometry and high-resolution spectra using 2-m Himalayan Chandra Telescope (HCT). Our work discovered several red clump super-Li rich giants for the first time with an unambiguous evolutionary phase based on asteroseismic analysis. The extensive systematic survey based on an unbiased sample of giants common among $Kepler$ and LAMOST surveys' fields provided a key evidence that Li enhancement is only associated with the He-core burning phase post-He-flash. Another key result that emerged from this study is the location of the Li enrichment site during the He-flashing phase, the transition phase between the evolution of stars from the end of RGB tip to the He-core burning phase of the red clump phase. Based on the analysis of spectroscopic and photometric data, we provided first-of-its-kind evidence in the form of a correlation between lithium abundances in giants and period spacing of g-mode oscillations derived using asteroseismology. The evidence being that all the super Li-rich giants are almost exclusively young red clump

giants compared to Li-poor red clump giants suggesting the direct connection between the He-flash occurrence and the presence of Li in red clump giants. We have set robust upper limits of 40 million years, since the on-set of He-flash, within which period Li enhancement occurred. However, data does indicate Li enhancement occurred much earlier, probably, during the period of He-flashing phase itself i.e within two million years from the on-set of He-flash at the tip of RGB. The later suggestion requires more refined data of a larger sample.

Contents

List of Figures

List of Tables

Abbreviations

APOGEE	The **A**pache **P**oint **O**bervatory **G**alactic **E**volution **E**xperiment
BBN	**B**ig **B**ang **N**ucleosynthesis
GALAH	The **GAL**actic **A**rcheology with the **H**ermes
GRC	**G**alactic **C**osmic **R**ay
HBB	**H**ot **B**ottom **B**urning
HCT	**H**imalayan **C**handra **T**elescope
HESP	**H**anle **E**chelle **SP**ectrograph
IRAF	**I**mage **R**eduction and **A**nalysis **F**acility
ISM	**I**nter **S**tellar **M**edium
LAMOST	**L**arge sky **A**rea **M**ulti-**O**bject fibre **S**pectroscopic **T**elescope
LTE	**L**ocal **T**hermodynamic **E**quilibrium
MESA	**M**odules for **E**xperiments in **S**tellar **A**strophysics
PDS	**P**ower **D**ensity **S**pectra
RC	**R**ed **C**lump
RGB	**R**ed **G**iant **B**ranch
SED	**S**pectral **E**nergy **D**istribution
SIMBAD	**S**et of **I**dentification, **M**easurement and **B**ibliography for **A**stronomical **D**ata
SLR	**S**uper **L**ithium **R**ich
SNR	**S**ignal to **N**oise **R**atio

Chapter 1

Stellar evolution of low mass stars and Li-rich giants

The main objective of the thesis is to understand the origin and evolution of excess lithium abundance in the photospheres of low mass red giant stars. This chapter consists of two parts; in the first part, we provide a brief description of relevant stellar evolution of low mass stars and, in the 2nd part we give introduction to lithium evolution in the universe and its sources, and the problem of Li excess in evolved stars with a particular emphasis on low mass red giants.

1.1 Low mass Stellar evolution

As stars evolve through different phases, they undergo changes in their internal structure and external properties. The evolution of star can be followed in the Hertzsprung-Russell diagram (HRD) which describes stars' evolution in terms

of two fundamental stellar parameters; luminosity (L) and effective temperature (T_{eff}).

1.1.1 The main sequence

The main sequence (MS) is one of the most stable evolutionary phases of low mass stars, where stars spend most of their life. The Sun is in the main sequence. After forming molecular clouds composed of dust and gas, stars continue to contract because of gravity through the proto-stellar phase to the pre-main sequence (PMS) phase. Contraction results in increasing central temperatures and densities. Once temperatures reach sufficiently high (**around 20 MK**), hydrogen begins to burn at the centre, signalling the star's arrival on the main sequence phase. The energy generated by nuclear fusion of H into He at the centre balances inward gravitational force, ensuring equilibrium between outward radiative and inward gravitational forces. During the MS phase, much of the energy output or luminosity comes from hydrogen burning into helium at the centre and forming the helium core. The star's brightness or Luminosity (L) is related to mass (M), and mean molecular weight (μ) as $L \propto M^3 \mu^4$ (**see details Salaris *et al.* (2002).**) Higher the star's mass, the higher the luminosity. Hydrogen fusion into helium occurs via two series of nuclear reactions; proton-proton chain (PP-chain) and Carbon-Nitrogen-Oxygen cycle (CNO cycle) (Bethe and Critchfield 1938; Bethe 1939). The PP-chain dominates in low mass stars like the Sun, where the core temperature is relatively low, and the CNO cycle is the main source of energy in higher mass stars, **starting from 1.3 $M_\odot$**, where the core temperature is high. The PP-chain series of reactions consist of the conversion of four protons into the nucleus of helium. We can subdivide the pp-chain into three different channels: PPI, PPII and PPIII. The relative efficiency of PPI to PPIII changes with increasing temperature. The PP-chain is dominant in temperature range of < 15 MK and energy generation rate, $\epsilon_{PP} \propto T^4$. The CNO cycle is an indirect channel of four proton fusion into

helium. C, N and O only act as a catalyst to facilitate hydrogen burning. Overall, **the sum of the abundances of C, N and O remains constant**, although with a small change in individual abundances. The CNO cycle goes through many sets of reactions where CNO elements get destroyed and produced again. CNO cycle is dominant in the temperature range of > 20 MK and energy production rate, $\epsilon_{\mathrm{CNO}} \propto T^{18}$. The CNO cycle has two subdivisions: CNO-I and CNO-II.

PP chain goes through following series of nuclear reactions:

$$^{1}\mathrm{H} + ^{1}\mathrm{H} \rightarrow ^{2}\mathrm{H} + \mathrm{e}^{+} + \nu$$

$$^{2}\mathrm{H} + ^{1}\mathrm{H} \rightarrow ^{3}\mathrm{He} + \gamma$$

$$^{3}\mathrm{He} + ^{3}\mathrm{He} \rightarrow ^{4}\mathrm{He} + ^{1}\mathrm{H} + ^{1}\mathrm{H}$$

PPI

$$^{3}\mathrm{He} + ^{4}\mathrm{He} \rightarrow ^{7}\mathrm{Be} + \gamma$$

$$^{7}\mathrm{Be} + \mathrm{e}^{-} \rightarrow ^{7}\mathrm{Li} + \nu$$
$$^{7}\mathrm{Li} + ^{1}\mathrm{H} \rightarrow ^{4}\mathrm{He} + ^{4}\mathrm{He}$$

PPII

$$^{7}\mathrm{Be} + ^{1}\mathrm{H} \rightarrow ^{8}\mathrm{B} + \gamma$$
$$^{8}\mathrm{B} \rightarrow ^{8}\mathrm{Be} + \mathrm{e}^{+} + \nu$$
$$^{8}\mathrm{Be} \rightarrow ^{4}\mathrm{He} + ^{4}\mathrm{He}$$

PPIII

The CNO main cycle or CNO-I has the following reactions:

$$^{12}\mathrm{C} + ^{1}\mathrm{H} \rightarrow ^{13}\mathrm{N} + \gamma$$

$$^{13}\mathrm{N} \rightarrow ^{13}\mathrm{C} + \mathrm{e}^{+} + \nu_{\mathrm{e}}$$
$$^{13}\mathrm{C} + ^{1}\mathrm{H} \rightarrow ^{14}\mathrm{N} + \gamma$$
$$^{14}\mathrm{N} + ^{1}\mathrm{H} \rightarrow ^{15}\mathrm{O} + \gamma$$
$$^{15}\mathrm{O} \rightarrow ^{15}\mathrm{N} + \mathrm{e}^{+} + \nu_{\mathrm{e}}$$
$$^{15}\mathrm{N} + ^{1}\mathrm{H} \rightarrow ^{12}\mathrm{C} + ^{4}\mathrm{He}$$

CNO-II cycle completes through following reactions:

$$^{15}\mathrm{N} + ^{1}\mathrm{H} \rightarrow ^{16}\mathrm{O} + \gamma$$
$$^{16}\mathrm{O} + ^{1}\mathrm{H} \rightarrow ^{17}\mathrm{F} + \gamma$$
$$^{17}\mathrm{F} \rightarrow ^{17}\mathrm{O} + \mathrm{e}^{+} + \nu_{\mathrm{e}}$$
$$^{17}\mathrm{O} + ^{1}\mathrm{H} \rightarrow ^{14}\mathrm{N} + ^{4}\mathrm{He}$$

Stars having their main source of energy from the pp-chain have radiative cores whereas stars having CNO-chain reactions as the main source of energy have convective cores. Figure 1.1 shows Hertzsprung-Russell diagram (in short HR-Diagram or HRD) of theoretical model evolution of sun-like stars starting from PMS to Asymptotic Giant Branch (AGB) phase. A few Key evolutionary phases are highlighted.)

1.1.2 Sub giant phase

Sub giant branch (SGB) is a transition phase between the main sequence and the red giant branch (RGB). MS phase ends with the exhaustion of H at the centre, forming a helium core. He-core continues to contract due to gravity and lack of nuclear fusion energy at the center. Core at the center gets compressed to higher density and temperature. The heat generated in the core leaks outward, increasing

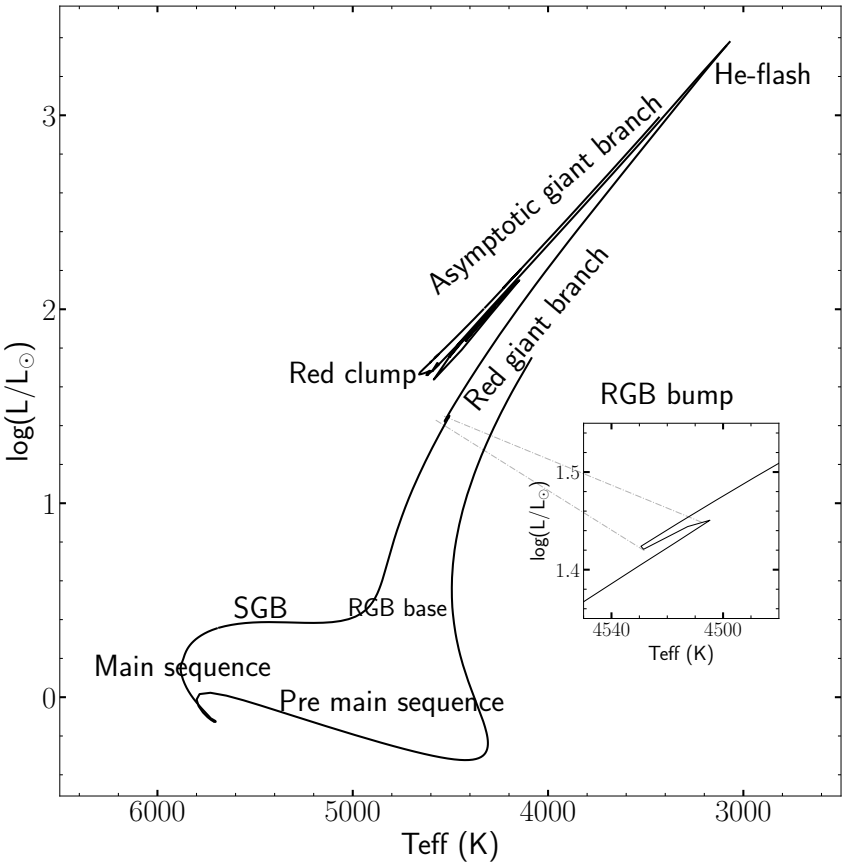

FIGURE 1.1: Hertzsprung-Russell diagram of a 1 $M_\odot$ star. Model evolution is computed from MESA stellar evolutionary code with solar metallicity. Different evolutionary phases are highlighted. Inset is the blown-up of luminosity function bump. **A star of 1 $M_\odot$ with solar metallicity has luminosity ranging from log($L/L_\odot$))= -0.12 to 0.36 and with almost constant radius while it is on the main sequence. Once the star reaches the RGB tip it will have log $L/L_\odot$ = 3.3 dex and its size increased to 165 $R_\odot$. Same will have reduced size and luminosity on RC with values of 1.65 dex and $\sim$ 15 $R_\odot$**, respectively.

the temperature of hydrogen layers immediately above He-core. With sufficient high temperature and density, H starts burning in a shell surrounding the inert He core. The core contracts continuously, and the outer envelope will expand with a fast decrease in T_{eff}. The inner core of low mass stars is made of electron degenerate gas. The electron degenerate pressure supports the core. Stars in the sub-giant branch spend a relatively short period.

1.1.3 Red giant phase

Base of RGB

At the RGB base, giants begin to ascend the RGB with increasing luminosity and no further significant cooling. During the RGB phase, He-core continues to grow in mass as H-burning adds more He ash to the core. Further core contraction results in more heat which in turn fuels more fusion in the H-burning shell. With the increased opacity and more energy generation, the temperature gradient becomes quite sharp between the inner and outer layers. The sharp gradient in temperature results in upper atmospheric layers to become unstable and expand (Salaris *et al.* 2002). As a result, stars become convective for efficient energy transport. The convective envelope progressively deepens, reaching close to the region where the chemical composition has been changed in MS. Near the RGB base, the convective envelope reaches maximum extent in mass and then recedes slowly towards the surface. The material containing the by-products of H-fusion in the MS phase starts mixing up with the stars' upper atmospheres resulting in changes in the chemical composition of stars' photosphere. The mixing occurs instantaneously throughout the convective envelope. The phenomenon is known as first dredge-up (1st dredge-up or FDU). According to canonical models, the first dredge-up increases abundance of He, ^{13}C and N, whereas decreases in abundance of Li, ^{12}C in the photosphere. The carbon isotopic ratio ^{12}C/^{13}C will be down from about 90 on the main sequence to 20-25 in the post first dredge-up. The theoretical predictions, in general, agree well with the observations.

Luminosity bump

The abrupt interruption in the increasing luminosity of low mass stars during their evolution ascending the RGB results in the concentration of stars at a particular stage on RGB. This is known as luminosity function bump or the luminosity bump, or in short, the bump on RGB. The bump was first observed among stars of the globular cluster (see (King *et al.* 1985)). During the interruption, star's luminosity falls abruptly and rises again to continue their ascension towards the RGB tip (Iben 1968; Christensen-Dalsgaard 2015), see inset in Figure 1.1. As a result, stars spend relatively more time in a narrow range of luminosity in the HR diagram compared to any other place on RGB, resulting in clumping of stars. This is known as the Luminosity bump on RGB. What causes the bump is not well understood. After the 1st dredge-up, the deep convective envelope retreats, creating a discontinuity in the H-abundance profile between the H-burning shell and the convective envelope. Because of the discontinuity, no further changes to the photospheric chemical composition are expected post first dredge-up. However, due to an increase in He-core mass at the bump, the H-burning shell moves outwards, encroaching the zone of discontinuity in the H-profile. As a result, the H-burning shell is provided with more hydrogen from the outer envelope resulting in a sudden fall in luminosity. The very low abundances of C, Li and $^{12}C/^{13}C$ seen in upper RGB giants compared to predictions of standard models of first dredge-up (FDU) on RGB are now understood to be due to some extra mixing process during giants' evolution RGB bump. The extra-mixing was not part of standard models. There are several proposals for extra-mixing, such as thermohaline mixing **(Charbonnel and Zahn 2007)** and meridional circulation(Talon and Charbonnel 1998).

The tip of RGB and He flash

The central He-core mass continues to grow due to the piling of He ash from the H-burning shell as stars evolve towards the RGB tip. The tip of the RGB (here onwards TRGB) is the endpoint of RGB evolution characterized by maximum luminosity and lowest temperature of RGB. The TRGB's luminosity is almost constant across the initial mass range of low mass giants ($\leq 2.0\ M_{\odot}$). Thus, TRGB is used for distance calibrations of nearby resolved galaxies(Lee *et al.* 1993) and it even allows measuring the Hubble constant, H_o, (Freedman *et al.* 2019). Low mass giants, in certain conditions, develop electron degeneracy pressure at the core to counter the inward gravitational force. Contrary to normal gas behaviour, material in the degeneracy does not increase in volume against the increased temperature. Thus, increased mass increases in temperature. When inert He core mass reaches 0.48 $M_{\odot}$ (the exact value of mass depends on the initial composition) near the TRGB, temperature and density in core reach to as high as 8×10^7 K and 10^6 gm cm^{-3}, respectively. These conditions initiate explosive He ignition near the core, causing He flashes. The He-flash takes place off-centre at the location of maximum temperature (neutrino cooling is maximum at the centre). It is predicted that these flashes are powerful, and the initial He-flash will produce luminosity close to a factor of a billion compared to the Sun's luminosity (Schwarzschild and Härm 1962a; Renzini and Fusi Pecci 1988). However, the effects are not seen on the surface except a drop in luminosity by order of magnitude from the TRGB luminosity. The immense He-flash energy goes into the lifting of central degeneracy, and some of it will be absorbed by the non-degenerate layers above the core. Stars undergo a series of He sub-flashes until the degeneracy is entirely removed and the central core is fully convective(Bildsten *et al.* 2012). Stars settle at the beginning of the horizontal branch burning helium quiescently under non-degenerate conditions. This phase is known as the red clump (RC) phase, with a central He-burning core surrounded by an H-burning shell. The TRGB's transition to red clump is very fast, about 2 Myr.

Red clump

Red clump (RC) stars are low mas giants burning helium quiescently in a convective core surrounded by an H-burning shell and enveloped by the outer convective zone. These are located at the beginning, cooler side, of the horizontal branch (Cannon 1970; Girardi 2016). Due to a small range in their mass and T_{eff}, these stars end up as a clump in L-T_{eff} plane, which is seen well in the case of globular clusters. Irrespective of their initial mass, at least among low mass giants, giants at the RC phase will have the same core mass and hence, the same luminosity. Due to this property, RC stars are generally used as standard candles for distance measurement of stars in Milky Way and neighboring galaxies (Stanek *et al.* 1998). He-burning powers giants in the RC phase at the centre and H-burning in the outer shell. Once He is exhausted at the core stars' RC phase ends. The He-fusion via triple α reactions at the centre forms a carbon core. Once He is exhausted at the centre, stars begin to move towards the early Asymptotic giant branch (AGB) phase. The RC phase is expected to last for about 100 Myr.

The location of red clump stars in the HR diagram overlaps with the giants ascending the RGB at many places, particularly with the bump on the RGB. Difference between stellar parameters between RC and ascending RGB phase depends on the mass and metallicity of stars, as seen in Figure 1.2. With increase in mass and metallicity separation reduces i.e. overlap increases, which makes distinguishing RC giants from those of RGB among field giants is a non-trivial problem. Asteroseismology of giants now enables separating RC and RGB giants as they exhibit characteristic oscillation frequencies associated with their central core properties **Kjeldsen** *et al.* (**2010**).

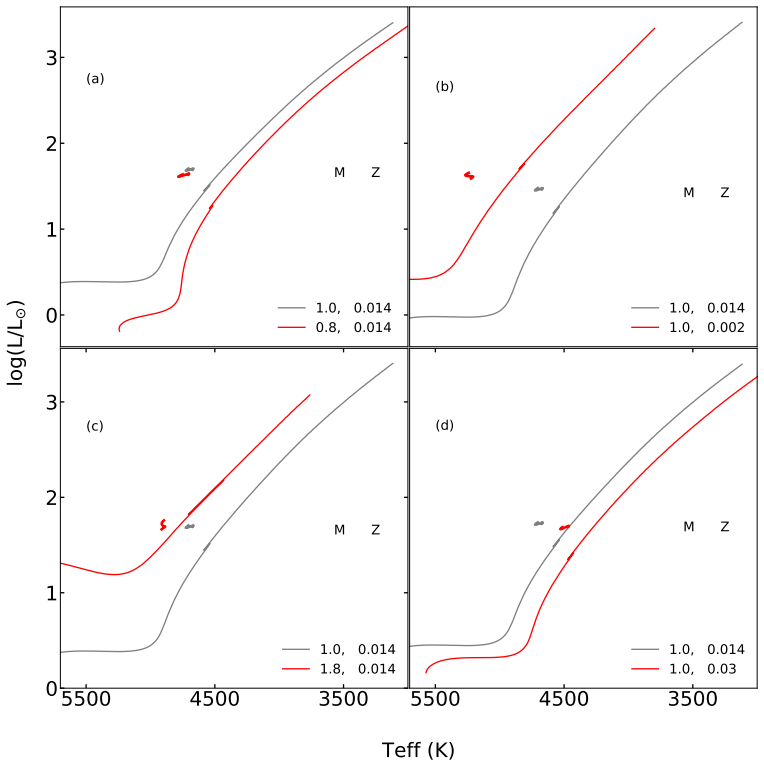

FIGURE 1.2: Figure Demonstrates the challenge of separating giants of RGB from those of RC. Shown in the figure are computed evolutionary models for different masses and metallicities. The gap between RC region and RGB (its bump region) is very small in L-T_{eff} plane.

1.1.4 Asymptotic giant branch

Post RC phase, stars enter into the asymptotic giant branch (AGB) phase. AGB is the final evolutionary phase of low and intermediate-mass stars before entering into planetary Nebulae and subsequent white dwarf phase. AGB stars are characterized by central electron degenerate C and O core surrounded by nuclear burning of He in the shell. A hydrogen-burning shell surrounds He-burning. In the early phase of AGB evolution, energy output from the He shell dominates the total energy production. Atmospheres of AGB stars are known to have enriched in elements like C, N, O and slow neutron capture elements or (s-process elements) like Y, Zr, Ba. Massive AGB stars ($> 3\,M_{\odot}$) are also known to produce Li in high quantities. In general, towards the end of the AGB phase, stars undergo intense mass loss due to thermal pulses. As a result, stars at this stage are shrouded by dust and

appear only in IR wavelengths. At the end of the AGB phase, stars appear as post-AGB stars and planetary nebulae (PN), which finally end up as C+O white dwarfs (Herwig 2005). Significant enrichment of interstellar medium (ISM) by various elements comes from the severe mass loss of AGB giants.

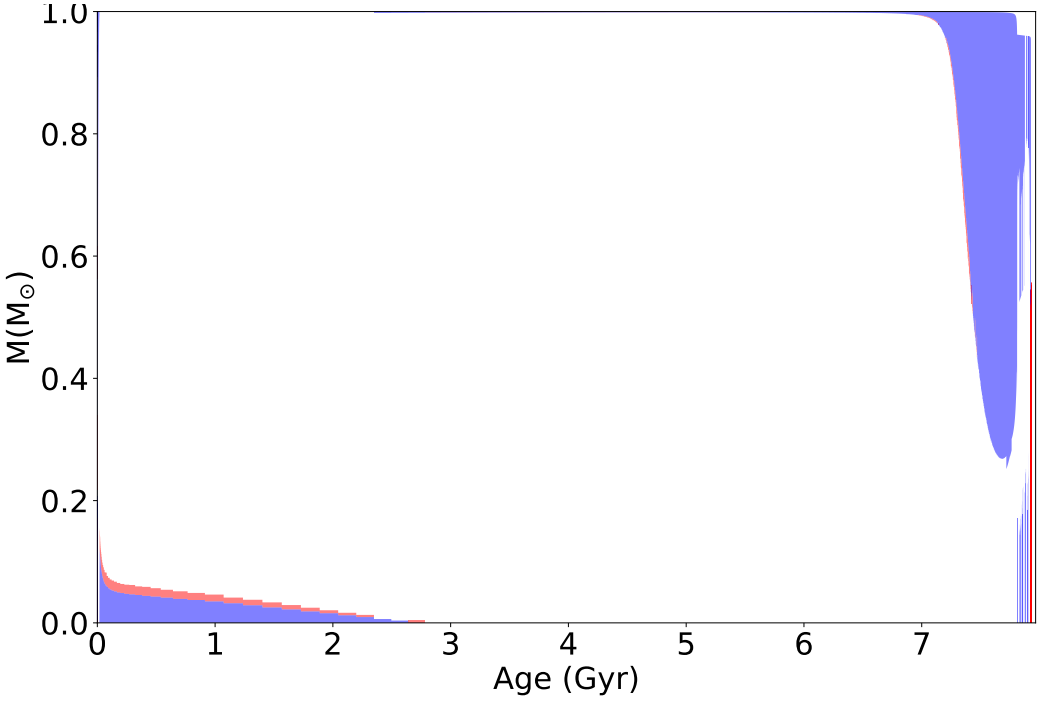

FIGURE 1.3: Evolution of convective region in 1 $M_{\odot}$ star as computed from MESA stellar evolutionary code. Blue color shows convection and red region is overshoot.

1.2 Li evolution in the universe and sources of its enrichment - the issue of large Li in red giants

Lithium (Li) is a unique alkaline element. In the periodic table, Li is the 3rd element (Z=3). It is one of the three elements known to have originated in the Big Bang nucleosynthesis(BBN). The other two are hydrogen (H) and helium (He). Of several isotopes of Li, isotopes ^{6}Li and ^{7}Li with mass numbers 6 and 7, respectively,

are the most common in nature. Current state-of-the-art Big Bang Nucleosynthesis (BBN) models with the latest measured input parameters such as photon to baryon density (η) using cosmic microwave background (CMB) experiments like Wilkinson Microwave Anisotropy Probe (*WMAP*), *Planck* predicts Li abundance of A(Li) = 2.72 ± 0.05 dex (Abundance are expressed in logarithmic scale relative to hydrogen, A(Li) = log N(Li)/N(H) + 12). This value is known in the literature as primordial Li abundance (Cyburt *et al.* 2016).

Are there Li abundances measured in stars or some other objects in the universe which can validate BBN Li abundance predictions? In other words, what is the observed Li abundance of the big bang? A key question over which a lot of observational efforts have gone into. Li abundance measured in relatively warmer, old and metal-poor dwarfs in the Galaxy is considered as the observed primordial value. The observed value is the value of Spite-plateau (Spite and Spite 1982) named after their discoverers is A(Li) = 2.2±0.1. Spite-plateau is remarkably constant over a large range in metallicity, with very little scatter. Spite-plateau Li abundance is known in the literature as the observed primordial Li abundance, see Figure 1.4. **However, the observed Li abundance in metal-poor stars is more than a factor of 3 less than the BBN predicted value**. There is no consensus on this yet. The difference in Li abundance between BBN and the observations has been known in the literature as the "cosmic Li problem".

There are two valid views for the discrepancy. Is the BBN theory overestimated Li abundance, or is there something to do with observations? There may be many channels where theory can be improved, such as the decay channel of ^{8}Be. What if ^{8}Be can decay into other elements apart from Li? If so, this will have a bearing on Li production in BBN. The other view being, the theory is correct because the other two BBN predicted elements (deuterium and helium) agree well with the observations, see Figure 1.5. Probably, Li in old stars has been depleted over the lifetime of the Universe due to slow mixing, such as the diffusion process. Also,

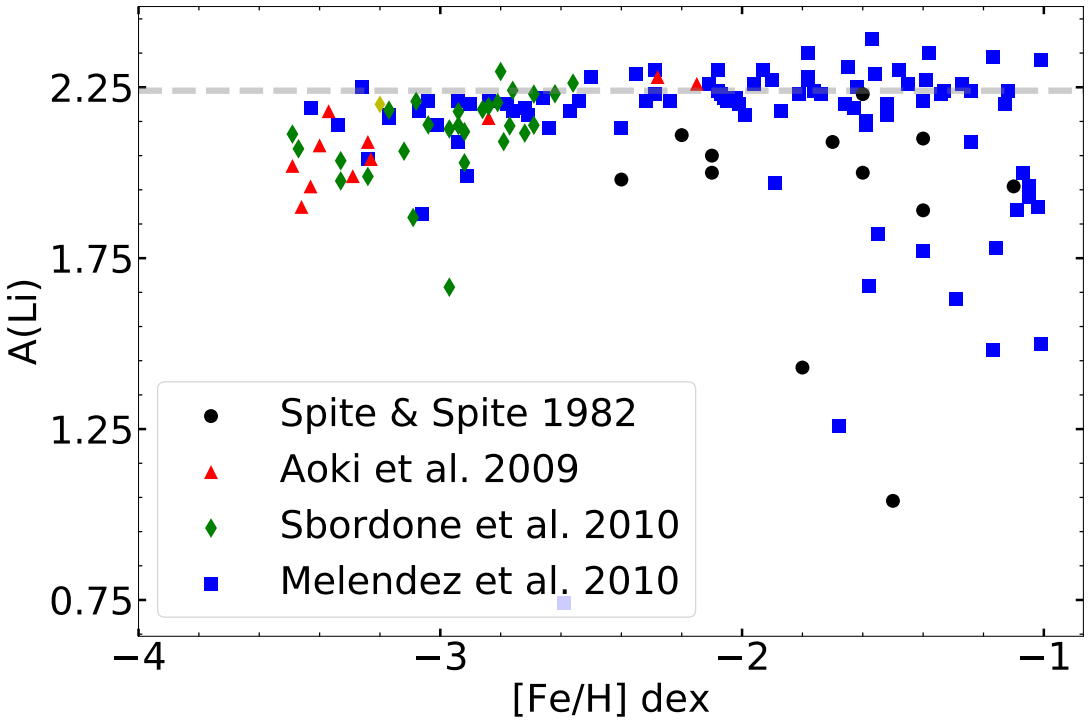

FIGURE 1.4: Li abundances among warmer metal-poor dwarfs. Dashed line is the Spite Plateau at A(Li) = 2.25 dex, a value known in the literature as the observed primordial abundance. Note, a trend of A(Li) decreasing from the plateau value starting from [Fe/H] $\sim$ -2.8 dex.

the new observations of Li in extremely metal-poor stars, claimed to be the first generation of stars formed with primordial soup, show significantly lower values compared to Spite value breaking the Spite-Plateau at the lower end of metallicity, at about [M/H] = -2.8 dex. The new Li observations in very metal-poor stars suggest Li is vulnerable to a complex set of stellar internal mechanisms, which are functions of age, metallicity and mass. It is fair to say that we do not yet have observed Li abundance that could be considered as a primordial value.

While the debate about the primordial Li abundance continues, studies also grapple with the issues related to Li enhancement in the Universe. The current value of A(Li) in the Universe as measured in young stars or interstellar medium (ISM) is A(Li) $\sim$ 3.32 dex (Knauth *et al.* 2003), meaning Li is enriched over the lifetime of the Galaxy irrespective of which value of Li is adopted as primordial value. If

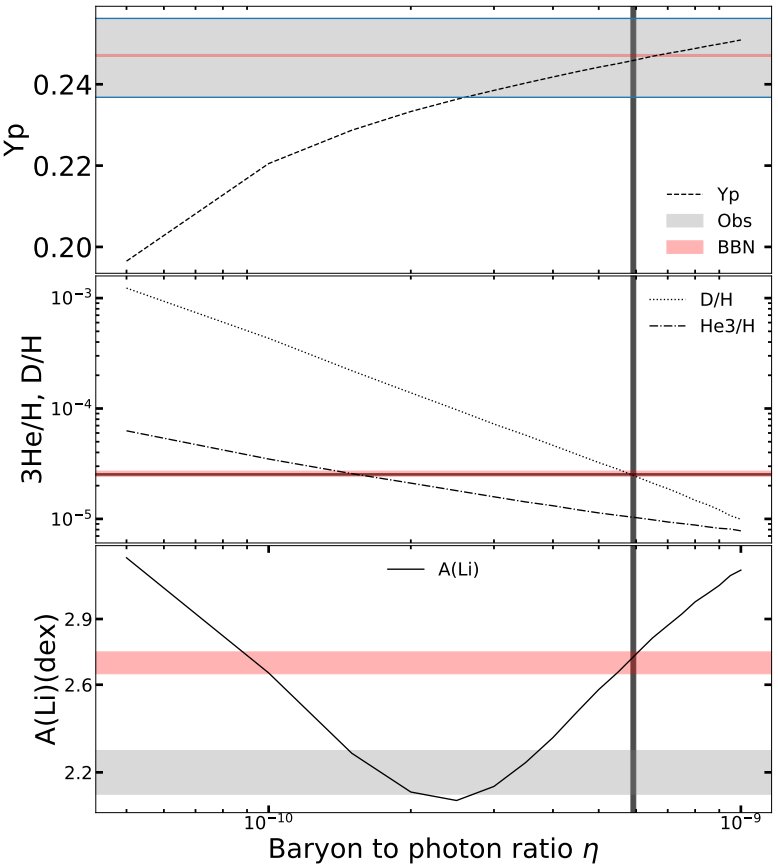

FIGURE 1.5: Observed abundances of the three primordial elements H, He and Li are compared with the Big Bang Nucleosynthesis models computed using the values of baryon-to-photon ratio, η, measured from *WMAP* and *Planck* space experiments. Horizontal lines represent observed values of respective elements. The vertical line is the adopted η in the BBN models. Except for the Li abundance the BBN models and observations are in good agreement for the other two primordial elements, H and He (Cyburt *et al.* 2016).

we take BBN prediction of A(Li) = 2.72 dex as the primordial abundance, Li increases by a factor of 4 or by order of magnitude if we take observed Spite-Plateau value since the time of Big Bang. Several sources were identified for the increased amount of Li in the Universe; cosmic ray spallation, evolved stars, and stellar explosive phenomena such as novae and supernovae (SNe). This thesis focuses on Li enrichment in evolved stars of a particular evolutionary phase called the red giant branch (RGB). For completeness, some of the suggested sources of Li enrichment in the Galaxy are briefly described below.

1.2.1 Cosmic ray spallation reactions

Galactic Cosmic rays (GCR) are high energy protons, alpha particles and nuclei of other heavy elements. The GCR flux interacts with the heavier atoms such as carbon, nitrogen and oxygen in the interstellar medium (ISM). The high energy particles split heavier atoms into smaller atoms like Li, Be and B (Reeves *et al.* 1970). Over a period of time, the spallation process($\mathrm{p}, \alpha + \mathrm{C}, \mathrm{N}, \mathrm{O} \rightarrow^{6,7}$ Li) can enrich the ISM significantly with light elements. Cosmic rays can also produce Li by fusion of α nucleons.

1.2.2 Novae and Super Novae

Novae and SNe are expected to produce Li during the thermonuclear runaway and contribute to Li enrichment of the ISM. Neutrino spallation reactions on helium and carbon-rich layers during SNe explosions in the massive stars seem to produce ^{7}Li and ^{11}B (Domogatskii *et al.* 1978). ^{7}Be production in Novae has been theoretically predicted. Depending on initial He abundance in white dwarf ^{7}Li can be produced in significant quantities during explosive H burning in novae (Starrfield *et al.* 1978). Direct detection of ^{7}Be in the near UV spectra of Nova Delphini 2013 Tajitsu *et al.* (2015) confirmed the predictions. With a half lifetime of 53.33 days, ^{7}Li will be produced from ^{7}Be with electron capture. Also, the Li resonance line was detected in the highly blue-shifted optical spectra of Novae V1369 Cen during the early phase of its outburst (Izzo *et al.* 2015).

1.3 Stars as Li sinks

In general, stars are known as Li sinks because Li gets destroyed at relatively low temperatures, $> 2.5 \times 10^6$ K, by converting back to helium. Li in stars survives mainly in the outer layers, which are relatively cool compared to the inner regions. Stellar interiors are hot and devoid of lithium. Convective mixing is common among evolved stars causing dilution of Li in the atmospheres by mixing the inner material with little/no Li in it. The complexity of Li is such that its depletion is not just associated with mixing in evolved stars; Li is also found to be depleted during their pre-main-sequence evolution before reaching the main sequence. For instance, Li abundance in the Sun's photosphere is A(Li) = 1.05±0.01 dex, more than two orders of magnitude less than in the Sun's birth clouds. During their lifetime, stars mostly destroy most of the initial Li with which they were formed. However, there are exceptions. A small group of RGB and AGB giants show very high levels of Li abundances, contrary to theoretical expectations.

1.3.1 Intermediate mass AGB stars

Asymptotic giant branch (AGB) star are known to produce Li internally (Scalo *et al.* 1975). Probably, AGBs contribute to the Li enrichment process via mass loss. Particularly, Li enhancement is seen mostly among intermediate mass ($> 3\,M_\odot$) AGB stars. It is known Li is produced in these stars via Cameron-Fowler (CF) mechanism (Cameron and Fowler 1971). In the CF mechanism, ^{3}He captures an α particle at high temperature (15 — 20 MK) and converts it into ^{7}Be. This freshly produced ^{7}Be can convert to B or decay into the ^{7}Li. The destruction temperature of Li is so low that it can not survive where it gets produced. Thus, there should be a mechanism that can safely transport the freshly synthesised ^{7}Be material into the cooler regions (T $<$ 2.5 MK) where ^{7}Li will be produced by electron capture.

In intermediate-mass stars ($3 < M(M_{\odot}) < 8$) base of the convective envelope is near the vicinity of the hydrogen burning shell where the temperature is high enough ($T_{bce} = 40\ MK$) for the CF mechanism to occur. The mechanism is known as hot bottom burning, just below the outer convective envelope, in which Li can be produced and quickly transported to outer layers (Scalo *et al.* 1975). HBB is not only a key mechanism for Li production in AGB stars it also produces N and C in the envelope of Carbon stars when the temperature at the base of convective envelope (T_{bce}) reaches 65 MK.

1.3.2 Li in red giants

The interest of the current thesis work is to understand Li production and evolution among low mass giants of the red giant branch (RGB) and red clump (RC). Once stars leave the main sequence after hydrogen exhaustion at the centre, they develop a deep convective envelope reaching the hydrogen-burning shell resulting mixing of material in stars. This mixing is known as the first 1st dredge-up. The first dredge-up causes the mixing up of processed material in the H-burning shell with the outer layers, altering the stars' photosphere's chemical composition. Notable changes to elemental abundances include by-products of PP chain and CN reactions: ^{7}Li, ^{12}C, ^{13}C, ^{14}N. While the abundances of Li and ^{12}C decrease, the abundances of ^{13}C, ^{14}N increase (Salaris *et al.* 2002). The observed abundances, in general, agree well with the theoretical models (Iben 1967; Lagarde *et al.* 2012).

However, there are exceptions. The notable exception being the Li abundance. Canonical models of stellar evolution predict a maximum A(Li) = 1.5 to 1.8 dex, depending on stars initial mass, for normal giants(Iben 1967). In most cases, observations agree with the predicted limits. However, a few outliers, contrary to theoretical models and general observational trends, show anomalously large excess in Li abundance. Studies adopted a value of A(Li) = 1.6 to 1.8 dex as

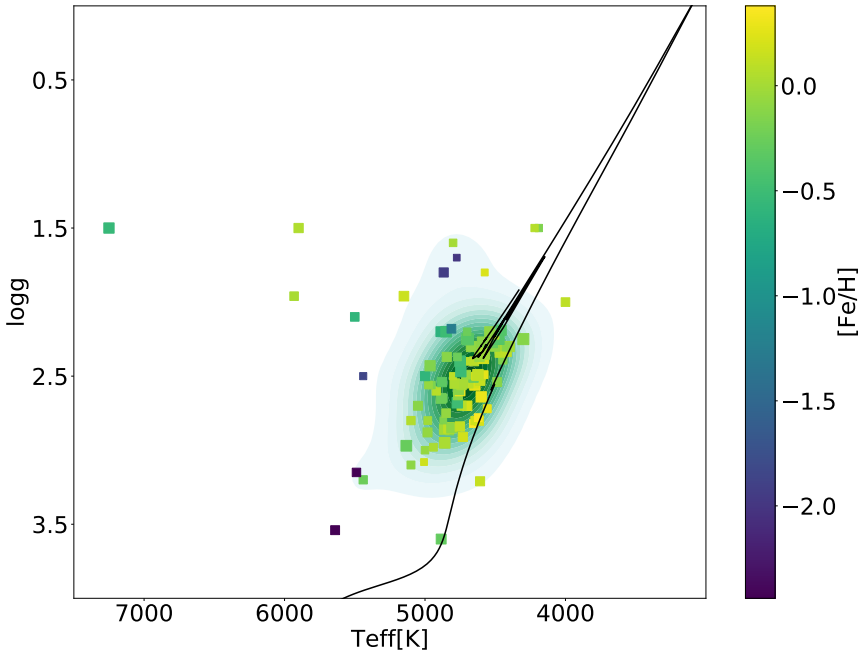

FIGURE 1.6: Location of Li-rich giants in the Hertzsprung-Russell diagram. Superimposed is the evolutionary track of a 1 $M_{\odot}$ star. Most of the Li-rich giants are confined to a narrow region overlapped by RGB bump and red clump phases. Li-rich giants data is taken from the compilation of Casey *et al.* (2016)

the upper limit for low mass giants ($M < 2.0\ M_{\odot}$). Giants with more A(Li) than the upper limit are classified as Li-rich giants. The excess Li amount was first reported by Wallerstein and Sneden (1982) in a typical red giant star HD 112127 with A(Li)=3.2 dex. Since then, the origin of Li excess in these stars remained a puzzle till date, though the number of Li-rich giants grew many-fold. Thanks to some extensive systematic surveys (Brown *et al.* 1989; Kumar *et al.* 2011; Casey *et al.* 2016; Kirby *et al.* 2016; Casey *et al.* 2019; Deepak and Reddy 2019) there are now a couple of hundred stars known as Li-rich giants with A(Li) $>$ 1.6 dex. Surveys show roughly 1 % giants having excess Li among red giants in the Galaxy (Brown *et al.* 1989; Kumar *et al.* 2011). Hence, Li-rich giants are known in the literature as a rare group of giants. Many theoretical and observational efforts are underway to understand the Li anomaly in giants otherwise well understood low mass stellar evolution.

1.3.3 Beryllium abundance in Li-rich giants

Another important light element is beryllium (Be) with Z=4. Beryllium too is fragile similarly to Li but gets destroyed at relatively higher temperatures. As a result, Be survives in relatively deeper layers than Li, which is mainly confined to cooler outer layers. Studies use Be to track the evolution of Li in stars. For example, low Be abundances in stars are indicative of severe convection and significant dilution of Li. An extensive survey carried out by Takeda and Tajitsu (2014) revealed severe depletion of Be in the red giants implying those red giants would have very little Li in their atmospheres. Be abundance evolves from its main sequence pop I stars, A(Be) = 1.38 ± 0.09 (Asplund *et al.* 2009) to as low as A(Be) = -1.0 dex in red giants (Takeda and Tajitsu 2017; Melo *et al.* 2005). There are no many studies in which A(Be) are measured in Li-rich giants. Castilho *et al.* (1999) studied two Li-rich giants for Be abundance and found very low levels of Be implying that the excess Li is probably produced freshly in stars. In figure 1.7 we have plotted Be abundance derived by Takeda and Tajitsu (2014) for red giants and main sequence stars adopted from the literature (Gálvez-Ortiz, M. C. *et al.* 2011, and reference therein). The A(Be) abundance trends shown in Figure 1.7 are similar to Li abundance trends among MS and RGB giants.

1.3.4 Li excess connection with other stellar properties: Infrared excess and rotational velocities

The above section clarifies that the Li excess seen in some red giants is **real meaning Li has been freshly produced in the stars, and it is not due to insufficient mixing**. Initial studies suggested that some of the giants with Li-excess are also found to have high rotational velocities ($vsini$) and infrared (IR) excess. The studies suggested that the Li excess in giants probably is due to the

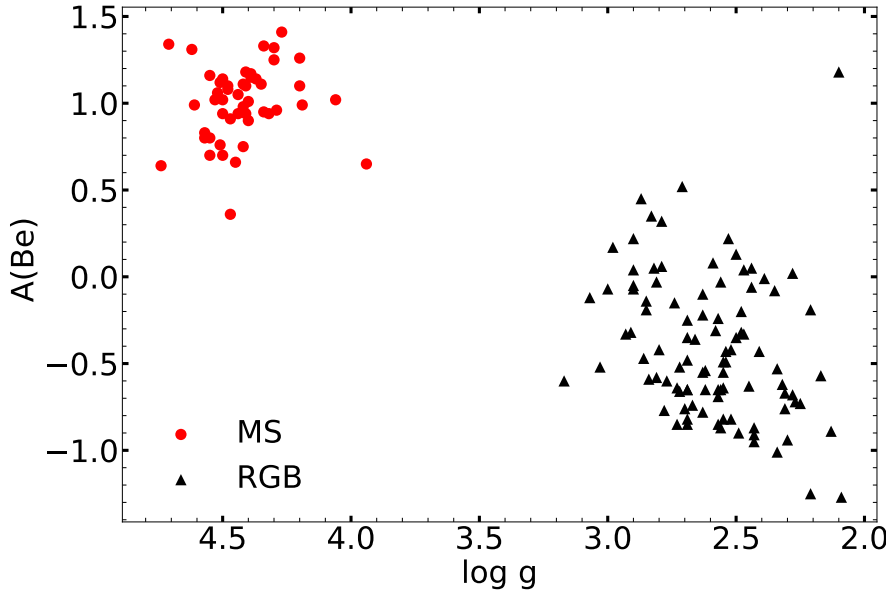

FIGURE 1.7: Evolution of Be abundance among stars evolving from the main sequence to red giants. Among red giants Be is significantly depleted. Be is similar to Li but gets destroyed slightly at higher temperatures. So, it is used to infer Li evolution i.e less Be abundance in red giants means severe mixing and much less Li abundance in those stars.

merging of planets or brown dwarfs that retained their original Li. Models indicate the possibility of mergers and the resulting increase in Li content. Merger theory also predicts increasing *vsini* due to transfer of angular momentum to the host star and infrared excess due to mass loss ejected at the time of merger event. However, a detailed survey of red giants for IR excess (Bharat Kumar *et al.* 2015; Rebull *et al.* 2015) showed no connection with Li excess. They concluded that a few stars that showed IR excess and very high Li abundances are merely a coincidence due to bias in the early sample selection (Zuckerman *et al.* 1995; Plets *et al.* 1997). As per the rotation, *vsini*, a few Li-rich giants do show very high values (De Medeiros *et al.* 2000; Drake *et al.* 2002; Carlberg *et al.* 2012; Smiljanic *et al.* 2018). However, there is no clear evidence of a correlation established yet between Li abundance and *visini* as the sample is small for which both the parameters are available. The correlation of *vsini* and Li excess among giants needs to be further probed.

1.4 Principal suggestions for Li excess in red giants

Almost six decades back Alexander (1967) suggested that Li excess seen in some evolved stars (probably in massive AGB stars) might be due to planet engulfment (a full 30 years before the discovery of exoplanets). However, much attention was paid to the Li excess issue in red giants only after the very high Li abundance reported in giants by Wallerstein and Sneden (1982). In the literature, there are three principal hypotheses for Li excess in giants. Each of them is described in brief below.

1.4.1 Preservation

According to this hypothesis, enhanced Li in the surface of evolved stars results from inefficient convective mixing at the base of RGB. However, this does not explain why the Li excess is seen only in a small fraction of giants. Further, very low carbon isotopic ratio ($^{12}C/^{13}C$ (Kumar *et al.* 2011), and observations of low Be abundances (Melo *et al.* 2005) rule out the preservation scenario for Li excess in red giants. Low $^{12}C/^{13}C$ ratios and Be abundance are robust indicators of deep stellar mixing in stars. Notably, the discovery of a few super Li-rich giants with A(Li) $\geq$ 3.2 dex (the ISM value) (de La Reza and da Silva 1995; de La Reza *et al.* 1996; Balachandran *et al.* 2000; Ruchti *et al.* 2011; Kumar *et al.* 2011; Casey *et al.* 2016) rules out the preservation scenario.

1.4.2 External sources

To explain excess Li in red giants, studies mooted the idea of an external source for Li excess origin in red giants, such as transfer of Li-rich material from intermediate-mass AGB stars, which are known to produce Li and engulfment of planets. The AGB mass transfer scenario requires evidence of binarity, which is not seen among Li-rich giants for which long term data is available (Jorissen *et al.* 2020). As per the planet or brown dwarf engulfment, serious studies are being made. There are issues to account for the original Li in giants' atmospheres. The shortage of close-in orbit planets around evolved stars, according to studies, is the evidence for such possibility. However, a merger scenario requires adding a substantial amount of planet material into the star's convective mass to match with the large observed Li enhancement in giants. For giants to have A(Li) = 2.2 dex, according to model estimates, giants require direct mixing of at least one thousand earth-sized planets in their outer convective envelopes. An external origin also requires observations of enhanced refractory elements like Fe, Ni etc., which is yet to be probed systematically. Also, models suggest that mergers cause higher rotation due to the transfer of angular momentum and infrared excess due to mass loss. IR excess studies among large red giants suggest a correlation with Li excess (Bharat Kumar *et al.* 2015). Relation between *vsini* and Li-excess needs to be probed further with a much large sample.

1.4.3 Internal production of Li

In-situ production of Li in stars is a widely acknowledged scenario for Li excess seen in red giants. Li production via a sequence of nuclear reactions in hydrogen burning shell via CF (Cameron and Fowler 1971) mechanism is well documented. However, according to current theoretical models, there is no viable known mechanism for

mixing up Li, in such a huge quantity, with the star's photosphere. The two key reactions that lead to Li production are: a) ^{3}He $(\alpha, \gamma)^{7}$Be, b) ^{7}Be(e^{-1}, ν) ^{7}Li. The ^{7}Be production reaction occurs at about $2\times$ 10^{7}K, and destruction of Li by capturing proton occurs at relatively much lower temperatures of about $2.5\times$ 10^{6}K. It is important to note that there must be a mechanism causing the large excess in Li by quickly transporting ^{7}Be to relatively cooler regions where ^{7}Li will be produced and survive for mixing with the outer photosphere. This mechanism is presently not understood. For completeness, we briefly mentioned below some of the ideas proposed for Li-excess. Some of them are now outdated due to the latest evidence from large observational data sets.

1.4.3.1 Li-flash

Charbonnel and Balachandran (2000) were the first to assemble all the known Li-rich giants (A(Li) $\geq$ 1.5 dex), till then, in Hertzsprung-Russel (HR) diagram of Luminosity-$T_{\rm eff}$. They used Hipparcos astrometry for luminosity. Based on stars grouping at luminosity bump region, they suggested that the bump region holds the key for Li production. This observational evidence led to various theories. One among them is Li-flash for enabling mixing of freshly produced Li with the upper atmosphere(Palacios *et al.* 2001). According to this scenario, ^{7}Li(proton, $\alpha)\alpha$ is a dominant reaction outside the H-burning shell, which creates a thin Li-burning shell. The Li-shell undergoes flashes causing instability in the shell, resulting in removing the molecular weight discontinuity barrier set post-1st-dredge-up. It will provide a way for safe transport of ^{7}Be to cooler regions. However, it is difficult to understand that the bump region, at which extra-mixing takes place causing very low Li abundances and ^{12}C/^{13}C ratios observed in upper red giants is also responsible for the high Li abundance. Extra-mixing mechanisms are successfully proposed for the very low abundance of Li and other elements observed in giants post-bump evolution relative to first dredge-up predictions.

1.4.3.2 Extra mixing mechanism

Extra mixing is the mechanism invoked to explain observed very low abundances of Li and $^{12}C/^{13}C$ compared to predictions from canonical models (Sweigart and Mengel 1979; Denissenkov and VandenBerg 2003; Charbonnel and Zahn 2007). Observations also showed that such severe depletion begins at the luminosity bump region in the HR diagram(Gratton *et al.* 2000). At the bump, the barrier for convection created post first dredge-up will be breached causing further dilution of photospheric Li and C abundance and increasing ^{13}C and N abundances. There are several scenarios proposed for this deep convection which was not part of standard models. The proposals include thermohaline mixing (Eggleton *et al.* 2006; Charbonnel and Zahn 2007; Cantiello and Langer 2010), rotational mixing (Talon and Charbonnel 1998), magneto-thermohaline mixing (Denissenkov *et al.* 2009) etc., which all come under the umbrella of the extra-mixing process. However, we do not know yet which one of these mixing processes or combination of them are responsible. However, extra-mixing must be responsible for connecting hydrogen-burning shell with outer envelope to have very low observed photospheric values of Li, C and much lower $^{12}C/^{13}C$ values.

1.4.3.3 Planet engulfment induced in-situ nucleosynthesis

Direct injection of Li-rich planetary material into the host star convective envelop will require the merger of hundreds of planets to account for Li excess seen in red giants. For example, Siess and Livio (1999) estimated about 0.1 $M_{\odot}$ planetary material mixing. Also, Aguilera-Gómez *et al.* (2016) estimated1 at least material mass of 15 $M_{Jupiter}$ required to show the maximum of A(Li)= 2.2 dex. Direct addition of external Li-rich material may not be sufficient to explain the large excess Li seen in red giants. Studies suggest that mergers apart from adding Li directly to the host star also trigger Li production and extra mixing process,

accounting for large Li excess seen in giants. One of them is the merger of a He-white dwarf with the red giant inert He-core creating He-flash at the centre Zhang and Jeffery (2013); Zhang *et al.* (2020). Also, tidal interactions by orbiting planets or brown dwarfs which break the stable radiative zone surrounding the H-burning shell creating a way to mix high Li with outer layers (see Denissenkov and Herwig (2004); Casey *et al.* (2019)).

1.4.3.4 The He-flash

The suggestion that the He-flash at the end of RGB is the plausible site for Li excess seen in RGB giants (Kumar *et al.* 2011) is a significant clue for Li excess origin search. This observational evidence was based on a large systematic and uniform study of 2000 giants. Since then, He-flash became one of the key contenders for Li origin site and attracted serious theoretical modelling and ideas. For example, Mocák *et al.* (2011) performed hydrodynamical simulations to see whether the entropy barrier between He- and H-shell burning could be overcome and mixing of their by-products with upper layers. They did succeed in creating such deep convection in their 3-D hydrodynamical simulations and reported Li abundances as high as A(Li) = 3.5 dex. Note, the merger models suggest severe mass loss, which most super-Li rich giants lack.

1.5 Summary

Excess Li in red giants is still a puzzle. Understanding its origin has important implications for overall Li enrichment in the Galaxy. Thanks to the advent of large data sets in the last couple of years, significant progress was made. Some of the key results from these large data sets form the current thesis work. The thesis is

arranged in the following way. Including the current chapter on stellar evolution and Li excess problem, the thesis consists of a total of 7 chapters. In Chapter 2, we provide basic information about the data used for this study and data sources. Also, it contains data reduction and analysis techniques of spectroscopic and time-resolved photometry (for asteroseismology). Chapter 3 provides our first discovery of two super Li-rich red giants for which asteroseismic analysis is available, along with two other super Li-rich giants for which secondary calibration based on asteroseismic analysis is available. Encouraged by our initial discoveries (Chapters 3) we performed a large systematic survey involving red giants, which are common among LAMOST spectroscopic and *Kepler* photometric surveys. Results of this large survey are described in Chapter 4. Chapter 5 contains a reanalysis of a particular Li-rich red giant KIC 9821622, earlier classified as a red giant ascending the RGB. If it is true, this would be the only Li-rich giant classified, based on asteroseismology, as a red giant with He-inert core posing serious implications for Li excess origins. Chapter 6 consists of key observational evidence and theoretical modelling for Li excess origin and its evolution during the short He-flashing phase. Concluding remarks are given in Chapter7.

Chapter 2

Observations, data sources and techniques

This chapter consists of a description of observational data, its sources and analysis techniques. We used data of high and low-resolution spectra, photometry and astrometry of a large sample of giants for this study. We obtained high-resolution spectra for a few selected Li-rich giants using Himalayan Echelle Spectrograph (HESP) mounted on the 2-m Himalayan Chandra telescope. We used low-resolution optical spectra from the LAMOST sky survey program and data of time-resolved photometric data for asteroseismology from the *Kepler* space telescope deep-sky survey. Other data we used in this study is astrometry which comes from the space-based Gaia telescope. For a few stars in the sample we also used high-resolution spectra of the large spectroscopic survey of APOGEE. Also, we used archival data from Subaru and Gemini 8-m class telescopes.

2.1 Spectroscopy

Spectroscopy is the technique that enables deciphering information about celestial objects by analysing the light emitted from them in the form of spectra. Stellar spectra are of three kinds: continuum spectra, emission spectra and absorption spectra. Hot stellar bodies with very high pressure, density, and very high rotational velocity act closely like black-body, emitting continuous spectra as all the emission lines are smeared out. Hot stars with relatively thin atmospheres in the absence of cool outer layers emit spectra of multiple emission lines. For this study, we investigated relatively cool stars, which in general emit absorption spectra. Each absorption line represents the energy of the photons taken out for exciting electrons from lower to higher energy states of corresponding atoms of a particular element. **Generally, in local thermodynamic equilibrium (LTE) conditions, if the temperature gradient is negative i.e. temperature of the layer is lower than the layer where the continuum is emitted, an absorption line is seen. If the temperature gradient is positive i.e. the temperature of the layer is higher compared to the layer contributing to the continuum, an emission line can arise. The radial temperature structure in real stellar atmosphere is fairly complicated and formation of lines of emission and absorption are subject to detailed ionization structure. Non local thermodynamic equilibrium (NLTE) also affects formation of spectral lines. Presence of emission lines in the spectra of hot stars (for example O type stars) can be explained in terms of high population in excited states caused by NLTE effects.** Depths of absorption lines are a function of atomic data of a particular transition such as excitation potential, transition probability, the number density of atoms of a particular element. Thus, by identifying and measuring the strengths of lines, one can derive abundances of various elements relative to hydrogen, the most abundant element close to 90% in stars. Spectra will be generated by allowing the stellar light to pass through an instrument called a spectrograph containing a grating for fine

separation of lines. The continuous spectra with multiple lines of emission and absorption superposed will be recorded on a detector attached at the end of the spectrograph as shown in the schematic diagram (Figure 2.1).

Shapes and strengths of line features in the recorded spectra are imprints of the stars' physical structure and its chemical composition. Depending on the topic to be investigated researchers obtain spectra with resolutions varying all the way from R($=\lambda/\Delta\lambda$) $\sim$500 to R$\sim$500,000, where λ and $\Delta\lambda$ represent wavelength of a particular transition and the smallest difference by which two adjacent lines could be resolved, respectively. For example, to measure accurate radial velocities and elemental abundances one would require spectra of good S/N. Higher the resolution better the accuracy in the derived parameters. Since obtaining good spectra requires relatively large flux as it spreads across wavelengths one would require relatively more observing time with larger aperture telescopes for high resolution spectra. In this thesis we have used spectra of various resolutions starting from low of R$\approx$1800, 7500 (LAMOST) to high resolution of R$\approx$25,000 (GALAH, APOGEE) to very high resolution spectra of R$\approx$60,000 from HCT. We describe briefly each of these spectroscopic facilities from which we obtained spectra.

2.1.1 HCT HESP

The Himalayan Chandra Telescope (hereafter HCT) is a 2-m altitude-over-azimuth mounted telescope located at Mount Saraswati of Indian astronomical Observatory (IAO), Hanle, at an altitude of 4500 m from sea level. IAO is run by the Indian Institute of astrophysics (IIA), Bengaluru. The HCT observations are carried out remotely at a distance of 3100 km from a campus of IIA, Centre for Research and Education in Science and Technology (CREST), Hoskote, through a dedicated satellite link. IAO site in the western Himalayas in the north of India is one of

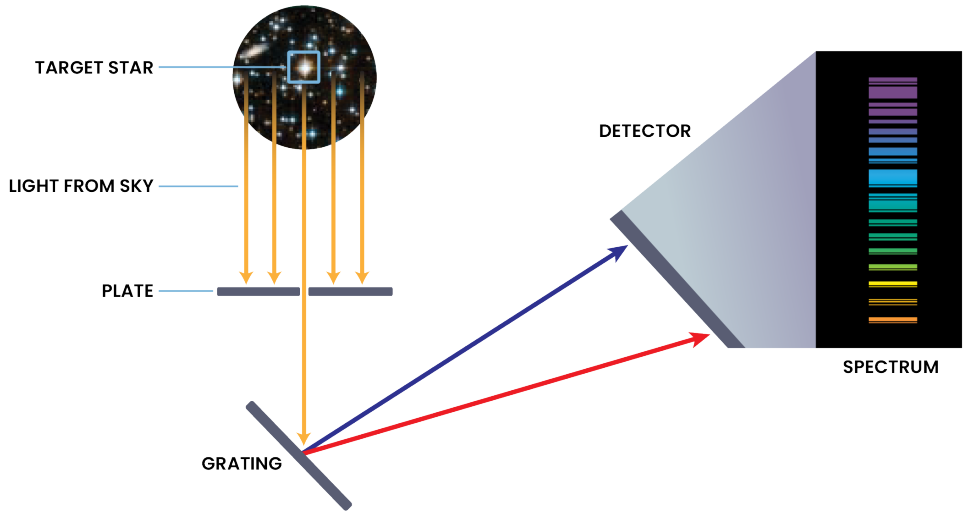

FIGURE 2.1: A schematic diagram for obtaining spectra of stars. Light coming from a star passes through a tiny hole in the plate to the grating which splits light into different wavelengths. The split spectra is recorded on a detector. Image credit https://hubblesite.org.

the driest sites in the northern hemisphere, well suited for astronomical observations of both optical and infrared wavelengths. HCT is equipped with an array of instruments for imaging and spectroscopy in both optical and infrared. For optical spectra, there are instruments; one is the Himalayan Chandra Fain Object spectrograph (HFOSC) which provides spectra of R≈745 - 4500, and the other is the HESP which gives high-resolution spectra at two resolutions of R≈30,000 and R≈60,000. HESP provides continuous spectra, covering the wavelength range from 3500 Å to 10000 Å without inter-order separation. The spectrograph is quite efficient (> 20 %), and one could obtain spectra of S/N∼100 for a star of brightness V∼10 in about 40 min integration.

2.1.2 LAMOST

The Large sky Area Multi-Object fibre Spectroscopic Telescope (LAMOST) was commissioned in late 2012 for a systematic spectroscopic survey of the northern

sky. LAMOST is operated by the National Astronomical Observatories (NAO), Chinese Academy of Sciences (CAS). It is a 4-m segmented mirror telescope with a large field of view 20 deg^2. LAMOST is equipped with a multi-object fibre fed spectrograph. LAMOST can obtain spectra of 4000 objects simultaneously using a set of 4000 fibres evenly spaced across the 1.75-m focal plane. LAMOST has two main science goals; 1) The LAMOST extragalactic survey (LEGAS), 2) LAMOST experiment for galactic understanding and exploration (LEGUE). Its original set-up was to obtain spectra of stars with limiting magnitudes V = 19 to 20 with spectral resolutions of R≈1800 and R≈500. After its success with original low resolutions set-ups, that data was released to the public as DR1, DR2, upto DR6. LAMOST was upgraded to provide better resolution spectra of R≈7500 under the project LAMOST-II. The new data was released to the public in late 2019 under DR6. Released data products include reduced spectra and a catalogue of derived parameters such as $T_{\rm eff}$, log g, values of radial velocities, and abundance of a few elements.

2.1.3 GALAH

The GALactic Archaeology with the Hermes (hereafter GALAH) spectrograph mounted on the 3.9-m Anglo-Australian Telescope (AAT) is the high-resolution spectroscopic survey of the southern hemisphere sky. AAT is located in the Siding Spring Observatory in New South Wales, operated by the Australian Astronomical Observatory (AAO). HERMES is a multi-object fibre fed spectrograph that provides simultaneous observation in four non-overlapping bands in the optical region. With its 400 fibres, one can obtain spectra of 400 objects simultaneously. It provides spectra with a spectral resolution of R≈28,000 with spectral coverage from 4700 Å to 7900 Å. Its resolution and spectral coverage are good enough to derive reasonably well various stellar parameters like $T_{\rm eff}$, log g, metallicity and abundances for several elements.

2.1.4 APOGEE

The Apache Point Observatory Galactic Evolution Experiment (hereafter APOGEE) using the 2.5-m located at Apache Point Observatory, the Sacramento Mountains in New Mexico, US, is an infrared spectroscopic survey in the northern sky. The APOGEE is a multi-object fibre fed spectrograph with 300 fibres and can obtain IR spectra in the wavelength range of 1.5 - 1.7 μ for 300 stars simultaneously. It has a large field of view of 3 degrees. It has a spectral resolution of R≈22,000. Stars in the survey were observed multiple times with a gap of one month for detecting binary stars and long time variables. The survey provides derived stellar parameters and abundance measurements of several elements.

2.2 HCT observations and Data Reduction

For a few selected Li enhanced giants based on low-resolution spectra of LAMOST, we performed high-resolution spectroscopic analysis using the spectra obtained from HESP spectrograph mounted on 2-m HCT. We obtained high-resolution spectra of R $\approx$ 60,000 for four Li-rich giant candidates with a very good signal of S/N$\sim$100 at Li wavelength region of 6700 Å. Observations were done on the nights of 1 May 2017 (KIC 12645107), 2 June 2017 (KIC 2305930), 28 September 2017 (TYC 1751-1713-1) and 30 December 2017 (HD 24960). We obtained a set of calibration images like bias and flat-field frames and Th-Ar wavelength calibration spectra each night. We also observed one hot and high rotating star to identify and remove atmospheric lines from the programme stars. Our stars brightness ranges from V = 8 - 11.5, which are relatively fainter for a 2.0 m class telescope for obtaining high resolution. To build good S/N, we performed 2 to 3 exposures, each lasting for about 30 to 40 minutes (except HD 24960, this is a relatively bright star (V = 8) so we took only one frame of 10 min exposure). Wavelength

calibration Th-Ar spectra were taken before and after the observations of each programme star.

For data reduction, we used Image Reduction and Analysis Facility (hereafter IRAF) data reduction software*. IRAF is a standard software package for image reduction and analysis which has various subroutines. We used the echelle package for HESP data reduction. After bias subtraction and corrected for pixel-to-pixel variation using flat frames, one-dimensional spectra were extracted using spectra sub-routines within IRAF. The 1-D spectra are the flux versus pixel number along the dispersion axis. Converting flux versus pixel number spectra into flux versus wavelength was done using Th-Ar calibration spectra. For transitions in the Th-Ar spectra, wavelengths are known from the laboratory measurements. We can get a 2 D polynomial relation between the pixel number and the wavelength of the known transitions. We converted flux versus pixel number spectra of programme stars into flux versus wavelength by applying this relation to the program spectra. Spectra is further reduced to continuum normalized spectra by dividing the spectra by the best-fit polynomial of the continuum. The spectra are ready for deriving stellar parameters. First among them is radial velocity, estimated by cross correlating high resolution Arcturus spectra, from Hinkle *et al.* (2000), with the observed spectra using $fxcor$ in IRAF.

2.3 Spectroscopic Data Analysis

Spectroscopic data analysis involves inspection of spectra and identification of lines corresponding to different elements. We used spectra of a bright K-giant Arcturus (Hinkle *et al.* 2000) for line identification and setting the continuum. Since the HCT spectra are very high resolution, we could pick several well defined clean

*http://ast.noao.edu/data/software

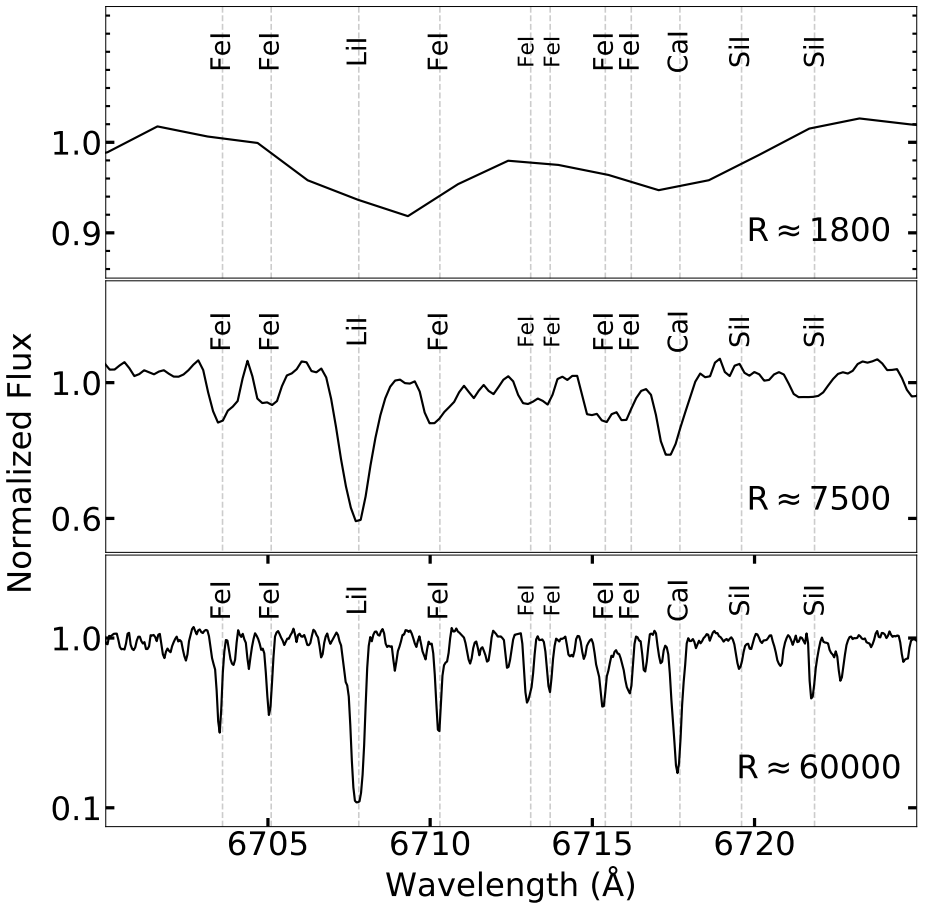

FIGURE 2.2: Representative spectra of a red giant, KIC12784683, in three different resolutions; LAMOST low resolution (R≈ 1800, top panel), medium resolution, (R≈ 7500, middle panel) are compared with HCT high resolution (R≈ 60000, bottom panel) spectra. One can notice sharper and more number of spectral lines with increasing spectral resolution.

lines with no known blends for many of the elements. Measurement of a large number of lines with different ionization stages (neutral, first ionized) and varying low excitation potentials (LEP) is particularly important to derive accurate stellar parameters($T_{\rm eff}$, log g, [Fe/H], $\xi_{\rm t}$, *vsini*) which are prerequisite for the derivation of accurate elemental abundances.

Measurement of stellar parameters can be accomplished using spectra either by measuring individual line strengths or equivalent widths (EWs) or comparing the

model spectra with the observed ones. Using the derived stellar parameters we extracted representative local thermodynamic equilibrium (LTE) model atmospheres from the Kurucz grid of stellar models Castelli and Kurucz (2004). Elemental abundances are derived for each element by matching the spectral strengths using radiative transfer code (here, we used MOOG) and LTE Kurucz models. In this section, we elaborated further on stellar parameters and model atmospheres used for high-resolution spectroscopic analysis.

2.3.1 Effective temperature

The effective temperature of a star is defined as the temperature of a black body emitting the same radiation per unit area (flux = $\sigma T_{\rm eff}^4$) as that of a star. Star is not a perfect black body; however, $T_{\rm eff}$ provides a good approximation of stellar photospheric temperature. The total radiation or luminosity (L) and $T_{\rm eff}$ are used to estimate stars' evolutionary phase by their location in the L-$T_{\rm eff}$ plane or commonly known as Hertzsprung-Russell diagram. Values of L and $T_{\rm eff}$ are related by the relation,

$$\mathrm{L} = 4\pi \mathrm{R}^2 \sigma \mathrm{T}_{\rm eff}^4$$

here $\sigma = 5.6705 \times 10^{-5} \mathrm{ergcm^{-2}K^{-4}s^{-1}}$ is Stefan-Boltzmann constant, R is radius of a star. Star's $T_{\rm eff}$ are estimated by either by using colours from photometry or by analysing spectral lines from the spectroscopy. For our study here we used high resolution spectra for deriving $T_{\rm eff}$ values.

2.3.2 Surface gravity

Surface gravity (g) is a measure of stars' photospheric pressure which in astronomy generally expressed in logarithmic scale, log g. The higher the value of log g

the denser the material, and the more compact stars are. Thus, the value of log g decreases as stars evolve from the main sequence to red giants and then to supergiants. Thus, log g is a good indicator of a star's evolutionary phase. Star's key parameters log g, T_{eff}, mass and L are expressed by the following relation;

$$\log g = \log g_{\odot} + \log\left(\frac{M}{M_{\odot}}\right) + 4\log\left(\frac{T}{T_{\odot}}\right) - \log\left(\frac{L}{L_{\odot}}\right)$$

The surface gravity of stars can be derived either by photometry or spectroscopy. log g values can be inferred from multi-band photometry by using some gravity sensitive features like MgH and Mg I triplet near 5150 Å (Lenz *et al.* 1998). The Ca II H and K lines (Lee *et al.* 2008) and Balmer lines (Wilhelm *et al.* 1999) are also useful to derive log g values. Combining Gaia parallaxes (for distances) and photometry could estimate log g values. Researchers using high-resolution spectra for elemental abundances generally rely on spectral line strengths of different ionization states for deriving log g values. The spectroscopic methods are further discussed in this chapter. With the recent availability of large data of time-resolved photometry of stars, asteroseismology emerged as another very reliable tool to measure stars' log g (Morel and Miglio 2012). For this study, we used either asteroseismology and high-resolution spectral analysis to estimate log g.

2.3.3 Microturbulance velocity

Microturbulance velocity, ξ_t, is measure of motion of particles at a microscopic level in a stellar atmosphere. ξ_t was introduced as a free parameter in stellar atmosphere codes to have same abundance from weak and strong lines for a set of given atomic data (Hundt 1973) and stellar parameters. Generally, ξ_t values are small, about 1-2 km s^{-1}, and are derived using lines of varying strengths of

a particular element for a given atomic data and stellar parameters. Values of ξ_t also could be inferred from empirical calibration relations (Kirby *et al.* 2009) **which is valid for giants of RGB's range of $T_{\rm eff}$ and log g which is given below;**

$$\xi_t(\mathrm{kms}^{-1}) = (2.13 \pm 0.05) - (0.23 \pm 0.03)\,\log\,\mathrm{g}$$

2.3.4 Projected rotational velocity

All stars rotate. Rotation is an inherited property of stars from their birth in molecular clouds. Typically, the measured velocities are projected velocities with respect to the line of sight of observations and are denoted by *vsini* ("i" is the inclination angle between the star's axis of rotation and the line of sight). Values of *vsini* vary across the spectral type of main-sequence stars. Generally, stars' rotation decreases from hot (O, B, A) stars to cool spectral types like F, G, K. Also, *vsini* values decrease as stars evolve off the main sequence and become giants as expected for conserving the angular momentum. Observations reveal that the bulk of red giants of spectral type late G and K having 2-4 km s^{-1} as expected. *visini* values are estimated using broadening stellar lines in the spectra after accounting for atmospheric turbulent velocities.

2.3.5 Equivalent width

Equivalent width is a measure of line strength in spectra. It is defined as the width of a rectangle whose area is equal to the area of a spectral line. As shown in the

Figure 2.3 EW can be expressed as:

$$\mathrm{EW} = \int_{\lambda_1}^{\lambda_2} (1 - \frac{\mathrm{F}_\lambda}{\mathrm{F}_\mathrm{c}})$$

Here F_λ is flux at wavelength λ and F_c is flux at continuum level. Using curve of growth (COG) method EW are used to measure abundances of elements. **COG is theoretical plot of equivalent width with optical depth. This curve can be divided into three regions depending on line strengths: Doppler part (linear region), shoulder region, and damping part. Only linear portion of COG is used for abundance measurements as this portion is quite sensitive to line equivalent widths and is directly proportional to the total number of absorbing atoms of a particular element**. Mathematical relation between EWs and abundance is:

$$\log\frac{\mathrm{EW}}{\lambda} = \log\ \mathrm{C} + \log(\mathrm{gf}\lambda) - \frac{5040}{\mathrm{T}_\mathrm{ex}}\xi + \log(\mathrm{N}) - \log(\kappa_\mathrm{c})$$

here C is a constant, g is the statistical weight, f the oscillator strength, T_ex the excitation temperature, ξ is the excitation potential of lower energy state, and κ_c continuum opacity.

2.4 Methodology for deriving elemental abundances

Elemental abundances are derived using standard procedure. Once we have reduced the spectra to normalized flux and wavelength, the next step would be to identify a good number of well-defined lines for each element of interest and gather well-measured atomic data. The atomic/**molecular** data for each line

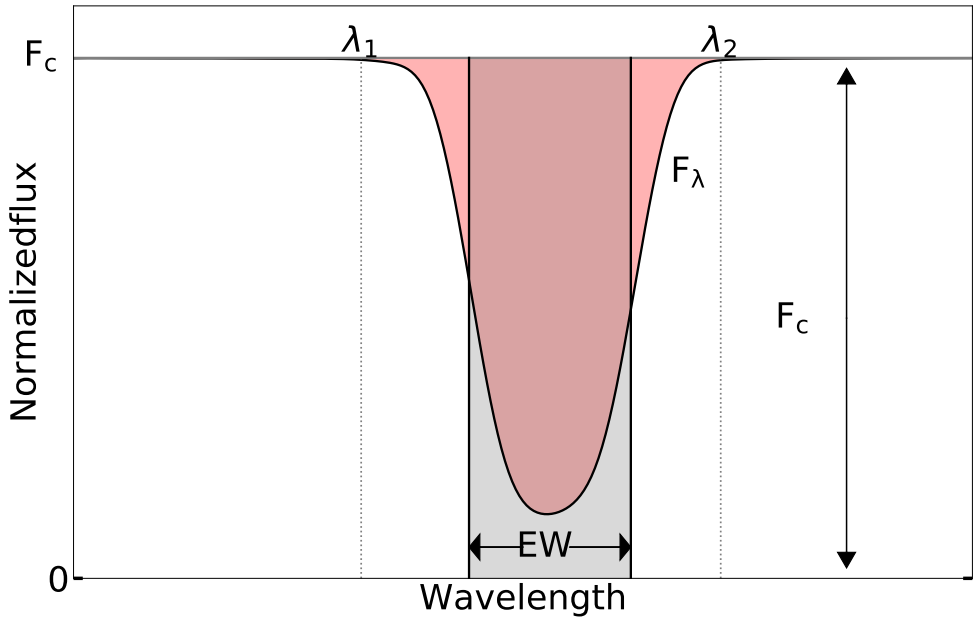

FIGURE 2.3: Definition of Equivalent width of a spectral line. The width of gray colored rectangle whose area is equal to the area under the absorption profile (red colored) is called the equivalent width (EW).

includes transition probability (or log gf), low excitation potential (LEP), dissociation energies etc. Observed line strengths or EWs and their atomic data form an input to a radiative transfer code to derive abundance by comparing with the theoretical atmospheric model star line EWs. This study used Kurucz LTE stellar atmospheric models and the revised radiative transfer code, MOOG originally written by Sneden (1973).

2.4.1 Line list

the compilation of line data is one of the key tasks in spectral analysis of stars for abundance determination. Since our stars are cool (mostly of K- spectral type), their spectra will be rich with atomic and molecular lines and bands. Even in high resolution, one will find many lines blended with some nearby lines. We searched the entire observed spectrum of each star and selected well-defined lines

of sharp and symmetric profiles. Individual lines in spectra are characterized by their central wavelength, oscillator strength (log gf), statistical weight, lower excitation states. Except log gf values, other values of lines are well determined. Wherever possible, we used only log gf values that are measured in the laboratory. We made use of a recent compilation of individual lines (Reddy *et al.* 2002, 2003; Ramírez and Allende Prieto 2011). We have also used Linemake code (Placco *et al.* 2021), which produces a line list in the MOOG (Sneden 1973) compatible format. Linemake code generates line list by merging Kurucz atomic and molecular line database(Kurucz 2011) [†] with updated transition probability and hyperfine structure data.

2.4.2 Stellar model atmosphere

There are quite a few stellar atmospheric models for deriving stars' atmospheric parameters and stellar composition. Stellar models computed using ATLAS atmospheric code by (Kurucz 1993) and MARCS models by (Gustafsson *et al.* 1999) are widely used in the literature. Here, we used Kurucz grid of atmospheric models (Kurucz 1979; Castelli and Kurucz 2004) which are tabulated with intervals of 250 K in T_{eff}, 0.25 dex in log g and 0.25 dex in metallicity [‡]. For interpolation of models for any desired set of atmospheric parameters, we used an interpolation routine called *kmod* [§]. The adopted models are 1-dimensional with plane-parallel geometry. Models are computed assuming stars atmospheres are in local thermodynamic equilibrium (LTE) and hydrostatic equilibrium. The assumptions may not entirely satisfy the actual atmospheric conditions of stars. Nevertheless, stars with moderate T_{eff} and masses such as those in our sample, these assumptions work well. Convective energy transport is modeled following mixing-length theory (Böhm-Vitense 1958) where mixing length parameter $\alpha_{MLT} = 1.25$. Kurucz stellar

[†] http://kurucz.harvard.edu/linelists.html
[‡] http://kurucz.harvard.edu/grids.html
[§] http://hebe.as.utexas.edu/stools/, C. Allende Prieto, Univ. of Texas, May 1999

model atmosphere assumes 72 parallel layers where Rosseland opacity (log τ_{Ross}) varies from -6.875 to +2.0 in steps of 0.125.

2.4.3 MOOG Code

MOOG is a radiative transfer code originally written by Chris Sneden of Univ. of Texas (Sneden 1973). This has gone into many revisions. The latest was in 2012. MOOG code solves radiative transfer equation in one dimension plane-parallel approximation for a given stellar atmospheric model. With MOOG, we could derive abundance either by the "synth" option or the "abun" option. In the "abun" option, MOOG requires a stellar atmospheric model and line list as input files. Line list includes wavelength, ionization state of the atom, low excitation potential, transition probability (log gf), and the observed EWs of a particular transition. MOOG code converges when the computed EWs equals the observed EWs for particular abundances. MOOG performs an iterative process internally by varying abundance for a given transition. In the "synth" option, the same input files but the line list will have all the transitions in the interesting range of spectra. In this case, we computed spectra by varying abundances for a given set of atmospheric parameters until the model spectra match the observed spectra. Depending on the situation, we used both the "synth" and "abun" options of the MOOG to derive elemental abundances.

2.4.4 Derivation of stellar parameters

In the case of low-resolution spectra from the LAMOST survey, we adopted stellar atmospheric parameters given in the LAMOST catalogue. From these spectra we estimated only Li abundance using a single line at 6707 Å based on its relative

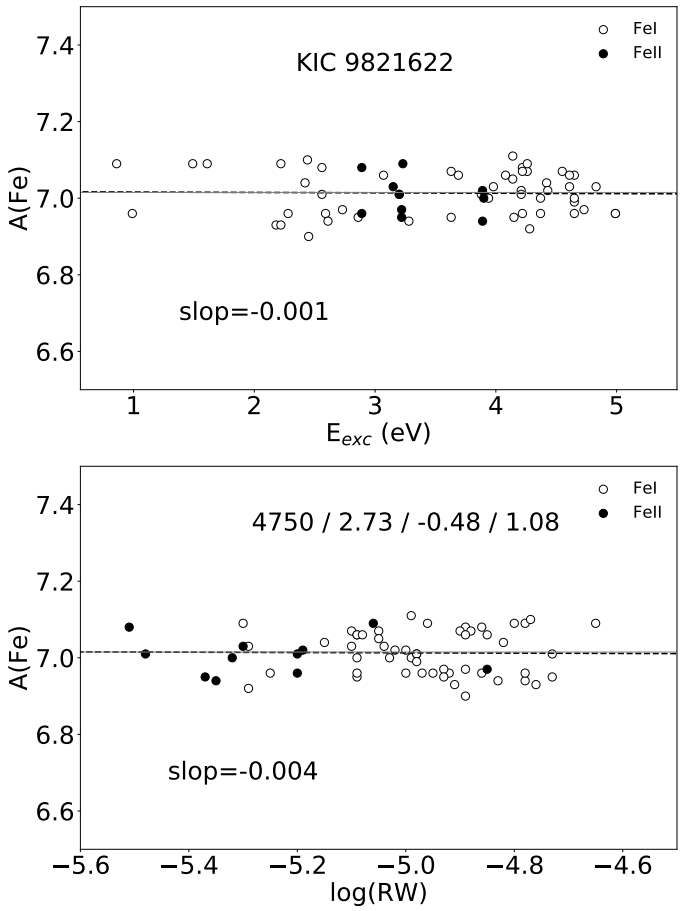

FIGURE 2.4: Derivation of stellar parameters (T_{eff}, log g, [Fe/H] and ξ_t) by Fe I (open circles) and Fe II (filled circles). The figure shows A(Fe) of individual lines against their low excitation potentials (upper panel) and against reduced EWs (bottom panel).

strength to its neighbouring Ca I line with similar LEP. A few of these very high Li abundance candidates were subjected to high-resolution spectroscopic analysis. **In the case of high resolution spectra we used the traditional method of deriving stellar parameters using the principle of excitation and ionization balance between the abundances of neutral and ionized lines for the giants studied in this case**.

Derivation of atmospheric parameters using high-resolution spectra requires identifying a sufficient number of Fe lines whose transitions are dominant in the spectra.

We identified 35 to 40 neutral Fe (Fe I) with varying LEPs and 10-12 singly ionized Fe (Fe II). Initial values of T_{eff} and log g are taken either from the LAMOST are estimated using the calibrations based on photometric colours Alonso *et al.* (1999); Gonzalez, O. A. *et al.* (2009). First, we fixed value of T_{eff} by computing abundances for a set of model atmospheres with varying T_{eff} but for the same log g and metallicity. Then the abundances of individual Fe I lines for each model are plotted against their LEP. The correct T_{eff} of a star is the one for which the slope between abundances of lines and their LEPs is zero. Similarly, the value of log g is fixed by computing abundances of individual lines of Fe I and Fe II for models of varying log g, but for a given T_{eff} (previously derived) and [Fe/H]. Correct log g is the one for which the mean abundance values of neutral and ionized lines are equal. Likewise we derived micro-turbulent velocity (ξ_t) by varying ξ_t for a given log g and T_{eff}. Correct ξ_t is the one for which the slope between abundances and reduced equivalent widths(REWs) [¶] of Fe I is zero. The derivation of the parameters is shown in Figure 2.4. It is an iterative process. The stellar model of converged stellar parameters is the most suitable stellar model that represents the observed spectrum or the star's stellar atmosphere.

2.5 Asteroseismology of red giants

In this section we will introduce asteroseismology as a tool to distinguish stellar evolutionary phases: in particular, to separate giants of inert He-core giants ascending red giant branch for the first time from those of red clump giants with He-core burning phase, post-He-flash.

The word "Asteroseismology" is made-up of astero (star) and seismology. Seismology is the mapping of the internal structure of the earth using quakes. A similar

[¶] REW = EW/λ

technique, known as Helioseismology, has been used to investigate interior regions of the sun by observing waves on its surface. This technique provided many breakthroughs, such as a detailed map of the solar interior, internal rotation profile and inputs for standard solar models. The oscillations are stochastically excited in the outer layers by turbulent convection (Goldreich and Keeley 1977; Goldreich and Kumar 1988) in the surface convection zone where part of the convection energy transferred to the oscillations. These types of oscillations are known as solar-like oscillations; the famous 5-minute oscillations first detected in the sun's surface Leighton *et al.* (1962). These pulsations are intrinsically stable. The excitation of oscillation and their amplitude are random due to a large number of convective elements in the convective zone. The presence of a surface convection zone is a necessary condition for stars to show solar-like oscillations.

The same technique could be used to understand stars other than the sun. The study of internal structure of stars using their oscillations is called asteroseismology. Unlike the sun, stars are point sources and fainter and cannot be spatially resolved. Oscillations on the surfaces are studies by using either variation in stars' brightness or by variation in the radial velocity of spectral profiles. Since the variations are tiny, it is challenging to get oscillations data for relatively fainter stars. Now thanks to space telescopes like the *Kepler* mission, asteroseismology became a key tool to study the internal structure of stars using intrinsic oscillations observed in the surface of stars.

Stars oscillate in various modes; for example, a radial mode where stars expand and shrink along the radial direction and the symmetry of stars is preserved. There are non-radial types of modes. Oscillations have their physical origins in two types of standing waves: the ones predominantly acoustic in nature known as p modes or pressure modes, where the gradient of pressure acts as restoring force and internal gravity waves where the restoring force is buoyancy. Modes of mixed character are also present. The mixed modes behave as g mode in the central

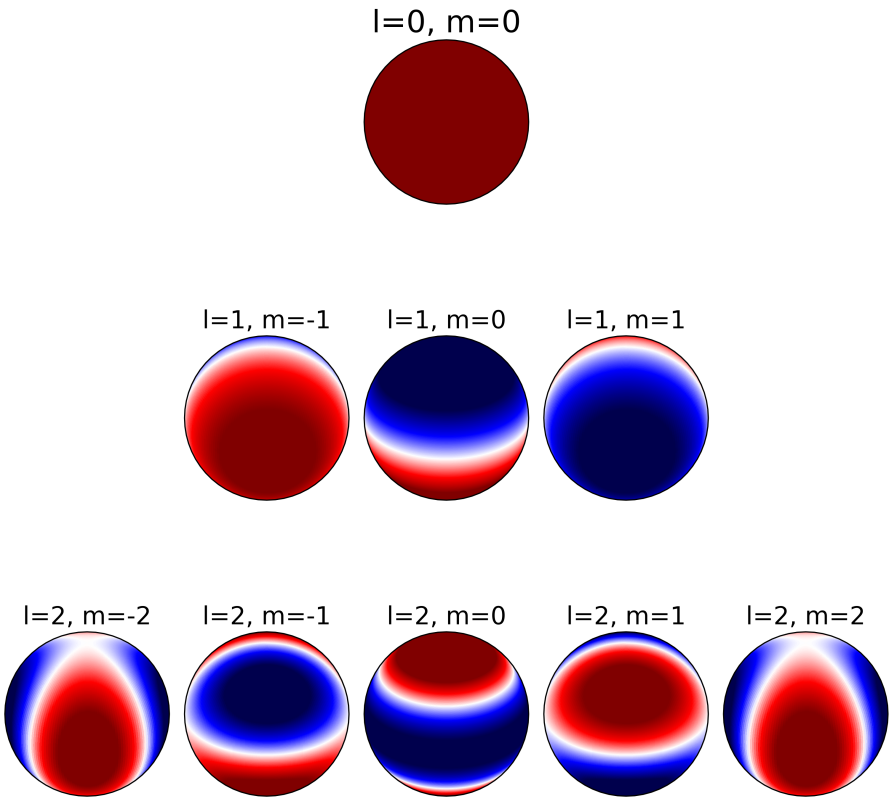

FIGURE 2.5: Various modes of oscillations in stars are represented in spherical harmonics. Value of l stands for total number of nodal lines on surface and m stands for a number of lines crossing the equator (m = 2l +1). Top panel shows radial oscillation (l=0 and m=0), middle panel shows dipole oscillations (l=1, m=-1,0,1) and bottom panel shows quadruple oscillations (l=2, m=-2, -1, 0, 1, 2).

region and p mode like in envelope. These modes are driven stochastically and damped intrinsically by vigorous turbulence in the surface convection zone. The oscillation spectra shown by red giants stars is very rich with multiple overtones excited to observable amplitude.

All modes of varying amplitude are excited in stochastic oscillations, resulting in the power excess in the Fourier space. Oscillations are described in terms of frequency (ω) and three quantum numbers; n, l, m. In the following sections we give a brief background of oscillation in stars.

In slowly rotating stars, oscillation frequencies with small amplitude can be modelled as spherical harmonics, ω_{nlm}. Dependency of eigenfunction on co-latitude θ and longitude ϕ angular part can be separated $\mathrm{Y_l^m}(\theta, \phi)$, where degree l is a measure of a total number of nodal lines on stellar surface and m is azimuthal order measures number of nodal lines crossing the equator. Radial order n represents the number of nodes in the radial directions. After separating angular term equation of adiabatic oscillations is reduced to the following form (Deubner and Gough 1984):

$$\frac{d^2X}{dr^2} = -K(r)X \tag{2.1}$$

where$X = c^2\,\rho^{1/2}\,div\,\delta r$ and δr is displacement vector, c is speed of **sound**, ρ is density and K is:

$$K = \frac{1}{c^2}\left[S_l^2\left(\frac{N^2}{\omega^2} - 1\right) + \omega^2 - \omega_c^2\right] \tag{2.2}$$

K depends on characteristic frequencies of star: Lamb frequency, $\mathrm{S_l}$, and buoyancy frequency, N and acoustic cutoff frequency (ω_c). Lamb frequency, $\mathrm{S_l}$, is the inverse of time needed to travel horizontal wavelength at local sound speed.

$$S_l^2 = \frac{l(l+1)c^2}{r^2}$$

and buoyancy frequency, N, is oscillation frequency of bubble vibrating vertically in hydrostatic equilibrium at any position of star.,

$$N^2 = g\left(\frac{1}{\Gamma_1}\frac{d\,lnp}{dr} - \frac{d\,ln\rho}{dr}\right)$$

Here g is local gravitational acceleration, and γ_1 is the adiabatic exponent. Frequency approximately satisfies following dispersion relation:

$$\int K^{1/2}dr = \left(n - \frac{1}{2}\right)\pi \tag{2.3}$$

Equation 2.1 determines the properties of the solution. If K $>$ 0 the solution oscillates, K $<$ 0 solution will exponentially decrease or increase, and K = 0 is called the turning point. The behaviour of Lamb frequency, S_l, is relatively simple. It decreases from core to the envelope with an increase in radius. The behaviour of buoyancy frequency is more complex. For condition of convective instability $N^2 < 0$. Therefore in the convective zone $N^2 < 0$, while in the radiative zone $N^2 > 0$. In Figure 2.6 variation of S_l and buoyancy frequency, N, is represented.

Based on Lamb frequency and buoyancy frequency, there are two conditions for positive K,

1. $\omega > S_l$ ($\omega >> N$).
2. $\omega < N$ ($\omega << S_l$).

The first case corresponds to the acoustic case where restoring force is pressure (p-mode), and the latter case corresponds to internal gravity waves where restoring force is buoyancy (gravity), g modes.

For p-modes dispersion relation, equation 2.3 can be represented in terms of cyclic frequency:

$$\nu_{nl} = \Delta\nu \left(n + \frac{l}{2} + \alpha + \frac{1}{4} \right) - d_{nl}$$

where

$$\Delta\nu = \left(2 \int \frac{dr}{c} \right)^{-1}$$

The equation shows that with neglecting small-term d_{nl}, frequencies are uniformly spaced in radial order, i.e. for two consecutive radial orders (n and n+1) for same

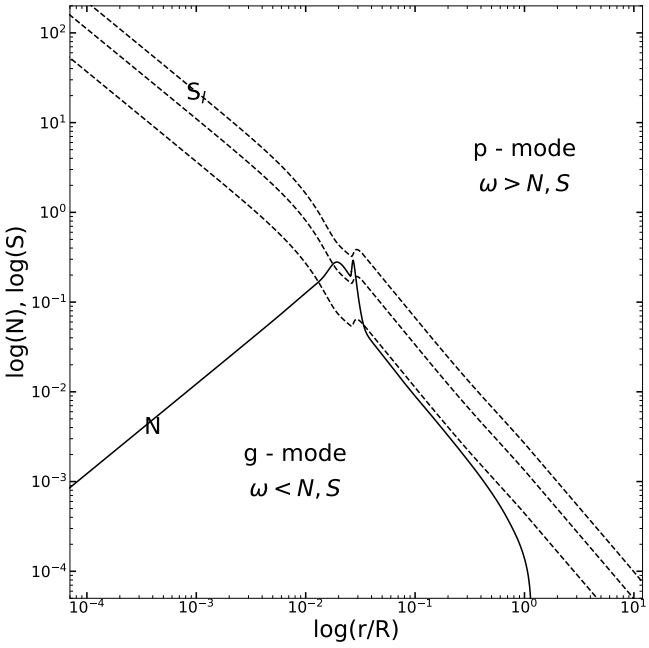

FIGURE 2.6: Propagation diagram of p and g modes inside stars of 1 $M_\odot$. Solid black line indicates buoyancy frequency (N) and dashed lines indicate Lamb frequency (S_l, l=1,2,3). Depending on the condition of g ($\omega < N, S_l$) and p-mode ($\omega > S_l, N$) the two cavity are marked where g and p-mode can propagate. In the inner region only g-mode oscillations propagate and and p-mode in the outer region.

angular degree l frequency separation is constant, $\Delta\nu$. This quantity is known as large frequency separation.

For g modes dispersion relation, equation 2.3 takes following form in term of period $\Pi = 2\pi/\omega$

$$\Pi = \frac{\Delta\Pi}{L}(n + \alpha_g)$$

Where

$$\Delta\Pi = 2\pi^2 \left(\int N \frac{dr}{r} \right)^{-1}$$

, L=l(l+1) and α_g is constant,

In this case, we get a period that is equally spaced in radial order. For two consecutive modes, period spacing is constant.

In the main sequence, buoyancy frequency is small, and Lamb frequency is large. Therefore detection of gravity modes on the surface is challenging, and we mainly see p modes. Post main sequence, stars evolve to SGB and RGB, where buoyancy frequency increases and Lamb frequency decreases. As a result frequency of g modes increases reaching closer to the range of p modes frequencies. When g modes frequency and p modes frequency come closer to each other, modes goes through avoided crossing (Aizenman *et al.* 1977). The modes resulting from the coupling of p and g modes are known as "mixed modes". Radial modes, l=0, are unaffected by coupling since no radial modes exist in the core (buoyancy does not support radial modes). Mainly dipole modes, l=1, get affected by coupling between dipole g modes in core and dipole p modes in the surface. The coupling causes a shift in the location of dipole modes. Stronger the coupling larger the shift in frequency of dipole modes. Coupling is very week in quadruple modes, l=2, because of geometric cancellation.

The essential requirement for asteroseismic analysis of stars is the availability of high-quality observational data. The initial hint of the presence of solar-type oscillations in giants came from radial velocity observations of a few stars such as Arcturus (Merline 1999), ε Ophiuchi (De Ridder *et al.* 2006) etc. and photometry in open cluster M67 (Stello *et al.* 2007). These studies suffered from poor signal to noise ratio in the observed data and interruptions in observations. Periods of solar-like oscillations in red giants vary from few hours to days. Thus, it requires long uninterrupted observations for clearly resolving oscillations. This is only possible by using space telescopes. Though the space observations of stars by HST (Edmonds and Gilliland 1996), WIRE (Buzasi *et al.* 2000), SMEI (Tarrant *et al.* 2007) and MOST (Barban *et al.* 2007) indicated the presence of oscillations, the first confirmed detection of radial and non-radial oscillation modes was possible by

using 150 long days of observation of space facility known as "Convection, Rotation and planetary Transits (CoRoT) satellite (De Ridder *et al.* 2009) in the 10-100μHz range. Later *Kepler* satellite demonstrated greater potential for asteroseismology. In the following section, we briefly describe details of the *Kepler* satellite.

2.6 Kepler

The *Kepler* spacecraft is a wide field Schmidt camera of 0.95 m front corrector lens feeding into the primary mirror of 1.4-m diameter. Its field of view is 105 square degrees. The mission is designed to make deep-sky observations towards the Cygnus-Lyra region in the northern hemisphere. NASA launched *Kepler* in early 2009 with an initial plan of operation of 3.5 years. However, this was later extended. NASA announced its retirement in late 2018. Its main goal was to observe the same part of the sky multiple times to detect earth-size planets around stars. Its primary instrument is a photometer with 42 CCDs of 2200 $\times$ 1024 pixels each. The *Kepler* satellite has observed more than 190 thousand stars of up to magnitude, V= 16. The *Kepler* (Borucki *et al.* 2010) satellite observed stars in two cadence modes; long cadence where sampling interval of 29.4 minutes and short cadence where sampling period is 58.85 seconds.

2.6.1 Analysis of Kepler data: Asteroseismic parameters calculations

One of the by-products of the high precision time-resolved photometry from the *Kepler* telescope is the data on a broad range of stellar variability, which could be used for the asteroseismic analysis of stars. Red giants show oscillations lasting for hours to months. The long cadence mode data of *Kepler* could be used to study the

characteristic properties of oscillations in the stellar atmospheres. *Kepler* observed stars in 17 quarters; Q0 has a cadence of 10 days, Q1 has 34 days, Q2 has 90 days etc. **In general, data of Kepler observations are transmitted back to data center on Earth once in a quarter i.e 90 days. However, in the initial period (Qo) and Q1), for some technical reasons, only a few days of observational data was sent.** In figure 2.7, we showed sample light curves of 17 quarters for a giant star, KIC 12784683. We used only data of stars with data for at least eight quarters to ensure high resolution for identifying modes accurately for our study. The *Kepler* data analysis includes conversion of light curve to the Fourier space and measurement of asteroseismic parameters such as $\nu_{\rm max}$, $\Delta\nu$ and period spacing. The Power density spectra or PDS of a sample giant, KIC 12784683, is shown in Figure 2.8.

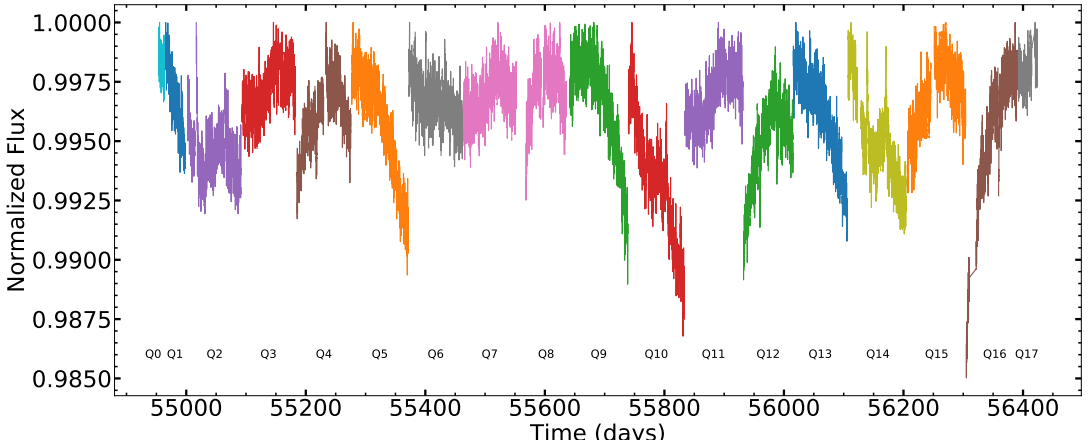

FIGURE 2.7: *Kepler* light curve of a representative star KIC 12784683 of all quarters. Vertical axis is normalized flux and horizontal axis is time.

2.6.2 Derivation of $\nu_{\rm max}$

The *Kepler* light curve of different quarters were first stitched together as shown in Figure 2.7 and transformed into the frequency space using Lomb-Scargle Fourier transform method. The resultant spectra of flux variation with frequency are called power density spectra (hereafter PDS) as shown in Figure 2.8 for a representative star KIC 12784683. PDS of stars with oscillations is first fitted with the

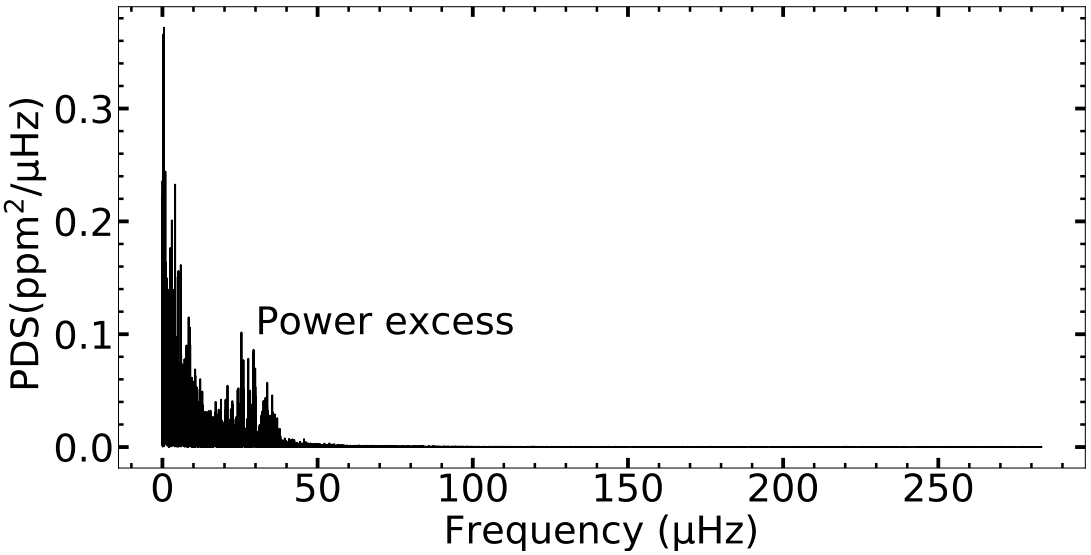

FIGURE 2.8: Power density spectra (PDS) of representative star KIC 12784683 of light curve shown in Figure 2.7. Note power excess in PDS which is typical in red giants oscillation spectra.

background model. The background signal of PDS contains white noise, three separate granulation components (modeled as super Lorentzian) and Gaussian power excess. The background model adopted here is

$$\mathrm{P_{bkg}} = \mathrm{W} + \mathrm{R}(\nu)[\mathrm{B}(\nu) + \mathrm{G}(\nu)]$$

Where W is white noise (flat noise), $R(\nu)$ is response function that considers sampling rate of long cadence *Kepler* data,

$$\mathrm{R}(\nu) = \mathrm{sinc}^2\left(\frac{\pi\nu}{2\nu_{\mathrm{Nyq}}}\right)$$

with Nyquist frequency $\nu_{\mathrm{Nyq}} = 283.212\mu$Hz. Super Lorentzian component are given by

$$\mathrm{B}(\nu) = \sum_{\mathrm{i}=1}^{3} \frac{\xi \mathrm{a_i^2} 2/\mathrm{b_i}}{1 + (\nu/\mathrm{b_i})^4}$$

where $\mathrm{a_i}$ is amplitude in ppm and b_i is characteristic frequency in μHz and $\xi = 2\sqrt{2}/\pi$ is normalization constant (Kallinger *et al.* 2014).

Power excess component in PDS is modeled in Gaussian form:

$$G(\nu) = H_{osc} \exp\left[-\frac{(\nu - \nu_{max})^2}{2\sigma_{env}^2}\right]$$

We fitted this background model to the observed data as shown in Figure 2.9 using the Markov chain Monte Carlo (MCMC) sampling method, and we used PyMC3 code [‖] for this purpose. The fit gives frequency corresponding to maximum power, ν_{max}.

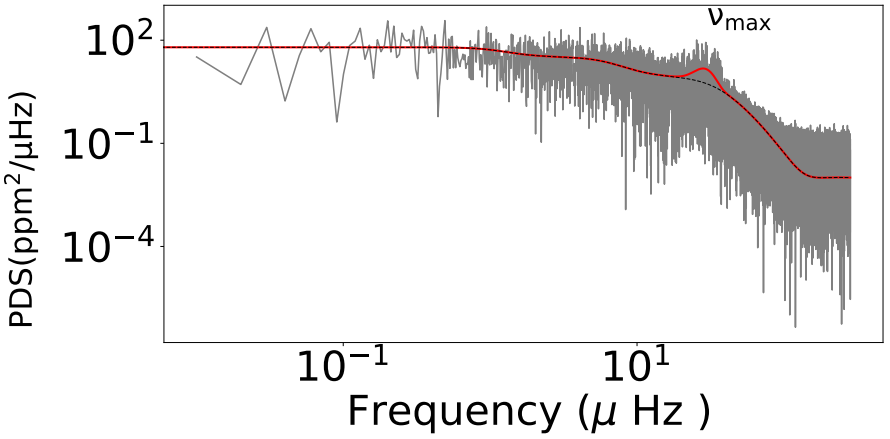

FIGURE 2.9: PDS of KIC 12784683 and background model fit to the data. Background model is consist of white noise, three super Lorentzian component and Gaussian component. Red line is the full background model and black line is background model without Gaussian component.

2.6.3 Large frequency separation

PDS of red giants contains large number of radial and non-radial modes as shown in Figure 2.10. We identified different modes in PDS and measured frequency to those modes. Frequency separation between the two consecutive radial modes is constant and given by:

$$\Delta\nu = \nu_{n+1} - \nu_n$$

[‖] https://github.com/pymc-devs/pymc3

We derived the frequency corresponding to the detected radial modes and measured large frequency separation, $\Delta\nu$, of stars.

2.6.4 Period spacing

Oscillations of dipole mixed-mode have approximately constant period spacing between the consecutive dipole modes.

$$\Delta \mathrm{P} = \frac{1}{\nu_{\mathrm{n,l}}} - \frac{1}{\nu_{\mathrm{n+1,l}}}$$

The measurement of dipole mode frequency requires identifying exact dipole modes, which requires a long cadence and high signal to noise ratio of PDS. Here we have measured average period spacing corresponding to the median of period spacing values derived for a given star.

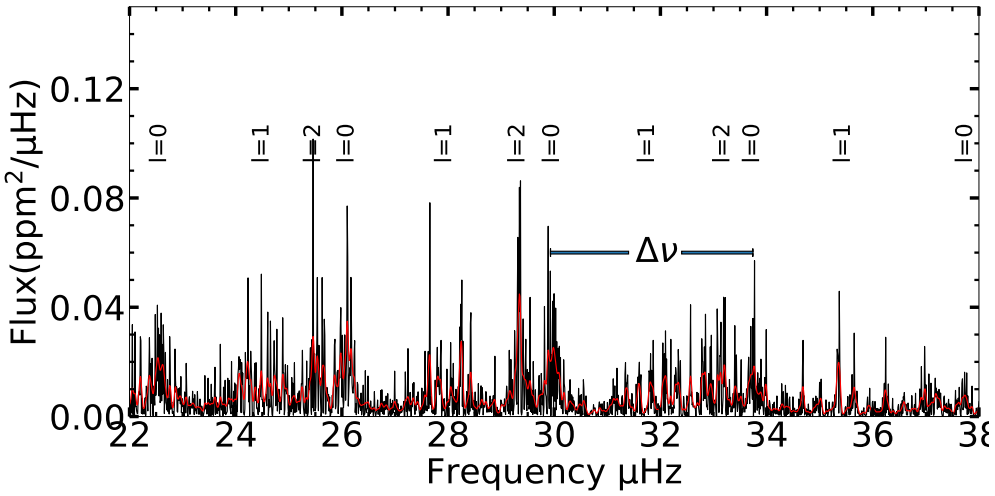

FIGURE 2.10: Different modes present in power density spectra of KIC 12784683. Black line is original PDS and red line is smoothed PDS. Radial and dipole modes are marked with degree l. Large frequency separation is also marked.

2.6.5 Global parameters: Mass, radius of stars

Stellar-mass and radius are two key parameters from which one could derive luminosity (L) and surface gravity (log g). It is shown that a star's mass and radius are related to the asteroseismic parameters mean large frequency separation, $\Delta\nu$ and frequency of maximum power, $\nu_{\rm max}$. Ulrich (1986) suggested that the parameter $\Delta\nu$ related to the sound travel time across the stellar diameter and provided a relation between $\Delta\nu$ and mass and size of a star as;

$$\frac{\Delta\nu}{\Delta\nu_{\odot}} = \left(\frac{\rm M}{\rm M_{\odot}}\right)^{1/2} \left(\frac{\rm R}{\rm R_{\odot}}\right)^{-3/2} \tag{2.4}$$

Later Brown *et al.* (1991) proposed that $\nu_{\rm max} \propto {\rm g\,T_{eff}^{-1/2}}$. Kjeldsen and Bedding (1995) provided a calibration relation between $\nu_{\rm max}$, M, R and $T_{\rm eff}$ as:

$$\nu_{\rm max} = \left(\frac{\rm M}{\rm M_{\odot}}\right) \left(\frac{\rm R}{\rm R_{\odot}}\right)^{-2} \left(\frac{\rm T_{eff}}{\rm T_{eff,\odot}}\right)^{-1/2} \tag{2.5}$$

By combining Equation 2.4 and 2.5 we get the following relations to derive mass and radius of stars:

$$\frac{\rm M}{\rm M_{\odot}} = \left(\frac{\nu_{\rm max}}{\nu_{\rm max,\odot}}\right)^{3} \left(\frac{\Delta\nu}{\Delta\nu_{\odot}}\right)^{-4} \left(\frac{\rm T_{eff}}{\rm T_{eff,\odot}}\right)^{3/2}$$

$$\frac{\rm R}{\rm R_{\odot}} = \left(\frac{\nu_{\rm max}}{\nu_{\rm max,\odot}}\right) \left(\frac{\Delta\nu}{\Delta\nu_{\odot}}\right)^{-2} \left(\frac{\rm T_{eff}}{\rm T_{eff,\odot}}\right)^{1/2}$$

Solar reference values adopted in this work are $\nu_{\max,\odot} = 3090 \pm 30\mu$Hz and $\Delta\nu_{\odot} = 135.1 \pm 0.1\mu$Hz (Huber *et al.* 2011).

Measuring the mass and radius of a star is quite complex. Generally, mass and radii are derived using a combination of stellar evolutionary models and the observed values stellar brightness, mV, [M/H], $T_{\rm eff}$ and log g. These will have larger uncertainties due to combined uncertainties in the measured parameters and evolutionary tracks. Asteroseismology provides an independent way of deriving L and log g by measuring mass and radii. It is shown for single stars that the derived mass and radius using the asteroseismic method are pretty accurate, with 10-15% uncertainty in mass and less than 5% uncertainty in radius (Yu *et al.* 2018).

2.7 Gaia

Knowing the accurate distance to stars is very important in astronomy to understand stars' evolution or the Galactic evolution. Measuring distances for a large number of stars far away from earth is quite difficult. By using ground-based observations only for nearby stars, reasonably accurate parallaxes could be measured. In the early 1990s,' European Space Agency (ESA) launched the space telescope " Hipparcos" for measuring accurate parallaxes. The Hipparcos measured astrometry for 100 thousand stars, and secondary calibrations provided astrometry for about two million stars. *Gaia* is the sequel to Hipparcos with an ambitious goal of measuring astrometry for more than a billion stars in the Galaxy and in the local group of galaxies. *Gaia* is placed at Lagrangian point 2 (L2) at about 1.5 million Km from Earth to have uninterrupted year-long observations while orbiting the Sun. *Gaia* consists of two identical primary mirrors of rectangular shape measuring 1.45m×0.5m. The two primary mirrors are pointing 106.5^o apart. Data are merged into a common path at the exit pupil. *Gaia* was launched in 2013 by

the European Space Agency (ESA) with a mission of operating it for at least five years. *Gaia*'s operation is now extended to 2025. It measures parallaxes with an unprecedented accuracy of about 24 microarcseconds (**it actually depends on magnitude**). Gaia is also designed to measure radial velocities and metallicities ([M/H]) for a couple of hundred million stars in addition to parallaxes and proper motions. The *Gaia* Data Processing and Analysis Consortium (DPAC) processes and analyses the raw data for public use.

2.7.1 Deriving stellar luminosity using Gaia parallaxes

The total brightness of stars or luminosity is an essential quantity in astronomy to understand the physical phenomenon of stars and galaxies. The luminosity of stars varies with the stars' evolution. Thus, luminosity will be used to indicate stars' evolutionary phase and distances for their given mass. *Gaia* provides unprecedented accurate parallaxes, which is a critical parameter. By combining the parallaxes with other less challenging parameters to measure (apparent magnitude, T_{eff}, [Fe/H]) we derived luminosity in the following way;

The apparent magnitude of star is defines as

$$V = -2.5 \log \left(\frac{F_{\lambda 4\pi R^2}}{4\pi d^2} \right) + C$$

where d is distance. Luminosity is the total amount of flux coming out from the surface of stars integrated **over the surface and over** all wavelengths. To account for fluxes in other wavebands, we made bolometric corrections for visual magnitude. We followed Alonso *et al.* (1999) empirical calibration relations for

bolometric corrections in the V band.

$$\mathrm{BC_V} = \frac{-0.0993}{\mathrm{X}} + 0.2887 + 2.275\mathrm{X} - 4.425\mathrm{X}^2 + 0.3505\mathrm{X[Fe/H]} \\ -0.05558[Fe/H] - 0.005375[Fe/H]^2$$

where $\mathrm{X} = \log(\mathrm{T_{eff}}) - 3.52$. The bolometric magnitude ($\mathrm{M_{bol}}$) independent of wavelength is written as

$$\mathrm{M_{bol}} = \mathrm{M_V} + \mathrm{BC_V}$$

Here M_V (= mV + 5 - 5 log (d))is the absolute magnitude in V band which is apparent magnitude of stars if they are placed at a distance of 10 pc .

Derivation of luminosity from $\mathrm{M_{bol}}$ is now straight forward:

$$\frac{\mathrm{L}}{\mathrm{L_\odot}} = 0.4(\mathrm{M_{bol,\odot}} - \mathrm{M_{bol}})$$

Here $\mathrm{M_{bol,\odot}} = 4.74$ is solar bolometric luminosity.

In this work, we have used unprecedented quality parallax measured by *Gaia* (Gaia Collaboration *et al.* 2016, 2018) satellite for distance measurement. We adopted apparent magnitudes from Set of identifications, measurements and bibliography for astronomical data (hereafter SIMBAD)(Wenger *et al.* 2000) `http://simbad.cfa.harvard.edu/simbad/`. We also corrected interstellar extinction in V band ($\mathrm{A_v} = 3.1 \times \mathrm{E(B-V)}$) using Green *et al.* (2015) reddening maps. Uncertainty in stellar parameters impacts the accuracy of luminosity. A major source of uncertainty in luminosity comes from parallax uncertainty.

Chapter 3

High resolution spectroscopic study of Li-rich giants

This Chapter has two parts. In part-1 (section 3.1), we describe our discovery of two red clump super Li-rich giants, for which the evolutionary phase is determined based on direct asteroseismic analysis. In part-2 (section 3.2), we report the finding of two more super Li-rich red giants classified as red clump giants based on indirect secondary calibration using asteroseismic parameters and stellar spectra. The evolutionary phase determination using asteroseismic analysis is robust and termed the " gold standard". Both methods are independent and superior compared to the methods used until recently using solely stars' position in the HR diagram. This Chapter is based on two published articles (Kumar, Singh et al. 2018, ApJL; Singh et al. 2019, MNRAS).

3.1 Part-I: Discovery of Two super Li rich giants in the Kepler field: KIC 2305930 and KIC 12645107

3.1.1 Introduction

A small class of red giant branch (RGB) stars, contrary to theoretical expectations, show an overabundance of Li in their photosphere. The expectation being that Li will be severely depleted, as a result of the 1st dredge-up (FDU) and deep convective envelope in low mass stars, from its initial value of main sequence, and shouldn't exceed A(Li) $\approx$ 1.6 dex in RGB stars (e.g. Iben 1967; Lagarde *et al.* 2012). In fact, observations show much less Li abundance (Brown *et al.* 1989) than the expected maximum value in RGB stars. Partly, this may be due to some Li depletion during main sequence and pre-main sequence phases. For example, the sun has Li abundance of A(Li)$\sim$1.05 dex which is about two orders of magnitude less than the initial Population I main sequence value of A(Li)$\sim$3.3 dex (e.g., Lambert and Reddy 2004). Thus, finding of large Li abundances in RGB stars and, in some cases, exceeding that of ISM value is a puzzle. Studies from systematic surveys found that Li-rich RGB stars are rare, just about 1% of all RGB stars, irrespective of stellar populations (Brown *et al.* 1989; Kumar *et al.* 2011; Monaco *et al.* 2011; Li *et al.* 2018). Now, there are more than one hundred ($\sim$150) Li-rich stars of which a dozen are super-Li rich stars with A(Li)$\geq$3.2 dex (See Casey *et al.* 2016). The rarity of Li-rich stars indicate Li enrichment on the RGB is a transient phenomenon. However, it is not understood how or at what stage of RGB phase such Li enrichment occurs. This has been a question to be answered ever since the first Li-rich K giant was discovered by Wallerstein and Sneden (1982).

One of the impediments in understanding Li origin in K-giants has been the lack of data from which their location in the Hertzsprung-Russel (HR) diagram can be fixed unambiguously. This is mainly due to uncertainties in derived key parameters: luminosity and T_{eff} which, in most cases, exceed the difference in T_{eff}-luminosity space between the suggested locations of Li-enrichment on RGB. For example, distinguishing stars of the red clump (RC) region post He-flash from the luminosity bump region is difficult. In particular, in the case of Population I stars in which the two regions in the HR diagram are separated just by 50-300 K in T_{eff}, and 0.1-0.4 dex in luminosity depending on metallicity and mass (Girardi 2016). As a result, studies based on solely spectroscopy and photometry couldn't draw conclusions on the origin of Li enhancement. Though astrometry from space based Hipparcos or *Gaia* missions provides relatively precise luminosities but found to be inadequate to resolve positional uncertainty of Li-rich K giants on the RGB (Kumar and Reddy 2009; Kumar *et al.* 2011). This may be the reason why many observational results show Li-rich K giants in overlapping regions in the HR diagram: below the luminosity bump (Casey *et al.* 2016; Martell and Shetrone 2013; Li *et al.* 2018), at the bump (Charbonnel and Balachandran 2000; Kumar and Reddy 2009), well above the bump closer to the RGB tip (Monaco *et al.* 2011), and the RC (Kumar *et al.* 2011; Silva Aguirre *et al.* 2014).

The lack of clarity on the precise location of Li-rich giants on the RGB led to an interesting speculations and theoretical modeling. They range from external causes such as engulfment of material of unburnt Li in massive planets (Siess and Livio 1999; Denissenkov and Herwig 2004) and accretion of material enriched with Li due to spallation in a binary companion, supernova explosions, or strong outbursts in X-ray binary systems, to in-situ synthesis and the dredge-up of Li-rich material to the photosphere. The current impasse may be addressed using asteroseismology which is regarded as a standard tool to separate stars of the core-He burning RC phase from the inert He-core Hydrogen shell burning RGB phase. *Kepler* space mission provides high precision photometry capable of measuring frequencies

sensitive to stellar evolutionary phases. Here, in the first part we described our discovery of two new *Kepler* field super Li-rich stars based on LAMOST survey and subsequent high resolution spectra.

3.1.2 Sample selection and Observations

LAMOST * observed millions of low resolution (R ≈1800) stellar spectra (Zhao *et al.* 2012). We have combed the LAMOST spectra to identify strong line at 6707.7 Å of Li transition. Using the technique developed by (Kumar *et al.* 2018a), a number of Li rich stars have been identified among high quality LAMOST spectra and estimated Li abundance. Among those identified giants with Li line two stars: J191712.49+514511.3 (KIC 12645107) and J192825.63+374123.3 (KIC 2305930) were found to have exceptionally strong Li line at 6707Å **for these stars there are** asteroseismic data from *Kepler* mission are available. The two Li-rich candidates were subjected to high resolution (R ≈ 60000) observations using Hanle Echelle Spectrograph (HESP) equipped to 2-m HCT. As stars are relatively fainter (mV>11), we obtained three spectra of 40 minutes exposure each for KIC 2305930 and two spectra of 40 minutes exposure each for KIC 12645107. For spectral calibration and telluric lines removal we obtained spectra of Th-Ar arc lamp and a hot star (HD 149630) with rapid rotation ($vsini$ ∼294 kms^{-1}), respectively. The raw two dimensional images were reduced in standard procedure using IRAF. The spectra have signal-to-noise ratio (SNR) of 50 at 6500 Å. Spectra were wavelength calibrated and continuum fitted. Sample spectra of two stars, observed in low resolution and high resolution, near the Li resonance line at 6707 Å are shown in Figure 3.3.

*For more details on LAMOST and HCT is provided on Chapter 2

3.1.3 Atmospheric Parameters and Abundances

The atmospheric parameters (T_{eff}, log g, [Fe/H], ξ_t) have been obtained using standard procedures based on high resolution spectra and local thermodynamic equilibrium (LTE) stellar model atmospheres with convection-on (Castelli and Kurucz 2004) using an iterative process as described in Chapter 2. For continuity, we describe briefly the procedure specific to these two stars. We used an updated version of spectral analysis code *MOOG* 2013 version (Sneden 1973) for deriving abundances and generating synthetic spectra. To derive accurate atmospheric parameters, a list of well calibrated Fe I and Fe II lines was adopted from the compilation of Reddy *et al.* (2003) and Ramírez and Allende Prieto (2011). Equivalent widths (EWs) of Fe I and Fe II absorption lines were measured from the continuum normalized radial velocity corrected spectra by fitting Gaussian function using splot task in IRAF. The final representative atmospheric model is the one for which the abundances of element Fe are independent of the lines' low excitation potential (LEP), equivalent widths and ionization state (in this case abundances of Fe I and Fe II lines should be same). We found best fit models of T_{eff} 4750 ±80K, log g = 2.38±0.1 dex, [M/H] = −0.50±0.1 dex and ξ_t = 1.5±0.1 km s^{-1} for KIC 2305930 and T_{eff} 4850 K±50, log g = 2.62±0.1, [M/H] = −0.20±0.05 and ξ_t = 1.4±0.1 for KIC 12645107. Uncertainties in the parameters were estimated using a range of model parameters and their sensitivity to abundance trends with LEP or EWs and differences between neutral and singly ionized Fe. The derived parameters in this study are in good agreement, within uncertainties, with the values derived from APOGEE spectra (DR13: Albareti *et al.* 2017). The derived values of T_{eff} based on 2MASS photometry and calibrations of Gonzalez, O. A. *et al.* (2009) are in very good agreement with the spectroscopic values. However, log g value derived using asteroseismic data (Pinsonneault *et al.* 2014; Vrard *et al.* 2016) for KIC 12645107 is about 0.25 dex more than the spectroscopic value. Derived atmospheric and other stellar parameters along with literature values are given in Table 3.1.

Abundance of Li was derived using Li resonance line 6707.8 Å and the subordinate line 6103.6 Å. In general, subordinate Li line is either too weak or absent in the spectra of red giants. However, because of very high Li abundance this line is quite strong in these two stars. We adopted spectral synthesis using LTE model atmospheres for deriving Li abundance. Line list and relevant atomic data including gf-values are taken from the compilation of Reddy *et al.* (2002). Hyperfine features are taken from Hobbs *et al.* (1999). Final abundances are corrected for Non-LTE using a recipe given by Lind *et al.* (2009a). The spectral synthesis of Li lines at 6707 Å and 6103 Å are shown in Figure 3.1. The derived Li abundances based on high resolution confirm the stars as super Li-rich K giants as identified from the LAMOST low resolution spectra.

Further, we derived C, N abundances and carbon isotopic ratio ($^{12}C/^{13}C$) which are key diagnostics for stars' evolutionary phase and level of mixing. Carbon abundance is derived from C I lines at 5052 Å and 5380 Å. However, the N abundance is based on molecular lines $^{12}C^{14}N$ by matching the observed spectrum with the synthetic spectrum in the region of 8003 Å to 8012 Å. Line list and molecular data such as dissociation energies and gf-values are taken from Sneden *et al.* (2014). The derived C and N abundances as input, we obtained ratio $^{12}C/^{13}C$ using $^{13}C^{14}N$ line at 8004.6 Å by performing spectral synthesis. Also, we synthesized 16745.3-16746.9 Å region in H-band APOGEE spectra[‡] to derive $^{12}C/^{13}C$ (See Figure 3.1) in a similar fashion described in Szigeti *et al.* (2018). The atmospheric parameters, elemental abundances, and isotopic ratios are given in Table 3.1.

3.1.4 Mass, *vsini* and Infrared Excess

For both the stars, masses have been derived using *Kepler* asteroseismic data combined with our spectroscopic T_{eff} values using the relation given in Kjeldsen and

[‡]https://dr13.sdss.org/infrared/spectrum/search

Parameters	KIC 2305930	KIC 12645107
R_v(LAMOST)	-126.4±8.3	-19.5±1.6
R_v(APOGEE)	-120.0±0.13	-13.63±0.0
T_{eff}(spec)	4750±80	4850±50
T_{eff}(phot)	4800±90	4765±90
T_{eff}(LAMOST)	4875±86	4841±80
T_{eff}(APOGEE)	4750±70	4825±70
log g_{Spec}	2.38±0.1	2.62±0.1
log g_{Spec}(LAMOST)	2.46±0.12	2.37±0.01
log g_{Spec}(APOGEE)	2.71±0.08	2.45±0.08
log g_{Seism}	2.37±0.01	2.37±0.01
log($L/L_\odot$)	1.69±0.05	1.78±0.02
$M/M_\odot$	0.92±0.11	1.05±0.04
vsini	12.5±1	1.5±0.5
[Fe/H]	-0.5±0.1	-0.2±0.05
[Fe/H](LAMOST)	-0.45±0.08	-0.23±0.01
[Fe/H](APOGEE)	-0.55±0.03	-0.21±0.03
$A(Li)_{LTE}$	4.2	3.24
$A(Li)_{NLTE}$	3.8	3.3
[C/Fe]	$0.36^{\dagger}$	−0.40
[N/Fe]	0.10^{a}	0.54
[C/N]	0.27	-0.94
$^{12}C/^{13}C$	10±2	6±1
[O/Fe]	0.27	0.04
[Na/Fe]	−0.13	−0.01
[Mg/Fe]	0.35	0.03
[Al/Fe]	−0.09	0.04
[Si/Fe]	0.01	0.01
[Ca/Fe]	0.128	−0.02
[TiI/Fe]	0.20	0.02

TABLE 3.1: Derived results of new super Li-rich red clump giants, KIC 2305930 and KIC 12645107 from high resolution spectra. Mass is derived from asteroseismology. For comparison, T_{eff}, log g and [Fe/H] from LAMOST and APOGEE is also provided.

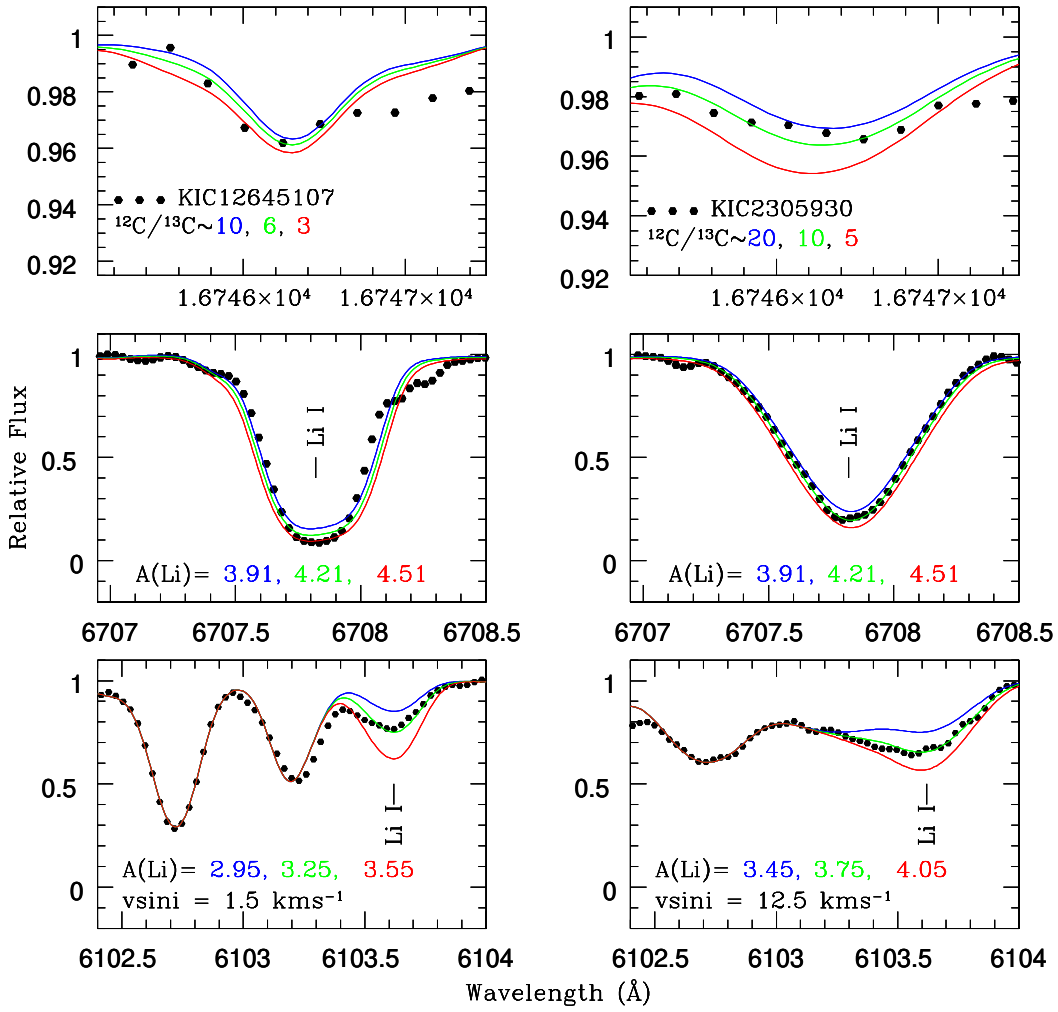

FIGURE 3.1: Derivation of carbon isotope ratio, $^{12}C/^{13}C$, (top two panels) from APOGEE IR spectra and Li abundances from Li resonance line and subordinate lines (bottom four panels) for two stars from optical HESP spectra.

Bedding (1995). Based on seismic values given in Vrard *et al.* (2016), we obtained a mass of 1.05 $M_\odot$ for KIC 12645107. Similarly, for KIC 2305930, we obtained a mass of 0.92 $M_\odot$ using seismic values given in Mosser *et al.* (2014). Projected rotational velocities (*vsini*) have been derived using two Fe I lines adjacent to Li line as described in Reddy *et al.* (2002), in which macroturbulence (V_m) and *vsini* are estimated simultaneously. Line profiles are fitted using χ^2 test for varying values of V_m and *vsini* for given Fe I abundance and instrumental profiles for which $\Delta\chi^2$ values are minimum. The method resulted *vsini* values of 1.5±0.5 km s^{-1} and

12.5±1.0 km s^{-1} for KIC 12645107 and KIC 2305930, respectively. Also, both the stars have been searched for possible infrared excess using observed IR photometry from a 2 Micron survey and mid-IR photometry from WISE (Cutri *et al.* 2003; Cutri and et al. 2013). Comparison of observed IR fluxes with model spectral energy distribution, and the color criteria for IR excess suggested by Rebull *et al.* (2015) and Bharat Kumar *et al.* (2015) do not indicate IR excess in either of the two stars.

3.1.5 Discussion

These are the first two super Li-rich low mass stars for which red clump evolutionary phase is known from an independent analysis of asteroseismic data. We also note that the discovery of one Li-rich K-giant, KIC 5000307 (Silva Aguirre *et al.* 2014), reported as He-core burning RC star based on asteroseismic data. It has Li abundance of A(Li) = 2.71 dex with an estimated mass of 1.52 $M_{\odot}$. Including our current results, these are only the three bonafide Li-rich stars in the red clump region known as of today. Though there are no systematic surveys, it is quite surprising that no giant classified as RGB giant, ascending RGB first time, based on asteroseismology reported in the literature as Li-rich giant. We note the recent report of a K-giant, KIC 9821622 (Jofré *et al.* 2015) which was classified as an RGB star below the bump using asteroseismic data, and was reported as a Li-rich K giant. We have performed a detailed re-analysis of this object for this thesis and the details are given in Chapter 5.

There are two broad scenarios for Li origin: a) internal production which is specific to a particular location, b) external origin, not specific to any particular location. Let us first look at internal production scenarios which are associated with internal changes to stellar structure such as extra mixing at the luminosity bump or He-flash at the RGB tip. At the luminosity bump, all low mass population I stars

below certain initial mass (M= 1.8 - 1.9 $M_{\odot}$) are expected to experience extra-mixing (Cassisi *et al.* 2016). At bump, giants will have central He-core surrounded by H-burning shell above which a radiative zone which inhibits convection into the outer convective envelope. However, during the bump evolution, the H-burning shell crosses the radiative zone barrier of mean molecular weight discontinuity and begins mixing processed material in the H-burning shell with the outer convective envelope (see Palacios *et al.* 2001; Denissenkov and Herwig 2004; Eggleton *et al.* 2008; Denissenkov and Merryfield 2011). As a consequence, models predict further decrease in $^{12}C/^{13}C$ from the values of 20 to 30 post 1st dredge-up, decrease in ^{12}C, and enhancement in N abundance. The extra mixing process seems to continue as the star ascends RGB as evidenced by observations of very low values of $^{12}C/^{13}C$ (e.g. Gilroy 1989). Extra mixing, as per model predictions, also seem to be responsible for high Li abundances seen in some of the RGB stars. To meet observed levels of Li abundances in super Li-rich giants, there must be an efficient mechanism by which ^{7}Be produced in hotter layers ($\geq 10^{8}K$) with seed nuclei of ^{3}He is transported to cooler regions where ^{7}Be is converted to ^{7}Li. To avoid destruction of freshly produced Li, this has to be quickly transported to the outer layers. Given the internal changes to the stellar structure, the associated extra mixing at the bump (e.g. Palacios *et al.* 2001), and the positional coincidence of observed Li-rich K-giants with bump region in the HR diagram, many studies (Charbonnel and Balachandran (2000); Kumar *et al.* (2011)) suggested that the luminosity bump may be the probable site for Li enhancement. However, there is no convincing data available based on which one could rule out the possibility that the luminosity bump as the site for Li enhancement.

In the case of two stars in this study, it is quite unlikely **that the** bump is the site at which Li enhancement happened. If bump is the site, one would expect the enhanced Li at the RGB bump to sustain all the way to the red clump via the RGB tip. Though few studies do report Li-rich stars beyond the luminosity bump and closer to the tip, their rate of occurrence seems to be much lower when

compared to Li-rich stars at the bump. If it is the bump, the very low rate of occurrence/absence of Li-rich giants beyond the bump may be explained by the rarity of Li-rich giants, about 1 in 100 RGB stars (Brown *et al.* 1989; Charbonnel and Balachandran 2000; Kumar *et al.* 2011) which suggests transient nature of Li enhancement among giants. It means giants with enhanced Li during the bump evolution stay as Li-rich for a short duration. It is very unlikely they remain Li-rich through the upper RGB to the red clump. Otherwise one would have observed many more Li-rich stars along the RGB. There is another argument saying that Li-rich giants could be either at RC and RGB due to rapid internal rotation and subsequent change in their T_{eff} resulting a kind of zig-zag motion in the T_{eff} - luminosity space in the HR diagram Denissenkov (2012). However, the zig-zag motion theory cannot be applied to the two super Li-rich stars reported here as they are known to be core He-burning stars settled at the RC which have possibly evolved through the He-flash at the RGB tip.

Since sustaining super Li enhancement is unlikely through post-bump and He-flash evolution, the next best scenario is that Li enhancement occurrence during the He-flash at the RGB tip as suggested by Kumar *et al.* (2011). He-flash is associated with internal changes as a result of He-core ignition and deep convection. The multi dimensional hydrodynamic simulations in low mass population I models (Eggleton *et al.* 2008; Mocák *et al.* 2011) do predict H injection into H-burning shell. This would further increase in ^{13}C (and hence low $^{12}C/^{13}C$, below 10), ^{14}N, and also high Li, assuming there is an ample amount of ^{3}He that survived from the previous evolution. Models also predict some increase in fresh ^{12}C, a by-product of triple-α reaction, depending on the star's metallicity and initial mass. Post He-flash, giants settle down at the red clump region with double shell structure of He- and H-shell burning. Evolution from the tip to the red clump region is quite fast, and one would expect the survival of Li for the short duration- if the Li is produced at the tip. Given the exceedingly large Li abundance in the current two stars, and their positions which seem to be at the beginning of the HB in the

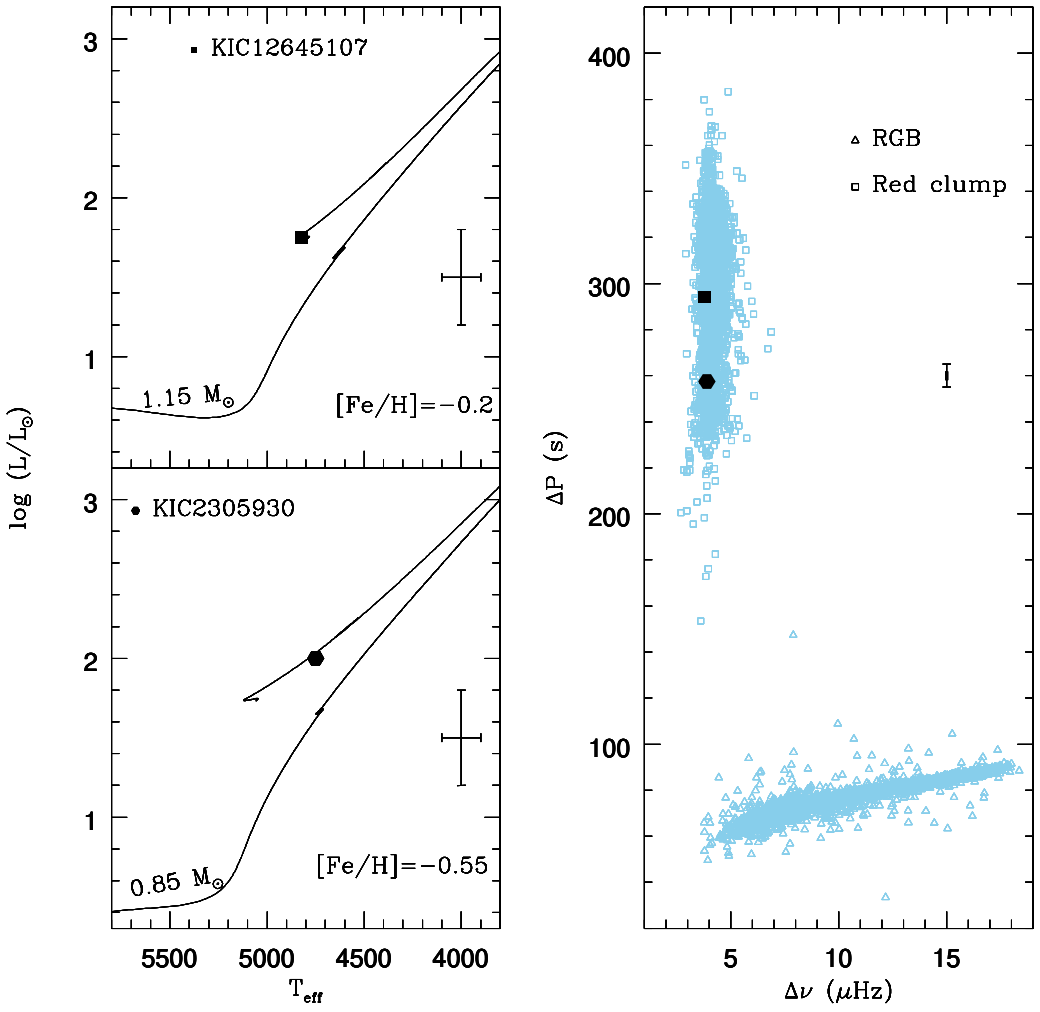

FIGURE 3.2: Location of the two sample stars on HR-diagram (left) and asteroseismic diagram HR diagram(right). Note, they occupy the red clump region in both panels.

HR diagram (See Figure 3.2), Li enhancement episode might have happened very recently. In that case it is very likely Li enhancement occurred during He-flash at the RGB tip, unless there is some kind of external source which is responsible for Li enrichment during red clump evolution.

Recent reports of more Li-rich giants and their locations all along the RGB in the HR diagram add complexity to the problem. In some cases, super Li-enhancement as high as A(Li) = 4.5 dex, reported in sub-giants and below the bump (Martell

and Shetrone 2013; Casey *et al.* 2016). Model predictions range from diffusion of Li in a narrow range of T_{eff} (e.g. Deliyannis *et al.* 2002) and large close-in giant planets engulfment with material of unburnt Li (e.g; see Siess and Livio 1999). It seems unlikely that any of these proposals would explain Li enhancement across the RGB. Alternatively, it is not an inconceivable proposition to make that many of the Li-rich giants are in fact misclassified (see e.g; da Silva *et al.* 2006) and they are most likely core He-burning stars. This argument may be strengthened by the fact that low mass stars spend a relatively much longer time at RC, of about 100 Myr, and as a result they have a higher probability of being detected as Li-rich stars. Another important suggestion which was not explored is by Zhang and Jeffery (2013) in which they predict the composition of early type R and J stars (early AGB stars) whose locations in the HR diagram are difficult to disentangle from their counter parts, red clump and upper RGB stars. They simulated various merger scenarios (such as accretion or subduction) of different He white dwarfs with the He-core of an RGB star. High mass He-dwarf accretion or subduction models predict convection of processed material from He- and H-burning shells which include higher ^{13}C, ^{14}N, and hence lower $^{12}C/^{13}C$. Also, by inserting a small fraction of ^{3}He left over, from the previous evolution, in the RGB envelopes into the He-burning shell, they suggested Li could be produced in the inner layers. If this is actually happening, then freshly born Li survived to be transported to the outer layers.

3.2 Part II: Spectroscopic study of the two new super Li-rich red clump giants whose evolutionary is based on secondary calibration.

In this section, we describe the discovery of two more new super Li-rich K-giants: HD 24960 and TYC 1751-1713-1 for which evolutionary phase is estimated based on secondary calibration using asteroseismology. We used high resolution ($R \approx 60,000$) spectra for deriving Li and other elements. Both the giants show Li abundances of A(Li)≈4.0 dex. Other elemental abundances are normal of typical K-giants. Low ratios of [C/N] ≤ -0.25 and $^{12}C/^{13}C \leq 10$ suggest that the stars are in upper RGB phase. Further, based on *Gaia* astrometry and secondary calibrations using *Kepler* asteroseismic and LAMOST spectroscopic data, we argue that both stars belong to red clump (RC) phase with core He-burning. These new results add to half a dozen already known red clump Li-rich K giants (including the results given in part-1 of this chapter). Results support the growing evidence that the origin of Li excess in RC giants seems to be associated with either He-flash at the tip of the red giant branch (RGB) or recent planet/ brown dwarf merger events closer to the RGB tip.

3.2.1 Introduction

When stars evolve off the main sequence to red giant branch standard stellar evolution models (these models don't include effect of magnetic field, rotation and diffusion) predict significant changes to photospheric abundances of some key isotopes: decrease in Li, ^{12}C and increase in ^{13}C and ^{14}N (Charbonnel 2005). Models predict ratio of $^{12}C/^{13}C$ in the range of 20 to 25 (Charbonnel 1994) from their main sequence value of about 89 (Asplund *et al.* 2009). Similarly, Li is

predicted to be a factor of about 40-60 less in RGB stars after the 1st dredge-up compared to their progenitors on the main sequence (Iben 1967, Lagarde *et al.* 2012). However, standard models do not predict further changes to abundances beyond the 1st dredge-up (Iben 1967).

In general, 1st dredge-up predictions agree well with the observations of RGB stars below the luminosity bump. However, giants at or above the bump, contrary to the standard predictions, show significantly changed abundances from the 1st dredge-up (Lind *et al.* 2009b, Kirby *et al.* 2016). The changes are in the same direction as 1st dredge-up but much severe. For example $^{12}C/^{13}C$ drops to less than 10 in most cases, and in some cases as low as its equilibrium value of 3 to 4 (Gilroy 1989, Gilroy and Brown 1991). Similarly, observed Li abundance in upper RGB stars is significantly low with typical value of A(Li) $\leq$ 0.5 dex (e.g. Brown *et al.* 1989) which is about three magnitudes less than the initial maximum main-sequence value of A(Li)$\sim$3.2 dex (Lambert and Reddy 2004). The rapid decrease of carbon isotopes post-1st dredge-up is attributed to some kind of extra-mixing during stellar evolution through luminosity bump (Denissenkov and VandenBerg 2003). It is not known what exactly causes extra-mixing. However, there are a number of possible mechanisms such as thermohaline mixing (Eggleton *et al.* 2006), magneto-thermohaline mixing (Denissenkov *et al.* 2009), rotationally induced mixing (Denissenkov and Herwig 2004) etc. The general understanding is that it happens at the luminosity bump at which H-burning shell advances upward causing the removal of chemical composition discontinuity (Christensen-Dalsgaard 2015), a barrier to mixing, left behind by the 1st dredge-up. The removal of discontinuity in the abundance profile revives the mixing with the outer convective envelope resulting further reduction in the values of $^{12}C/^{13}C$ and Li abundance.

Contrary to these general observational trend and theoretical predictions, a small group of low mass RGB stars show large amounts of Li, A(Li) $\geq$ 1.6 dex. In some

giants enhancements are 2 to 4 orders of magnitude above the expected values, exceeding the initial maximum main sequence or ISM values of A(Li) = 3.2 dex (Knauth *et al.* 2003; Lambert and Reddy 2004), which are known as super Li-rich giants (e.g. Kumar *et al.* 2011). Presently, there are close to 200 Li-rich K giants of which about 2 dozen are super Li-rich (e.g. Casey *et al.* 2016; Smiljanic *et al.* 2018). In spite of finding a large number of Li-rich stars on RGB, there is no consensus on the origin of Li excess. Though Li-rich stars were reported to be across RGB starting from sub-giant phase (e.g. Martell and Shetrone 2013; Li *et al.* 2018) to all the way to red clump with He-core burning phase (e.g. Silva Aguirre *et al.* 2014; Bharat Kumar *et al.* 2018), majority of them are known to be concentrated in a narrow luminosity range of $1.4 \leq log(L/L_{\odot}) \leq 2.0$ overlapping with the luminosity bump region as well as the red clump region (Charbonnel and Balachandran 2000, Kumar *et al.* 2011). Since bump is associated with stellar internal changes many studies explored to explain the anomalous Li enhancement during the bump as a consequence of extra-mixing (e.g. Palacios *et al.* 2001).

However, the recent discovery of Li-rich K-giants (e.g. Silva Aguirre *et al.* 2014; Bharat Kumar *et al.* 2018; Smiljanic *et al.* 2018) which are in *Kepler* or CoRoT field, and determining their evolutionary phase as red clump based on asteroseismic analysis (Bedding *et al.* 2011) shifted the focus of Li enhancement to the He-flash or post He-flash phase. Precise determination of stellar evolutionary phase of Li-rich stars on RGB has important implications since Li enhancement scenarios vary with evolutionary phase.

Here, in part 2 of this chapter, we describe our high resolution spectroscopic analysis of two new super Li-rich K giants: HD 24960 and TYC 1751-1713-1 for which no prior spectroscopic analysis of elemental abundances was reported. Results in this paper will add to half a dozen known Li-rich K giants of red clump. These are results are published (Singh et al. 2020, MNRAS).

3.2.2 Observations

LAMOST[§] low resolution (R=1800) spectra of the two stars were screened out from the spectra of much larger sample of K-giants which were scanned for finding new Li-rich K giants. Sample LAMOST spectra of two stars showing Li line at 6707 Å are shown in Fig 4.3 (top panels). Line at 6707 Å is quite strong and characteristic of unusual Li abundance (Kumar *et al.* 2018b). Subsequently, the two candidate Li-rich K giants were observed with 2.0-m Himalayan Chandra Telescope (HCT) equipped with the high resolution spectrograph or HESP (Hanle Echelle Spectrograph). Single spectrum of 10 minutes exposure for HD 24960 (mV = 8.00) and three spectra of 30 minutes exposure each for TYC 1751-1713-1 (mV = 9.42) were obtained. Spectra have good signal-to-noise ratio of SNR $>$ 100.

Standard reduction procedure such as bias, flat field corrections, and extraction of one dimensional spectra of flux versus pixel were followed using IRAF tools. For identification and removal of atmospheric lines, we observed HD 5394, a bright hot star of spectral type BIV with very high rotational velocity of $vsini = 265\ Kms^{-1}$ during the same night. Stellar spectra were wavelength calibrated using Th-Ar arc calibration spectra obtained immediately after each star's observation. Finally spectra were continuum fitted for the measurement of equivalent widths (EWs). Cross correlation of stellar spectra with a template spectrum yields radial velocity (RV) of -36.1 km s^{-1} and 5.06 km s^{-1} for HD 24960 and TYC 1751-1713-1, respectively.

[§]http://dr3.lamost.org/

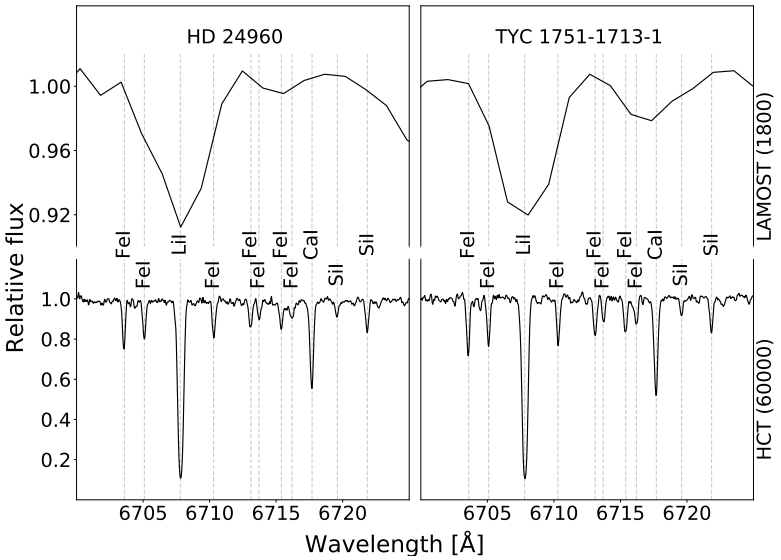

FIGURE 3.3: Sample spectra of stars in the Li region: Low resolution spectra from LAMOST (top two panels) and the corresponding high resolution spectra (bottom two panels).

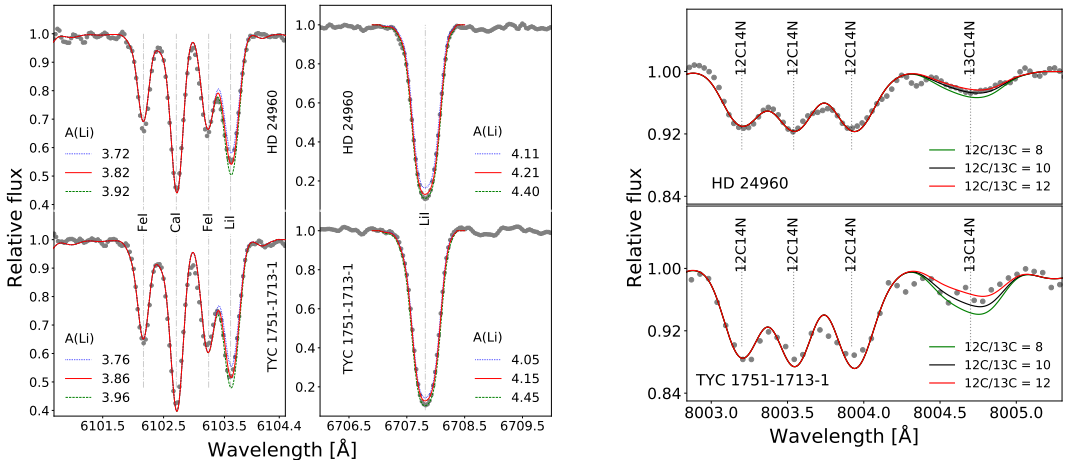

FIGURE 3.4: Left panel: Synthetic spectra (continuous line) around resonance Li line 6707.8 Å and subordinate Li line at 6104 Å for different abundances compared with observed spectra (dotted line). Right panel: Synthesis of ^{13}CN spectral line compared with observed spectra (dotted line).

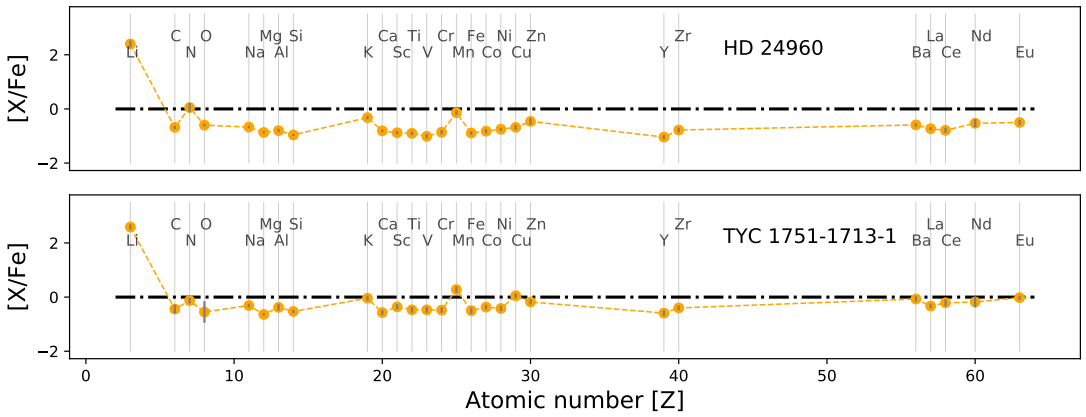

FIGURE 3.5: Elemental abundance of TYC 1751-1713-1 and HD 24960.

3.2.3 Analysis and Results

Abundances have been obtained for 24 chemical elements. For each element a number of representative lines of moderately strong, free of known blends and having reliable atomic data were identified based on a typical K-giant, Arcturus (α-Boo) spectral atlas (Hinkle *et al.* 2000). Line strengths i.e equivalent widths (EWs) are measured from continuum-normalized spectra using *IRAF* tools. Depending on line strengths and possible blends such as Hyper fine structure (HFS), abundances are derived either by matching observed spectra with the synthetic spectra or matching individual line EWs with the predicted EWs in case of clean lines with free of blends. For the analysis, we used LTE stellar atmospheric models from Kurucz (Castelli and Kurucz 2004), and the recently updated radiative transfer code MOOG 2013 version (Sneden 1973).

3.2.3.1 Atmospheric parameters

Atmospheric parameters: T_{eff}, log g, microturbulance velocity (ξ_t) and [Fe/H] were derived using a set of well defined Fe I and Fe II lines taken from the compilation of Reddy *et al.* (2003) and Ramírez and Allende Prieto (2011). A total of 40

Fe I and 10 Fe II lines with EWs less than about 110 mÅ were used. Standard iterative procedure was adapted for deriving T_{eff}, log g and ξ_t. We chose T_{eff} and ξ_t of an atmospheric model for which Fe I lines' abundances are independent of their corresponding lower excitation potential (LEP) and their EWs, respectively. In case of log g, models were varied until neutral average Fe I abundance is equal to that of singly ionized Fe II abundance. Derived parameters along with the uncertainties are given in Table 3.2. We estimated Uncertainties using sensitivity of abundance trends to changes in small steps to respective parameters. We found no appreciable effect on lines' abundance versus LEP relation for a change up to $\delta T_{eff} = \pm$ 70 K for TYC 1751-1713-1 and 35 K for HD 24960. Thus, $\pm$ 70 K and 35 K is taken as uncertainty in the determination of T_{eff}. Also, values of T_{eff} and log g derived using photometry combined with Gaia parallaxes (Gaia Collaboration *et al.* 2018). Photometry was taken from from 2MASS (Skrutskie *et al.* 2006) and Simbad[¶]. The de-reddened colors of $(V-K)_\odot$ and $(J-K)_\odot$ combined with empirical relations from González Hernández and Bonifacio (2009) yield an average T_{eff} of 4870±60 K for TYC 1751-1713-1 and 4800±80 K for HD 24960. Reddening value of E(B-V) = 0.09 is taken from dust maps (Green *et al.* 2015) in the direction of stellar sources. Values of log g are also derived using a relation;

$$\log g = \log g_\odot + \log\left(\frac{M}{M_\odot}\right) - \log\left(\frac{L}{L_\odot}\right) + 4 \times \log\left(\frac{T}{T_\odot}\right)$$

Masses are estimated using stellar evolutionary tracks (Paxton *et al.* 2011, 2018) with corresponding stellar metallicity that pass through respective positions of Luminosity and T_{eff} in the HR-diagram. Derived T_{eff} and log g values using astrometry and photometry along with spectroscopic values are given in Table 3.2. Values are in good agreement within the quoted uncertainties. We adopt values from spectroscopic analysis.

[¶]http://simbad.u-strasbg.fr/simbad/sim-fbasic

	TYC 1751-1713-1	HD 24960
RA	01:21:41.845	03:59:27.632
DEC	+25:15:06.79	+36:19:06.53
mV (mag)	9.42	8.00
HESP Spectra SNR	110	120
Parallax (mas)	1.95 ± 0.04	3.67 ± 0.04
logg(gms^{-2})	2.58 ± 0.17	2.39 ± 0.19
log $g_{photometric}$	2.45 ± 0.04	2.40 ± 0.03
T_{eff} [K]	4830 ± 70	4835 ± 35
$T_{eff,photometric}$	4870 ± 60	4800 ± 80
$\xi_t(kms^{-1})$	1.47 ± 0.15	1.41 ± 0.04
[Fe/H](dex)	-0.25 ± 0.10	-0.45 ± 0.04
vsini (kms^{-1})	4.40 ± 0.8	6.0 ± 1
V_m (kms^{-1})	3.60 ± 0.10	4.0 ± 0.20
[C/Fe]	0.06 ± 0.20	0.21 ± 0.09
[N/Fe]	0.37 ± 0.16	0.94 ± 0.18
[O/Fe]	0.11 ± 0.17	0.33 ± 0.12
$^{12}C/^{13}C$	10 ± 1	10 ± 2
$A(Li)_{LTE,6103}$ Å	3.86 ± 0.13	3.82 ± 0.07
$A(Li)_{NLTE,6103}$ Å	3.97 ± 0.13	3.94 ± 0.07
$A(Li)_{LTE,6708}$ Å	4.15 ± 0.15	4.21 ± 0.10
$A(Li)_{NLTE,6708}$ Å	4.05 ± 0.15	4.06 ± 0.10
Age (Gyr)	8.8	8.1
Mass ($M_\odot$)	1.3 ± 0.05	1.2 ± 0.05
Sptype	K2III	K2III

TABLE 3.2: Stellar parameters (T_{eff}, log g, [Fe/H], $vsini$),ξ_t, abundances (A(Li), [C/Fe], [N/Fe], [O/Fe]) and carbon isotopic ratio of TYC 1751-1713-1 and HD 24960 derived from high resolution and high SNR optical spectra. Mass of stars is derived from evolutionary tracks.

3.2.3.2 Abundances

Lithium: Li abundance was derived from resonance line at 6707.8 Å and a subordinate line at 6103.6 Å. Abundances were derived using spectral synthesis to account for weak blends, and hyperfine structure (HFS). For line synthesis, we adopted line list along with oscillator strengths from the compilation of Reddy *et al.* (2002) and HFS from Hobbs *et al.* (1999). Spectral synthesis of respective lines yields Li abundances of A(Li) = 4.15[‖] and 3.86 dex for TYC 1751-1713-1 and A(Li) = 4.18 and 3.82 dex for HD 24960. Comparison of observed spectra with the predicted spectra for different Li abundances for both stars are shown in left panel of Figure 3.4. Since both the transitions are known to have affected by non-LTE effects (Lind *et al.* 2009a) and the derived abundances were corrected using their procedure. The average non-LTE corrected abundances are: A(Li)=4.0 dex for TYC 1751-1713-1 and 4.01 dex for HD 24960 (See Table 3.2).

C,N,O & $^{12}C/^{13}C$: Abundance ratios of C/N and, in particular, isotopic ratios of $^{12}C/^{13}C$ are key tracers of evolution on RGB. We have derived carbon abundance using three well defined atomic lines at 5052.15 Å, 5380.36 Å and 6587.62 Å with gf values taken from (Wiese *et al.* 1996). Atomic N lines in the spectra are quite weak as the stars are too cool and the N transitions in the visible spectra are of high voltage lines. For N abundance, we relied on a few selected CN lines in the red region of optical spectra , 8000-8006 Å and with the derived C abundance as input. Basic line data of CN lines for spectral synthesis was taken from de Laverny and Gustafsson (1998). Oxygen abundances was based on two forbidden [OI] lines at 6300.30 Å and 6363.78 Å. In case of 6300.30 Å synthesis, we included line list with atomic data given in (Allende Prieto *et al.* 2001). Values for isotopic ratio $^{12}C/^{13}C$ were derived using a molecular line of $^{13}C^{14}N$ at 8004.6 Å, see right panel of Figure 3.4. Derived C, N,O and $^{12}C/^{13}C$ ratios are given in Table 3.2.

[‖] A(Li) = log(N(Li)/N(H)

Element	HD 24960			TYC 1751-1713-1		
	A(X)	[X/Fe]	$\sigma_{[X/Fe]}$	A(X)	[X/Fe]	$\sigma_{[X/Fe]}$
(1)	(2)	(3)	(4)	(5)	(6)	(7)
Li	4.00	...	...	4.01	...	...
C	8.20	0.21	0.09	8.24	0.06	0.20
N	8.33	0.94	0.18	7.95	0.37	0.16
[O]	8.58	0.33	0.12	8.55	0.11	0.17
Na I	5.95	0.15	0.08	6.12	0.13	0.14
Mg I	7.19	0.03	0.08	7.29	-0.06	0.13
Al I	6.05	0.04	0.08	6.30	0.10	0.13
Si I	6.99	-0.08	0.08	7.17	-0.09	0.14
Ca I	5.94	0.04	0.09	6.16	0.07	0.15
Sc II	2.70	-0.01	0.11	3.05	0.15	0.16
Ti II	4.46	-0.05	0.10	4.73	0.03	0.17
V II	3.33	-0.16	0.10	3.70	0.02	0.16
Cr I	5.22	0.02	0.08	5.35	-0.04	0.16
Fe I	7.01	0.00	0.09	7.20	0.00	0.17
Co I	4.46	-0.09	0.11	4.87	0.13	0.15
Ni I	5.84	0.06	0.09	5.98	0.01	0.17
Cu I	3.85	0.10	0.12	4.28	0.34	0.18
Zn I	4.15	0.03	0.14	4.29	-0.02	0.18
Y I	1.53	-0.24	0.12	1.98	0.02	0.15
Zr I	2.16	0.02	0.11	2.38	0.05	0.18
Ba II	2.02	0.28	0.10	2.27	0.34	0.20
La II	0.87	0.18	0.12	1.07	0.19	0.15
Ce II	1.24	0.10	0.14	1.35	0.02	0.19
Nd II	0.96	-0.05	0.17	1.49	0.29	0.22

TABLE 3.3: Summary of elemental abundances of TYC 1751-1713-1 and HD 24960. Uncertainties in abundances is quadratic sum of uncertainties propagated from errors in T_{eff}, log g,[Fe/H] and ξ_t. Solar abundance is adopted from Asplund *et al.* (2009)

Other Elements: In addition to key elements like Li, C, N and $^{12}C/^{13}C$, we have derived abundances of other elements to look for any possible trends with Li excess. Atomic data for most of the transitions were taken from the compilation of Reddy *et al.* (2003) and Ramírez and Allende Prieto (2011). The derived average abundances of elements from Li to Nd for which we could measure reliable EWs are tabulated in Table 3.3. Except the abundance of Li, other elemental abundances defined by [X/Fe] (= $[X/H]_{star} - [Fe/H]_{star}$) do not suggest any abnormality, and they are typical for stars on the RGB. Also, abundance patterns are typical of Galactic thin disk component to which both stars belong as per the kinematic measurements with probability of being thin disk by more than 95% (Reddy *et al.* 2006).

Uncertainties: Quoted errors in average abundances given in Table 3.2 & 3.3 are quadratic sum of uncertainties in respective abundances due to estimated uncertainties in model parameters: ΔT_{eff}, Δlog g, Δ[Fe/H] and $\Delta\xi_t$. Also included is the estimated uncertainty in measuring EWs (ΔEW) which is a function of S/N ratio of spectra (Cayrel 1988). The individual uncertainties in each of these parameters are assumed to be independent, and the net error in each abundance is given by

$$X_{error} = \sqrt{\Delta Teff^2 + \Delta log\ g^2 + \Delta\xi_t^2 + \Delta[Fe/H]^2 + \Delta EW^2}$$

As expected, abundances from neutral lines are more sensitive to ΔT_{eff}, ionized species (Fe II, Ba II etc.) to Δlog g, and the abundances derived using stronger lines are more sensitive to $\Delta\xi_t$. Effect of Δ[Fe/H] is very little or nil on abundances.

3.2.3.3 *vsini* and infrared excess

Many studies speculated on the possible correlation between Li-excess, and *vsini* and IR excess which could be one of the key evidences for planet/sub-dwarf merger scenarios (Carlberg *et al.* 2010). In general, average stellar rotational velocities (*vsini*) for K-giants are low, at about 2 Km s^{-1}, compared to their progenitors on the main sequence (de Medeiros *et al.* 1996). As stars evolve off to RGB their *vsini* drops significantly due to angular momentum conservation. However, a few Li-rich giants do show higher *vsini* values than the typically observed values prompting speculations of correlation between *vsini* and Li-excess (Drake *et al.* 2002). In the case of two stars in this study, we derived derived *vsini* values using two neutral Fe I lines 6703.5 Å and 6705.1 Å. Observed spectral profiles were compared with the profiles predicted for given input atomic data, abundance, and instrumental broadening derived from Th-Ar calibration spectrum. By varying values of *vsini* and macro turbulence(V_m) simultaneously, we found best fits with minimum χ^2 value for *vsini*= 6±1 km s^{-1} and V_m= 4.0±0.2 km s^{-1} for HD 24960, and 4.4±0.8 km s^{-1} and V_m= 3.6±0.1 km s^{-1} for TYC 1751-1713-1. Values of V_m and *vsini* are given in Table 3.2.

For estimating IR excess, we used spectral energy distribution (SED) fitting in virtual observatory SED analyzer (VOSA, Bayo *et al.* (2008))**. The observed available fluxes in different bands were fitted with theoretical Kurucz atmospheric flux models (Castelli *et al.* 1997) for a set of derived atmospheric parameters. We used mid IR fluxes from AKARI (Ishihara *et al.* 2010) and WISE (Wright *et al.* 2010), and near IR fluxes from 2MASS (Skrutskie *et al.* 2006) survey. The data for optical bands (G, G_{BP}, G_{RP}) comes from Gaia survey (Gaia Collaboration *et al.* 2016, 2018). Near- and mid-IR fluxes of both stars are of very good quality as indicated by flags in respective catalogues. As shown in left panel of Figure 3.6

**http://svo2.cab.inta-csic.es/theory/vosa/

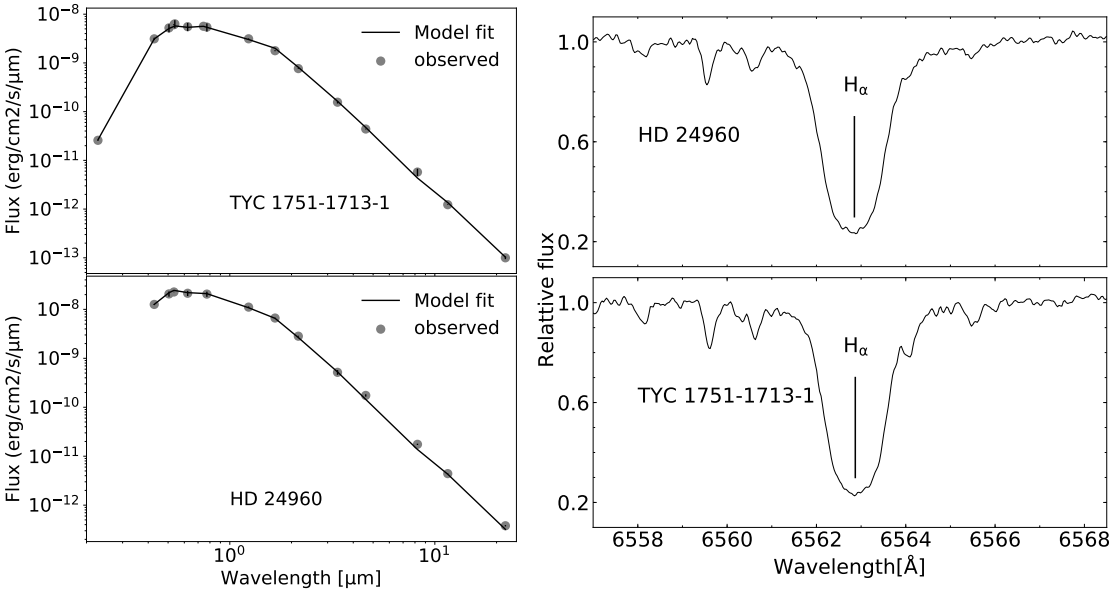

FIGURE 3.6: Left panel: Model SED fits (continuous line) of TYC 1751-1713-1 and HD 24960 with observed fluxes (filled circles). Right panel: Observed H_α of profiles show no asymmetry. Central line is a bisector of profiles.

neither of the stars show evidence of IR excess at least in the near- and mid-IR regime. Stars may have excess in far IR due to cold dust for which we don't have data because far IR fluxes of 24 μ, 60 μ and 100 μ given in IRAS catalogue (Moshir *et al.* 1990) are upper limits which were not considered in fitting SEDs. Lack of IR excess, at least in the near IR, suggests lack of mass loss activity either at present or in the recent past. This is further corroborated by the near symmetric H_α profiles (Mészáros *et al.* 2009) (see right panel of Figure 3.6) as asymmetric profiles are generally used for stellar mass-loss.

3.2.4 Evolutionary Status

Evolutionary phase of Li-rich stars is one of the key issues which is yet to be resolved unambiguously for most of the Li-rich RGB stars. The resolution of the issue is closely tied to the understanding of Li excess origin in K giants. Here,

we used two different methods to determine stellar evolutionary phase. First one involves traditional method of simply placing stars in the HR diagram of luminosity versus T_{eff} plane and compare with theoretical evolutionary tracks. As shown in left panel of Figure 3.7 evolutionary tracks from MESA (Paxton *et al.* 2011, 2018) with corresponding metallicity suggest that stars are at the red clump region, post He-flash at the RGB tip. Errors in luminosity due to errors in parallaxes, and T_{eff} are shown as vertical and horizontal bars. Parallaxes are taken from *Gaia* survey (Gaia Collaboration *et al.* 2016, 2018). Other source of error in determining star's position in the HR-diagram is the metallicity. We plotted two tracks for each star for upper and lower limits of [Fe/H] (tracks with broken lines). Tracks for given average metallicities of masses of 1.2 ± 0.05 $M_{\odot}$ for HD 24960 and 1.3 ± 0.05 $M_{\odot}$ for TYC 1751-1713-1 best converge with stars positions in $\log(L/L_{\odot})$ - T_{eff} plane. Though the position appears to coincide well with the red clump region it would be difficult to completely rule out the possibility of their location on the RGB either at or close to the luminosity bump in HR diagram. This is because the gap between the clump and the bump of field stars of metallicities closer to the sun is very small which is one of the main difficulties to separate stars of RC from that of the bump (Kumar *et al.* 2011).

Second method pertains to asteroseismology for differentiating RGB stars with H-shell burning from stars of red clump with He-core burning (Bedding *et al.* 2011). Unfortunately, the stars in the current study are not in the *Kepler* survey field. However, secondary calibration based on LAMOST and APOGEE spectra of stars that have *Kepler* asteroseismic data is possible. This is an useful tool based on which one could classify giants as either red clump or RGB stars (Ting *et al.* 2018). Oscillations in red giants vary depending on core density. The average period spacing between oscillations of gravity mode (g- mode) and acoustic pressure mode (p-mode), and the frequency separation ($\Delta\nu$) between p-modes are found to be key parameters to separate RC stars of He-core burning from those of H-shell burning RGB stars. Stars with $\Delta P \geq 150$ sec and $\Delta\nu \leq 5$ μHz have been classified as

RC stars (Bedding *et al.* 2011; Vrard *et al.* 2016). The criterion is often termed as gold standard for segregating RC and RGB stars. (Ting *et al.* 2018) estimated ΔP = 275 sec and $\Delta\nu$ = 4.04 μHz for HD 24960 and ΔP = 249.3 sec and $\Delta\nu$ = 4.18 μHz for TYC 1751-1713-1 suggesting that both the stars belong to the RC. Using the estimated seismic parameters (ΔP, $\Delta\nu$), other stellar parameters such as $\nu_{\rm max}$, mass and Radius of the stars (See Table 3.4) were derived using equations given in Kjeldsen and Bedding (1995). We found M = 1.27 $M_{\odot}$ for HD 24960 and M = 1.26 $M_{\odot}$ for TYC 1751-1713-1 which are very close to the values obtained using the stellar evolutionary tracks. Further, one can also infer stars evolutionary phase based on the relative level of changes in C and N abundances. RC stars that have gone through the RGB phase are expected to have lower C compared to stars which are still on the RGB phase. For example ratios of [C/N] versus [Fe/H] can be used to separate RC stars from RGB stars (see Masseron *et al.* 2017; Hawkins *et al.* 2016). In Table 3.5, we have given values of [C/N] and [Fe/H] of our two stars along with seven other known Li-rich giants, of which evolutionary phase for six stars is known based on asteroseismic analysis, and based on CMD for one in open cluster Trumpler 5. We have shown all of them in a plot (see right panel of Figure 3.7) of [C/N] versus [Fe/H] of asteroseismically classified normal RC and RGB stars. The two stars in our study with [C/N] ≤ -0.25 show that they are indeed RC stars.

3.2.5 Discussion

Derived abundances of Li, ratios of [C/N] and $^{12}C/^{13}C$ of two stars in this study, HD 24960 and TYC 1751-1713-1, along with six other known RC giants are summarized in Table 3.5. All of them have three features in common: a) Large Li abundance which is about 1 or 2 orders of magnitude more than the maximum predicated value of A(Li)=1.5 dex on RGB (Iben 1967; Lagarde *et al.* 2012), and 2 to 3 orders of magnitude more than the generally observed values in post bump

	HD 24960	TYC1751-1713-1
ΔP [sec]	275.99	249.31
$\Delta\nu[\mu$Hz]	4.04	4.18
$\nu_{\rm max}[\mu$Hz]	33.86	35.36
M [$M_\odot$]	1.27	1.26
R [$R_\odot$]	11.25	10.96
log g	2.44	2.46
$\log(\frac{L}{L_\odot})$	1.80	1.78

TABLE 3.4: Asteroseismic parameters derived from spectral calibration. Period spacing and frequency separation are directly adopted from (Ting *et al.* 2018). Mass, radius, log g and luminosity have been derived using scaling relations.

stars (Lind *et al.* 2009b), b) low $^{12}C/^{13}C$ ratios which are a factor of 2 to 3 lower (except for KIC 4937011, see table 3.5) than the predicted values suggesting some kind of extra mixing post 1st dredge-up episode, c) low [C/N] values (≤ -0.25), indicating stars have evolved through the RGB tip and are in RC phase(Hawkins *et al.* 2018). However, Li-rich giant, KIC 2305930, though it is a bonafide RC star based on asteroseismic data, has [C/N] value which is positive falling in the category of RGB stars (See right panel of Figure 3.7). In their paper, Bharat Kumar *et al.* (2018) commented that because of its large $vsini$=12.5 km s^{-1}, and hence relatively broader spectral lines, they couldn't derive C and N abundances. They have adopted C and N abundances given in APOGEE DR13 catalog which are based on infrared spectra of resolution R$\approx$ 22,000. So, [C/N] value of this star should be treated with caution.

With the recent findings of new super Li-rich red clump stars (part-1 of this chapter), a question arises whether there is a single mechanism that is responsible for all the Li-rich RGB stars, or there are multiple mechanisms for Li enhancement depending on their evolutionary phase on RGB. To answer this question

it is necessary to have evolutionary phase unambiguously determined. Presently, there are just 7 giants which are reported as Li-rich for which evolutionary phase is determined based on asteroseismic analysis (see Table 3.5). Of which giant KIC 9821612 reported by Jofré *et al.* (2015) is the only RGB Li-rich giant. Also, KIC 9821612 stands out from other Li-rich giants in Table 3.5 by having least amount of Li abundance A(Li)=1.80 dex. Recent analysis by (Takeda and Tajitsu 2017) also gives similar mean abundance of A(Li) = 1.76 dex. With the commonly applied criterion of A(Li) $>$ 1.5 dex, KIC 9821612 can be qualified as a Li-rich giant. However, as mentioned in Jofré *et al.* (2015), its abundance is at the limit of normal Li-rich giants of A(Li) $\leq$ 1.8 dex as indicated in recent studies (e.g. Ruchti *et al.* 2011; Liu *et al.* 2014). Given its relatively higher value of $^{12}C/^{13}C$ coupled with its position in HR diagram, below the bump, it is important to understand whether this star is genuinely Li-rich i.e its photosphere is enriched with Li while star is on RGB. Also, one can't rule out the possibility of insufficient dilution of Li from its initial value. On other hand, its reported over-abundances of α- and r-process elements seem to be in odds with its RGB evolutionary phase. A more detailed study of this star is given in Chapter 5 as it has important implications for constraining Li-enhancement models.

There are two main hypotheses for Li-excess in RGB stars. One being the in-situ nucleosynthesis and subsequent extra mixing, and second is external origin. The apparent concentration of a large number of Li-rich giants at luminosity bump as reported by observations (Charbonnel and Balachandran 2000; Casey *et al.* 2016; Ruchti *et al.* 2011) led to construction of many theoretical models around in-situ nucleosynthesis and extra-mixing at the bump. Note, extra-mixing is also responsible for observed severe depletion of Li and very low values of $^{12}C/^{13}C$ and [C/N]. However, under some special conditions models (e.g. Palacios *et al.* 2001; Denissenkov and Herwig 2004; Eggleton *et al.* 2008; Denissenkov and Merryfield 2011; Denissenkov 2012) predict high levels of Li abundances seen in Li-rich stars. Given the relatively longer stellar evolutionary time scales at the bump and the

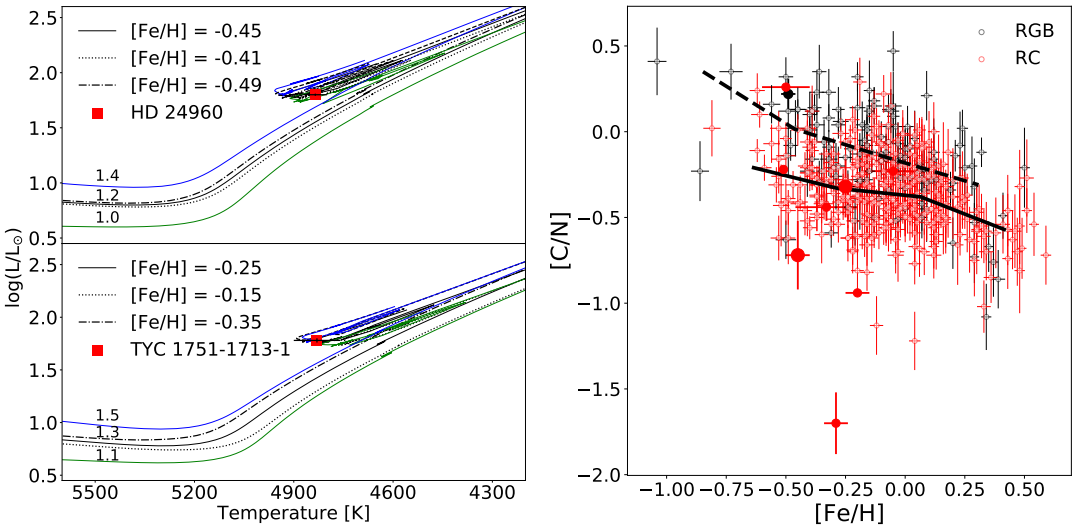

FIGURE 3.7: Left panel: Location of two super Li-rich stars (filled squares) in the HR diagram. Shown are the MESA evolutionary tracks Paxton *et al.* (2011) for masses 1.2, 1.3 $M_{\odot}$ with corresponding metallicities. Right panel: Plot of [C/N] vs [Fe/H] of known normal RC (red open circles) and RGB (black open circles) stars. Li-rich RC stars from Table 4 are shown as red filled circle and the lone Li-rich RGB star KIC 9821622 is shown as filled black circle. Black solid and black dashed lines are running median of [C/N] abundance of RC and RGB stars, respectively. Note, two stars in this study (large filled red circles) are well within RC regime of the plot.

expected brief life span of enhanced Li, models seem to explain the reported observational results: a) concentration of Li-rich stars at the bump, b) very few or lack of Li-rich stars in between the bump and RGB tip.

Star name	[C/N]	[Fe/H]	A(Li)	12C/13C	vsini	status	method
Trumpler 5 3416	-0.22	-0.51	3.75	14 ± 3	2.8	RC	HRD
KIC 9821622	$+0.22 \pm 0.09$	-0.49 ± 0.03	1.80	$18 \pm .7$	$1.01 \pm .7$	RGB	Asteroseismology
KIC 5000307	-1.70 ± 0.18	-0.29 ± 0.05	2.71	< 20	...	RC	Asteroseismology
KIC 4937011	-0.23 ± 0.08	$+0.05 \pm 0.12$	2.30	25 ± 5	8.5 ± 1.1	RC	Asteroseismology
KIC 12645107	-0.94 ± 0.00	-0.20 ± 0.05	3.30	10 ± 1	1.5 ± 0.5	RC	Asteroseismology
KIC 2305930	$+0.26 \pm 0.00$	-0.50 ± 0.10	3.80	6 ± 1	12.5 ± 1	RC	Asteroseismology
2MASS 19265195+0044004	-0.44 ± 0.08	-0.33 ± 0.13	2.94	$- - -$	2.1 ± 2.7	RC	Asteroseismology
TYC 1751-1713-1	-0.30 ± 0.18	-0.25 ± 0.10	4.01	9 ± 2	4.4 ± 0.8	RC	HRD & [C/N]
HD 24960	-0.70 ± 0.20	-0.45 ± 0.05	4.00	8 ± 2	6.0 ± 1.0	RC	HRD & [C/N]

TABLE 3.5: Summary of key parameters of all the known red clump Li-rich K giants including the two from this study for which evolutionary phase is determined either from asteroseismology or secondary calibration based on LAMOST spectra and asteroseismology data.

The above scenario may explain Li-rich stars if they are either at the bump or just evolved off the bump. In case of Li-rich giants at red clump, it would be difficult to explain sustaining of Li abundance at the level shown in Table 3.4 if Li-enhancement occurred during the bump on RGB. The continued deep convection post-bump evolution seems to rapidly deplete remaining Li from 1st dredge-up or Li that has been produced at the bump. This has been well illustrated by observations (e.g. Lind *et al.* 2009b). Also, relatively much shorter Li depletion time scales compared to stellar evolutionary time scales from the bump to red clump (e.g. Bharat Kumar *et al.* 2015) add to the argument in favour that the enhanced Li at the bump is very unlikely to survive all the way to red clump. Alternately, accretion of Li-rich material from sub-stellar objects such as planets or brown dwarfs may enhance photospheric Li abundance (Alexander 1967). Since planet engulfment can happen anywhere along the RGB a single mechanism may be sufficient to explain reported Li-rich stars along RGB: sub-giants (Li *et al.* 2018), below the bump (Adamów *et al.* 2014; Casey *et al.* 2016), at the bump (Charbonnel and Balachandran 2000), between the bump and the RGB tip, even at the red clump. External scenarios explain relatively high occurrence of Li-rich stars either at bump or at the clump may be due to relatively longer evolutionary time scales at the respective phases.

Though, at the outset, the external hypothesis seems to explain Li excess, there are genuine concerns on its ability to explain the level of Li excess observed in stars by Li-rich material accretion alone. For example Aguilera-Gómez *et al.* (2016) shows a maximum limit of A(Li) = 2.2 dex in RGB stars by way of accretion of sub-stellar companion of mass lower than 15 M_j in a regime where extra-mixing does not operate. Above this mass limit, Li is expected to be depleted in the interiors of sub-stellar objects (Chabrier *et al.* 1996). Also, Siess and Livio (1999) computations showed enhancement of photospheric Li abundance by mixing Li rich material of sub stellar objects of masses as high as 0.1 $M_\odot$ to meet observed levels of Li. Results from these studies, in the absence of induced mixing, imply

that multiple number of planets and/or sub-stellar objects are required to reach the level of Li abundances observed in super Li-rich giants. However, one can't rule out the possibility of merger induced extra-mixing that brings up Li produced in H-burning shell. Yet, we don't have evidence for such large accretion of external material in the form of enhanced metal abundances such as Fe-peak elements. One of the key evidences for the addition of external Li rich material is the enhanced abundance of ^{6}Li which has not been observed either in RGB stars or in main sequence dwarfs with planets (Reddy *et al.* 2002). Also, models based on external events predict infrared excess as well as enhanced rotation as a consequence of accretion process which do not seem to be evident in many of the Li-rich stars (Bharat Kumar *et al.* 2015; Rebull *et al.* 2015). Of course, IR excess may not be a stringent criterion as Li and dust shells evolve on different time scales (Bharat Kumar *et al.* 2015). As per *vsini* values, as shown in Table 3.5 among 9 Li-rich giants at least 4 stars do show projected *vsini* which are two to three times of the average observed values for K-giants de Medeiros *et al.* (1996).

In case of two stars in this study and other RC giants in Table 3.4, their very large Li abundance and relatively shorter Li depletion time scales suggest that the Li enhancement event occurred very recently either by material accretion or by in-situ nucleosynthesis, and subsequent mixing. In case of in-situ, He-flash at the RGB tip could be an alternate site to the luminosity bump for excess Li seen in RC stars. He-flash at RGB tip, an immediate preceding phase of red clump phase, is a significant event on RGB at which He ignition at the core begins. There are couple of studies that dealt with nucleosynthesis during He-flash and its effects on stellar photosphere abundances. For example, Mocák *et al.* (2011) show injection of hydrogen into He-layers and mixing up of interior material with outer layers resulting in very low ^{12}C/^{13}C, large Li abundances, and enhanced N. Models also predict enhanced C as well. In case of external scenario, one can think of merger events closer to the tip. Zhang and Jeffery (2013) explored mergers of He white dwarfs with He-core of RGB stars to explain Li in early AGB stars,

and predict enhanced Li and lower $^{12}C/^{13}C$ values along with infrared excess for certain combination of masses of He-WD and central He-cores.

3.2.6 Summary

In this chapter, we have described the discovery of four new super Li-rich K giants with A(Li) $\approx$ 4.0 dex. We argued they are in red clump phase with He-burning at the core. Two of them are classified as RC giants based on direct asteroseismic analysis and the other two using an indirect secondary calibration using again asteroseismology. The four stars add to the growing list of Li-rich red clump giants. Large Li abundances coupled with their RC evolutionary phase imply that the Li enhancement occurred very recently either by internal nucleosynthesis during He-flash at the RGB tip or by external events such as merger of sub-stellar objects near the tip. Including four stars in this chapter there are 8 Li-rich K giants for which RC evolutionary phase is firmly established. Out of which five are super Li-rich stars with A(Li) $\geq$ 3.2 dex including four from this study. KIC 9821622 is the only Li-rich RGB star reported whose evolutionary phase is based on asteroseismology. Though the numbers are too small to deduce firm conclusion, it would be interesting to comment on the large difference in number of known Li-rich giants among RC and RGB phases. Whether the difference in numbers is due to large difference in stellar evolutionary time scales between the two phases; red clump evolutionary time scales (100 Myr) are relatively much longer compared to the bump time scales (few thousand years) (Bharat Kumar *et al.* 2015). A systematic survey of Li among the known RGB and RC giants is warranted to find clues for the origin of Li-excess. A large systematic survey in this direction is necessary. In the next chapter we have provided results of our survey of common giants among *Kepler* photometric survey and LAMOST spectroscopic survey fields.

Chapter 4

Survey of Li-rich giants in LAMOST-Kepler field

Inspired by our recent discovery of bona-fide red clump giants (Chapter 3) of He-core burning phase we performed a systematic survey of red giants which are common between large spectroscopic survey of LAMOST and time resolved photometric survey of *Kepler* space mission. This survey is to find whether the Li enhancement is associated with only red giants of He-inert core or only with red clump giants or with both the phases. The survey resulted in discovering of 24 new super Li-rich giants and all of them found to be red clump giants. Results are based on systematic search of a large sample of about 12,500 giants common to the LAMOST spectroscopic and *Kepler* time resolved photometric surveys. The two key parameters derived from *Kepler* data; average period spacing (ΔP) between $l = 1$ mixed gravity dominated g-modes and average large frequency separation ($\Delta\nu$) $l = 0$ acoustic p-modes, suggest all the Li-rich giants are in He-core burning phase. This is the first unbiased survey subjected to a robust technique of asteroseismic analysis to unambiguously determine evolutionary phase of Li-rich giants. The results provide a strong evidence that Li enhancement phenomenon

is associated with giants of He-core burning phase, post He-flash, rather than any other phase on RGB with inert He-core surrounded by H-burning shell. In this chapter, we describe survey strategy and results. The results given in this chapter are published in Astrophysical Journal Letters (Singh et al. 2019, ApJL).

4.1 Introduction

It is firmly established that Li-rich giants do exist though they are not very common(they comprise about 1% of red giants). Thanks to recent large surveys such as LAMOST(Cui *et al.* 2012) and GALAH(De Silva *et al.* 2015) there are now a few hundred Li-rich giants which have Li abundance of $A(\mathrm{Li}) \geq 1.5$ dex, a commonly adopted upper limit for normal giants of red giant branch (RGB; Iben 1967). For example, recent large study by Deepak and Reddy (2019) discovered more than 300 Li-rich giants from GALAH spectroscopic survey doubling the number of Li-rich giants known till then since the first discovery of Li-rich giant by Wallerstein and Sneden (1982). However, there is no consensus on the origin of Li excess in red giants which has been elusive for decades. This is because there is no clarity on their evolutionary phase, a key parameter for identifying the source of Li enhancement.

Presently, evolutionary phase of most of the Li-rich giants is based on their location in the T_{eff} - L plane of Hertzsprung-Russell (HR) diagram. Such determination is fraught with ambiguity. Uncertainties in derived stellar parameters arising from different methodologies by different studies are often larger than the differences in stellar parameters of T_{eff} and L between different locations in HR diagram. As a result, different scenarios for origin of Li excess in Red giants were suggested. For example, diffusion of Li upwards (in case of sub-giants), some kind of extra-mixing associated with luminosity bump (e.g.,Palacios *et al.* 2001), nucleosynthesis and

dredge-up during He-flash in case of red clump (Kumar *et al.* 2011), and external scenario such as mergers of planet or sub-stellar objects for occurrence of Li-rich giants any where along the RGB (Lebzelter, T. *et al.* 2012). It is important to address the question whether Li-rich phenomenon is confined to a single evolutionary phase or to multiple phases on RGB. For this to be answered one would require independent method.

Asteroseismic analysis is one of the robust methods to separate giants ascending RGB with He-inert core from those with core He-burning (Bedding *et al.* 2011) red clump giants, post He-flash. One could make use of *Kepler* (Borucki *et al.* 2010) time resolved photometric data for this purpose. Unfortunately, none of the known Li-rich giants are in the *Kepler* fields barring a few recently reported ones. To date, there are only six Li-rich giants that were analyzed using *Kepler* and CoRoT asteroseismic data. With the exemption of one (Jofré *et al.* 2015), all the five giants have been found to be He-core burning giants of red clump (Silva Aguirre *et al.* 2014; Carlberg *et al.* 2015; Bharat Kumar *et al.* 2018; Smiljanic *et al.* 2018). It is necessary to conduct a large unbiased systematic survey of Li-rich giants which have asteroseismic data.

In this chapter we discuss the evolutionary phase of Li-rich giants derived based on global asteroseismic parameters of large red giant sample stars. Outline of chapter is as follows. In section 2, we discuss about sample selection. Derivation of Li abundances using low resolution LAMOST spectra and derivation of asteroseismic parameters namely $\nu_{\rm max}$, $\Delta\nu$, ΔP using Kepler data are given in section 3 and 4, respectively. In section 5, we discuss the results.

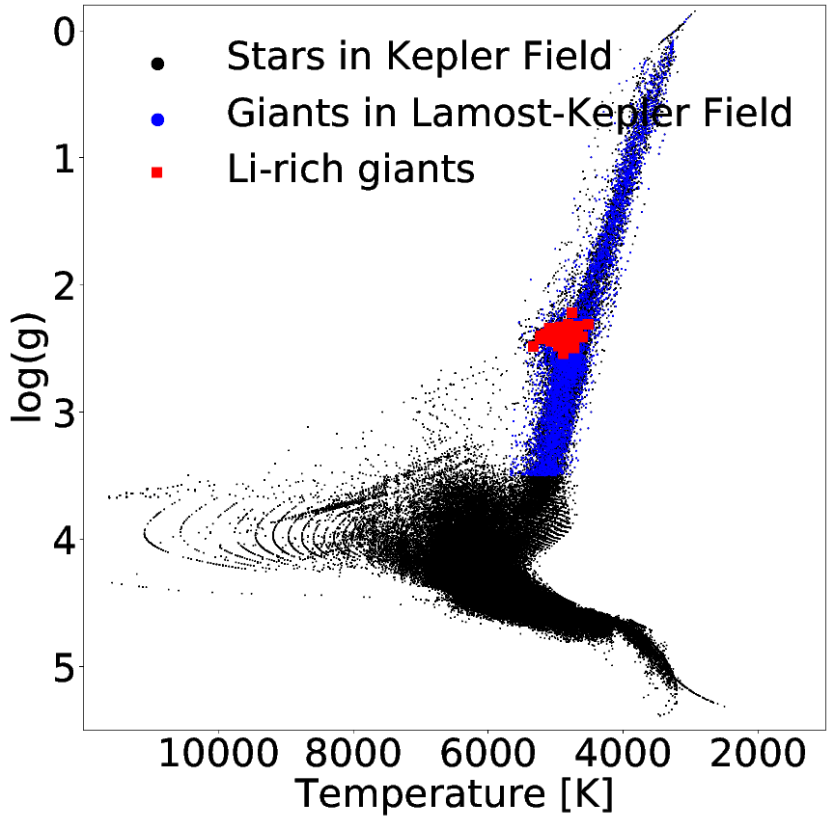

FIGURE 4.1: Survey sample of 12,500 giants (Blue symbols) along with the entire sample from the *Kepler* catalogue as background (black symbols). Red symbols represent giants with strong Li line at 6707Å.

4.2 Sample selection

By applying criterion of log $g \leq 3.5$ and $T_{eff} \leq 5500$ K for RGB giants, we found a sample of 23,000 giants in the *Kepler* Input Catalogue of 197,000 stars. Of which about 12,500 giants are found to be common in LAMOST catalogue of data release 4 (DR4) *. LAMOST is a low resolution ($R = 1800$) spectroscopic survey of stars covering wavelength range of 3700 – 9000 Å. Continuum fitted spectra have been inspected for the presence of Li resonance line at 6707 Å and found 78 spectra with strong Li line. Common sample of giants among *Kepler* and LAMOST (blue dots) along with the entire sample from *Kepler* catalogue (Mathur *et al.* 2017) as background (black dots) are shown in Fig 4.2. Stars that show strong Li line

*http://dr4.lamost.org/

at 6707Å are shown as red squares. Note that all of them are concentrated in a particular range of log g which coincides with positions of both red clump and luminosity bump in HR-diagram.

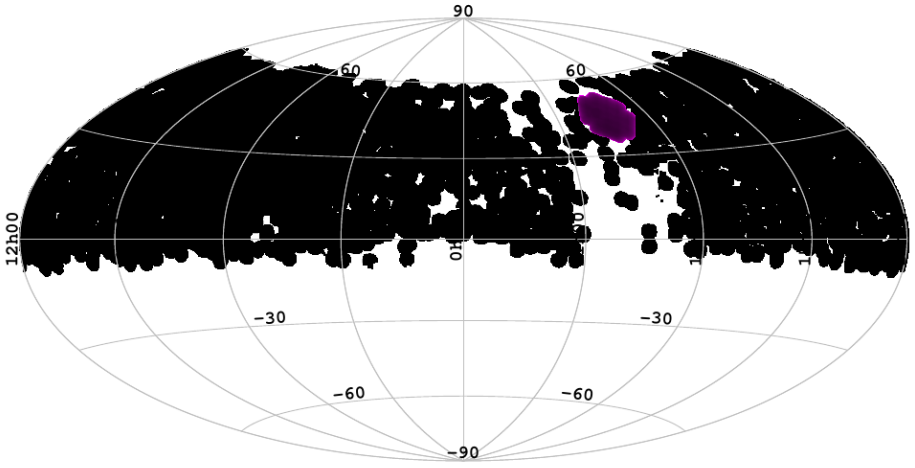

FIGURE 4.2: LAMOST spectroscopic survey field (black colored symbol) compared with the Kepler photometric survey field (red colour). Kepler's survey is a deep survey of a small patch in the sky (100 square degrees).

4.3 Lithium abundance

Spectra of Li-rich giants with strong Li resonance line at 6707 Å are shown in Figure 4.3 along with the known Li-rich giant KIC 12645107 on the top and a normal Li giant at the bottom. For estimating Li abundance from low resolution spectra we used a method that was successfully demonstrated previously by Kumar *et al.* (2011) and Kumar *et al.* (2018a). This method involves measuring of Li line strength at 6707 Å relative to an adjacent Ca I line at 6717 Å, both are zero low excitation potential lines and show similar sensitivity to T_{eff}. The derived ratios of Li 6707 Å core strength to Ca 6717 Å are plugged into correlations between Li abundance and line strength ratios derived by Kumar *et al.* (2018a).

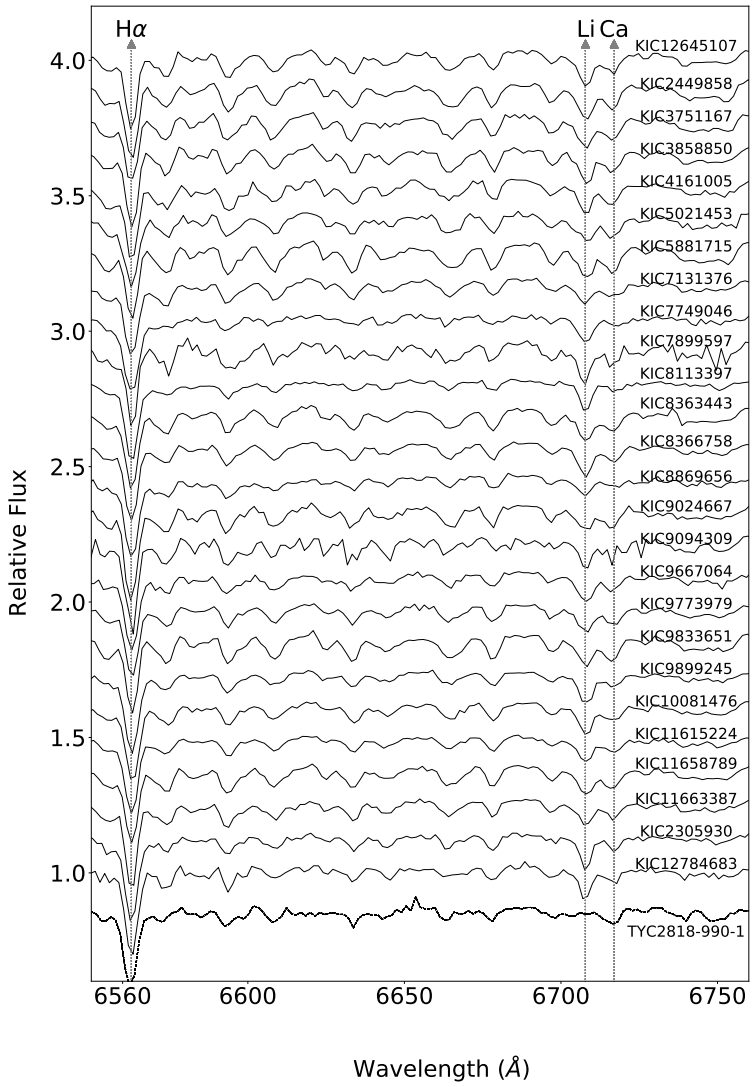

FIGURE 4.3: Spectra of 26 Li-rich giants showing exceptionally strong Li resonance line at 6707Å. Also, shown are the two reference spectra of known super Li-rich giant (KIC 12645107, KIC 2305930) of A(Li)=3.3, 4.1 dex and a normal Li giant of A(Li) = 0.5 dex (bottom, TYC 2818-990-1).

$$\mathrm{A(Li)} = \frac{(\mathrm{Li/Ca}) - (0.133 \pm 0.175)}{0.5447 \pm 0.0572} \tag{4.1}$$

To derive strength ratio of Li and CaI line we first did continuum normalization of wavelength calibrated spectra obtained from LAMOST in IRAF. Then we did radial velocity correction and finally measured strength of Li resonance line at 6708 Å and Ca I line at 6717 Å. Since uncertainties are relatively higher, 0.3 –

0.4 dex, sample has been restricted to only giants with very strong Li line or the estimated Li abundance A(Li) $\geq$ 3.0 dex. This is to avoid mistaking of normal giants with A(Li) $\leq$ 1.8 dex (Iben 1967). We found 26 giants with A(Li) $\geq$ 3.0 dex and half a dozen have A(Li) $\geq$ 4.0 dex, about an order of magnitude more than the current ISM value (3.3 dex), and about a factor of 100 more than the the maximum predicted abundance of A(Li) = 1.8 dex (Iben 1967). Estimated Li abundances along with [Fe/H], $T_{\rm eff}$ and log g (stellar parameters from LAMOST DR4 catalogues) are given in Table 4.1. Two of these have been recently reported as Li-rich giants (Bharat Kumar *et al.* 2018) based on high resolution spectra. We compared difference between Li abundance derived using calibration relations and synthesis method and found that mean difference between the estimated A(Li) in this study and the literature values based on high resolution spectra is 0.2 dex, which agrees well within uncertainties.

4.4 Analysis of asteroseismic data

All the 26 Li-rich giants that are given in Table 4.1 have long cadence (29.4 min) of 10 to 17 quarters *Kepler* photometric data. It is known that red giants show oscillations of mixed modes of gravity (g-mode) arising from the central core and acoustics modes (p-modes) arising in the convective envelope (De Ridder *et al.* 2009; Beck *et al.* 2011). In this work we have used lightkurve package (`https://github.com/KeplerGO/lightkurve`) for merging individual quarters into a combined light curve, and converting the combined light curve into power density spectrum (PDS) using Lomb-Scargle Fourier transform. In Fig 4.4a, power density spectra (PDS) for one of the sample stars of KIC 11615224 from Table 4.1 is given in which solid line is the fitting for background. Background subtracted and smoothed PDS (Fig 4.4b) is used to identify modes and measuring their frequencies.

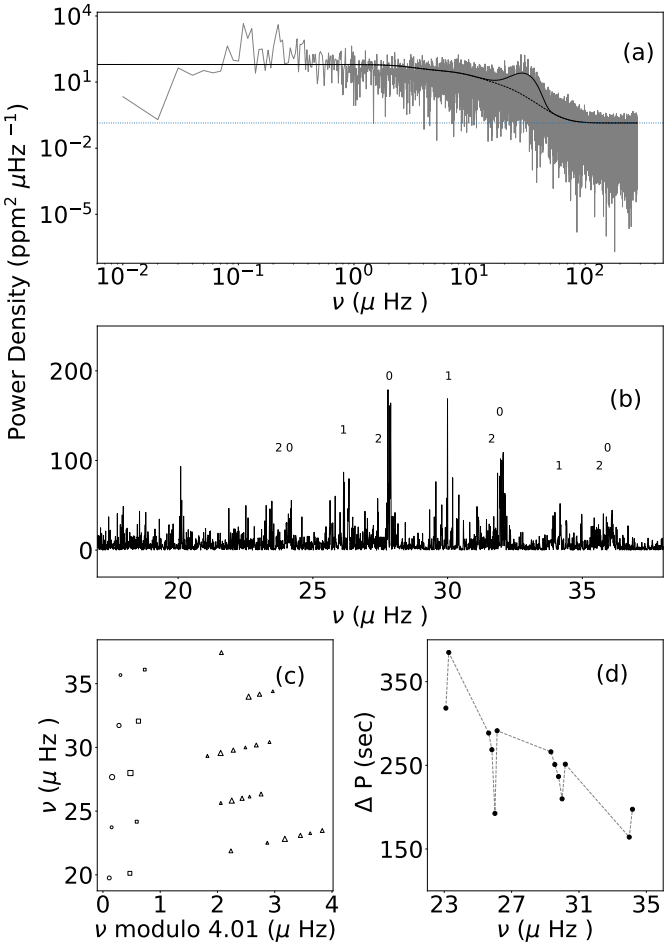

FIGURE 4.4: Top panel: gray region in background is PDS of KIC 11615224 and solid black line is global background fit to the **PDS**. Middle panel: $l = 0, 1, 2$ modes in the **PDS**. Bottom panel: Measurement of large frequency separation and gravity mode period spacing of star. In the bottom left panel circle are modes corresponding to $l = 0$, square corresponding to $l = 2$ and triangle corresponding to $l = 1$ modes.

There are two key parameters: frequency separation between two consecutive radial ($l = 0$) modes ($\Delta\nu$) and period separation between two consecutive dipole ($l = 1$) modes (ΔP) which are used to separate red giants of He-burning core of red clump and He-inert core of RGB (Bedding *et al.* 2011). From the smoothed PDS radial modes $l = 0$, dipole modes ($l = 1$) and quadruple modes ($l = 2$) have been identified and the corresponding frequencies for 4–5 modes ($l = 0$) in each star's PDS are measured. Values of $\Delta\nu$ are those for which modulo or remainder of $\nu/\Delta\nu$ is same for the frequencies of respective measured mode. In Fig 4.4c, this

has been illustrated for a typical giant, KIC 1165224. For its modes of $l = 0$, $l = 2$ and $l = 1$, we found a value of $\Delta\nu = 4.01$ μHz for which modulo is same for all the frequencies. The values of derived large frequency separation, $\Delta\nu$ are given in Table 4.1. After measuring frequency corresponding to detected dipole modes ($l = 1$, g-modes), we calculate the period of dipole modes and period spacing between the consecutive dipole modes which are given in Fig 4.4d. Median value of derived period spacing is considered as gravity mode period spacing of a star (Stello *et al.* 2013). Derived values of $\Delta\nu$ and ΔP, given in Table 4.1, suggest all the Li-rich giants are He-core burning red clump stars. Our analysis agrees well with the recent study done by Yu *et al.* (2018). Average difference between ours and Yu *et al.* (2018) for $\Delta\nu$ and $\nu_{\rm max}$ is 0.8 and 0.1 μHz respectively.

Stellar parameters such as radius and mass have been derived using the seismic parameters and the calibrations are given by (Kjeldsen and Bedding 1995). All the giants are low mass with M $\leq$ 2.0 $M_{\odot}$ (Table 4.1). Further, light curves show no indication of a major flaring activity which is in agreement with lack of visible asymmetry or emission profiles of H_{α} in the spectra (Fig 4.3) indicating no significant stellar activity in the photospheres of the stars.

Galactic membership

Based on precise *Gaia* astrometry and estimated radial velocities from LAMOST spectra we computed kinematic motion (U, V, W) of individual stars in the sample. Further, following the recipe given in Reddy *et al.* (2006) we estimated probability percentage for each giant for being in thin disk, thick disk and halo of the Galaxy. Results show of 26 giants 19 belong to thin disk, 6 belongs to thick disk and one is halo giant.

KIC	Vmag	ΔP	$\Delta\nu$	ν_{max}	A(Li)	T_{eff}	M($M_\odot$)	R($R_\odot$)	log g	[Fe/H]
2305930	11.02	226	4.1	27.2	4.0	4861 ± 40	0.71 ± 0.1	9.40 ± 0.7	2.40 ± 0.1	-0.50 ± 0.0
2449858	13.38	235	3.3	26.8	3.5	4840 ± 30	1.15 ± 0.1	12.1 ± 0.5	2.50 ± 0.1	-0.15 ± 0.0
3751167	13.83	419	4.0	26.1	3.6	4777 ± 239	0.91 ± 0.2	10.9 ± 1.0	2.25 ± 0.2	-1.06 ± 0.2
3858850	12.44	192	3.3	25.9	3.5	4434 ± 50	0.90 ± 0.1	11.1 ± 0.6	2.62 ± 0.1	0.27 ± 0.1
4161005	13.93	247	3.3	29.1	3.9	4897 ± 40	0.93 ± 0.2	10.7 ± 0.8	2.35 ± 0.1	-0.52 ± 0.0
5021453	11.25	314	4.0	31.8	4.0	4754 ± 26	1.02 ± 0.1	10.5 ± 0.6	2.55 ± 0.1	-0.08 ± 0.0
5881715	11.64	191	3.8	30.9	3.4	4786 ± 35	1.85 ± 0.2	14.2 ± 0.7	2.35 ± 0.1	-0.15 ± 0.0
7131376	13.99	190	3.8	34.8	4.1	4696 ± 80	1.18 ± 0.1	10.8 ± 0.4	2.68 ± 0.1	0.08 ± 0.1
7749046	13.47	235	4.2	29.9	3.8	4891 ± 26	1.13 ± 0.1	11.2 ± 0.4	2.36 ± 0.1	-0.71 ± 0.0
7899597	13.61	224	3.9	31.6	3.8	4710 ± 50	1.26 ± 0.2	11.7 ± 0.9	2.49 ± 0.1	-0.10 ± 0.1
8113379	13.13	273	3.2	31.2	3.9	4757 ± 40	1.06 ± 0.1	10.7 ± 0.4	2.53 ± 0.1	-0.06 ± 0.0
8363443	10.95	217	3.5	32.4	3.8	4490 ± 40	1.28 ± 0.1	11.8 ± 0.3	2.58 ± 0.1	0.23 ± 0.0
8366758	12.50	218	3.8	26.4	3.9	4664 ± 50	0.67 ± 0.1	9.3 ± 0.3	2.57 ± 0.1	0.18 ± 0.0
8869656	9.34	240	4.1	30.7	3.8	4764 ± 30	1.15 ± 0.1	11.3 ± 0.5	2.44 ± 0.1	-0.30 ± 0.0
9024667	12.28	449	3.4	25.2	3.5	4555 ± 35	0.83 ± 0.1	10.7 ± 0.7	2.59 ± 0.1	0.16 ± 0.0
9094309	14.31	253	4.0	33.2	4.1	4919 ± 129	1.16 ± 0.1	10.8 ± 0.5	2.55 ± 0.2	-0.32 ± 0.1
9667064	13.35	176	4.4	30.2	3.6	4678 ± 211	1.34 ± 0.2	12.4 ± 0.7	2.28 ± 0.2	-0.10 ± 0.2
9773979	14.30	487	3.2	32.6	4.0	4622 ± 86	1.15 ± 0.2	11.0 ± 0.6	2.48 ± 0.1	-0.05 ± 0.1
9833651	12.52	174	3.6	38.8	4.2	4683 ± 44	1.47 ± 0.1	11.4 ± 0.4	2.67 ± 0.1	0.09 ± 0.0
9899245	13.04	150	3.4	33.2	3.9	4700 ± 30	1.30 ± 0.3	11.6 ± 0.8	2.72 ± 0.1	0.10 ± 0.0
10081476	13.84	211	3.8	26.6	3.4	4453 ± 50	1.07 ± 0.2	11.9 ± 0.8	2.52 ± 0.1	0.24 ± 0.0
11615224	11.16	257	3.3	30.0	4.0	4746 ± 25	0.85 ± 0.1	9.80 ± 0.4	2.40 ± 0.1	-0.04 ± 0.02
11658789	13.36	228	3.9	31.2	4.3	4999 ± 75	0.81 ± 0.1	9.30 ± 0.6	2.48 ± 0.1	-0.70 ± 0.1
11663387	12.59	217	4.0	32.7	4.1	4642 ± 40	1.01 ± 0.1	10.4 ± 0.2	2.49 ± 0.1	0.02 ± 0.0
12645107	11.40	243	3.5	30.4	3.8	4853 ± 40	1.14 ± 0.1	11.2 ± 0.4	2.39 ± 0.1	-0.22 ± 0.0
12784683	11.10	239	3.4	28.7	3.7	4862 ± 25	1.11 ± 0.2	11.4 ± 0.7	2.33 ± 0.1	-0.28 ± 0.0

TABLE 4.1: List of Li-rich giants discovered in this work. A(Li), ΔP and $\Delta\nu$ derived in present work and stellar parameters (T_{eff}, log g, [Fe/H]) are taken from LAMOST DR4 catalog. A(Li) derived from empirical calibration relation, provided in equation 4.1 are also given.

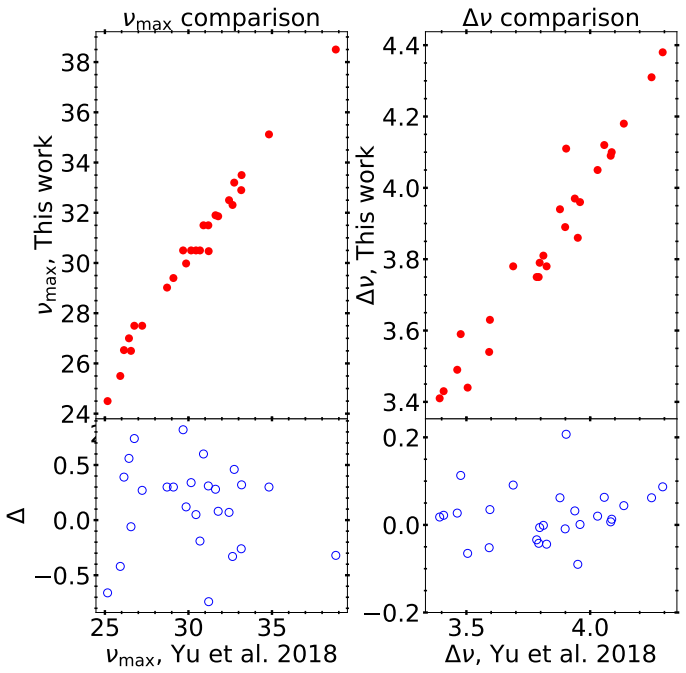

FIGURE 4.5: Comparison of values of large frequency separation, $\Delta\nu$, and frequency of maximum power, $\nu_{\max}$, derived in this study with the values given in the literature Yu *et al.* (2018).

4.5 Discussion

This is the first of its kind survey based on a large unbiased sample survey of giants that are common among LAMOST spectroscopic and *Kepler* photometric surveys. Analysis yielded a total of 26 super Li-rich giants (of which two are already known in the literature). Abundance results along with the derived asteroseismic parameters; $\Delta\nu$ and ΔP are given in Table 4.1, and are shown in the plot of Δp and $\Delta\nu$ (Figure 4.6). Known RC and RGB giants based on asteroseismic analysis form background. As shown in Figure 4.6, all the Li-rich giants from this study show a large values of $\Delta P \geq 150$ sec and small values of $\Delta\nu \leq 5$ μHz, and occupy the He-core burning phase region of $\Delta\nu - \Delta$P diagram (Bedding *et al.* 2011). Interestingly, none of the Li-rich giants found in this survey are on ascending RGB. Results imply Li enhancement phenomenon is most probably associated with He-flash at the tip of RGB or post He-flash rather than on RGB.

KIC	RA	DEC	plx	pmra	pmdec	RV	U	V	W	Pthin	Pthick	Phalo	Membership
2305930	292.11	37.68	1.035±0.02	-5.60	-2.45	-131.28±4.07	-22.880	-132.211	-3.850	11.173	87.430	1.395	2
2449858	292.87	37.70	0.279±0.01	-2.74	-5.88	-45.72±3.49	89.684	-77.506	-12.630	75.312	24.550	0.136	1
3751167	292.57	38.86	0.221±0.01	-2.88	-8.24	-37.85±8.48	165.811	-88.244	-33.129	1.972	93.463	4.564	2
3858850	293.68	38.98	0.602±0.03	-1.86	3.744	-32.07±3.54	-28.843	-28.454	21.620	96.977	3.0188	0.003	1
4161005	292.39	39.23	0.245±0.02	-1.33	-6.99	-2.27±4.83	126.879	-35.766	-39.358	53.042	46.694	0.262	1
5021453	294.66	40.10	0.769±0.02	-6.33	-12.50	-12.35±3.81	79.680	-35.234	-4.6116	96.444	3.549	0.006	1
5881715	293.50	41.14	0.576±0.02	-6.99	-7.46	7.42±3.92	79.072	-18.402	23.065	90.662	9.321	0.016	1
7131376	295.60	42.68	0.297±0.02	-2.77	-3.82	-50.68±4.05	60.739	-67.490	1.0189	91.844	8.132	0.023	1
7749046	290.41	43.42	0.243±0.01	-10.54	-7.13	-250.91±4.34	138.368	-317.535	65.417	0.0001	0.002	99.997	3
7899597	294.70	43.64	0.263±0.01	-2.078	-5.82	-67.29±4.27	93.230	-86.219	-28.407	45.605	53.948	0.445	1
8113379	296.93	43.93	0.365±0.03	-0.49	-7.77	5.15±4.04	91.452	-6.903	-42.862	81.684	18.278	0.0364	1
8363443	291.03	44.38	1.050±0.02	-5.17	-15.03	-29.16±3.45	63.131	-42.350	-14.842	96.965	3.0295	0.005	1
8366758	292.27	44.39	0.591±0.03	-3.19	-6.80	-14.63±3.78	55.577	-27.239	-4.5221	98.319	1.6783	0.002	1
8869656	284.87	45.13	2.060±0.02	-13.20	-16.45	-23.75±4.13	38.156	-37.716	6.496	97.974	2.0225	0.0025	1
9024667	292.81	45.36	0.599±0.02	-1.86	-9.97	-27.61±3.49	70.815	-37.768	-27.625	94.792	5.198	0.009	1
9094309	293.84	45.41	0.178±0.01	-1.46	-5.36	-34.9±4.92	135.525	-56.319	-37.378	30.861	68.453	0.685	2
9667064	298.18	46.36	0.269±0.02	-1.50	-0.92	-1.27±4.15	26.4111	-8.051	14.353	98.281	1.717	0.001	1
9773979	293.28	46.54	0.215±0.01	-3.93	-8.90	-76.83±4.10	196.306	-111.191	-27.426	0.0576	79.554	20.387	2
9833651	292.98	46.66	0.495±0.02	-4.21	-6.61	3.57±3.56	73.632	-12.177	8.383	96.938	3.057	0.004	1
9899245	295.17	46.77	0.357±0.02	-1.45	-4.50	-13.59±3.10	58.928	-21.633	-13.408	98.280	1.717	0.002	1
10081476	294.30	47.07	0.274±0.01	-1.73	-5.12	-38.76±3.61	85.087	-50.367	-21.966	91.443	8.533	0.023	1
11615224	294.14	49.64	0.700±0.03	-16.27	-25.27	-41.07±3.48	194.471	-71.458	11.322	1.5714	91.966	6.462	2
11658789	290.09	49.71	0.307±0.01	4.05	-6.13	-128.64±6.37	45.458	-105.908	-126.795	0.0001	86.267	13.732	2
11663387	292.72	49.71	0.518±0.02	-1.83	-5.87	1.02±3.72	55.561	-4.780	-7.674	98.606	1.392	0.001	1
12645107	289.30	51.75	0.697±0.02	-0.65	-11.75	-15.77±4.55	73.937	-16.316	-30.279	95.412	4.580	0.006	1
12784683	290.12	52.05	0.757±0.02	-6.74	-7.70	-10.23±3.84	58.898	-22.277	15.914	96.426	3.568	0.004	1

TABLE 4.2: Membership study of sample stars. Parallax and proper motion adopted from *Gaia* DR2 and radial velocity is taken from LAMOST DR4 catalog. We gave membership based on maximum probability except one star KIC 7899597 where probability are almost similar. We consider this star as thin disk star (its metallicity [Fe/H]=-0.10).

As earlier stated, there are only six Li-rich giants for which evolutionary phase is determined directly using asteroseismology. All of them were discovered serendipitously. Of which five are unambiguously classified as giants of He-core burning phase in red clump region (Silva Aguirre *et al.* 2014; Carlberg *et al.* 2015; Bharat Kumar *et al.* 2018; Smiljanic *et al.* 2018) and one as RGB near the bump(Jofré *et al.* 2015). The lone exception being the KIC 9821622 (Jofré *et al.* 2015). Though this is a bonafide RGB star with inert He-core and H-burning shell ($\Delta\nu$ =6.07 μHz and $\Delta P = 67.6$ sec) its categorization as Li-rich giant is not beyond doubt as the Li abundance (LTE: A(Li)= 1.49 dex and NLTE: 1.65 dex) measured from well defined and much stronger line at 6707 Å is at the borderline. It is important

to establish whether this particular star is indeed a Li-rich giant as it has serious implications for identifying source of Li enrichment in red giants.

Of course, there are many Li-rich giants in literature which were reported as being on RGB based on their positions in the HR-diagram. This method found to be uncertain in determining exact evolutionary phase. For example, of the five asteroseismically known Li-rich RC giants, KIC 4937011 was initially reported as RGB star below the bump by Anthony-Twarog *et al.* (2013); Carlberg *et al.* (2015) based on its location in HR diagram. However, its derived asteroseismic parameters $\Delta\nu = 4.15$ μHz and $\Delta P = 249.9$ sec (Vrard *et al.* 2016) firmly puts the giant in He-core burning phase. This illustrates the difficulty of determining their precise evolutionary phase. We also note another recent study by Yan *et al.* (2018) in which they reported TYC 429-2097-1 as the most Li-rich giant with A(Li)= 4.51 dex and located at the bump based on their location in HR-diagram. This star is not in the *Kepler* field. However, its derived ratio of $[C/N] = -0.47 \pm 0.10$ is more compatible with it being in red clump (Hawkins *et al.* 2016; Singh *et al.* 2019b). In fact, Casey *et al.* (2016) made an important observation that although the stellar parameters of majority of Li-rich giants is consistent with being on RGB at or below the luminosity bump, they are each individually consistent with being RC. However, they couldn't conclude that they are indeed RC giants based on available data to them. Does this mean, a number of Li-rich giants that are reported as RGB giants based on L and T_{eff} are misclassified? Results in this study seem to suggest false classification is a real possibility.

Due to ambiguity in their evolutionary phase, numerous models have been constructed to explain Li excess with prevailing conditions at each of the suggested multiple phases on RGB. Broadly, theoretical models fall into two categories: external and in-situ scenarios. One of the external scenarios is merger of planets or sub-stellar objects such as brown dwarfs. This is invoked with the expectation that planet or brown dwarfs contain reservoir of primordial Li with little/no depletion,

and their mergers will enhance star's photospheric Li abundance either by direct addition of Li reservoir to the photosphere or by induced mixing due to angular momentum transfer to the star or a combination of the both (see e.g.; Siess and Livio 1999; Casey *et al.* 2016). This scenario gained merit with the evidence that the large planets in close-in orbits among sub-giants are less frequent compared to their counter parts on main sequence stars (Villaver *et al.* 2014).

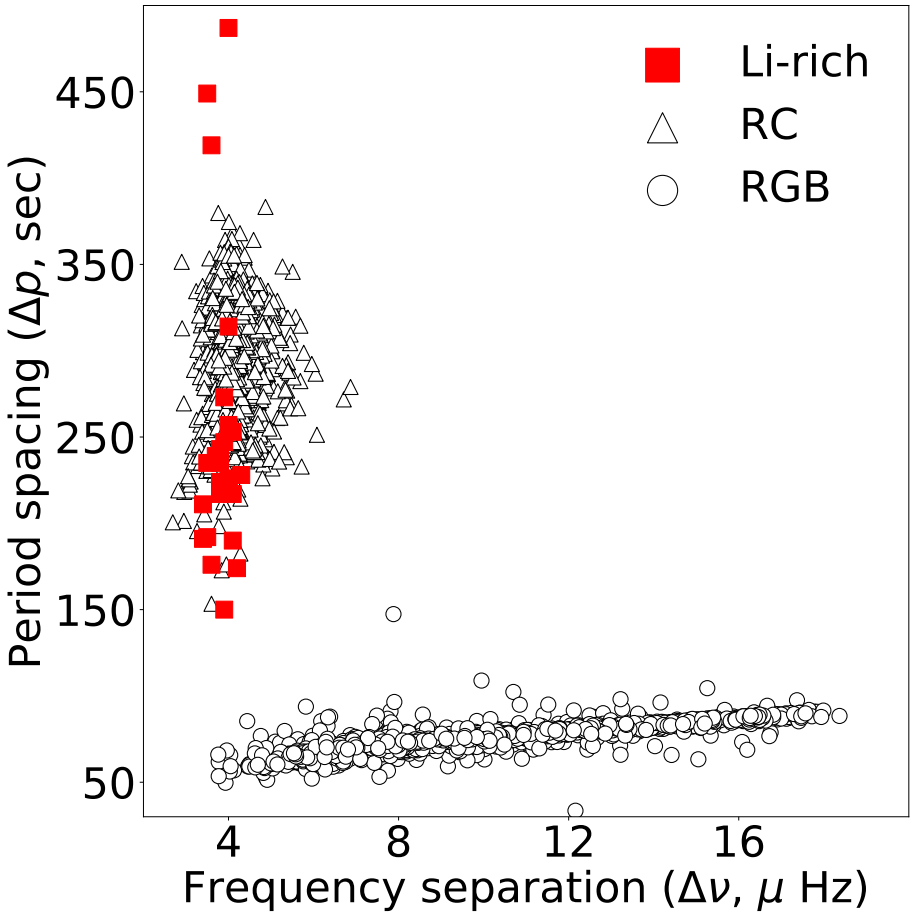

FIGURE 4.6: Li-rich giants discovered in this study (red squares) are shown in $\Delta\nu - \Delta P$ asteroseismic diagram. Giants classified based on asteroseismic analysis form the background: He-core burning RC giants (open triangle) and inert He-core giants ascending RGB first time (open circle). Note, all the Li-rich giants fall in the RC region of the diagram.

However, to account for levels of Li seen in many of the super Li-rich giants, one would require merger of several Jupiter size planets having undiluted Li reservoir (Carlberg *et al.* 2012). Merger of such large number of planets is very unlikely.

Also, theoretical models put a maximum limit of Li abundance due to such mergers at A(Li)= 2.2 dex (Aguilera-Gómez *et al.* 2016). Further, contrary to our results engulfment scenario suggests occurrence of Li-rich giants anywhere along the RGB and presence of infrared excess as a result of merger impact. Results support the argument by Deepak and Reddy (2019) against external scenario based on the frequency of Li-rich giants occurring at various phases. They show that disproportionately large number of Li-rich giants belong to red clump compared to any other phase on RGB.

Second scenario is in-situ origin which is Li production via Cameron & Fowler mechanism (Cameron and Fowler 1971), $^{3}\mathrm{He}(\alpha,\gamma)^{7}\mathrm{Be}(e^{-},\nu)^{7}\mathrm{Li}$. In case of Li enhancement in the photospheres of highly evolved massive ($\geq 3-4\ M_{\odot}$) asymptotic giants branch (AGB) stars (Smith and Lambert 1989) this mechanism is expected to operate just below the convective envelope which is hot enough to produce ^{7}Be and close enough for ^{7}Be to get transported to cooler upper layers where it can form ^{7}Li. This process is known as Hot Bottom burning (HBB). In case of low mass RGB giants convection between the H-burning shell and the outer convective layers is inhibited by the radiative zone, and standard models (Iben 1967) do not predict changes in abundances post 1st dredge-up. However, observations of giants post 1st dredge-up do show severe depletion of Li and reduction in the $^{12}\mathrm{C}/^{13}\mathrm{C}$ ratios (Gilroy and Brown 1991) compared to standard models of 1st dredge-up on RGB Iben (1967). For example, severe depletion of Li starting from the bump has been well illustrated for giants in globular cluster NGC 6397 by Lind *et al.* (2009b). These anomalies were explained by extra mixing at the luminosity bump at which the barrier for the deep mixing is erased (see for example Eggleton *et al.* 2008). Ironically, bump has also been suggested as a source of Li enhancement (Palacios *et al.* 2001; Charbonnel 2005; Denissenkov *et al.* 2009) as many early observations showed Li-rich giants coinciding with the bump in the HR-diagram (Charbonnel and Balachandran 2000; Kumar and Reddy 2009). It would be a challenging task for explaining Li enhancement at the same phase where severe Li

depletion is known to occur. Even if we assume bump as the origin for Li excess, it is unlikely Li can survive through deep convection phase from bump to the clump, and importantly, sustaining high levels of Li abundances seen in many of the super Li-rich giants. Given the Li-rich phase of RGB is a transient phenomenon lasting for a short period of about 6 M years (Palacios *et al.* 2001) compared to, for example, 50–100 M years (see also Deepak and Reddy (2019)) long evolutionary period from the bump to the RGB tip, it is very unlikely the high Li abundances seen in these red clump stars originated at the luminosity bump.

4.6 Summary

In this study we addressed one of the long standing problems of precisely determining stellar evolutionary phase of Li-rich giants. Results are based on a large unbiased sample of 12,500 low mass RGB giants common among *Kepler* photometric and LAMOST spectroscopic surveys. We found 24 new Li-rich giants with Li abundance of A(Li) $\geq$ 3.0 dex, more than an order of magnitude larger compared to the maximum predicted abundance of A(Li) = 1.80 dex. Importantly, the derived asteroseismic parameters; $\Delta\nu$ and ΔP show all the Li-rich giants are in He-core burning phase, and are at red clump region. This is the most unambiguous evidence so far suggesting that the Li enhancement phenomenon is probably associated only with He-core burning phase rather than on RGB with inert He-core. He-flash at the tip, an immediate preceding event to red clump, may be explored for Li excess in red clump giants. We explored this issue further in Chapter 6.

Chapter 5

Reanalysis of KIC 9821622: A bona fide RGB giant classified as Li-rich

This chapter provides a detailed description of the reanalysis of the only reported Li-rich giant (KIC 9821622), which has been classified as a giant ascending RGB for the 1st time. We did this analysis to understand whether Li enhancement in RGB giants has multiple sources or a single source. Our results are based on reanalysis of multiple high-resolution spectra, which resulted in $A(Li)_{LTE} = 1.42 \pm 0.05$ dex. After correcting for non-local thermodynamic equilibrium (NLTE), we have $A(Li)_{NLTE} = 1.57 \pm 0.05$ dex, which is significantly less than the reported $A(Li) = 1.80 \pm 0.2$ dex. We found that the subordinate line at 6103 Å is too weak or absent from measuring Li abundance. The derived abundance is normal for red giants undergoing dilution during the first dredge-up. Since all known *Kepler* field Li-rich giants belong to the red clump region, this clarification removes the anomaly and strengthens the evidence that Li enhancement in low-mass giants may be associated only with the He-core burning phase. The origin of Li excess

probably lies during the He flash at the RGB tip, a phase immediately preceding the red clump. The results in this chapter are published in MNRAS (Singh et al. 2020).

5.1 Introduction

It is now accepted that a small group of red giants exists with significantly higher photospheric Li abundances compared with the maximum values of A(Li) = 1.6–1.8 dex predicted by standard models(Iben 1967; Lagarde *et al.* 2012). In some cases, Li abundances in these giants exceed predictions by a factor of 10-1000 (Brown *et al.* 1989; Yan *et al.* 2018). However, the origin of high Li abundance in these giants has been a subject of debate for over three decades since their first discovery in 1982 (Wallerstein and Sneden 1982). This is mainly because of a lack of precise determination of the exact location of Li-rich giants on the red giant branch (RGB; see e.g. Charbonnel and Balachandran (2000)). In particular, there is uncertainty in determining whether a particular Li-rich giant is at the RGB bump or the red clump, as their positions overlap in the T_{eff}–L plane (Kumar *et al.* 2011). This uncertainty has led to multiple theories (e.g. (de La Reza *et al.* 1996; Drake *et al.* 2002; Siess and Livio 1999; Palacios *et al.* 2001; Denissenkov and Herwig 2004; Denissenkov 2012)).

Now it is possible, thanks to *Kepler* (Borucki *et al.* 2010) asteroseimic data, to separate giants with inert He-core ascending RGB for the first time from those of red clump giants of He-core burning (Bedding *et al.* 2011). A recent study by Singh *et al.* (2019a) showed that all Li-rich giants for which asteroseismic analysis is available are indeed red clump giants in the He-core burning phase. This is quite significant as this survey is based on large unbiased data set drawn from *Kepler* (Borucki *et al.* 2010) and LAMOST (Cui *et al.* 2012) catalogs. This study

reconfirms earlier serendipitous discoveries of five Li-rich giants, all of them have been classified as red clump giants based on asteroseismic data (Silva Aguirre *et al.* 2014; Carlberg *et al.* 2015; Bharat Kumar *et al.* 2018; Smiljanic *et al.* 2018). The mounting evidence that Li-rich phenomenon is probably associated only with He-core burning giants, post-He-flash, has been further strengthened by a recent large survey of Li-rich giants among GALAH (De Silva *et al.* 2015) and Gaia (Gaia Collaboration *et al.* 2016, 2018) catalogs by Deepak and Reddy (2019), in which they showed a vast majority of Li-rich giants belong to red clump region.

KIC 9821622 is the lone exception among Li-rich giants for which stellar evolutionary phase is determined using robust asteroseismic technique. Exception being, it is the only bonafide red giant with inert He-core reported as Li-rich giant (Jofré *et al.* 2015) and all the others are associated with core He-burning phase of red clump, post He flash. It is interesting to see whether this star is indeed a Li-rich giant as its Li abundance is very close to the border. Understanding of its Li-rich status has implications for Li origin scenarios. If this is indeed a Li-rich giant as reported, one may have to revoke multiple theories for Li enrichment among red giants such as planet engulfment for occurrence of Li-rich giants anywhere along the RGB (e.g.; Siess and Livio 1999) or extra mixing during bump luminosity, and He-flash combined with non-canonical mixing for Li-rich RC giants, etc. Otherwise, these results will constrain models to look for Li-excess origin among red clump giants.

In this chapter, we have discussed the re-analysis of KIC 9821622, a lone Li-rich giants classified as RGB. The chapter is outlined as follows: Section 2 describe data acquisition and analysis. Section 3 explain estimation of A(Li) using currently derived stellar parameters. Section 4 presents discussion with other literature data and section 6 contains conclusions..

5.2 Data acquisition

For this study, we used wavelength calibrated and continuum normalized spectra taken using GRACES spectrograph equipped to Gemini telescope https://www.gemini.edu/sciops/instruments/graces/2015-onsky-tests. The Gemini Observatory is made of two 8.1 meter diameter optical-infrared telescope. They are located in Hawaii and Chile. Spectra has spectral resolution of R≈67500, wavelength range of 3990 -10479 Å, and S/N ≈ 150 for median combined spectra. We also used reduced spectra from Subaru archive https://smoka.nao.ac.jp/ with spectral resolution of R≈80000 and S/N ≈ 50. This star was observed using High Dispersion Spectrograph (HDS) instrument mounted in the Subaru Telescope. Subaru Telescope is a 8.2 m primary mirror telescope located in Hawaii, Maunakea peak at altitude of 4139m. Subaru Telescope is operated by National Astronomical Observatory of Japan (NAOJ). We did continuum normalization of this spectra following standard technique in IRAF.

5.3 Atmospheric Parameters and Li abundance

Stellar atmospheric parameters ($T_{\rm eff}$, log g, [Fe/H]) and $\xi_{\rm t}$ were derived using LTE stellar atmospheric models (Castelli and Kurucz 2004) and MOOG (Sneden 1973). For this, a good number of Fe I and Fe II with well determined oscillator strengths and relatively free of blends were taken from Reddy *et al.* (2003); Ramírez and Allende Prieto (2011); Carlberg *et al.* (2012). $T_{\rm eff}$ was derived through iterative process in which derived Fe I abundance is independent of line low excitation potential for a set of given log g, microturbulance (ξ_t) and [Fe/H]. Similarly, $\xi_{\rm t}$ was derived for which Fe I abundance is independent of line equivalent widths, and log g is the one for which derived abundances of Fe I and Fe II are equal. Uncertainties in $T_{\rm eff}$ and $\xi_{\rm t}$ were evaluated based on sensitivity of the slope of

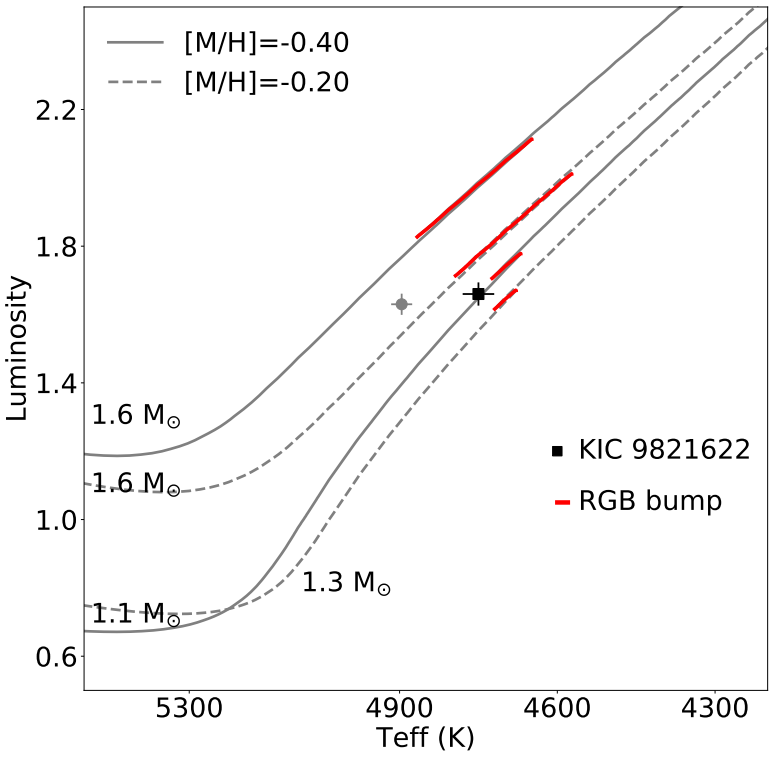

FIGURE 5.1: KIC 9821622 in the HR-diagram. Evolutionary tracks are from Parsec model grids. Dotted tracks are scaled up tracks for $[\alpha/\mathrm{Fe}] = 0.32$ for the same derived mass of 1.6 $M_{\odot}$ (see text for more details). Note, star's position is below the luminosity bump.

relation between abundances and LEP, and abundances and EWs to changes in respective parameters. The derived values are given in Table 5.1. T_{eff} was also derived from photometry using (V-K) calibration from Alonso *et al.* (1999) (See Table 5.2). Our derived values are similar to the values derived by Jofré *et al.* (2015) and infrared APOGEE spectra (Majewski *et al.* 2017). However, these values are cooler by about 140 K compared to two other recent studies by Takeda and Tajitsu (2017); Yong *et al.* (2016) (See Table 5.1). The stellar age along with mass, radius, and log$g$ are computed from asteroseismic parameters (ν_{max}, $\Delta\nu$) and derived spectroscopic parameters ([Fe/H], T_{eff}) using PARAM based on Bayesian statistics* code (da Silva *et al.* 2006). Derived values are given in Table 5.2. However, the calibration relation (Kjeldsen and Bedding 1995) for the same input

*http://stev.oapd.inaf.it/cgi-bin/param_1.3

Parameter	J15	T17	Y16	This work
T_{eff} (K)	4725 ± 20	4896	4895	4750±30
[Fe/H]	-0.49 ± 0.03	-0.25	-0.40	-0.49±0.06
ξ_t (Km s^{-1})	1.12 ± 0.04	1.03	1.18	1.08±0.1
log g	2.71 ± 0.09	2.91	2.71	2.73±0.1
vsini (Km s^{-1})	1.01 ± 0.77	1.9	—	1.9±0.5
A(Li)6103	1.80 ± 0.04	1.67	—	—
A(Li)6707	1.49 ± 0.02	1.85	1.63	1.42±0.05

TABLE 5.1: Stellar parameters and Li abundance of KIC 9821622 from 4 different studies, three from literature and one current study. J15 stands for Jofré *et al.* (2015), T17 for Takeda and Tajitsu (2017) and Y16 for Yong *et al.* (2016).

asteroseismic parameters and derived T_{eff} returns mass of 1.62 ± 0.05 $M_\odot$. Note, there is no [Fe/H] parameter in this relation.

The adopted T_{eff} = 4750 K and luminosity, derived using *Gaia* astrometry, combined with PARSEC evolutionary tracks (Bressan *et al.* 2012) as shown in Figure 5.1 suggest stellar mass is close to 1.1 $M_\odot$ which is significantly less than the mass = 1.62 $M_\odot$ derived from asteroseismology. However, higher T_{eff} = 4890 K derived by Yong *et al.* (2016); Takeda and Tajitsu (2017) yield mass which is close to the value derived from asteroseismology. In either case, star's position is below the luminosity bump (See Figure 5.1). We tested whether the input value of T_{eff} in deriving mass using asteroseismic parameters plays a role. We find little difference in mass ($\approx$ 0.1 $M_\odot$) from the two values of T_{eff}. Since the adopted T_{eff} in this study seems to be robust as this agrees well with the least extinction affected (V-K) colour temperature and values from the APOGEE infrared spectra (see Table 5.2), the discrepancy in T_{eff} and, thereby, in its mass is, probably, due to giant's peculiar nature. KIC 9821622 is a known member of a small group of young α- and r-process enriched giants (Matsuno *et al.* 2018). It has [α/Fe] =

0.32 dex, which is quite high for its [Fe/H] = −0.49 dex (Reddy *et al.* 2003). If we use α-enhanced evolutionary tracks instead of normal ones, the discrepancy in mass will significantly reduce as α enhanced tracks of same mass are relatively cooler compared to normal ones (see, Fu *et al.* 2018). A scaled-up model based on Fu *et al.* (2018) study will be metal-rich by about 0.3 dex for [α/Fe] = 0.32 dex enhanced models. The scaled model of 1.6 $M_{\odot}$ is shown as dotted lines in Figure 5.1. As shown, the discrepancy in mass derived from asteroseismic analysis and α-element enhanced evolutionary tracks is small about 0.15 $M_{\odot}$. For the same parameters with scaled-up [Fe/H] = -0.2 dex, PARAM returns a mass of 1.51 $M_{\odot}$. This amounts to a gap of 40 K to 50 K in $T_{\rm eff}$ between the two extreme masses. Also, note among various RGB evolutionary tracks there is an uncertainty of about 50 - 60 K (see e.g.; Tayar *et al.* 2017; Choi *et al.* 2018).

Li-abundance is derived from Li-resonance line at 6707.78 Å using GRACES spectrum of S/N ≈ 150 by comparing synthetic spectra to observed one (see left panel of Figure 5.2). Synthetic spectra is generated using Kurucz model atmosphere (Castelli and Kurucz 2004) and LTE radiative transfer code MOOG, using 'synth' driver (Sneden 1973). For spectral synthesis, we used line list compiled by Reddy *et al.* (2002) for a resonance line at 6707 Å which includes hyperfine structure and molecular lines. We also examined spectra synthesized using the same line list used by Jofré *et al.* (2015) and find no significant difference between the two line lists. Synthetic spectra computed for A(Li)= 1.42 dex well matches with the observed line profile with an uncertainty of 0.05 dex which is a cumulative uncertainty estimated by quadratic sum of uncertainties in derived stellar parameters. Our derived abundance is very similar to the value A(Li) = 1.49 dex obtained by Jofré *et al.* (2015) from the same Li line. However, our value is about 0.2 dex lower than the value derived by Yong *et al.* (2016) which is expected as their $T_{\rm eff}$ is higher by about 150 K. Both Jofré *et al.* (2015) and Yong *et al.* (2016) used Gemini GRACES spectra. On the other hand Takeda and Tajitsu (2017) used Subaru spectra of S/N ≈ 50. They report significantly higher A(Li) = 1.85 dex.

Star	KIC 9821622	Remarks
RA	19:08:36.16	
Dec	46:41:21.25	
Vmag	12.22 ± 0.04	APASS
Parallax (mas)	0.556 ± 0.02	Gaia DR2
$\log(L/L_{\odot})$	1.66 ± 0.034	
$\Delta\Pi_1$ (sec)	67.6 ± 1.6	Mosser *et al.* (2014)
$\Delta\nu$	6.02 ± 0.015	Yu *et al.* (2018)
$\nu_{\rm max}$	63.39 ± 0.57	Yu *et al.* (2018)
log g_{seis}	2.71 ± 0.03	
Vmacro	3.7	
A(Li)$_{LTE}$	1.42 ± 0.05	
A(Li)$_{NLTE}$	1.57 ± 0.05	
[Eu/Ba]	0.53 ± 0.1	
[C/N]	0.20 ± 0.02	
N/O	0.15	
Age (Gyr)	2.482 ± 0.164	PARAM
Mass ($M_{\odot}$)	1.465 ± 0.033	PARAM
R ($R_{\odot}$)	8.942 ± 0.095	PARAM
log g	2.693 ± 0.003	PARAM
Photometry		
(B-V)	1.012 ± 0.04	
Teff (B-V)	4665 ± 60	
(V-K)	2.378 ± 0.04	
Teff (V-K)	4730 ± 40	
APOGEE		
$T_{\rm eff}$	4744 ± 69	
log g	2.493 ± 0.08	
[Fe/H]	-0.358 ± 0.029	

TABLE 5.2: Asteroseismic parameters, Li abundance and abundance ratio of few other elements of KIC 9821622.For comparison stellar parameters from APOGEE data and derived using photometry are also provided. Age, mass, radius and log g are derived using online code PARAM (http://stev.oapd.inaf.it/cgi-bin/param).

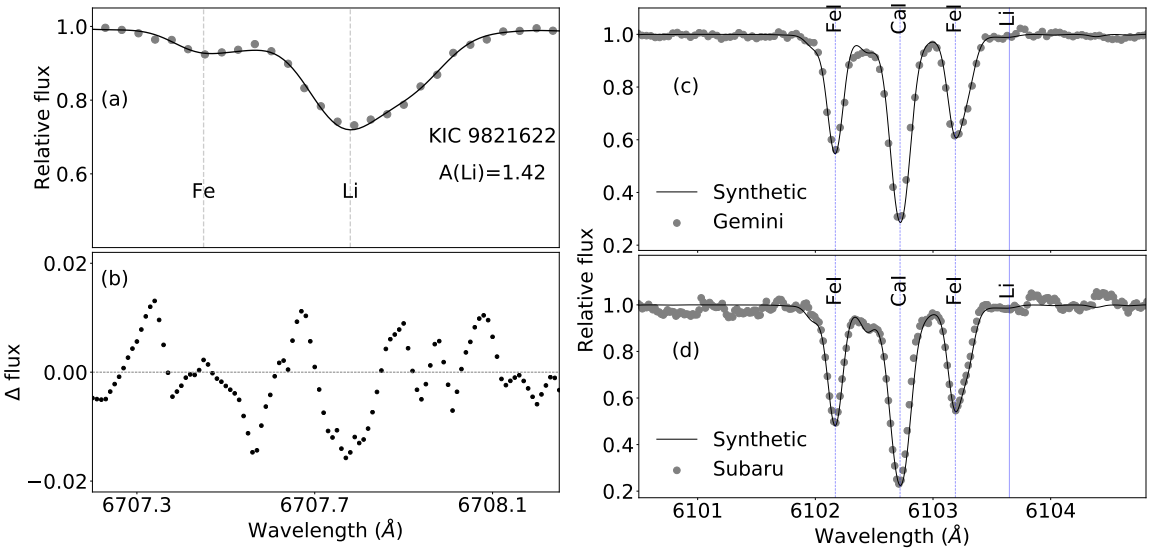

FIGURE 5.2: Panel (a): Comparison of observed Gemini and synthetic spectra at Li resonance line, 6707.78 Å for different Li abundances. Synthetic spectra (black solid line) for A(Li)=1.42 dex best fits the observed line. In panel (b) difference between observed and best fit synthetic spectra is shown. In panel (c) and (d): Synthesis of Gemini and Subaru spectra in the region of 6100–6105 Å respectively. Subordinate Li line is not visible because of relatively low SNR.

Derived Li abundance from all the three studies along with ours are given in Table 5.1. Apart from the resonance line at 6707 Å there is another Li transition of Li at 6103 Å which is weak, generally seen in stars with large Li abundances. In right panel of Figure 5.2, we displayed spectra of KIC 9821622 at 6103 Å region taken from both Gemini GRACES and Subaru. Li transition at 6103 Å line is not seen in either of the spectra. The reported A(Li) = 1.80 dex from this line by Jofré *et al.* (2015) appears to be an upper limit. Yong *et al.* (2016) performed abundance analysis but didn't report Li abundance from 6103 Å line. Given the well defined Li transition at 6707 Å and its reliability for A(Li) measurement, and absence of Li transition at 6103 Å, we don't consider Li abundance reported from 6103 Å line any further.

Other elemental abundances

We also derived abundances of other elemental abundances using EW and synthesis methods. Apart from Li and CNO elements we derived abundances of other elements as given table 5.3. Abundance of carbon, nitrogen and *s*-process elements (Ba, Y and La) are consistent with the typical star in red giant branch phase in comparable metallicity range. KIC 9821622 has abnormally high abundance of α-elements (O, Mg, Si, Ca, Ti) with $[\alpha/\mathrm{Fe}] = 0.32$ dex. This is unusually high for star of age 2.48±0.16 Gyr. Fe-peak elements ((Sc, V, Cr, Ni)) abundance of this star also deviate from usual trend.

5.4 Discussion

What is the expected photospheric Li abundance in RGB stars? According to standard models (Iben 1967) Li abundance is a function of stellar mass and its initial Li abundance with which stars evolved off. Also, to certain extent, it is metallicity dependent. Opacity is relatively lower in lower metallicity stars, and hence less efficient mixing during their evolution on RGB compared to metal-rich stars of same metallicity (Lagarde *et al.* 2012). As a result, rate of photospheric Li abundance depletion is lower in low metallicity giants of same mass. Further, standard models predict depletion of Li abundance only during 1st dredge-up, and expected no further dilution as the convection envelope recedes from the hydrogen burning shell. Standard models (Iben 1967) set 1st dredge-up depletion upper limits of about A(Li) = 1.6 to 1.8 dex for Li normal giants of mass between 1.0 to 1.5 $M_{\odot}$.

However, dilution of Li post 1st dredge-up seems to happen as giants evolve with luminosity via bump as neatly illustrated by observations of giants in globular

X	[X/H]	[X/Fe]	J15[X/Fe]
NaI	-0.20±0.13	0.29 ±0.13	0.23±0.01
MgI	-0.02± 0.05	0.48 ±0.06	0.28±0.08
AlI	0.04± 0.05	0.54 ±0.05	0.35±0.04
SiI	-0.00± 0.03	0.50 ±0.03	0.30±0.06
KI	0.23± 0.07	0.73 ±0.07	—
CaI	-0.24± 0.04	0.26 ±0.02	0.20±0.04
ScI	-0.33± 0.08	0.17 ±0.06	0.10±0.03
ScII	-0.27± 0.08	0.20 ±0.05	0.10±0.03
TiI	-0.14± 0.06	0.36 ±0.04	0.28±0.04
TiII	-0.19± 0.08	0.28 ±0.05	0.28±0.04
VI	-0.25± 0.07	0.25 ±0.05	0.18±0.03
CrI	-0.46± 0.05	0.04 ±0.02	0.00±0.04
CrII	-0.21± 0.05	0.26 ±0.02	0.00±0.04
MnI	-0.39± 0.09	0.11 ±0.07	-0.13±0.04
CoI	-0.34± 0.06	0.16 ±0.04	0.04±0.04
NiI	-0.27± 0.06	0.23 ±0.02	0.03±0.04
CuI	-0.35± 0.09	0.15 ±0.07	0.04±0.04
YII	-0.44± 0.09	0.03 ±0.07	-0.03±0.06
BaII	-0.49± 0.10	-0.02 ±0.07	-0.14±0.06
LaII	-0.30± 0.09	0.17 ±0.06	0.13
CeII	-0.49± 0.10	-0.02 ±0.08	—
NdII	-0.32± 0.09	0.15 ±0.06	0.05±0.17
EuII	0.07± 0.09	0.54 ±0.07	0.52±0.12

TABLE 5.3: The elemental abundance of KIC 9821622. Errors in abundances are quadratic sum of errors propagated from uncertainties in T_{eff}, log g, [Fe/H] and ξ_t. In the last column, abundances are provided from Jofré *et al.* (2015) for comparison. We measured abundance of two more elements, K and Ce, which were not present in Jofré *et al.* (2015). The elemental abundances of the sun are adopted from Asplund *et al.* (2009).

cluster NGC 6397 (Lind *et al.* 2009b) and predicted by theoretical models of extra mixing (e.g. Lagarde *et al.* 2012). Thus, apart from mass and metallicity, it is important to consider giants' evolutionary phase as well to determine whether Li abundance is normal or enhanced in any particular giant (Kirby *et al.* 2016). It's position in HR diagram (Figure 5.1) coupled with the derived values of $^{12}C/^{13}C$ and [C/N] ratios (see Table 5.2) confirms that the star is not evolved past the luminosity bump.

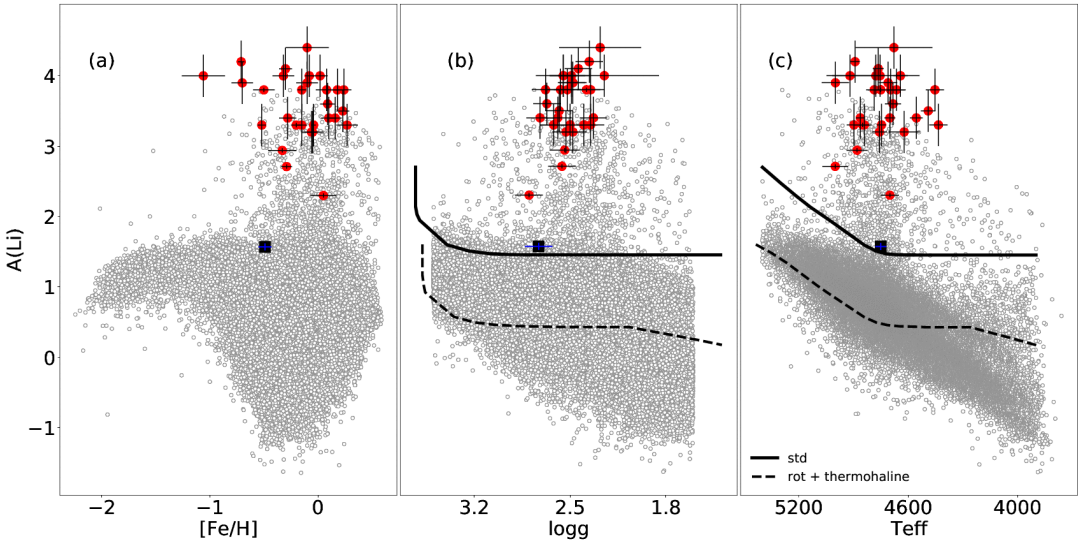

FIGURE 5.3: Location of KIC 9821622 in A(Li) vs [Fe/H], vs log$g$, and vs T_{eff} plots. Background stars are from the catalogue of GALAH survey. Sample giants are low mass ($M \leq 2\ M_{\odot}$) red giants with $Flag_{canon} = 0$. Solid and dashed lines are models of 1.5 $M_{\odot}$ from Lagarde *et al.* 2012 for standard mixing and thermohaline mixing with rotation included, respectively. In all the panels red filled circles are the known Li-rich giants classified as red clump giants using asteroseismic analysis.

Let us examine model prediction of Li abundance upper limit for KIC 9821662 at its present evolutionary position for its stellar parameters and initial A(Li). We don't have exact Li abundance with which this particular star might have evolved off. However, we can use general trends of A(Li) with mass and [Fe/H] among main sequence dwarfs. We adopt initial A(Li) from a study of Lambert and Reddy (2004) who provides plots of A(Li) versus stellar mass for different bins of [Fe/H]. For metallicity of [Fe/H] $\approx$ -0.5 and M $\approx$ 1.5 $M_{\odot}$ we find maximum initial abundance in the range of A(Li) = 3.0 to 2.8 dex. Combining this information

with Iben (1967) models we find Li deletion factor of about 12 for KIC 9821662 for its derived $T_{\rm eff}$ = 4750 K and for 1.5 $M_{\odot}$ model which correspond to values of about A(Li) = 1.92 dex, post 1st dredge-up. Even if we assume lower initial values of A(Li) = 2.8 dex, we find A(Li) = 1.72 dex at the end of 1st dredge-up. We find even higher upper limits for higher values of $T_{\rm eff}$ = 4890 K as reported by Yong *et al.* (2016); Takeda and Tajitsu (2017). For example, for the same 1.5 $M_{\odot}$, models predict less Li depletion with final values corresponding to 2.0 and 1.89 dex for the respective initial values of Li abundance. This is in good agreement with the empirical relation between A(Li) and Mv derived based on cluster data by Kirby *et al.* (2016). For its Mv = 0.99 (log ($L/L_{\odot}$) = 1.66) the relation suggests giant should have a value more than A(Li) = 1.66 dex, in other words, the measured A(Li) = 1.57 dex for KIC 9821622 is normal for giants below the bump luminosity.

Observations of Li abundance in numerous studies (e.g. Brown *et al.* 1989) confirm upper limits of Li for normal giants predicted by classical models. This has been beautifully illustrated in a plot of A(Li) versus [Fe/H] for a large sample of giants taken from GALAH catalogue and shown by Deepak and Reddy (2019) (See Figure 5.3). Within large [Fe/H] range, as defined by observations, upper limit is about 1.7 dex as measured by eye. Upper limits are low at the extreme ends of sample metallicity range. We won't comment on it as this is not a focus of present study. In the same figure, we have over plotted all the Li-rich giants (red symbols) for which asteroseismic classification is available including the star in question, KIC 9821622 (black square). Same data is shown as A(Li) vs log g (Figure 5.3 b) and A(Li) vs $T_{\rm eff}$ (Figure 5.3 c) along with the standard Li depletion models evolved from initial A(Li) of 3.3 dex (Lagarde *et al.* 2012) for 1.5 $M_{\odot}$. Note, KIC 9821622 is the only giant with significantly less A(Li) which falls closer to the upper limit.

5.5 Summary

We have performed a review of the reported Li-rich status of KIC 9821622, a bonafide red giant ascending RGB. Re-analysis of the spectra based on high resolution archival spectra of Gemini GRACES and Subaru, and comparison with theoretical models suggest the giant is most probably a normal Li giant (A(Li) $= 1.57 \pm 0.05$ dex) at the end of 1st dredge-up. The sub-ordinate line at 6103 Å is very weak or absent for deriving Li-abundance contrary to previous report by Jofré *et al.* (2015). Till date, all the Li-rich giants for which evolutionary phase was determined by a robust technique using asteroseismic analysis, are red clump giants with He-core burning phase. This clarification will constrain theoretical models to understand Li-excess origin scenarios around red clump giants and its immediate preceding phase, He-flash event. In next chapter we probe Li-excess origin during He-flashing phase of 2 Myr.

Chapter 6

Observational evidence of Li-production during the He-flashing phase of low mass stars

This chapter describes our novel observational method leading to the first observational evidence on the evolutionary status of lithium-rich giant stars. This was accomplished by combining asteroseismic and lithium abundance data. Comparing observations and models of the asteroseismic gravity-mode period spacing $\Delta\Pi_1$, which varies with stellar evolution, we discovered that super-Li-rich giants (SLR, A(Li) $>$ 3.2 dex) are almost exclusively young red-clump (RC) stars. Depending on the exact phase of evolution, which requires more data to refine, SLR stars are either (i) less than $\sim$ 2 Myr or (ii) less than $\sim$ 40 Myr past the main core helium flash (CHeF). If they are only $<$ 2 Myr post-CHeF, this will imply that all low-mass stars must go through an SLR phase. Our observations set a robust upper limit for the inferred Li-enrichment phase of $<$ 40 Myr post-CHeF,

lending support to the idea that lithium is produced somewhere between the very late red giant branch and the early RC phase, possibly around the time of the CHeF. In contrast, the more evolved RC stars (> 40 Myr post-CHeF) in our sample generally have low lithium abundances (A(Li) < 1.0 dex). Between the young, super-Li-rich phase, and the mostly old, Li-poor RC phase, there is an average reduction of lithium by about three orders of magnitude. The Li-destruction seems to occur rapidly, either almost immediately before reaching the RC or within the first $\sim 40\%$ of their RC lifetime. We find the situation less clear with stars having Li abundances between the two extremes of super-Li-rich and Li-poor. This group, the 'Li-rich' stars (3.2 > A(Li) > 1.0 dex), shows a wide range of evolutionary states. These results are published in Astrophysical Journal Letters (Singh et al. 2021, ApJL).

6.1 Introduction

He-flash: Low mass giants (≤ 2 $M_\odot$) while ascending the red giant branch (RGB) develop electron degenerate core due to continued accumulation of He at the centre from the outer hydrogen-burning shell. According to theoretical models (Schwarzschild and Härm 1962b; Thomas 1967) initiation of off-centre helium flash near the core terminates the RGB evolution by removing electron degeneracy at the core. The He-flash is very short-lived, of about 2 Myr, beginning with a strong He-flash followed by a series of sub-flashes progressively weakening until the core becomes fully convective (Bildsten *et al.* 2012; Deheuvels, S. and Belkacem, K. 2018). Because of its short duration not much is known about the He-flash and its effects on physical properties of stars during the flashing period.

Thanks to high precision time-resolved photometric surveys such as *Kepler* space mission (Borucki *et al.* 2010) it is now possible to probe the internal structure of the

stars before and after the RGB tip at which the transition begins from RGB to red clump phase. Identification of characteristic frequencies of oscillations associated with the central core properties of giants enabled to separate RGB giants of He-core burning from those of inert He-core giants ascending RGB (Beck *et al.* 2011; Bedding *et al.* 2011). However, there is no observational evidence for the He-flash phase apart from a sudden drop in brightness by 2-3 orders of magnitude. This is because the He-flash phase itself is very short and importantly, it is expected to affect only in changing internal structure rather than the outer structure, which could be observed.

Li-excess problem and Red Clump giants: On the other hand, the origin of strong lithium abundance excess in red giants - 'Li-rich giants' - has been a long-standing problem ever since its discovery about four decades ago (Wallerstein and Sneden 1982; Brown *et al.* 1989). In the last few years significant progress has been made (see Chapter 3 & 4) with increased sample of Li-rich stars thanks primarily to large datasets of ground-based spectroscopic sky surveys such as LAMOST (Cui *et al.* 2012), GALAH (De Silva *et al.* 2015) and Gaia-ESO (Gilmore *et al.* 2012) and the space-based *Gaia* astrometric (Gaia Collaboration *et al.* 2016, 2018) and *Kepler* time-resolved photometric surveys (Borucki *et al.* 2010). Studies using data from these surveys have now confirmed the early suspicions (eg. Kumar *et al.* 2011; Silva Aguirre *et al.* 2014) that Li-rich giants are predominantly in the He-core burning phase of stellar evolution, also known as the red clump (RC; Singh *et al.* 2019a; Bharat Kumar *et al.* 2018; Smiljanic *et al.* 2018; Casey *et al.* 2019; Yan *et al.* 2020). This new development has significantly narrowed the search for finding the origin of the lithium enhancement.

In particular, with the arrival of *Kepler* data significant progress has been made in understanding internal structure of stars in all evolutionary phases using stellar oscillation properties. Observed frequencies can be used to study internal structure such as evolutionary phase(Bedding *et al.* 2011; Mosser *et al.* 2014; Vrard

et al. 2016; Yu *et al.* 2018), internal core rotation, magnetic field etc which were previously hidden from direct photometric or spectroscopic observations. This path breaking novel technique has revolutionized understanding of Li-rich giant problem in low mass stars. Since first discovery of Li-rich giant, these stars were considered as RGB stars until the pioneering work by Kumar *et al.* (2011). Kumar *et al.* (2011) first suggested that these stars are red clump stars based on HRD. Subsequent study by Martell and Shetrone (2013); Monaco *et al.* (2014) also suggested that few of stars in their sample may be in the red clump phase. But these were only claims on small sample size. First breakthrough in exactly pin pointing evolutionary phase came from Silva Aguirre *et al.* (2014) who studied single star KIC 5000307 in *Kepler* field and found that this is a Li-rich giant (A(Li) = 2.71 dex) at red clump phase. Later study by Carlberg *et al.* (2015); Bharat Kumar *et al.* (2018) in *Kepler* field found Li-rich giants in red clump and based on spectroscopically determined [C/N] Singh *et al.* (2019b) found that Li-rich giants were indeed red clump stars. These sporadic discoveries of red clump Li-rich giants contrary to the belief that Li-rich stars are associated with RGB warranted a large systematic survey. This was conducted by Singh *et al.* (2019a) in which they assembled common giants between LAMOST and *Kepler* observed fields (see for details Chapter 4). Recent similar survey by Yan *et al.* (2020) also found that majority of Li-rich stars are red clump and all the super Li-rich stars are core He burning stars.

Li depletion along the RGB: Also, it is also well established that Li is almost totally destroyed during the phase of evolution just preceding the RC, the red giant branch (RGB; Brown *et al.* 1989; Lind *et al.* 2009a; Kumar *et al.* 2020), reaching values as low as A(Li) $\sim$ -1.0 dex. In contrast, the average Li abundance on the RC is A(Li) = +0.7 dex (Kumar *et al.* 2020). As discussed by Kumar *et al.* (2020), this implies that there must be a lithium production phase between the late RGB and RC. Since that study two theoretical models have been put forward for Li production. The first is by Mori *et al.* (2020) whose model produces Li

at the RGB tip, before the onset of He-flash, via the inclusion of the neutrino magnetic moment. The second proposed model produces Li during the main CHeF, by assuming some mixing during the extremely energetic flash (Schwab 2020). Schwab (2020) studied Li production during He-flash with a specific ad-hoc mixing procedure. They suggested excess ^{7}Li in the red clump phase could be explained by in situ production of Li in single stars by Cameron-Fowler mechanism (Cameron and Fowler 1971). The amount of ^{7}Be present outside the H burning shell is enough for production of observed ^{7}Li abundances in RC stars if their assumed mixing works during the strong first off-centre He-flash. For efficient Li synthesis, one of the critical requirements is the safe transportation of ^{7}Be to the outer cooler layers in which ^{7}Be can be converted to Li which is available for mixing-up with the photosphere. According to their models, such mixing can be accomplished by internal gravity waves (IGW) excited by turbulent convection created during the most energetic first He sub-flash ($L_{He} = 10^{9}$ $L_{\odot}$), and subsequent sub-flashes are weaker for causing any such mixing, and Li starts only depleting during the sub-flash phase. On the other hand Mori *et al.* (2020) state that it is very difficult to reproduce such high Li abundances in their model with their neutrino magnetic moment scenario. Other proposals for producing Li in red giants include tidal interactions between binary stars (eg. Casey *et al.* 2019), and merger events between a white dwarf and a red giant (Zhang and Jeffery 2013; Zhang *et al.* 2020). These scenarios can produce Li at different phases of evolution.

In summary, although the temporal location of the inferred Li production phase has been narrowed down substantially, the exact phase (and nature of event) at which it occurs is still unknown. Further, it is unknown if the Li-rich and SLR giants maintain their extreme Li abundances for the entire RC phase ($\sim$ 100 Myr at 1 $M_{\odot}$; eg. Constantino *et al.* 2017), or if the Li is quickly depleted early on the RC. Having this information would shed light on the frequency of the Li-production event(s), and help narrow the possibilities for the site further.

In this chapter, we discussed the detailed analysis of correlation between $\Delta\Pi_1$ and A(Li) in a sample of stars selected from literature and complemented by common stars in LAMOST-MRS and *Kepler* field. The chapter is outlined as follows: In section 2, we described sample selection process from literature and LAMOST-MRS survey in *Kepler* field. In section 3 we gave details of measurement of A(Li) and $\Delta\Pi_1$. In section 4, we described correlation between A(Li) and $\Delta\Pi_1$ and other quantities. In section 5 we provide discussion of our results in comparison to theoretical models. In section 6 consist of conclusions.

6.2 Sample selection

We have extracted a sample of 14509 giants (7554 RGB and 6955 RC) in the *Kepler* field for which evolutionary phase is provided in the literature (Bedding *et al.* 2011; Mosser *et al.* 2012b, 2014; Stello *et al.* 2013; Vrard *et al.* 2016; Yu *et al.* 2018). The classification is based on asteroseismic data from the *Kepler* space mission (Borucki *et al.* 2010). The sample comprises low mass giants ($M \leq 2\ M_{\odot}$) with luminosity in the range $0.53 \leq \log(L/L_{\odot}) \leq 2.50$, covering the RGB and RC evolutionary phases. Of these, we found 90 giants (32 RGB and 58 RC stars) with Li abundance measurements in the literature (Anthony-Twarog *et al.* 2013; Silva Aguirre *et al.* 2014; Bharat Kumar *et al.* 2018; Takeda and Tajitsu 2017; Singh *et al.* 2019a, 2020; Yan *et al.* 2020). Most of the measurements are based on high-resolution spectra ($R \geq 30{,}000$) except a few for which Li abundances are based on low resolution ($R \approx 1800$) LAMOST spectra (Singh *et al.* 2019a). For some of these giants Li abundances were derived using high resolution spectra Yan *et al.* (2020). Their abundances are in agreement with the Singh *et al.* (2019a) values.

To increase the sample size, we also searched for *Kepler* field stars in the recently released catalogue of medium resolution (MRS, $R \approx 7{,}500$) spectroscopic data of

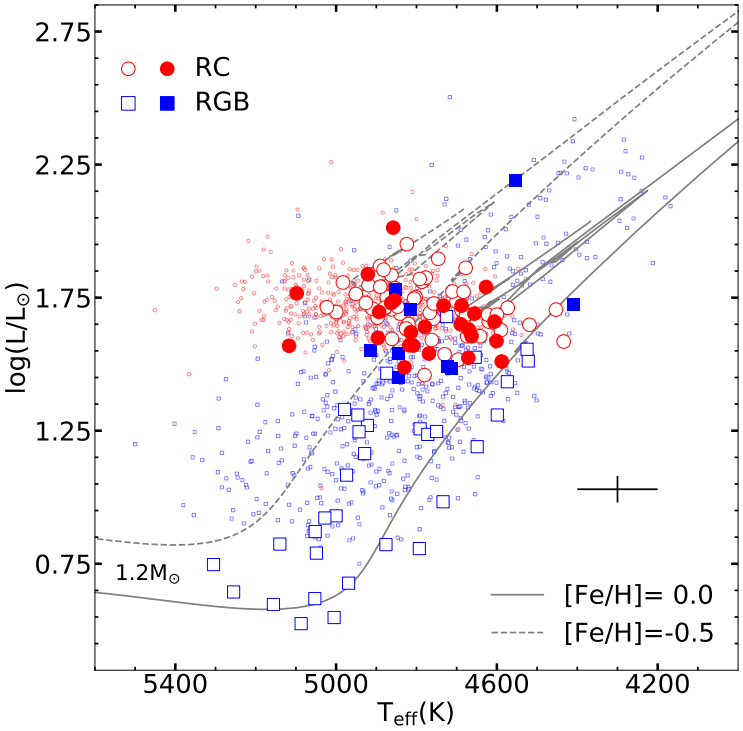

FIGURE 6.1: HR diagram showing our sample of 120 giant stars (large symbols) which have measured Li abundances as well as evolutionary phase known from asteroseismology (large symbols). RC stars are shown as circles and RGB stars as squares. Stars for which Li abundances are available in the literature are shown as open symbols and those with abundances derived in this study are shown as filled symbols. For context, the entire overlap sample of 1158 giants in background between Kepler and LAMOST MRS catalogues forms the background (small symbols). Typical uncertainties are represented by the error cross on the right. Overplotted are two stellar model tracks, both 1.2 $M_{\odot}$ but with two different metallicities.

the LAMOST* survey (Liu *et al.* 2020). Spectra are available in two wavelength regions: a blue region of 4980 – 5380 Å and a red region of 6300 – 6880 Å (Liu *et al.* 2019), spectra of a representative star is given in shown in Figure 6.2. The red region of the MRS survey spectra contains the Li resonance line at 6707.8 Å. We found a total of 1158 giants (581 RGB giants and 577 RC stars) in common between the two catalogues, location of selected stars in shown in Figure 6.1 and spectra of all the stars in show in Figure 6.3. One striking feature in Figure 6.3 is absence of strong Li absorption line in bottom panel which represents spectra of RGB while in upper panel, which represents RC stars, has significant number

*http://dr6.lamost.org/

of spectra with strong Li absorption feature. However, due to the low spectral resolution of the LAMOST data we found only 30 giants (22 RC and 8 RGB) with Li lines strong enough for reliable measurement (see Sec. 6.3.1). Combining this sample with the literature sample, we have a total of 120 giants with evolutionary phase and accurate Li abundances. Our sample is shown in Figure 6.1 along with the entire overlap sample of LAMOST-MRS and the *Kepler* catalogue. All of the stars have precise astrometry from *Gaia* DR2 (Gaia Collaboration *et al.* 2018). Luminosity were derived using the *Gaia* distances.

6.3 Results

We briefly describe estimation of lower limit in EWs in selecting the 30 LAMOST-MRS giants spectra and derivation of Li abundances. We also describe derivation of gravity mode period spacing values of 48 giants for which asteroseismic parameters are are not given in the literature.

6.3.1 LAMOST MRS Lithium abundances

Li abundances were derived by matching the synthetic spectra with the the observed Li line at 6707.78 Åin the medium-resolution LAMOST spectra using spectral synthesis. We used the 2013 version of the local thermal equilibrium (LTE) radiative transfer code MOOG (Sneden 1973), in combination with the Kurucz ATLAS atmospheric models (Castelli and Kurucz 2004). Atmospheric parameters ($T_{\rm eff}$, log g, [Fe/H]) were taken from the Yu *et al.* (2018) catalogue. Values of microturbulent velocity ($\xi_{\rm t}$) were derived using the calibration relation of Kirby *et al.* (2009). We synthesized the spectral region covering the wavelength range 6700 – 6715 Å for a given set of atmospheric parameters with varying Li abundance to

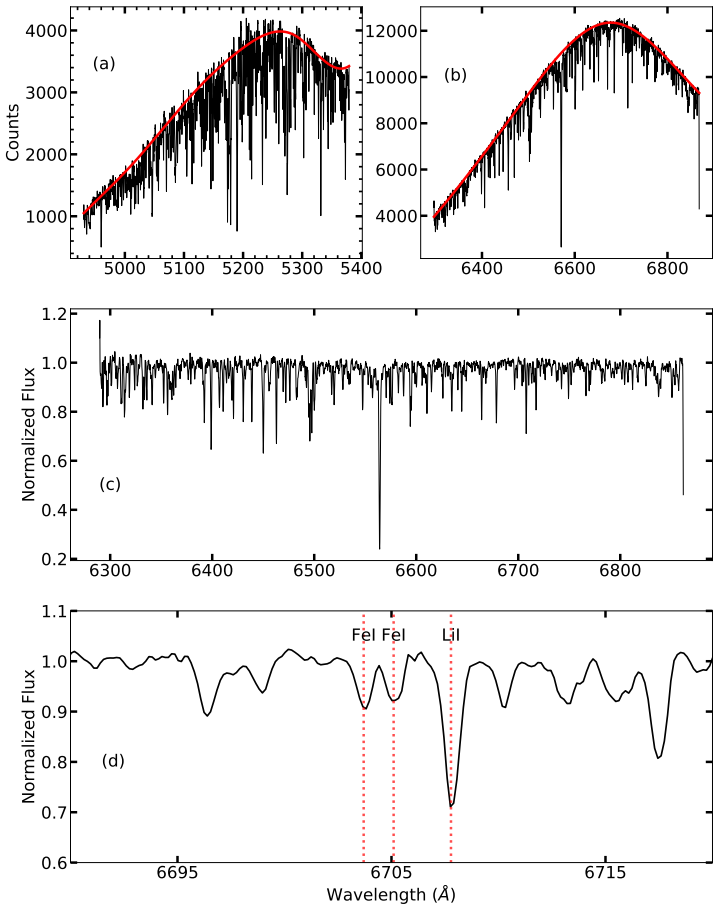

FIGURE 6.2: Sample spectra of LAMOST medium resolution survey (R = 7500). In the topmost panel we see wavelength calibrated spectra in two different regions: blue region from 4800–5350 Å and in red region: 6300—6800 Å. Middle panel shows continuum normalized spectra in red region. Bottom panel shows zoomed spectral region near Li resonance line at 6707.78Å.

match the observed Li line at 6707.78 Å. Our line list, with atomic and molecular data, was compiled using the Linemake code[†]. Figure 6.4 shows a comparison of synthetic spectra with the observed spectra of a few representative stars in the increasing order of Li abundances. The estimated uncertainty in Li abundance is the quadratic sum of uncertainties in Li abundance caused by the estimated uncertainties in atmospheric parameters for each individual star ($T_{\rm eff}$, log g, [Fe/H]; see Table 6.1). Li abundances were corrected for non-LTE) effects using the $\Delta_{\rm NLTE}$ values provided by Lind *et al.* (2009a).

[†] https://github.com/vmplacco/linemake

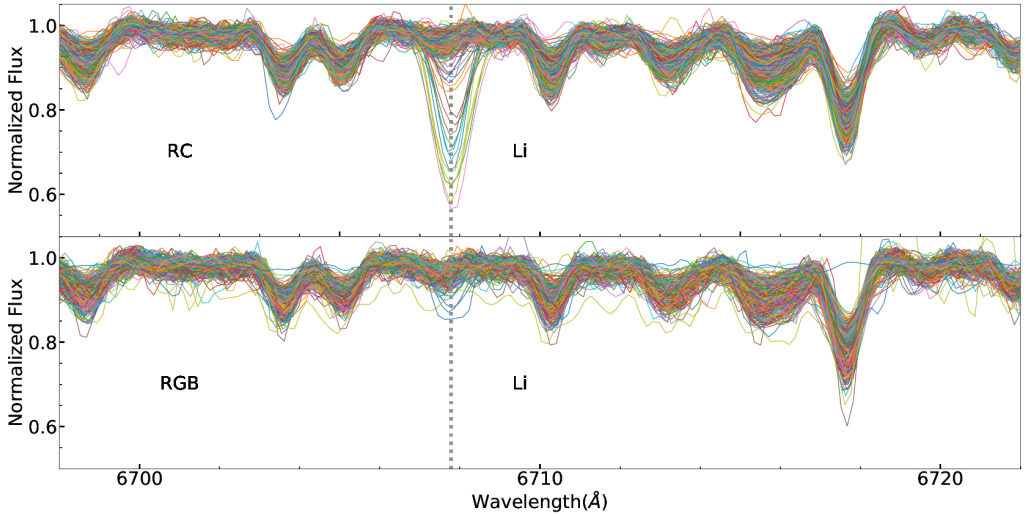

FIGURE 6.3: Observed spectra of all the RC and RGB stars selected from LAMOST MRS survey. In the top panel we have plotted 577 RC stars from which we found 22 RC with measurable Li. In the bottom panel we see that none of the RGB star has excess Li. Depth of Li line is very weak.

Due to the moderate resolution of the spectra, not all stars will have reliable Li abundances. We estimated the lower detectability limit in equivalent width (EW) for our data using the Cayrel (1988) formulation for estimating uncertainties in EW for a given spectral quality: $\delta\mathrm{EW} = 1.6(\mathrm{w} \times \delta\mathrm{x})^{1/2}\epsilon$, where w is the full width half maximum (FWHM) of the line, $\epsilon = 1/\mathrm{SNR}$ and δx is the pixel width. For the LAMOST MRS spectra the pixel width is 0.12 Å (Wang *et al.* 2019) and FWHM = 0.89 Å (for R $\approx$ 7500), and range in SNR = 55 – 150 consistent with our spectra. We estimated the uncertainty in equivalent width: δEW $\approx$ (3.5 – 9.4) mÅ. To err on the conservative side, we adopted a lower limit of 3$\times$ δEW = (10.6 – 28.2) mÅ, which translates to lower limit abundances in the range of +0.7 to +1.1 dex, depending on stellar parameters (see Fig. 6.4). This criterion resulted in 30 giants (22 RC and 8 RGB stars) for which we could reliably derive Li abundances (Table 6.1).

KIC	V‡	plx	T_{eff}	log g	[Fe/H]	log($L/L_{\odot}$)	A(Li)	A(Li)N
				RC				
5079905	12.56	0.55	4769±139	2.38±0.01	0.03±0.30	1.54±0.04	2.64	2.66±0.21
6593240	11.11	1.03	4808±80	2.41±0.01	0.0±0.15	1.57±0.03	2.71	2.74±0.15
6774006	10.99	0.98	4656±139	2.32±0.02	0.50±0.3	1.69±0.04	3.31	3.26±0.20
7020392	12.40	0.48	4893±100	2.39±0.01	-0.25±0.15	1.83±0.04	1.26	1.45±0.16
7023331	11.16	0.94	4690±100	2.46±0.02	0.01±0.30	1.65±0.03	1.40	1.66±0.15
7184162	12.98	0.33	5098±163	2.46±0.01	0.07±0.30	1.92±0.05	1.88	2.06±0.20
7595155	12.12	0.66	4601±100	2.36±0.01	0.30±0.30	1.74±0.03	0.91	1.23±0.20
7612438	12.88	0.33	4921±80	2.54±0.01	0.07±0.15	1.96±0.08	1.68	1.86±0.15
7807614	11.85	0.63	4688±100	2.41±0.01	0.50±0.30	1.72±0.03	1.21	1.53±0.15
7954197	10.90	1.06	4814±139	2.42±0.01	0.12±0.30	1.62±0.03	1.13	1.32±0.20
8363443	10.88	1.05	4606±80	2.41±0.01	0.38±0.15	1.81±0.03	3.65	3.55±0.12
8366758	12.50	0.59	4671±80	2.32±0.01	0.28±0.15	1.62±0.04	3.29	3.14±0.15
8619916	12.90	0.43	5117±160	2.44±0.01	-0.05±0.30	1.71±0.06	2.66	2.71±0.25
8819748	11.71	0.61	4896±171	2.44±0.01	0.38±0.30	1.93±0.06	1.74	1.92±0.24
8879518	11.22	0.81	4863±80	2.57±0.01	0.14±0.15	1.73±0.03	3.60	3.51±0.12
9024667	12.28	0.60	4818±100	2.31±0.02	0.28±0.15	1.73±0.04	3.19	3.03±0.15
9346108	12.78	0.47	4663±80	2.39±0.01	0.22±0.15	1.71±0.04	2.03	2.15±0.15
9785675	11.88	0.81	4588±80	2.28±0.01	0.35±0.15	1.51±0.04	2.66	2.62±0.12
9848308	12.28	0.51	4733±80	2.49±0.01	0.06±0.15	1.72±0.04	2.57	2.59±0.12
9907856	12.45	0.45	4855±80	2.41±0.01	-0.17±0.15	1.73±0.01	2.57	2.56±0.13
10603958	11.42	0.48	4858±100	2.36±0.02	-0.42±0.15	2.21±0.12	1.04	1.23±0.15
11129153	12.09	0.72	4830±100	2.37±0.03	-0.37±0.15	1.63±0.08	1.26	1.45±0.16
				RGB				
4446405	12.10	0.66	4846±100	2.68±0.01	-0.13±0.15	1.54±0.03	1.38	1.58±0.15
5350163	11.49	0.62	4712±80	2.78±0.01	0.34±0.15	1.87±0.04	0.95	1.20±0.15
6262706	11.53	0.85	4915±100	2.69±0.01	-0.17±0.15	1.55±0.02	1.44	1.63±0.14
7033467	10.38	1.57	4723±80	2.76±0.01	0.22±0.15	1.49±0.03	0.98	1.17±0.15
8160419	10.89	1.11	4410±80	2.27±0.01	0.16±0.15	1.67±0.04	0.87	1.29±0.13
8167335	11.32	1.06	4844±80	2.81±0.01	-0.01±0.15	1.45±0.02	1.10	1.31±0.14
8802374	11.10	0.77	4853±100	2.41±0.01	-0.30±0.15	1.81±0.04	1.21	1.40±0.16
11288888	9.90	0.93	4553±80	2.08±0.01	-0.09±0.15	2.19±0.03	0.85	1.08±0.15

TABLE 6.1: Derived Li abundances and stellar parameters for 30 giants (22 RC and 8 RGB) for which A(Li) values are derived from LAMOST-MRS spectra. Stellar parameters (T_{eff}, log g and [Fe/H]) are adopted from Yu *et al.* (2018)) and parallax from *Gaia* DR2. Also given NLTE corrected Li abundances in the last column. Note, A(Li) of RC stars varies from 1.23— 3.55 dex whereas maximum A(Li) of RGB is 1.63 dex.

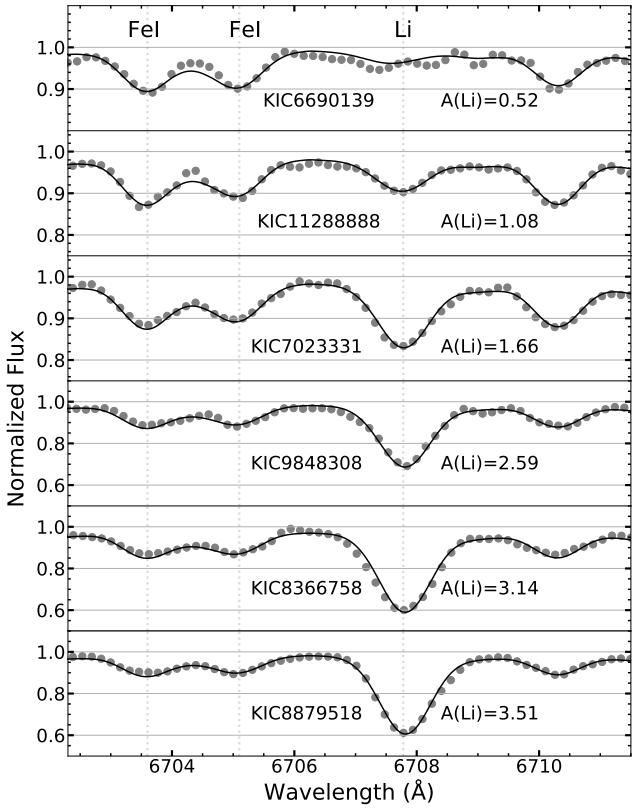

FIGURE 6.4: Derivation of Li abundances for a few representative giants using spectral synthesis of the 6707.78 Å Li line (solid lines) in the LAMOST medium resolution spectra (dots). The spectrum in the top panel is for KIC 6690139 for which A(Li) = +0.52 dex is known in literature based on high resolution spectra. LAMOST MRS data is only useful for stars with A(Li) $\sim$ +0.7 dex.

6.3.2 Asymptotic gravity-mode period spacing, $\Delta\Pi_1$

Cross-matching our sample of 120 stars with the literature we found $\Delta\Pi_1$ for 72 of them(Mosser *et al.* 2012a, 2014; Vrard *et al.* 2016). There are other parameters such as the average mixed-mode period spacing $\Delta P_{g,ave}$ (eg. Stello *et al.* 2013; Singh *et al.* 2019a) or the log g - mass method for separating RGB and RC stars (eg. Yu *et al.* 2018). However, these parameters do not give precise enough evolutionary status for our purposes. For the remaining 48 giants for no literature values of $\Delta\Pi_1$ are not available, we attempted to derive it ourselves. We downloaded the time series data from the *Kepler* archive and converted them to the frequency domain

using the Lightkurve package[§] (Lightkurve Collaboration *et al.* 2018). Details of our method of $\Delta\Pi_1$ estimation are given in Mosser *et al.* (2014) and Vrard *et al.* (2016). We were able to derive asymptotic values for 16 of the 48 stars (Table 6.2). The rest did not have sufficient SNR in their power density spectra (PDS). The asymptotic gravity mode period spacing method requires data of high cadence with good SNR which many of the sources do not have. For the remaining 32 stars after identifying mixed modes present in the power density spectra, we measured the period spacing of consecutive mixed modes and adopted the median value of the period spacing, $\Delta P_{g,ave}$ (see eg. Stello *et al.* 2013). These values are useful for determining 'bulk' evolutionary state (RC vs RGB), however they do not give precise evolutionary state along the phases so we do not use them in our this analysis. Average value of period spacing is smaller than the asymptotic value by factor of 1.3–1.6 (Bedding *et al.* 2011). There is no direct relation connecting average values to asymptotic values. This leaves 88 stars (59 RC, 29 RGB) for which we have A(Li) and $\Delta\Pi_1$ values. As we can see in Table 6.1 none of the RGB stars can be considered as Li -rich. Therefore we restricted sample to only RC stars with known (from literature or derived in this study) asymptotic period spacing for present study. $\Delta\Pi_1$ of 16 RC stars measured in the present study are given in Table 6.2.

6.4 A(Li) vs $\Delta\Pi_1$: Evolution of Li along the RC

Since our aim is to understand Li excess among RC giants we focused only on the RC stars of the sample for which we have A(Li) and $\Delta\Pi_1$. RGB stars are considered Li-rich if they have A(Li) $> 1.5 - -1.8$ dex (Iben 1967). None of the RGB stars in our sample were found to be Li-rich. On the other hand, Kumar *et al.* (2020) showed that RC stars should be considered Li-enhanced if they have

[§] https://github.com/NASA/Lightkurve

KIC	ν_{max}	$\Delta\nu$	M($M_\odot$)	R($R_\odot$)	$\Delta\Pi_1$
3751167	26.14 ± 1.59	3.59 ± 0.12	0.95 ± 0.22	11.04 ± 1.02	260.0 ± 12.86
5079905	29.82 ± 0.72	3.94 ± 0.03	0.92 ± 0.09	10.27 ± 0.37	297.9 ± 20.28
7020392	29.85 ± 0.84	3.94 ± 0.09	0.97 ± 0.13	10.45 ± 0.59	298.7 ± 19.91
7131376	34.82 ± 0.71	4.13 ± 0.03	1.25 ± 0.11	11.00 ± 0.37	250.8 ± 18.24
7612438	42.43 ± 0.65	4.36 ± 0.02	1.87 ± 0.12	12.14 ± 0.30	279.3 ± 32.24
7899597	31.62 ± 1.06	3.79 ± 0.13	1.28 ± 0.23	11.76 ± 0.95	267.4 ± 18.0
7954197	32.49 ± 0.73	3.93 ± 0.04	1.23 ± 0.12	11.32 ± 0.41	268.7 ± 2.37
8363443	32.43 ± 0.61	3.78 ± 0.02	1.34 ± 0.10	11.94 ± 0.34	247.9 ± 1.97
8869656	30.69 ± 0.83	3.81 ± 0.04	1.21 ± 0.13	11.51 ± 0.47	235.5 ± 13.45
9667064	30.16 ± 1.27	3.59 ± 0.05	1.40 ± 0.20	12.57 ± 0.67	260.9 ± 16.46
9833651	38.82 ± 0.79	4.24 ± 0.04	1.50 ± 0.13	11.50 ± 0.39	266.4 ± 2.70
11129153	28.88 ± 1.66	3.69 ± 0.06	1.12 ± 0.22	11.45 ± 0.80	227.6 ± 11.25
11615224	29.68 ± 0.88	4.05 ± 0.06	0.85 ± 0.10	9.80 ± 0.44	257.7 ± 2.20
11658789	31.21 ± 1.40	4.29 ± 0.08	0.87 ± 0.14	9.51 ± 0.59	256.0 ± 2.03
11805390	31.55 ± 0.79	3.51 ± 0.06	1.82 ± 0.20	13.92 ± 0.64	333.0 ± 2.47
12784683	28.72 ± 1.02	3.68 ± 0.08	1.16 ± 0.18	11.58 ± 0.73	282.3 ± 17.55

TABLE 6.2: Asymptotic gravity mode period spacing, $\Delta\Pi_1$, of 16 Li-rich red clump stars for which asteroseismic analysis is done in the present study. Masses and radius are derived using the calibration relation given in Kjeldsen and Bedding (1995). Out of total 16, six stars are from present study and 10 stars are from literature.

abundances greater than the preceding phase of evolution, the late RGB. They estimated a limit for Li-enhancement in RC stars of A(Li) > -0.9 dex. All of our RC stars can therefore be considered Li-enhanced, to varying degrees. In Figure 6.5 we display A(Li) vs $\Delta\Pi_1$ for the RC stars. We divide the sample into three groups depending on their Li abundance:

- Li-normal (LN): A(Li) > 1.0 dex
- Li-rich (LR): $1.0 <$ A(Li) < 3.2 dex
- Super-Li-rich (SLR): A(Li) > 3.2 dex

The A(Li) $= 1.0$ dex delineation is based on the Kumar *et al.* (2020) study's distribution on the RC (peaked at +0.7 dex), whilst the A(Li) $= 3.2$ dex delineation is based on the ISM value (Knauth *et al.* 2003). Our key result emerges from Figure 6.5 – the great majority ($12/15 = 80\%$) of the SLR stars have $\Delta\Pi_1$ peaked at low values (mean $= 257 \pm 23$ s). We note that two of the three outliers in the SLR group have masses 2σ from the mean mass of our RC sample (~ 1.8 $M_\odot$, where the sample mean mass is 1.2 ± 0.3 $M_\odot$). Removing the three outliers the average remains the same, at 255 s, but the dispersion is halved ($\sigma = 10$ s), as expected from the histogram in Fig. 6.5. In contrast, the Li-normal stars all have higher $\Delta\Pi_1$, ranging from 280 s up to ~ 330 s. Their mean is 306 ± 14 s, much higher than the SLR group. The Li-rich stars (Fig. 6.5) show more complex behaviour. They have a very broad distribution of $\Delta\Pi_1$ values rather than forming a coherent group.

We now discuss the implications of the $\Delta\Pi_1$-A(Li) observations in relation to stellar evolution.

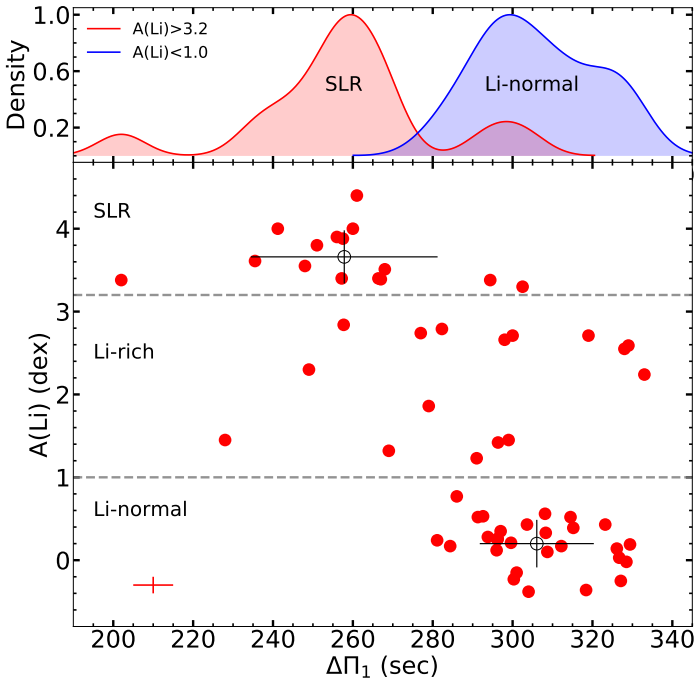

FIGURE 6.5: Variation of A(Li) with asymptotic gravity mode period spacing $\Delta\Pi_1$ in RC stars. The open circles with error bars show the mean and 1σ dispersion of the groups. Due to the broadness of the Li-rich group we do not assign a mean to it. The top panel shows Gaussian kernel density histograms for the SLR and LN groups. Since $\Delta\Pi_1$ tracks the evolution of the stars (from left to right, see Fig. 6.10), it can be seen that the average Li abundance reduces with evolution. Typical A(Li) and $\Delta\Pi_1$ uncertainties are represented by the error cross at bottom left.

6.4.1 Mass and metallicity distribution

To find that whether correlation between A(Li) and $\Delta\Pi_1$ is arising because of different mass and metallicity of stars we checked any sort of dependency between them and found that average mass of SLR group is 1.21±0.32 $M_\odot$, Li-rich group is 1.14±0.33 $M_\odot$ and LN group is 1.22±0.23 $M_\odot$. All the three group is almost similar mass, see top panel of Figure 6.7. Similarly metallicity of SLR group is -0.26±0.38, Li-rich group is -0.06±0.19 and LN group is -0.10±0.19. Metallicity of SLR group is slightly lower but within 1-σ all the group has same metallicity, see bottom panel of Figure 6.7.

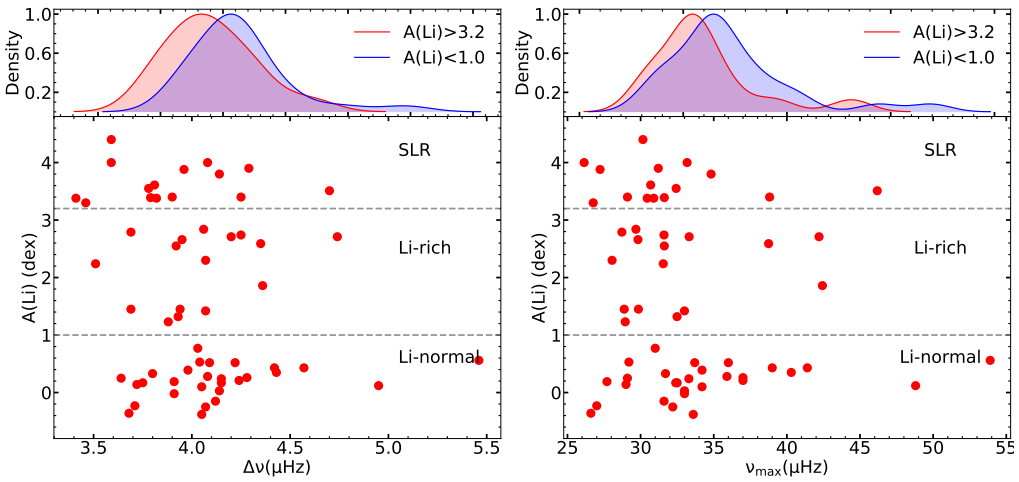

FIGURE 6.6: Left panel: $\Delta\nu$ variation w.r.t A(Li) of red clump stars. As clear in kernel density estimation SLR have lower $\Delta\nu$ than Li-normal stars. Right panel: $\nu_{\rm max}$ variation w.r.t A(Li). SLR stars have slightly lower $\nu_{\rm max}$ than Li-normal stars.

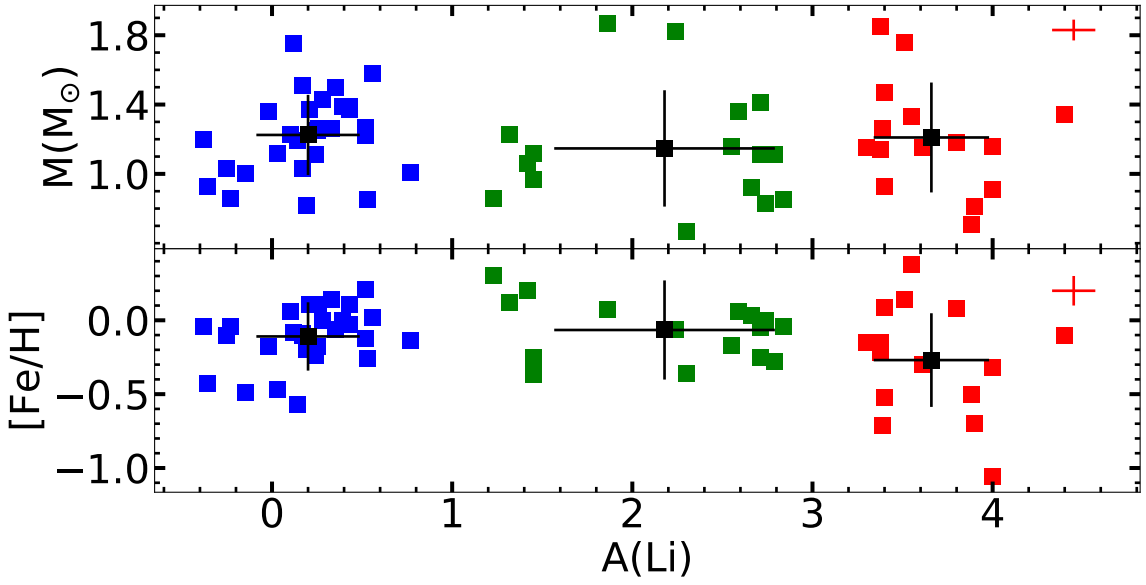

FIGURE 6.7: Variation of Li abundance with mass and metallicity of 59 sample stars. Typical error bar is presented at the upper right corner. Black square is average mass and metallicity in SLR, Li-rich and LN group. No correlation is seen between observed mass and Li abundances among SLR, LR and LN groups.

6.5 Discussion

6.5.1 Possible biases in stellar sample

Of our 59 RC giants 30 are taken from Takeda and Tajitsu (2017). This forms our low-Li sample of stars as their A(Li) are based on high resolution spectra. The Takeda and Tajitsu (2017) sample, which only used brightness as a selection criterion, was itself taken from the original sample of Mosser *et al.* (2012b) who derived $\Delta\Pi_1$ for 95 RC stars that had long cadence observations of the *Kepler* field.

At no stage did we select on the basis of $\Delta\Pi_1$. Our A(Li) values are however limited in a couple of cases. Firstly, the abundances from the LAMOST medium-resolution spectra are limited to A(Li) > 0.7 dex (Sec. 6.3.1). This does not affect the detection of Li-rich and SLR stars, since their abundances are above this limit, but it biases against low-Li stars. Secondly, we used the sample from Singh *et al.* (2019a) whose Li measurements were restricted only to very strong Li lines due to low spectral resolution (LAMOST, R $\approx$ 1800). This resulted in a bias towards SLR stars in their sample, which is mapped to our sample. By combining these samples biased to Li-rich stars with the low-Li sample of Takeda and Tajitsu (2017), we cover the whole range of A(Li). Super-Li-rich stars are central to our main result. The *Kepler* field is known to have 26 SLR stars in total (Singh *et al.* 2019a; also Table 6.1), they are rare objects. Of these, we have 15 in our sample with $\Delta\Pi_1$ measurements. As such our sample represents a very substantial fraction (58%) of all the known SLR stars in the *Kepler* field.

A possible bias against observing low $\Delta\Pi_1$ values was reported by Constantino *et al.* (2015), based on comparisons between models and the Mosser *et al.* (2012a) sample. At low $\Delta\Pi_1$ their models predict more stars than are observed. This

could be a problem with the models or the observations, or both. As mentioned, our sample contains 58% of all known *Kepler* field SLR stars. We have $\Delta\Pi_1$ for all of these stars, and our main result is that they are strongly peaked at low values. This shows that we, and others, have been able to measure low values of $\Delta\Pi_1$ in the majority of these stars. We see no reason why the detectability of $\Delta\Pi_1$ should depend on Li abundance. In Figure 6.8, we provide histograms comparing the distributions of $\Delta\Pi_1$ and A(Li) in our sample with large survey samples. Our sample covers the whole range of A(Li) and $\Delta\Pi_1$ present in the larger samples. As discussed above, our sample has proportionally more (S)LR stars than an unbiased survey, which is seen clearly in Fig. 6.8. The $\Delta\Pi_1$ distribution, despite being independent of our sampling, has an unusual peak at low $\Delta\Pi_1 \sim 255$ s – this is our main result, that SLR stars have predominately low $\Delta\Pi_1$.

6.5.2 Observations versus Stellar Evolution

Low mass giants (≤ 2 $M_\odot$) while ascending the red giant branch develop electron degenerate cores due to continued piling up of He ash at the centre from the outer hydrogen-burning shell. Initiation of an off-centre helium flash in the core terminates the RGB evolution (Schwarzschild and Härm 1962b; Thomas 1967). The main He-flash is very short-lived, lasting about 1000 years. After the main flash a series of progressively weaker flashes ensues (see Fig. 6.10 and Bildsten *et al.* 2012), each igniting closer and closer to the centre, progressively removing the electron degeneracy in the core. The entire He-flashing phase lasts $\sim 1.5-2$ Myr. Finally the very centre of the core becomes convective, marking the start of the RC phase (quiescent core helium burning), which lasts for ~ 100 Myr. Throughout this evolution $\Delta\Pi_1$ varies predictably, as seen in Fig. 6.10 (also see Bildsten *et al.* 2012; Constantino *et al.* 2015; Bossini *et al.* 2017; Deheuvels, S. and Belkacem, K. 2018). Our new observational data enables us to compare the observed $\Delta\Pi_1$ with model predictions.

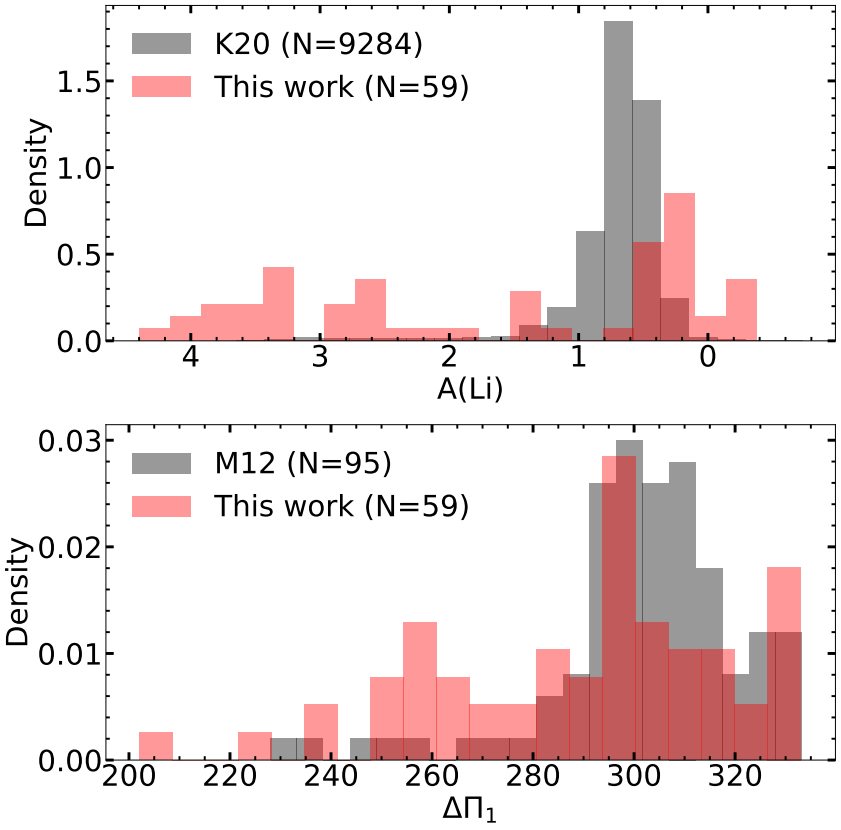

FIGURE 6.8: Histogram showing the distribution of A(Li) (top) and $\Delta\Pi_1$ (bottom) of our RC sample compared to the large GALAH sample (K20; Kumar *et al.* 2020) and the Mosser *et al.* (2012b) (M12) catalogue. We note that at low A(Li) the K20 sample has a systematic shift relative to the Takeda and Tajitsu (2017) sample, of $\sim +0.3$ dex. This could be due to the lower resolution and SNR of GALAH. The bias to high Li can be seen in our sample, as can the unusual peak in $\Delta\Pi_1$ at ~ 255 s associated with the SLR stars (our main result).

We have calculated a series of stellar models using the MESA code (Paxton *et al.* 2011, 2019; version 12778). In Figure 6.10 we show a representative model that matches the mean mass of our sample, 1.2 $M_\odot$, and is of solar metallicity (the mean [Fe/H] of our sample is -0.14 ± 0.26 dex). RGB mass loss was modelled using the Reimers (1975) formula ($\eta = 0.3$). As Bossini *et al.* (2017) showed, the very early RC $\Delta\Pi_1$ evolution is not dependent on mass, however it has some dependence on metallicity. Comparing the dispersion of [Fe/H] in our sample (0.26 dex) with the models in Figure 3 of Bossini *et al.* (2017), we expect a variation of ~ 5 s in $\Delta\Pi_1$. This is approximately the same as our observational error bars (Fig. 6.5).

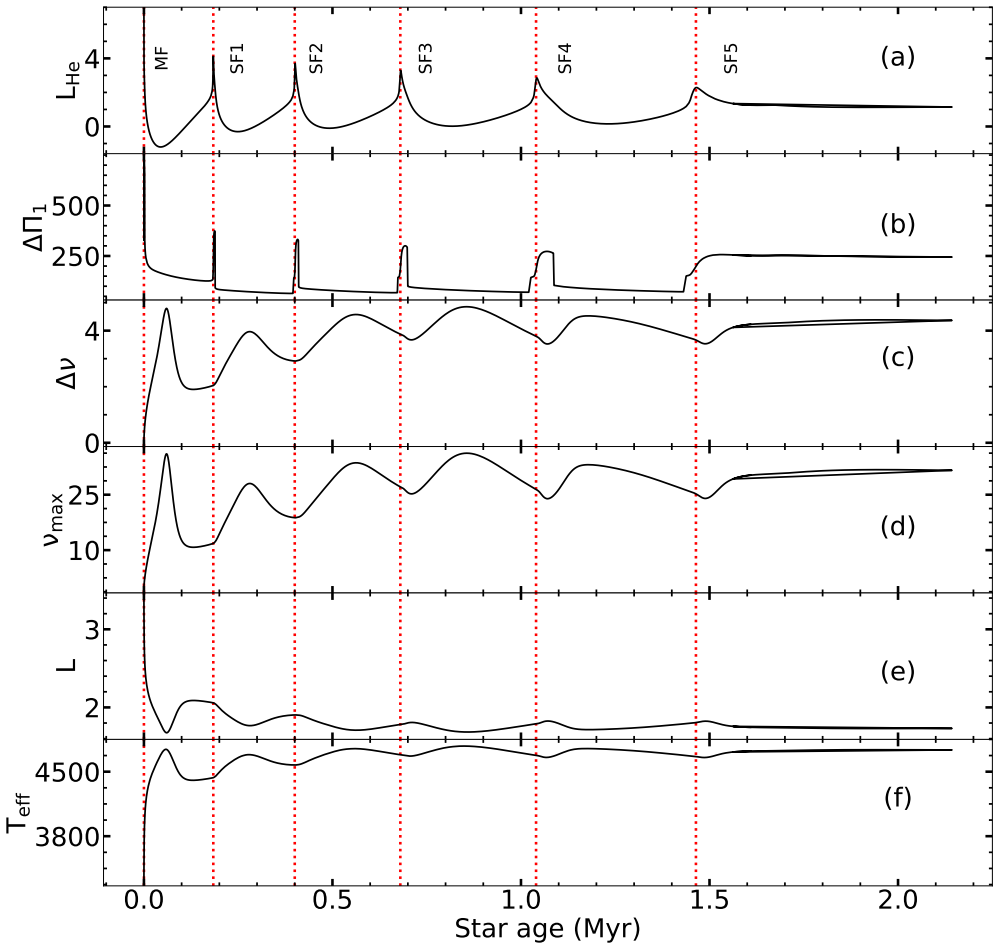

FIGURE 6.9: MESA model of 1.2 $M_\odot$ mass star with solar metallicity during He flash near the RGB tip. Figure shows variation of stellar parameters (L_{He}, $\Delta\Pi_1$, $\Delta\nu$, ν_{max}, L, T_{eff}) during the He flash near the tip of RGB in panels a, b, c, d, e, f, respectively. As shown after first major He flash strength of the subsequent subflashes diminishes. Flash duration is very short, stars spend most of the time in-between the flashes. During the flashing values of $\Delta\Pi_1$ are relatively high compared to stars in-between the flashes.

On the other hand, the late RC is affected by overshoot (eg. Constantino *et al.* 2015; Bossini *et al.* 2017). To match the highest $\Delta\Pi_1$ values ($\sim$ 330 s) we adopted exponential overshoot with overshoot parameter $f_{OS} = 0.07$.

We display the model evolution of $\Delta\Pi_1$ versus time in the top panels of Figure 6.10. Over plotted are the 2σ intervals of $\Delta\Pi_1$ for the observations of the SLR and Li-normal groups. It can be seen that the high values of $\Delta\Pi_1$ present in the Li-normal

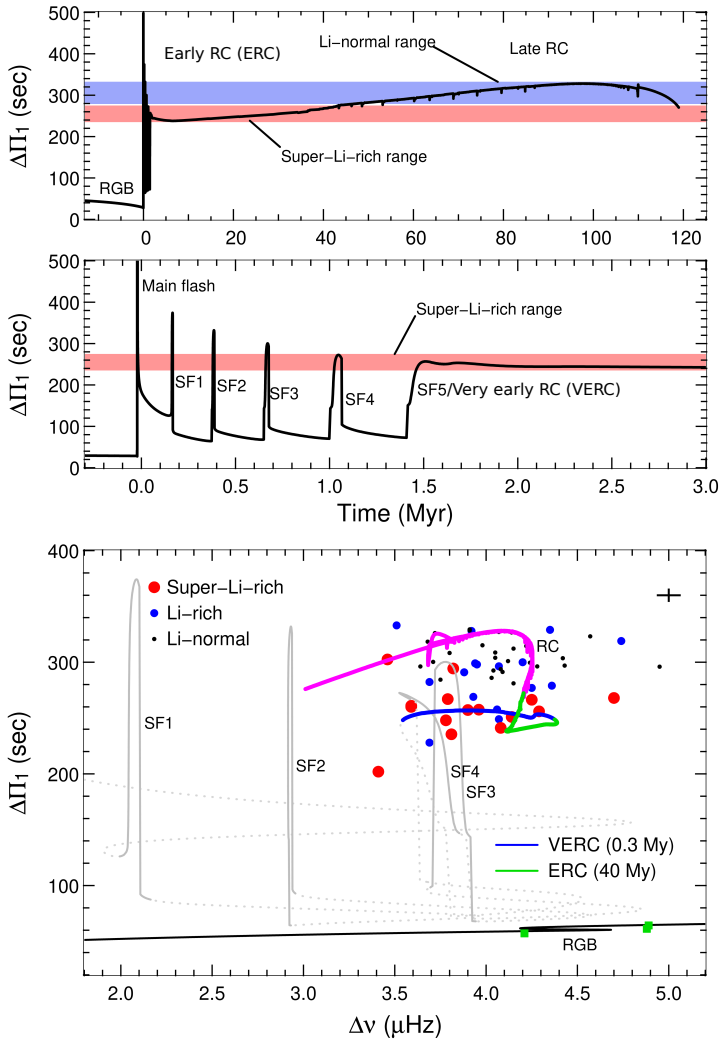

FIGURE 6.10: Stellar model showing evolution of $\Delta\Pi_1$ and $\Delta\nu$. **Top panel:** $\Delta\Pi_1$ evolution through the late RGB, the brief helium core flash phase, and the entire RC phase. The shaded bands show the 2σ intervals of $\Delta\Pi_1$ for the SLR (red) and LN stars (blue), corresponding to the distributions in Fig. 6.5. **Middle panel:** Same as above but magnified to focus on the helium flashing phase and the early RC. **Bottom panel:** Model evolution in the $\Delta\Pi_1$-$\Delta\nu$ plane (lines), compared to observations. Dotted lines are used for the evolution between (sub)flashes for clarity. Included are 3 of our RGB data points for reference (green squares).

stars are only available in the second half of the RC evolution (from $\sim$ 40 Myr onwards), or for extremely brief periods ($\sim$ 0.005 Myr) during the early helium flashes, which are unlikely to be observed in such numbers. We thus identify the Li-normal stars as more evolved RC stars. In contrast, the low $\Delta\Pi_1$ values present in the SLR stars are only consistent with young RC stars ($<$ 40 Myr in the 1.2 $M_\odot$

model). Interestingly we find there is very little overlap between the Li-normal and SLR populations. This may indicate a rapid Li-depletion event.

6.5.3 Are SLR Stars He-flash Stars?

It has been hypothesised that the Li in SLR stars is produced during the main core He-flash (CHeF; e.g. Kumar *et al.* 2011; Kumar *et al.* 2020; Schwab 2020). Here we explore the possibility that our sample of SLR stars are currently experiencing the CHeF, or are in the following sub flashing phases. In Figure 6.10 it can be seen that there is some degeneracy in $\Delta\Pi_1$ during the early phases of the RC evolution. This makes identifying the exact young RC phase that the SLR stars reside in more difficult.

The vertical portions of the $\Delta\Pi_1$ evolution are extremely short-lived, so it is very unlikely to find stars in these phases. Adding the extra dimension of $\Delta\nu$ (bottom panel of Fig. 6.10), we see that the $\Delta\nu$ values of the model's early subflashes are inconsistent with our sample. This is also true of the main CHeF (not pictured), which has $\Delta\nu \sim 0.04$ μHz. In addition, the main flash has $\Delta\Pi_1 = 700$ s, well outside our observed range. Thus we can rule out our SLR stars being in the main core helium flash. The third subflash (SF3) has $\Delta\Pi_1 \sim 300$ s, well above the SLR average value of 257 s, so we rule this out also. Three possibilities remain, defined by the SLR $\Delta\Pi_1$ band:

- The first ~ 40 Myr of RC evolution, 'early RC' (ERC in Fig. 6.10);
- The first ~ 0.3 Myr of evolution, which encompasses the 'merged' subflash SF5, named 'very early RC' (VERC: $1.6 - 1.9$ Myr range in Fig.6.10);
- The final separated helium subflash, SF4, which has a lifetime of 0.04 Myr and $\Delta\nu$ values within the range of our observations.

More information is required to distinguish between these three possible scenarios. We compared the average SLR $\Delta\nu$ and $\nu_{\rm max}$ values to the Li-normal average values and found that for both of these parameters the SLR stars have slightly lower values: 3.90 ± 0.08 vs 4.13 ± 0.07 μHz for $\Delta\nu$, and 31.97 ± 1.31 vs 34.43 ± 1.15 μHz for $\nu_{\rm max}$, see Figure 6.6. The differences in both cases are at the 1σ level. We note that systematically lower values of $\Delta\nu$ and $\nu_{\rm max}$ (at low $\Delta\Pi_1$, see Fig. 6.10) are more consistent with the SLR stars being subflashing stars (SF4 in Fig. 6.10) or VERC stars, rather than the more evolved ERC stars which have higher $\Delta\nu$. We checked for mass dependence of $\Delta\nu$ amongst the SLR stars and found no trend. Large surveys give us statistical information on Li-rich giants that may also help in identifying the exact phase of SLR stars. Using the large samples of Kumar *et al.* (2020) and Singh *et al.* (2019a) we have calculated the SLR fractions to be 0.3% and 0.5%, respectively. If we hypothesise that all stars go through a SLR phase, then we can estimate timescales of the SLR phase. The RC phase lasts for $\sim$ 100 Myr, implying that the SLR phase would last around $0.3 - 0.5$ Myr. The lifetime of SF4 is only 0.04 Myr, so this is inconsistent with the timescale estimated from the surveys. Put another way, we find too many SLR stars for the SF4 scenario, by a factor of $\sim$ 10. Further, we estimated the probability of finding even one SF star in our sample and found an expectation of 0.02 stars. We therefore conclude that the SLR stars are highly unlikely to be in a flashing phase.

6.5.4 How young are the SLR stars?

To attempt to distinguish between the two remaining phases we calculated a series of models, to quantify the theoretical versus observational dispersion in $\Delta\Pi_1$ and $\Delta\nu$. The models had the same parameters as the representative 1.2 $M_\odot$ model shown in Figure 6.10, but vary in mass ($M = 0.9, 1.2, 1.4$ $M_\odot$) and metallicity ([Fe/H]$= -0.4, +0.0$), to cover the bulk of our observational sample. We found

that the various stellar tracks covered the observed range of $\Delta\nu$ for the SLR stars. Other model parameters, such as the convective mixing length $\alpha_{\rm MLT}$ would further increase the dispersion in $\Delta\nu$ (Constantino *et al.* 2015; Bossini *et al.* 2017). Thus we are unable to distinguish between the VERC and ERC scenarios with our data. In contrast, as discussed above, $\Delta\Pi_1$ does not vary much with mass in the early RC phases (eg. Bossini *et al.* 2017) – the low $\Delta\Pi_1$ values we observe are always found in the ERC or VERC, reinforcing the finding that the objects are all young, or very young, RC stars.

In the ERC case only a small proportion, $\sim 1\%$, of stars would be super-Li-rich. This is a factor of 2-3 higher than the fraction found when taking into account all RC stars, consistent with the SLR stars being only found in the first $\sim 40\%$ of the RC lifetime. In the VERC case $\sim 100\%$ of low-mass stars would be SLR. That is, super-Li-richness would be a universal phase of low-mass stars. They would already be super-Li-rich as they start the RC, which would be consistent with the model of Schwab (2020), where the Li-enrichment occurs during the main CHeF although they report that their model depletes Li substantially before settling onto the RC. A universal SLR phase would also resonate with the finding of Kumar *et al.* (2020), who report that all low-mass stars appear to go through a Li-enrichment phase, albeit to more moderate abundances – although this difference would be explained by our Li-normal group, which indicates that strong depletion occurs during the RC.

In summary, the evidence tends to suggests that the SLR stars are possibly in a very early phase of RC evolution, i.e. less than ~ 2 Myr since the main core helium flash. Further, the statistics from large surveys suggests that they are not in a 'separated' subflashing phase, but are most likely in the initial RC phase, We can detect stars in these subflashes because of longer timescale relative to the major He flash and first few He subflashes. 3rd or 4th sub-flashes are also overlapped by the early RC phase.

6.5.5 The Li-rich group

Our normal-Li sample suggests that the majority of stars end up depleting Li to a similar degree. However the Li-rich group (Fig. 6.5) is more difficult to interpret, since the $\Delta\Pi_1$ distribution is so broad. One possible hypothesis is that the higher $\Delta\Pi_1$ stars in this group are subflashing stars. However, the probability of observing a star undergoing this phase is very low. We speculate that the higher $\Delta\Pi_1$ stars in this group may be subflashing stars. The remaining Li-rich stars could be stars in a phase of evolution intermediate to the SLR and Li-normal stars, currently depleting Li on their way to the late RC. This aligns with their $\Delta\Pi_1$ distribution being peaked at 290 s, which is between that of the SLR group (257 s) and the Li-normal group (306 s). Clearly more information is needed to disentangle the evolutionary state(s) of the Li-rich group.

6.6 Conclusion

By combining asteroseismic and spectroscopic measurements for a sample of giant stars we discovered a strong correlation between A(Li) and $\Delta\Pi_1$, whereby super-Li-rich stars are almost universally young RC stars, and Li-normal stars are predominately older RC stars. The simplest explanation for this is that (i) there is a Li-enrichment phase before the start of the RC, either near the RGB tip or during the core flashing phase, and (ii) Li is depleted during the early phases of RC evolution. The exact time of the Li depletion, which could be in very early phases of RC evolution ($\sim 0.3\%$ of RC lifetime) or later during the early RC (first $\sim 40\%$ of RC evolution) is indistinguishable with our current data. If it occurs in the very early RC phase then it implies that *all* low-mass stars go through a SLR phase. If it occurs later then $\sim 1\%$ go through a SLR phase. More data is required to separate these scenarios. Also, probably, if confirmed, the correlation

would be the first observational evidence for the theoretically predicted phase of converting an inert, degenerate He-core into a fully convective helium burning core (Schwarzschild and Härm 1962b; Thomas 1967).

Chapter 7

Conclusions

In this thesis, we have focused on understanding lithium excess among a small group of red giants. Li excess has been a long-standing problem for over four decades since its serendipitous discovery in the 1980s. It remained as a puzzle since then. Both the standard models and new extra-mixing models of low mass stars predict only severe depletion of lithium from their initial values on the main sequence, let alone producing Li in enormous quantities seen in a small group of red giants. Also, the problem remained unsolved because the number of classified giants as Li-rich was very small until very recently. It is because that most of the Li-rich giants' discoveries were mainly based on high-resolution spectra that, too, by serendipity. Since getting high-resolution spectra is quite time-consuming, there were no large survey efforts for searching Li-rich giants. Another reason being the establishment of a correct evolutionary phase of Li-rich giants. It was generally done until very recently by placing them in the HR diagram. Given the uncertainties in stellar parameters like mass, $T_{\rm eff}$, and log g and their small differences between stars of different evolutionary phases studies suggested different evolutionary phases for Li-rich giants. Phases include giants below the RGB bump, at the bump, or anywhere on RGB and red clump region leading to variety

of process for Li excess in giants.

Our goal is to understand whether the Li-excess is due to multiple processes as suggested in literature or due to some single process at a particular evolutionary phase. To meet the goal, we required assembling large data of spectra for Li determination and also identifying some independent way of knowing the evolutionary phase of Li-rich giants other than using HRD and theoretical evolutionary tracks.

We assembled large data sets from LAMOST low-resolution spectroscopic survey of the northern hemisphere, *Kepler* photometric survey and *Gaia* astrometry with a follow-up study of high-resolution spectra obtained for few stars using 2-m HCT. While low-resolution spectra from LAMOST enabled us to search for Li-rich candidates among a large set of giants, the high cadence time-resolved *Kepler* photometric survey provided data to determine the unambiguous evolutionary phase of giants. In particular, *Kepler* data is used to derive characteristic asteroseismic parameters like period spacing between the dipole mixed modes (p- and g-modes) and frequency separation between two consecutive radial modes by which we could separate giants ascending the RGB for the first time, i.e. with inert He-core from those of in the red clump phase, post-He-flash, with He-burning at the center.

Initial Results and Clues: Our suspicion that there may be only one unique process at a particular evolutionary phase of stars is responsible for Li-excess in giants was strengthened by our discovery of four new super Li-rich giants (Chapter 3). Two of which are from the *Kepler* field and their evolutionary phase was determined directly from the asteroseismic analysis. The other two were classified as red clump giants not using the direct asteroseismic method but using secondary calibration based on spectra and asteroseismology. We could also ascertain their evolutionary phase from the analysis of their high-resolution spectra for the all four super Li-rich giants. Derived elemental abundances like [C/N] and $^{12}C/^{13}C$ which are sensitive to evolutionary phase confirmed giants' RC classification based

on asteroseismology. Both the parameters are relatively much lower for RC giants compared to their counterparts on RGB. However, since the *Kepler* survey has minimal sky coverage, not many Li-rich giants could be found common in the *Kepler* field. There were only two Li-rich giants in the *Kepler* field until this study, and both were classified as RC. Our discovery of the four super Li-rich RC giants strengthened the idea that Li enhancement probably lies beyond the RGB phase with He-inert core. Our initial results Bharat Kumar *et al.* (2018); Singh *et al.* (2019b) prompted us to undertake a large systematic survey of giants common among *Kepler* and LAMOST fields.

Large Survey results: We performed for the first time the largest survey of its kind for searching Li-rich giants among spectroscopic (for Li abundances) and photometric surveys (for asteroseismology) to determine the precise evolutionary phase of Li-rich giants and the associated mechanism. We found that about 12,500 giants in the *Kepler* space telescope field are also in LAMOST spectroscopic survey fields. However, we limited our Li estimation to giants for which the Li resonance line at 6707Å is strong so that it yields A(Li) $\geq$ 3.2 dex. We made this choice because of low spectral resolution and to avoid picking up any normal giants A(Li) $\leq$ 1.8 dex as Li-rich giants. We performed the asteroseismic analysis of these high Li-rich giants using *Kepler* data. We found 26 giants (of which 24 are new) with estimated A(Li) $\geq$ 3.2 dex and all of them with asteroseismic analysis parameters: $\Delta P > 150$ sec and $\Delta\nu < 7\,\mu$Hz) implying at least all the super Li-rich giants are red clump giants. This is one of the key results (Singh *et al.* 2019a).

Our study based on a large, unbiased sample reinforced the suggestion that Li excess origin lies among red clump giants rather than anywhere else on RGB. These results prompted other studies (e.g. Kumar *et al.* (2020)) to systematically look for the Li-rich phenomenon among RC giants leading to a conclusion that Li enhancement is ubiquitous among red clump giants. The average Li abundance of

RC giants is a factor of 40 or more than their counterparts on upper RGB. Studies also showed Li abundances are very low among RGB giants and reach as low as A(Li) = −0.9 dex as giants approach the tip of RGB. Very low values of A(Li) on RGB agree well with the theoretical models with the extra-mixing mechanism. Since the He-flash event at the RGB tip is the only major event between the very low Li abundance phase of upper RGB and Li enriched RC giants, the He-flashing event and its associated mixing process was identified as possible mechanisms for the Li excess in RC giants. After firmly establishing that Li enhancement is only associated with red clump giants, we further undertook a novel study to understand the underlying process causing the Li enrichment among RC giants.

He-flashing phase & **Site of lithium enhancement:** Is the overabundance of Li seen among red clump giants caused by some process during the giants' red clump evolution of 100 My or prior to it, just after the termination of RGB? RGB phase is understood to be terminated by He-flash at the centre. He flashing will convert inert He-degenerate core into a convective He-core burning through a series of sub-flashes after the main He-flash. The entire process is predicted to last for about two Myr. It is predicted from the models that g-mode period spacing ($\Delta\Pi_1$) of stellar oscillations vary with the evolution of the central He-core. Values of $\Delta\Pi_1$ increase with progressively waning of central degeneracy at the centre. This means giants with fully convective cores burning He-at the centre have relatively larger $\Delta\Pi_1$ values (300 s) than giants with He-degenerate cores (150-200). In between, during the sub-flashing phase, $\Delta\Pi_1$ values are predicted to be somewhere between the values of fully convective core and degenerate cores of RGB.

We did a novel study (Chapter 6) in which we assembled a sample of RC giants for which $\Delta\Pi_1$ and Li abundance could be measured reliably. Derivation of $\Delta\Pi_1$ (asymptotic period spacing) values requires very high quality and high cadence

time-resolved photometry. We found 59 RC giants for which we could get values of $\Delta\Pi_1$ using *Kepler* survey data and accurate Li abundances measurements either from literature or by deriving in this study using recently released LAMOST medium-resolution spectroscopic data. Interestingly, we found a correlation between A(Li) values and $\Delta\Pi_1$ values of red clump giants. In that, all the super Li-rich giants seem to belong to exclusively the very early stage of the He-flashing phase, i.e. having low values of $\Delta\Pi_1$ and very low Li-abundance RC giants or normal RC giants, belong to the late stage of RC, i.e., having high values of $\Delta\Pi_1$ (see Chapter 6). For giants in between the two extremes (with A(Li) $>$ 1.0 dex and $<$ 3.2 dex) there is not much clarity as they seem to have a large range in $\Delta\Pi_1$. Our computed models, based on MESA stellar codes for the evolution of $\Delta\Pi_1$, starting from the initiation of He-flash at the core, suggest a robust upper limit for the age of 40 Myr within which Li enhancement occurred. The upper limit could be much shorter. For example, the estimated SLRs fractions (0.3 to 0.5% of total RC giants) among the recent large surveys, including our own, suggest super Li-rich giants are about 300 - 500 thousand years old. This implies that Li enhancement occurred immediately after the main flash or within the period of initial flashes. These observations suggest SLRs formed at least within 2 Myr. The correlation between the two independent parameters like A(Li) and a parameter related to stellar oscillations is a very key result from which one could draw the following suggestion: a) Li is indeed produced during the He-flashing period of 2 Myr with conservative upper limit of 40 Myr from the start of He-flash ignition, b) A small fraction of SLRs among RC giants implies Li enhancement among RC giants is a transient phenomenon further indicating a rapid depletion of A(Li), nearly 2-3 orders of magnitude, from high SLRs phase to its normal Li phase, c) Evolution of A(Li) along with $\Delta\Pi_1$ would also serve as observational evidence for the transition phase of converting an entirely inert degenerate He-core into a fully convective He-core burning RC giant which was predicted in the late 1950s.

7.1 Future prospect

Our immediate goal would be to gather more data of RC giants with well-determined asteroseismic parameters and accurate Li abundances for firming the relation between A(Li) and $\Delta\Pi_1$ values, which would help to identify the location in which Li gets enriched in these stars. For example, it is essential to understand whether the Li is brought up to the surface during the individual He-flashes. Actual flashing periods last only a few hundred to thousand years. Identifying Li-rich RC giants during the flashing requires an extensive data set with accurate A(Li) and $\Delta\Pi_1$. This would lead to a better understanding of stellar evolution and nucleosynthesis aspects during the He-flashing period, a transition phase between the tip of RGB and the RC phase, which are known very little.

Further, these studies could be expanded by tracking Li evolution across RC giants starting from the end of RGB tip to asymptotic giant branch (AGB) stars via early AGB giants, a successive phase of RC. Many early AGB giants are also known to have enriched Li, and the cause for it is not well understood. It would be worth pursuing any connection between the Li excess seen in early AGB and the Li production during the He-flashing phase prior to the RC phase. In particular, understanding Li enrichment and its precise evolution among AGB stars known to have a copious mass loss would help quantify Li's contribution to the ISM.

One of the larger goals of Li study in stars is to understand Li evolution in the universe, its sources and sinks. Would stars contribute to a 4 - 6 fold increase of Li in the universes from its initial or primordial value to its present value of A(Li) $\approx$ 3.2 dex measured in young stars or interstellar medium? Though it is now established that low mass stars do undergo Li production in stars during their RC evolution, it is not understood how much they contribute to ISM and the overall Li enhancement in the Galaxy/Universe. Generally, ISM gets enriched by large-scale material, enriched by chemical elements, outflow via mass loss, or

stellar explosions. It would be important to gather mass loss information of the RC giants and other evolved stars in which Li is known to have enhanced to address the bigger picture.

Bibliography

Adamów, M., Niedzielski, A., Villaver, E., Wolszczan, A. and Nowak, G., 2014, "The Penn State - Toruń Centre for Astronomy Planet Search stars. II. Lithium abundance analysis of the red giant clump sample", *Astron. Astrophys.*, **569**, A55. [DOI], [ADS], [arXiv:1407.4956 [astro-ph.SR]]

Aguilera-Gómez, C., Chanamé, J., Pinsonneault, M. H. and Carlberg, J. K., 2016, "On Lithium-rich Red Giants. I. Engulfment of Substellar Companions", *Astrophys. J.*, **829**, 127. [DOI], [ADS], [arXiv:1605.05332 [astro-ph.SR]]

Aizenman, M., Smeyers, P. and Weigert, A., 1977, "Avoided Crossing of Modes of Non-radial Stellar Oscillations", *Astron. Astrophys.*, **58**, 41. [ADS]

Albareti, F. D., Allende Prieto, C., Almeida, A., Anders, F., Anderson, S., Andrews, B. H., Aragón-Salamanca, A., Argudo-Fernández, M., Armengaud, E., Aubourg, E. and et al., 2017, "The 13th Data Release of the Sloan Digital Sky Survey: First Spectroscopic Data from the SDSS-IV Survey Mapping Nearby Galaxies at Apache Point Observatory", *Astrophys. J. Suppl.*, **233**, 25. [DOI], [ADS], [arXiv:1608.02013]

Alexander, J. B., 1967, "A possible source of lithium in the atmospheres of some red giants", *The Observatory*, **87**, 238–240. [ADS]

Allende Prieto, C., Lambert, D. L. and Asplund, M., 2001, "The Forbidden Abundance of Oxygen in the Sun", *Astrophys. J. Lett.*, **556**, L63–L66. [DOI], [ADS], [astro-ph/0106360]

Alonso, A., Arribas, S. and Martínez-Roger, C., 1999, "The effective temperature scale of giant stars (F0-K5). II. Empirical calibration of T_{eff} versus colours and [Fe/H]", *Astron. Astrophys. Suppl.*, **140**, 261–277. [DOI], [ADS]

Anthony-Twarog, B. J., Deliyannis, C. P., Rich, E. and Twarog, B. A., 2013, "A Lithium-rich Red Giant Below the Clump in the Kepler Cluster, NGC 6819", *Astrophys. J. Lett.*, **767**, L19. [DOI], [ADS], [arXiv:1303.2984 [astro-ph.SR]]

Asplund, M., Grevesse, N., Sauval, A. J. and Scott, P., 2009, "The Chemical Composition of the Sun", *Ann. Rev. Astron. Astrophys.*, **47**, 481–522. [DOI], [ADS], [arXiv:0909.0948 [astro-ph.SR]]

Balachandran, S. C., Fekel, F. C., Henry, G. W. and Uitenbroek, H., 2000, "Two K Giants with Supermeteoritic Lithium Abundances: HDE 233517 and HD 9746", *Astrophys. J.*, **542**, 978–988. [DOI], [ADS]

Barban, C., Matthews, J. M., De Ridder, J., Baudin, F., Kuschnig, R., Mazumdar, A., Samadi, R., Guenther, D. B., Moffat, A. F. J., Rucinski, S. M., Sasselov, D., Walker, G. A. H. and Weiss, W. W., 2007, "Detection of solar-like oscillations in the red giant star Ophiuchi by MOST spacebased photometry", *Astron. Astrophys.*, **468**(3), 1033–1038. [DOI], [ADS]

Bayo, A., Rodrigo, C., Barrado Y Navascués, D., Solano, E., Gutiérrez, R., Morales-Calderón, M. and Allard, F., 2008, "VOSA: virtual observatory SED analyzer. An application to the Collinder 69 open cluster", *Astron. Astrophys.*, **492**(1), 277–287. [DOI], [ADS], [arXiv:0808.0270 [astro-ph]]

Beck, P. G., Bedding, T. R., Mosser, B., Stello, D., Garcia, R. A., Kallinger, T., Hekker, S., Elsworth, Y., Frandsen, S., Carrier, F., De Ridder, J., Aerts, C., White, T. R., Huber, D., Dupret, M.-A., Montalbán, J., Miglio, A., Noels, A., Chaplin, W. J., Kjeldsen, H., Christensen-Dalsgaard, J., Gilliland, R. L., Brown, T. M., Kawaler, S. D., Mathur, S. and Jenkins, J. M., 2011, "Kepler Detected Gravity-Mode Period Spacings in a Red Giant Star", *Science*, **332**, 205. [DOI], [ADS]

Bedding, T. R., Mosser, B., Huber, D., Montalbán, J., Beck, P., Christensen-Dalsgaard, J., Elsworth, Y. P., García, R. A., Miglio, A., Stello, D., White, T. R., De Ridder, J., Hekker, S., Aerts, C., Barban, C., Belkacem, K., Broomhall, A.-M., Brown, T. M., Buzasi, D. L., Carrier, F., Chaplin, W. J., di Mauro, M. P., Dupret, M.-A., Frandsen, S., Gilliland, R. L., Goupil, M.-J., Jenkins, J. M., Kallinger, T., Kawaler, S., Kjeldsen, H., Mathur, S., Noels, A., Silva Aguirre, V. and Ventura, P., 2011, "Gravity modes as a way to distinguish between hydrogen- and helium-burning red giant stars", *Nature*, **471**, 608–611. [DOI], [ADS], [arXiv:1103.5805 [astro-ph.SR]]

Bethe, H. A., 1939, "Energy Production in Stars", *Physical Review*, **55**(5), 434–456. [DOI], [ADS]

Bethe, H. A. and Critchfield, C. L., 1938, "The Formation of Deuterons by Proton Combination", *Physical Review*, **54**(4), 248–254. [DOI], [ADS]

Bharat Kumar, Y., Reddy, B. E., Muthumariappan, C. and Zhao, G., 2015, "Far-infrared study of K giants in the solar neighborhood: Connection between Li enrichment and mass-loss", *Astron. Astrophys.*, **577**, A10. [DOI], [ADS], [arXiv:1503.01548 [astro-ph.SR]]

Bharat Kumar, Y., Singh, R., Eswar Reddy, B. and Zhao, G., 2018, "Two New Super Li-rich Core He-burning Giants: A New Twist to the Long Tale of Li Enhancement in K Giants", *Astrophys. J. Lett.*, **858**, L22. [DOI], [ADS], [arXiv:1804.10955 [astro-ph.SR]]

Bildsten, Lars, Paxton, Bill, Moore, Kevin and Macias, Phillip J., 2012, "Acoustic Signatures of the Helium Core Flash", *Astrophys. J. Lett.*, **744**(1), L6. [DOI], [ADS], [arXiv:1111.6867 [astro-ph.SR]]

Böhm-Vitense, E., 1958, "Über die Wasserstoffkonvektionszone in Sternen verschiedener Effektivtemperaturen und Leuchtkräfte. Mit 5 Textabbildungen", *Z. Astrophys.*, **46**, 108. [ADS]

Borucki, W. J., Koch, D., Basri, G., Batalha, N., Brown, T., Caldwell, D., Caldwell, J., Christensen-Dalsgaard, J., Cochran, W. D., DeVore, E., Dunham, E. W., Dupree, A. K., Gautier, T. N., Geary, J. C., Gilliland, R., Gould, A., Howell, S. B., Jenkins, J. M., Kondo, Y., Latham, D. W., Marcy, G. W., Meibom, S., Kjeldsen, H., Lissauer, J. J., Monet, D. G., Morrison, D., Sasselov, D., Tarter, J., Boss, A., Brownlee, D., Owen, T., Buzasi, D., Charbonneau, D., Doyle, L., Fortney, J., Ford, E. B., Holman, M. J., Seager, S., Steffen, J. H., Welsh, W. F., Rowe, J., Anderson, H., Buchhave, L., Ciardi, D., Walkowicz, L., Sherry, W., Horch, E., Isaacson, H., Everett, M. E., Fischer, D., Torres, G., Johnson, J. A., Endl, M., MacQueen, P., Bryson, S. T., Dotson, J., Haas, M., Kolodziejczak, J., Van Cleve, J., Chandrasekaran, H., Twicken, J. D., Quintana, E. V., Clarke, B. D., Allen, C., Li, J., Wu, H., Tenenbaum, P., Verner, E., Bruhweiler, F., Barnes, J. and Prsa, A., 2010, "Kepler Planet-Detection Mission: Introduction and First Results", *Science*, **327**, 977. [DOI], [ADS]

Bossini, D., Miglio, A., Salaris, M., Vrard, M., Cassisi, S., Mosser, B., Montalbán, J., Girardi, L., Noels, A., Bressan, A., Pietrinferni, A. and Tayar, J., 2017, "Kepler red-clump stars in the field and in open clusters: constraints on core mixing", *Mon. Not. Roy. Astron. Soc.*, **469**(4), 4718–4725. [DOI], [ADS], [arXiv:1705.03077 [astro-ph.GA]]

Bressan, A., Marigo, P., Girardi, L., Salasnich, B., Dal Cero, C., Rubele, S. and Nanni, A., 2012, "PARSEC: stellar tracks and isochrones with the PAdova and TRieste Stellar Evolution Code", *Mon. Not. Roy. Astron. Soc.*, **427**, 127–145. [DOI], [ADS], [arXiv:1208.4498 [astro-ph.SR]]

Brown, J. A., Sneden, C., Lambert, D. L. and Dutchover, Jr., E., 1989, "A search for lithium-rich giant stars", *Astrophys. J. Suppl.*, **71**, 293–322. [DOI], [ADS]

Brown, Timothy M., Gilliland, Ronald L., Noyes, Robert W. and Ramsey, Lawrence W., 1991, "Detection of Possible p-Mode Oscillations on Procyon", *Astrophys. J.*, **368**, 599. [DOI], [ADS]

Buzasi, D., Catanzarite, J., Laher, R., Conrow, T., Shupe, D., Gautier, T. N., III, Kreidl, T. and Everett, D., 2000, "The Detection of Multimodal Oscillations on α Ursae Majoris", *Astrophys. J. Lett.*, **532**(2), L133–L136. [DOI], [ADS], [arXiv:astro-ph/0002512 [astro-ph]]

Cameron, A. G. W. and Fowler, W. A., 1971, "Lithium and the s-PROCESS in Red-Giant Stars", *Astrophys. J.*, **164**, 111. [DOI], [ADS]

Cannon, R. D., 1970, "Red giants in old open clusters.", *Mon. Not. Roy. Astron. Soc.*, **150**, 111. [DOI], [ADS]

Cantiello, M. and Langer, N., 2010, "Thermohaline mixing in evolved low-mass stars", *Astron. Astrophys.*, **521**, A9. [DOI], [ADS], [arXiv:1006.1354 [astro-ph.SR]]

Carlberg, J. K., Smith, V. V., Cunha, K., Majewski, S. R. and Rood, R. T., 2010, "The Super Lithium-rich Red Giant Rapid Rotator G0928+73.2600: A Case for Planet Accretion?", *Astrophys. J. Lett.*, **723**, L103–L107. [DOI], [ADS], [arXiv:1010.2954 [astro-ph.SR]]

Carlberg, J. K., Smith, V. V., Cunha, K., Majewski, S. R., Mészáros, S., Shetrone, M., Allende Prieto, C., Bizyaev, D., Stassun, K. G., Fleming, S. W., Zasowski, G., Hearty, F., Nidever, D. L., Schneider, D. P., Holtzman, J. A. and Frinchaboy, P. M., 2015, "The Puzzling Li-rich Red Giant Associated with NGC 6819", *Astrophys. J.*, **802**, 7. [DOI], [ADS], [arXiv:1501.05625 [astro-ph.SR]]

Carlberg, Joleen K., Cunha, Katia, Smith, Verne V. and Majewski, Steven R., 2012, "Observable Signatures of Planet Accretion in Red Giant Stars. I. Rapid Rotation and Light Element Replenishment", *Astrophys. J.*, **757**(2), 109. [DOI], [ADS], [arXiv:1208.1775 [astro-ph.SR]]

Casey, A. R., Ruchti, G., Masseron, T., Randich, S., Gilmore, G., Lind, K., Kennedy, G. M., Koposov, S. E., Hourihane, A., Franciosini, E., Lewis, J. R., Magrini, L., Morbidelli, L., Sacco, G. G., Worley, C. C., Feltzing, S., Jeffries, R. D., Vallenari, A., Bensby, T., Bragaglia, A., Flaccomio, E., Francois, P.,

Korn, A. J., Lanzafame, A., Pancino, E., Recio-Blanco, A., Smiljanic, R., Carraro, G., Costado, M. T., Damiani, F., Donati, P., Frasca, A., Jofré, P., Lardo, C., de Laverny, P., Monaco, L., Prisinzano, L., Sbordone, L., Sousa, S. G., Tautvaišienė, G., Zaggia, S., Zwitter, T., Delgado Mena, E., Chorniy, Y., Martell, S. L., Silva Aguirre, V., Miglio, A., Chiappini, C., Montalban, J., Morel, T. and Valentini, M., 2016, "The Gaia-ESO Survey: revisiting the Li-rich giant problem", *Mon. Not. Roy. Astron. Soc.*, **461**, 3336–3352. [DOI], [ADS], [arXiv:1603.03038 [astro-ph.SR]]

Casey, Andrew R., Ho, Anna Y. Q., Ness, Melissa, Hogg, David W., Rix, Hans-Walter, Angelou, George C., Hekker, Saskia, Tout, Christopher A., Lattanzio, John C., Karakas, Amanda I., Woods, Tyrone E., Price-Whelan, Adrian M. and Schlaufman, Kevin C., 2019, "Tidal Interactions between Binary Stars Can Drive Lithium Production in Low-mass Red Giants", *Astrophys. J.*, **880**(2), 125. [DOI], [ADS], [arXiv:1902.04102 [astro-ph.SR]]

Cassisi, S., Salaris, M. and Pietrinferni, A., 2016, "The red giant branch phase transition: Implications for the RGB luminosity function bump and detections of Li-rich red clump stars", *Astron. Astrophys.*, **585**, A124. [DOI], [ADS], [arXiv:1510.07870 [astro-ph.SR]]

Castelli, F. and Kurucz, R. L., 2004, "New Grids of ATLAS9 Model Atmospheres", *ArXiv Astrophysics e-prints*. [ADS], [astro-ph/0405087]

Castelli, F., Gratton, R. G. and Kurucz, R. L., 1997, "Notes on the convection in the ATLAS9 model atmospheres.", *Astron. Astrophys.*, **318**, 841–869. [ADS]

Castilho, B. V., Spite, F., Barbuy, B., Spite, M., de Medeiros, J. R. and Gregorio-Hetem, J., 1999, "Beryllium abundance in lithium-rich giants", *Astron. Astrophys.*, **345**, 249–255. [ADS]

Cayrel, R., 1988, "Data Analysis", in *The Impact of Very High S/N Spectroscopy on Stellar Physics*, (Eds.) Cayrel de Strobel, G., Spite, M., IAU Symposium, 132, [ADS]

Chabrier, G., Baraffe, I. and Plez, B., 1996, "Mass-Luminosity Relationship and Lithium Depletion for Very Low Mass Stars", *Astrophys. J. Lett.*, **459**, L91. [DOI], [ADS]

Charbonnel, C., 1994, "Clues for non-standard mixing on the red giant branch from C-12/C-13 and C-12/N-14 ratios in evolved stars", *Astron. Astrophys.*, **282**, 811–820. [ADS]

Charbonnel, C., 2005, "Mixing Along the Red Giant Branch: Where Do We Stand?", in *Cosmic Abundances as Records of Stellar Evolution and Nucleosynthesis*, (Eds.) Barnes, III, T. G., Bash, F. N., Astronomical Society of the Pacific Conference Series, 336, [ADS]

Charbonnel, C. and Balachandran, S. C., 2000, "The Nature of the lithium rich giants. Mixing episodes on the RGB and early-AGB", *Astron. Astrophys.*, **359**, 563–572. [ADS], [arXiv:astro-ph/0005280 [astro-ph]]

Charbonnel, C. and Zahn, J. P., 2007, "Thermohaline mixing: a physical mechanism governing the photospheric composition of low-mass giants", *Astron. Astrophys.*, **467**(1), L15–L18. [DOI], [ADS], [arXiv:astro-ph/0703302 [astro-ph]]

Choi, Jieun, Dotter, Aaron, Conroy, Charlie and Ting, Yuan-Sen, 2018, "On the Red Giant Branch: Ambiguity in the Surface Boundary Condition Leads to ≈100 K Uncertainty in Model Effective Temperatures", *Astrophys. J.*, **860**(2), 131. [DOI], [ADS], [arXiv:1805.04112 [astro-ph.SR]]

Christensen-Dalsgaard, J., 2015, "On the red-giant luminosity bump", *Mon. Not. Roy. Astron. Soc.*, **453**, 666–670. [DOI], [ADS], [arXiv:1507.05531 [astro-ph.SR]]

Constantino, Thomas, Campbell, Simon W., Christensen-Dalsgaard, Jørgen, Lattanzio, John C. and Stello, Dennis, 2015, "The treatment of mixing in core helium burning models - I. Implications for asteroseismology", *Mon. Not. Roy. Astron. Soc.*, **452**(1), 123–145. [DOI], [ADS], [arXiv:1506.01209 [astro-ph.SR]]

Constantino, Thomas, Campbell, Simon W. and Lattanzio, John C., 2017, "The treatment of mixing in core helium-burning models - III. Suppressing core breathing pulses with a new constraint on overshoot", *Mon. Not. Roy. Astron. Soc.*, **472**(4), 4900–4909. [DOI], [ADS], [arXiv:1709.06381 [astro-ph.SR]]

Cui, X.-Q., Zhao, Y.-H., Chu, Y.-Q., Li, G.-P., Li, Q., Zhang, L.-P., Su, H.-J., Yao, Z.-Q., Wang, Y.-N., Xing, X.-Z., Li, X.-N., Zhu, Y.-T., Wang, G., Gu, B.-Z., Luo, A.-L., Xu, X.-Q., Zhang, Z.-C., Liu, G.-R., Zhang, H.-T., Yang, D.-H., Cao, S.-Y., Chen, H.-Y., Chen, J.-J., Chen, K.-X., Chen, Y., Chu, J.-R., Feng, L., Gong, X.-F., Hou, Y.-H., Hu, H.-Z., Hu, N.-S., Hu, Z.-W., Jia, L., Jiang, F.-H., Jiang, X., Jiang, Z.-B., Jin, G., Li, A.-H., Li, Y., Li, Y.-P., Liu, G.-Q., Liu, Z.-G., Lu, W.-Z., Mao, Y.-D., Men, L., Qi, Y.-J., Qi, Z.-X., Shi, H.-M., Tang, Z.-H., Tao, Q.-S., Wang, D.-Q., Wang, D., Wang, G.-M., Wang, H., Wang, J.-N., Wang, J., Wang, J.-L., Wang, J.-P., Wang, L., Wang, S.-Q., Wang, Y., Wang, Y.-F., Xu, L.-Z., Xu, Y., Yang, S.-H., Yu, Y., Yuan, H., Yuan, X.-Y., Zhai, C., Zhang, J., Zhang, Y.-X., Zhang, Y., Zhao, M., Zhou, F., Zhou, G.-H., Zhu, J. and Zou, S.-C., 2012, "The Large Sky Area Multi-Object Fiber Spectroscopic Telescope (LAMOST)", *Research in Astronomy and Astrophysics*, **12**, 1197–1242. [DOI], [ADS]

Cutri, R. M. and et al., 2013, "VizieR Online Data Catalog: AllWISE Data Release (Cutri+ 2013)", *VizieR Online Data Catalog*, **2328**, 0. [ADS]

Cutri, R. M., Skrutskie, M. F., van Dyk, S., Beichman, C. A., Carpenter, J. M., Chester, T., Cambresy, L., Evans, T., Fowler, J., Gizis, J., Howard, E., Huchra, J., Jarrett, T., Kopan, E. L., Kirkpatrick, J. D., Light, R. M., Marsh, K. A., McCallon, H., Schneider, S., Stiening, R., Sykes, M., Weinberg, M., Wheaton, W. A., Wheelock, S. and Zacarias, N., 2003, *2MASS All Sky Catalog of point sources.*. [ADS]

Cyburt, R. H., Fields, B. D., Olive, K. A. and Yeh, T.-H., 2016, "Big bang nucleosynthesis: Present status", *Reviews of Modern Physics*, **88**(1), 015004. [DOI], [ADS], [arXiv:1505.01076]

da Silva, L., Girardi, L., Pasquini, L., Setiawan, J., von der Lühe, O., de Medeiros, J. R., Hatzes, A., Döllinger, M. P. and Weiss, A., 2006, "Basic physical parameters of a selected sample of evolved stars", *Astron. Astrophys.*, **458**, 609–623. [DOI], [ADS], [astro-ph/0608160]

de La Reza, R. and da Silva, L., 1995, "Lithium abundances in strong lithium K giant stars: LTE and non-LTE analyses", *Astrophys. J.*, **439**, 917–927. [DOI], [ADS]

de La Reza, R., Drake, N. A. and da Silva, L., 1996, "Lithium Enrichment–Mass-Loss Connection in K Giant Stars", *Astrophys. J. Lett.*, **456**, L115+. [DOI], [ADS]

de Laverny, P. and Gustafsson, B., 1998, "On the determination of carbon isotopic ratios in cool carbon stars", *Astron. Astrophys.*, **332**, 661–671. [ADS]

de Medeiros, J. R., Melo, C. H. F. and Mayor, M., 1996, "Rotational velocity for lithium-rich evolved stars.", *Astron. Astrophys.*, **309**, 465–468. [ADS]

De Medeiros, J. R., do Nascimento, Jr., J. D., Sankarankutty, S., Costa, J. M. and Maia, M. R. G., 2000, "Rotation and lithium in single giant stars", *Astron. Astrophys.*, **363**, 239–243. [ADS], [arXiv:astro-ph/0010273]

De Ridder, J., Barban, C., Carrier, F., Mazumdar, A., Eggenberger, P., Aerts, C., Deruyter, S. and Vanautgaerden, J., 2006, "Discovery of solar-like oscillations in the red giant Ophiuchi", *Astron. Astrophys.*, **448**(2), 689–695. [DOI], [ADS]

De Ridder, J., Barban, C., Baudin, F., Carrier, F., Hatzes, A. P., Hekker, S., Kallinger, T., Weiss, W. W., Baglin, A., Auvergne, M., Samadi, R., Barge, P. and Deleuil, M., 2009, "Non-radial oscillation modes with long lifetimes in giant stars", *Nature*, **459**, 398–400. [DOI], [ADS]

De Silva, G. M., Freeman, K. C., Bland-Hawthorn, J., Martell, S., de Boer, E. Wylie, Asplund, M., Keller, S., Sharma, S., Zucker, D. B., Zwitter, T., Anguiano, B., Bacigalupo, C., Bayliss, D., Beavis, M. A., Bergemann, M., Campbell, S., Cannon, R., Carollo, D., Casagrande, L., Casey, A. R., Da Costa, G., D'Orazi, V., Dotter, A., Duong, L., Heger, A., Ireland, M. J., Kafle, P. R., Kos, J., Lattanzio, J., Lewis, G. F., Lin, J., Lind, K., Munari, U., Nataf, D. M., O'Toole, S., Parker, Q., Reid, W., Schlesinger, K. J., Sheinis, A., Simpson, J. D., Stello, D., Ting, Y. S., Traven, G., Watson, F., Wittenmyer, R., Yong, D. and Žerjal, M., 2015, "The GALAH survey: scientific motivation", *Mon. Not. Roy. Astron. Soc.*, **449**, 2604–2617. [DOI], [ADS], [arXiv:1502.04767 [astro-ph.GA]]

Deepak and Reddy, B. E., 2019, "Study of Lithium-rich giants with the GALAH spectroscopic survey", *Mon. Not. Roy. Astron. Soc.*, **484**, 2000–2008. [DOI], [ADS], [arXiv:1901.03832 [astro-ph.SR]]

Deheuvels, S. and Belkacem, K., 2018, "Seismic characterization of red giants going through the helium-core flash", *A&A*, **620**, A43. [DOI]URL: https://doi.org/10.1051/0004-6361/201833409

Deliyannis, C. P., Steinhauer, A. and Jeffries, R. D., 2002, "Discovery of the Most Lithium-rich Dwarf: Diffusion in Action", *Astrophys. J. Lett.*, **577**, L39–L43. [DOI], [ADS]

Denissenkov, P. A. and Herwig, F., 2004, "Enhanced Extra Mixing in Low-Mass Red Giants: Lithium Production and Thermal Stability", *Astrophys. J.*, **612**, 1081–1091. [DOI], [ADS]

Denissenkov, P. A. and Merryfield, W. J., 2011, "Thermohaline Mixing: Does it Really Govern the Atmospheric Chemical Composition of Low-mass Red Giants?", *Astrophys. J. Lett.*, **727**, L8. [DOI], [ADS], [arXiv:1011.2191 [astro-ph.SR]]

Denissenkov, P. A., Pinsonneault, M. and MacGregor, K. B., 2009, "Magneto-Thermohaline Mixing in Red Giants", *Astrophys. J.*, **696**, 1823–1833. [DOI], [ADS], [arXiv:0806.4346]

Denissenkov, Pavel A., 2012, "A New Twist in the Evolution of Low-mass Stars", *Astrophys. J. Lett.*, **753**(1), L3. [DOI], [ADS], [arXiv:1203.1948 [astro-ph.SR]]

Denissenkov, Pavel A. and VandenBerg, Don A., 2003, "Canonical Extra Mixing in Low-Mass Red Giants", *Astrophys. J.*, **593**(1), 509–523. [DOI], [ADS]

Deubner, Franz-Ludwig and Gough, Douglas, 1984, "Helioseismology: Oscillations as a Diagnostic of the Solar Interior", *Ann. Rev. Astron. Astrophys.*, **22**, 593–619. [DOI], [ADS]

Domogatskii, G. V., Eramzhian, R. A. and Nadezhin, D. K., 1978, "Production of the Light Elements due to Neutrinos Emitted by Collapsing Stellar Cores", *Astrophys. Space Sci.*, **58**(2), 273–299. [DOI], [ADS]

Drake, N. A., de la Reza, R., da Silva, L. and Lambert, D. L., 2002, "Rapidly Rotating Lithium-rich K Giants: The New Case of the Giant PDS 365", *Astron. J.*, **123**, 2703–2714. [DOI], [ADS], [astro-ph/0202158]

Edmonds, Peter D. and Gilliland, Ronald L., 1996, "K Giants in 47 Tucanae: Detection of a New Class of Variable Stars", *Astrophys. J. Lett.*, **464**, L157. [DOI], [ADS]

Eggleton, P. P., Dearborn, D. S. P. and Lattanzio, J. C., 2006, "Deep Mixing of ^{3}He: Reconciling Big Bang and Stellar Nucleosynthesis", *Science*, **314**, 1580. [DOI], [ADS], [astro-ph/0611039]

Eggleton, P. P., Dearborn, D. S. P. and Lattanzio, J. C., 2008, "Compulsory Deep Mixing of ^{3}He and CNO Isotopes in the Envelopes of Low-Mass Red Giants", *Astrophys. J.*, **677**, 581–592. [DOI], [ADS], [arXiv:0706.2710]

Freedman, Wendy L., Madore, Barry F., Hatt, Dylan, Hoyt, Taylor J., Jang, In Sung, Beaton, Rachael L., Burns, Christopher R., Lee, Myung Gyoon, Monson, Andrew J., Neeley, Jillian R., Phillips, M. M., Rich, Jeffrey A. and Seibert,

Mark, 2019, "The Carnegie-Chicago Hubble Program. VIII. An Independent Determination of the Hubble Constant Based on the Tip of the Red Giant Branch", *Astrophys. J.*, **882**(1), 34. [DOI], [ADS], [arXiv:1907.05922 [astro-ph.CO]]

Fu, Xiaoting, Bressan, Alessandro, Marigo, Paola, Girardi, Léo, Montalbán, Josefina, Chen, Yang and Nanni, Ambra, 2018, "New parsecdata base of -enhanced stellar evolutionary tracks and isochrones – I. Calibration with 47 Tuc (NGC 104) and the improvement on RGB bump", *Monthly Notices of the Royal Astronomical Society*, **476**(1), 496–511. [DOI], [http://oup.prod.sis.lan/mnras/article-pdf/476/1/496/24243860/sty235.pdf]URL: https://doi.org/10.1093/mnras/sty235

Gaia Collaboration, Prusti, T., de Bruijne, J. H. J., Brown, A. G. A., Vallenari, A., Babusiaux, C., Bailer-Jones, C. A. L., Bastian, U., Biermann, M., Evans, D. W. and et al., 2016, "The Gaia mission", *Astron. Astrophys.*, **595**, A1. [DOI], [ADS], [arXiv:1609.04153 [astro-ph.IM]]

Gaia Collaboration, Brown, A. G. A., Vallenari, A., Prusti, T., de Bruijne, J. H. J., Babusiaux, C. and Bailer-Jones, C. A. L., 2018, "Gaia Data Release 2. Summary of the contents and survey properties", *ArXiv e-prints*. [ADS], [arXiv:1804.09365]

Gálvez-Ortiz, M. C., Delgado-Mena, E., González Hernández, J. I., Israelian, G., Santos, N. C., Rebolo, R. and Ecuvillon, A., 2011, "Beryllium abundances in stars with planets - Extending the sample", *A&A*, **530**, A66. [DOI]URL: https://doi.org/10.1051/0004-6361/200913827

Gilmore, G., Randich, S., Asplund, M., Binney, J., Bonifacio, P., Drew, J., Feltzing, S., Ferguson, A., Jeffries, R., Micela, G., Negueruela, I., Prusti, T., Rix, H. W., Vallenari, A., Alfaro, E., Allende-Prieto, C., Babusiaux, C., Bensby, T., Blomme, R., Bragaglia, A., Flaccomio, E., François, P., Irwin, M., Koposov, S., Korn, A., Lanzafame, A., Pancino, E., Paunzen, E., Recio-Blanco, A., Sacco, G., Smiljanic, R., Van Eck, S., Walton, N., Aden, D., Aerts, C., Affer, L., Alcala, J. M., Altavilla, G., Alves, J., Antoja, T., Arenou, F., Argiroffi, C.,

Asensio Ramos, A., Bailer-Jones, C., Balaguer-Nunez, L., Bayo, A., Barbuy, B., Barisevicius, G., Barrado y Navascues, D., Battistini, C., Bellas Velidis, I., Bellazzini, M., Belokurov, V., Bergemann, M., Bertelli, G., Biazzo, K., Bienayme, O., Bland-Hawthorn, J., Boeche, C., Bonito, S., Boudreault, S., Bouvier, J., Brandao, I., Brown, A., de Bruijne, J., Burleigh, M., Caballero, J., Caffau, E., Calura, F., Capuzzo-Dolcetta, R., Caramazza, M., Carraro, G., Casagrande, L., Casewell, S., Chapman, S., Chiappini, C., Chorniy, Y., Christlieb, N., Cignoni, M., Cocozza, G., Colless, M., Collet, R., Collins, M., Correnti, M., Covino, E., Crnojevic, D., Cropper, M., Cunha, M., Damiani, F., David, M., Delgado, A., Duffau, S., Edvardsson, B., Eldridge, J., Enke, H., Eriksson, K., Evans, N. W., Eyer, L., Famaey, B., Fellhauer, M., Ferreras, I., Figueras, F., Fiorentino, G., Flynn, C., Folha, D., Franciosini, E., Frasca, A., Freeman, K., Fremat, Y., Friel, E., Gaensicke, B., Gameiro, J., Garzon, F., Geier, S., Geisler, D., Gerhard, O., Gibson, B., Gomboc, A., Gomez, A., Gonzalez-Fernandez, C., Gonzalez Hernandez, J., Gosset, E., Grebel, E., Greimel, R., Groenewegen, M., Grundahl, F., Guarcello, M., Gustafsson, B., Hadrava, P., Hatzidimitriou, D., Hambly, N., Hammersley, P., Hansen, C., Haywood, M., Heber, U., Heiter, U., Held, E., Helmi, A., Hensler, G., Herrero, A., Hill, V., Hodgkin, S., Huelamo, N., Huxor, A., Ibata, R., Jackson, R., de Jong, R., Jonker, P., Jordan, S., Jordi, C., Jorissen, A., Katz, D., Kawata, D., Keller, S., Kharchenko, N., Klement, R., Klutsch, A., Knude, J., Koch, A., Kochukhov, O., Kontizas, M., Koubsky, P., Lallement, R., de Laverny, P., van Leeuwen, F., Lemasle, B., Lewis, G., Lind, K., Lindstrom, H. P. E., Lobel, A., Lopez Santiago, J., Lucas, P., Ludwig, H., Lueftinger, T., Magrini, L., Maiz Apellaniz, J., Maldonado, J., Marconi, G., Marino, A., Martayan, C., Martinez-Valpuesta, I., Matijevic, G., McMahon, R., Messina, S., Meyer, M., Miglio, A., Mikolaitis, S., Minchev, I., Minniti, D., Moitinho, A., Momany, Y., Monaco, L., Montalto, M., Monteiro, M. J., Monier, R., Montes, D., Mora, A., Moraux, E., Morel, T., Mowlavi, N., Mucciarelli, A., Munari, U., Napiwotzki, R., Nardetto, N., Naylor, T., Naze, Y., Nelemans,

G., Okamoto, S., Ortolani, S., Pace, G., Palla, F., Palous, J., Parker, R., Penarrubia, J., Pillitteri, I., Piotto, G., Posbic, H., Prisinzano, L., Puzeras, E., Quirrenbach, A., Ragaini, S., Read, J., Read, M., Reyle, C., De Ridder, J., Robichon, N., Robin, A., Roeser, S., Romano, D., Royer, F., Ruchti, G., Ruzicka, A., Ryan, S., Ryde, N., Santos, N., Sanz Forcada, J., Sarro Baro, L. M., Sbordone, L., Schilbach, E., Schmeja, S., Schnurr, O., Schoenrich, R., Scholz, R. D., Seabroke, G., Sharma, S., De Silva, G., Smith, M., Solano, E., Sordo, R., Soubiran, C., Sousa, S., Spagna, A., Steffen, M., Steinmetz, M., Stelzer, B., Stempels, E., Tabernero, H., Tautvaisiene, G., Thevenin, F., Torra, J., Tosi, M., Tolstoy, E., Turon, C., Walker, M., Wambsganss, J., Worley, C., Venn, K., Vink, J., Wyse, R., Zaggia, S., Zeilinger, W., Zoccali, M., Zorec, J., Zucker, D., Zwitter, T. and Gaia-ESO Survey Team, 2012, "The Gaia-ESO Public Spectroscopic Survey", *The Messenger*, **147**, 25–31. [ADS]

Gilroy, K. K., 1989, "More About $^{12}C/^{13}C$ Ratios in Cluster Giants Subgiants", in *Bulletin of the American Astronomical Society*, , 21, [ADS]

Gilroy, K. K. and Brown, J. A., 1991, "Carbon isotope ratios along the giant branch of M67", *Astrophys. J.*, **371**, 578–583. [DOI], [ADS]

Girardi, Léo, 2016, "Red Clump Stars", *Ann. Rev. Astron. Astrophys.*, **54**, 95–133. [DOI], [ADS]

Goldreich, P. and Keeley, D. A., 1977, "Solar seismology. II. The stochastic excitation of the solar p-modes by turbulent convection.", *Astrophys. J.*, **212**, 243–251. [DOI], [ADS]

Goldreich, Peter and Kumar, Pawan, 1988, "The Interaction of Acoustic Radiation with Turbulence", *Astrophys. J.*, **326**, 462. [DOI], [ADS]

González Hernández, J. I. and Bonifacio, P., 2009, "A new implementation of the infrared flux method using the 2MASS catalogue", *Astron. Astrophys.*, **497**, 497–509. [DOI], [ADS]

Gonzalez, O. A., Zoccali, M., Monaco, L., Hill, V., Cassisi, S., Minniti, D., Renzini, A., Barbuy, B., Ortolani, S. and Gomez, A., 2009, "Li-rich red giant branch stars in the Galactic bulge", *A&A*, **508**(1), 289–295. [DOI]URL: https://doi.org/10.1051/0004-6361/200912469

Gratton, R. G., Sneden, C., Carretta, E. and Bragaglia, A., 2000, "Mixing along the red giant branch in metal-poor field stars", *Astron. Astrophys.*, **354**, 169–187. [ADS]

Green, G. M., Schlafly, E. F., Finkbeiner, D. P., Rix, H.-W., Martin, N., Burgett, W., Draper, P. W., Flewelling, H., Hodapp, K., Kaiser, N., Kudritzki, R. P., Magnier, E., Metcalfe, N., Price, P., Tonry, J. and Wainscoat, R., 2015, "A Three-dimensional Map of Milky Way Dust", *Astrophys. J.*, **810**, 25. [DOI], [ADS], [arXiv:1507.01005]

Gustafsson, B., Karlsson, T., Olsson, E., Edvardsson, B. and Ryde, N., 1999, "The origin of carbon, investigated by spectral analysis of solar-type stars in the Galactic Disk", *Astron. Astrophys.*, **342**, 426–439. [ADS], [arXiv:astro-ph/9811303]

Hawkins, K., Masseron, T., Jofré, P., Gilmore, G., Elsworth, Y. and Hekker, S., 2016, "An accurate and self-consistent chemical abundance catalogue for the APOGEE/Kepler sample", *Astron. Astrophys.*, **594**, A43. [DOI], [ADS], [arXiv:1604.08800]

Hawkins, K., Ting, Y.-S. and Walter-Rix, H., 2018, "Photospheric Diagnostics of Core Helium Burning in Giant Stars", *Astrophys. J.*, **853**, 20. [DOI], [ADS]

Herwig, F., 2005, "Evolution of Asymptotic Giant Branch Stars", *Ann. Rev. Astron. Astrophys.*, **43**, 435–479. [DOI], [ADS]

Hinkle, K., Wallace, L., Valenti, J. and Harmer, D., 2000, *Visible and Near Infrared Atlas of the Arcturus Spectrum 3727-9300 A*. [ADS]

Hobbs, L. M., Thorburn, J. A. and Rebull, L. M., 1999, "Lithium Isotope Ratios in Halo Stars. III.", *Astrophys. J.*, **523**, 797–804. [DOI], [ADS]

Huber, D., Bedding, T. R., Stello, D., Hekker, S., Mathur, S., Mosser, B., Verner, G. A., Bonanno, A., Buzasi, D. L., Campante, T. L., Elsworth, Y. P., Hale, S. J., Kallinger, T., Silva Aguirre, V., Chaplin, W. J., De Ridder, J., García, R. A., Appourchaux, T., Frandsen, S., Houdek, G., Molenda-Żakowicz, J., Monteiro, M. J. P. F. G., Christensen-Dalsgaard, J., Gilliland, R. L., Kawaler, S. D., Kjeldsen, H., Broomhall, A. M., Corsaro, E., Salabert, D., Sanderfer, D. T., Seader, S. E. and Smith, J. C., 2011, "Testing Scaling Relations for Solar-like Oscillations from the Main Sequence to Red Giants Using Kepler Data", *Astrophys. J.*, **743**(2), 143. [DOI], [ADS], [arXiv:1109.3460 [astro-ph.SR]]

Hundt, E., 1973, "Microturbulence in Stellar Spectroscopy", *Astron. Astrophys.*, **29**, 17. [ADS]

Iben, Jr., I., 1967, "Stellar Evolution.VI. Evolution from the Main Sequence to the Red-Giant Branch for Stars of Mass 1 M_{sun}, 1.25 M_{sun}, and 1.5 M_{sun}", *Astrophys. J.*, **147**, 624. [DOI], [ADS]

Iben, Icko, Jr., 1968, "Low-Mass Red Giants", *Astrophys. J.*, **154**, 581. [DOI], [ADS]

Ishihara, D., Onaka, T., Kataza, H., Salama, A., Alfageme, C., Cassatella, A., Cox, N., García-Lario, P., Stephenson, C., Cohen, M., Fujishiro, N., Fujiwara, H., Hasegawa, S., Ita, Y., Kim, W., Matsuhara, H., Murakami, H., Müller, T. G., Nakagawa, T., Ohyama, Y., Oyabu, S., Pyo, J., Sakon, I., Shibai, H., Takita, S., Tanabé, T., Uemizu, K., Ueno, M., Usui, F., Wada, T., Watarai, H., Yamamura, I. and Yamauchi, C., 2010, "The AKARI/IRC mid-infrared all-sky survey", *Astron. Astrophys.*, **514**, A1. [DOI], [ADS], [arXiv:1003.0270 [astro-ph.IM]]

Izzo, Luca, Della Valle, Massimo, Mason, Elena, Matteucci, Francesca, Romano, Donatella, Pasquini, Luca, Vanzi, Leonardo, Jordan, Andres, Fernand

ez, José Miguel, Bluhm, Paz, Brahm, Rafael, Espinoza, Nestor and Williams, Robert, 2015, "Early Optical Spectra of Nova V1369 Cen Show the Presence of Lithium", *Astrophys. J. Lett.*, **808**(1), L14. [DOI], [ADS], [arXiv:1506.08048 [astro-ph.SR]]

Jofré, E., Petrucci, R., García, L. and Gómez, M., 2015, "KIC 9821622: An interesting lithium-rich giant in the Kepler field", *Astron. Astrophys.*, **584**, L3. [DOI], [ADS], [arXiv:1510.07192 [astro-ph.SR]]

Jorissen, A., Van Winckel, H., Siess, L., Escorza, A., Pourbaix, D. and Van Eck, S., 2020, "Li-rich K giants, dust excess, and binarity", *Astron. Astrophys.*, **639**, A7. [DOI], [ADS], [arXiv:2007.05442 [astro-ph.SR]]

Kallinger, T., De Ridder, J., Hekker, S., Mathur, S., Mosser, B., Gruberbauer, M., García, R. A., Karoff, C. and Ballot, J., 2014, "The connection between stellar granulation and oscillation as seen by the Kepler mission", *Astron. Astrophys.*, **570**, A41. [DOI], [ADS], [arXiv:1408.0817 [astro-ph.SR]]

King, C. R., Da Costa, G. S. and Demarque, P., 1985, "The luminosity function on the subgiant branch of 47 Tucanae : a comparison of observation and theory.", *Astrophys. J.*, **299**, 674–682. [DOI], [ADS]

Kirby, E. N., Guhathakurta, P., Zhang, A. J., Hong, J., Guo, M., Guo, R., Cohen, J. G. and Cunha, K., 2016, "Lithium-rich Giants in Globular Clusters", *Astrophys. J.*, **819**, 135. [DOI], [ADS], [arXiv:1601.01315 [astro-ph.SR]]

Kirby, Evan N., Guhathakurta, Puragra, Bolte, Michael, Sneden, Christopher and Geha, Marla C., 2009, "Multi-element Abundance Measurements from Medium-resolution Spectra. I. The Sculptor Dwarf Spheroidal Galaxy", *Astrophys. J.*, **705**(1), 328–346. [DOI], [ADS], [arXiv:0909.3092 [astro-ph.GA]]

Kjeldsen, H. and Bedding, T. R., 1995, "Amplitudes of stellar oscillations: the implications for asteroseismology.", *Astron. Astrophys.*, **293**, 87–106. [ADS], [astro-ph/9403015]

Kjeldsen, H., Christensen-Dalsgaard, J., Handberg, R., Brown, T. M., Gilliland, R. L., Borucki, W. J. and Koch, D., 2010, "The Kepler Asteroseismic Investigation: Scientific goals and first results", *Astronomische Nachrichten*, **331**, 966. [DOI], [ADS], [arXiv:1007.1816 [astro-ph.SR]]

Knauth, D. C., Federman, S. R. and Lambert, D. L., 2003, "An Ultra-high-Resolution Survey of the Interstellar ^{7}Li/^{6}Li Isotope Ratio in the Solar Neighborhood", *Astrophys. J.*, **586**, 268–285. [DOI], [ADS], [astro-ph/0212233]

Kumar, Y. B. and Reddy, B. E., 2009, "HD 77361: A New Case of Super Li-Rich K Giant with Anomalous Low $^{12}C/^{13}CRatio''$, $Astrophys.J.Lett.$, **703**, $L46 --L50$.[DOI], [ADS]

Kumar, Y. B., Reddy, B. E. and Lambert, D. L., 2011, "Origin of Lithium Enrichment in K Giants", *Astrophys. J. Lett.*, **730**, L12. [DOI], [ADS], [arXiv:1102.2299 [astro-ph.SR]]

Kumar, Y. B., Reddy, B. E. and Zhao, G., 2018a, "Identifying Li-rich giants from low-resolution spectroscopic survey", *Journal of Astrophysics and Astronomy*, **39**, 25. [DOI], [ADS]

Kumar, Y. B., Reddy, B. E. and Zhao, G., 2018b, "Identifying Li-rich giants from low-resolution spectroscopic survey", *Journal of Astrophysics and Astronomy*, **39**, 25. [DOI], [ADS]

Kumar, Yerra Bharat, Reddy, Bacham E., Campbell, Simon W., Maben, Sunayana, Zhao, Gang and Ting, Yuan-Sen, 2020, "Discovery of ubiquitous lithium production in low-mass stars", *Nature Astronomy*. [DOI]URL: http://dx.doi.org/10.1038/s41550-020-1139-7

Kurucz, R. L., 1979, "Model atmospheres for G, F, A, B, and O stars.", *Astrophys. J. Suppl.*, **40**, 1–340. [DOI], [ADS]

Kurucz, R. L., 1993, "A New Opacity-Sampling Model Atmosphere Program for Arbitrary Abundances", in *IAU Colloq. 138: Peculiar versus Normal Phenomena in A-type and Related Stars*, (Ed.) M. M. Dworetsky, F. Castelli, & R. Faraggiana, Astronomical Society of the Pacific Conference Series, 44, [ADS]

Kurucz, Robert L., 2011, "Including all the lines", *Canadian Journal of Physics*, **89**, 417–428. [DOI], [ADS]

Lagarde, N., Decressin, T., Charbonnel, C., Eggenberger, P., Ekström, S. and Palacios, A., 2012, "Thermohaline instability and rotation-induced mixing. III. Grid of stellar models and asymptotic asteroseismic quantities from the pre-main sequence up to the AGB for low- and intermediate-mass stars of various metallicities", *Astron. Astrophys.*, **543**, A108. [DOI], [ADS], [arXiv:1204.5193 [astro-ph.SR]]

Lambert, D. L. and Reddy, B. E., 2004, "Lithium abundances of the local thin disc stars", *Mon. Not. Roy. Astron. Soc.*, **349**, 757–767. [DOI], [ADS], [astro-ph/0401259]

Lebzelter, T., Uttenthaler, S., Busso, M., Schultheis, M. and Aringer, B., 2012, "Lithium abundances along the red giant branch: FLAMES-GIRAFFE spectra of a large sample of low-mass bulge stars", *A&A*, **538**, A36. [DOI]URL: https://doi.org/10.1051/0004-6361/201117743

Lee, Myung Gyoon, Freedman, Wendy L. and Madore, Barry F., 1993, "The Tip of the Red Giant Branch as a Distance Indicator for Resolved Galaxies", *Astrophys. J.*, **417**, 553. [DOI], [ADS]

Lee, Young Sun, Beers, Timothy C., Sivarani, Thirupathi, Allende Prieto, Carlos, Koesterke, Lars, Wilhelm, Ronald, Re Fiorentin, Paola, Bailer-Jones, Coryn A. L., Norris, John E., Rockosi, Constance M., Yanny, Brian, Newberg, Heidi J., Covey, Kevin R., Zhang, Hao-Tong and Luo, A. Li, 2008, "The SEGUE Stellar Parameter Pipeline. I. Description and Comparison of Individual Methods", *Astron. J.*, **136**(5), 2022–2049. [DOI], [ADS], [arXiv:0710.5645 [astro-ph]]

Leighton, Robert B., Noyes, Robert W. and Simon, George W., 1962, "Velocity Fields in the Solar Atmosphere. I. Preliminary Report.", *Astrophys. J.*, **135**, 474. [DOI], [ADS]

Lenz, Dawn D., Newberg, Jo, Rosner, Robert, Richards, Gordon T. and Stoughton, Chris, 1998, "Photometric Separation of Stellar Properties Using SDSS Filters", *Astrophys. J. Suppl.*, **119**(2), 121–140. [DOI], [ADS]

Li, H., Aoki, W., Matsuno, T., Bharat Kumar, Y., Shi, J., Suda, T. and Zhao, G., 2018, "Enormous Li Enhancement Preceding Red Giant Phases in Low-mass Stars in the Milky Way Halo", *Astrophys. J. Lett.*, **852**, L31. [DOI], [ADS]

Lightkurve Collaboration, Cardoso, J. V. d. M., Hedges, C., Gully-Santiago, M., Saunders, N., Cody, A. M., Barclay, T., Hall, O., Sagear, S., Turtelboom, E., Zhang, J., Tzanidakis, A., Mighell, K., Coughlin, J., Bell, K., Berta-Thompson, Z., Williams, P., Dotson, J. and Barentsen, G., 2018, "Lightkurve: Kepler and TESS time series analysis in Python", [ADS]

Lind, K., Asplund, M. and Barklem, P. S., 2009a, "Departures from LTE for neutral Li in late-type stars", *Astron. Astrophys.*, **503**, 541–544. [DOI], [ADS], [arXiv:0906.0899 [astro-ph.SR]]

Lind, K., Primas, F., Charbonnel, C., Grundahl, F. and Asplund, M., 2009b, "Signatures of intrinsic Li depletion and Li-Na anti-correlation in the metal-poor globular cluster NGC 6397", *Astron. Astrophys.*, **503**, 545–557. [DOI], [ADS], [arXiv:0906.2876 [astro-ph.SR]]

Liu, Chao, Fu, Jianning, Shi, Jianrong, Wu, Hong, Han, Zhanwen, Chen, Li, Dong, Subo, Zhao, Yongheng, Chen, Jian-Jun, Zhang, Haotong, Bai, Zhong-Rui, Chen, Xuefei, Cui, Wenyuan, Du, Bing, Hsia, Chih-Hao, Jiang, Deng-Kai, Hou, Jinliang, Hou, Wen, Li, Haining, Li, Jiao, Li, Lifang, Liu, Jiaming, Liu, Jifeng, Luo, A-Li, Ren, Juan-Juan, Tian, Hai-Jun, Tian, Hao, Wang, Jia-Xin, Wu, Chao-Jian, Xie, Ji-Wei, Yan, Hong-Liang, Yang, Fan, Yu, Jincheng, Zhang, Bo, Zhang, Huawei, Zhang, Li-Yun, Zhang, Wei, Zhao, Gang, Zhong,

Jing, Zong, Weikai and Zuo, Fang, 2020, "LAMOST Medium-Resolution Spectroscopic Survey (LAMOST-MRS): Scientific goals and survey plan", *arXiv e-prints*, arXiv:2005.07210. [ADS], [arXiv:2005.07210 [astro-ph.SR]]

Liu, Nian, Fu, Jian-Ning, Zong, Weikai, Shi, Jian-Rong, Luo, A. Li, Zhang, Hao-Tong, Cui, Xiang-Qun, Hou, Yong-Hui, Pan, Yang, Shan, Xin-Rui, Chen, Jian-Jun, Bai, Zhong-Rui, Chen, Jian-Xing, Du, Bing, Hou, Wen, Liu, Yu-Chen, Tian, Hao, Wang, Jiang-Tao, Wang, Jia-Xin, Wu, Ke-Fei, Wu, Yu-Zhong, Yan, Hong-Liang and Zuo, Fang, 2019, "Radial velocity measurements from LAMOST medium-resolution spectroscopic observations: a pointing towards the Kepler field", *Research in Astronomy and Astrophysics*, **19**(5), 075. [DOI], [ADS], [arXiv:1901.00619 [astro-ph.SR]]

Liu, Y. J., Tan, K. F., Wang, L., Zhao, G., Sato, B., Takeda, Y. and Li, H. N., 2014, "The Lithium Abundances of a Large Sample of Red Giants", *Astrophys. J.*, **785**, 94. [DOI], [ADS], [arXiv:1404.1687 [astro-ph.SR]]

Majewski, Steven R., Schiavon, Ricardo P., Frinchaboy, Peter M., Allende Prieto, Carlos, Barkhouser, Robert, Bizyaev, Dmitry, Blank, Basil, Brunner, Sophia, Burton, Adam, Carrera, Ricardo, Chojnowski, S. Drew, Cunha, Kátia, Epstein, Courtney, Fitzgerald, Greg, García Pérez, Ana E., Hearty, Fred R., Henderson, Chuck, Holtzman, Jon A., Johnson, Jennifer A., Lam, Charles R., Lawler, James E., Maseman, Paul, Mészáros, Szabolcs, Nelson, Matthew, Nguyen, Duy Coung, Nidever, David L., Pinsonneault, Marc, Shetrone, Matthew, Smee, Stephen, Smith, Verne V., Stolberg, Todd, Skrutskie, Michael F., Walker, Eric, Wilson, John C., Zasowski, Gail, Anders, Friedrich, Basu, Sarbani, Beland, Stephane, Blanton, Michael R., Bovy, Jo, Brownstein, Joel R., Carlberg, Joleen, Chaplin, William, Chiappini, Cristina, Eisenstein, Daniel J., Elsworth, Yvonne, Feuillet, Diane, Fleming, Scott W., Galbraith-Frew, Jessica, García, Rafael A., García-Hernández, D. Aníbal, Gillespie, Bruce A., Girardi, Léo, Gunn, James E., Hasselquist, Sten, Hayden, Michael R., Hekker, Saskia, Ivans, Inese, Kinemuchi, Karen, Klaene, Mark, Mahadevan, Suvrath, Mathur, Savita,

Mosser, Benoît, Muna, Demitri, Munn, Jeffrey A., Nichol, Robert C., O'Connell, Robert W., Parejko, John K., Robin, A. C., Rocha-Pinto, Helio, Schultheis, Matthias, Serenelli, Aldo M., Shane, Neville, Silva Aguirre, Victor, Sobeck, Jennifer S., Thompson, Benjamin, Troup, Nicholas W., Weinberg, David H. and Zamora, Olga, 2017, "The Apache Point Observatory Galactic Evolution Experiment (APOGEE)", *Astron. J.*, **154**(3), 94. [DOI], [ADS], [arXiv:1509.05420 [astro-ph.IM]]

Martell, S. L. and Shetrone, M. D., 2013, "Lithium-rich field giants in the Sloan Digital Sky Survey", *Mon. Not. Roy. Astron. Soc.*, **430**, 611–620. [DOI], [ADS], [arXiv:1301.0163 [astro-ph.SR]]

Masseron, T., Lagarde, N., Miglio, A., Elsworth, Y. and Gilmore, G., 2017, "Nitrogen depletion in field red giants: mixing during the He flash?", *Mon. Not. Roy. Astron. Soc.*, **464**, 3021–3028. [DOI], [ADS]

Mathur, S., Huber, D., Batalha, N. M., Ciardi, D. R., Bastien, F. A., Bieryla, A., Buchhave, L. A., Cochran, W. D., Endl, M., Esquerdo, G. A., Furlan, E., Howard, A., Howell, S. B., Isaacson, H., Latham, D. W., MacQueen, P. J. and Silva, D. R., 2017, "Revised Stellar Properties of Kepler Targets for the Q1-17 (DR25) Transit Detection Run", *Astrophys. J. Suppl.*, **229**, 30. [DOI], [ADS], [arXiv:1609.04128 [astro-ph.SR]]

Matsuno, Tadafumi, Yong, David, Aoki, Wako and Ishigaki, Miho N., 2018, "Optical High-resolution Spectroscopy of 14 Young α-rich Stars", *Astrophys. J.*, **860**(1), 49. [DOI], [ADS], [arXiv:1804.08818 [astro-ph.SR]]

Melo, C. H. F., de Laverny, P., Santos, N. C., Israelian, G., Randich, S., Do Nascimento, J. D., Jr. and de Medeiros, J. R., 2005, "On the nature of lithium-rich giant stars. Constraints from beryllium abundances", *Astron. Astrophys.*, **439**(1), 227–235. [DOI], [ADS], [arXiv:astro-ph/0504133 [astro-ph]]

Merline, W. J., 1999, "Precise Velocity Observation of K-Giants: Evidence for Solar-Like Oscillations in Arcturus", in *IAU Colloq. 170: Precise Stellar Radial*

Velocities, (Eds.) Hearnshaw, J. B., Scarfe, Colin David, Astronomical Society of the Pacific Conference Series, 185, [ADS]

Mészáros, S., Avrett, E. H. and Dupree, A. K., 2009, "Mass Outflow from Red Giant Stars in M13, M15, and M92", *Astron. J.*, **138**, 615–624. [DOI], [ADS], [arXiv:0906.3420 [astro-ph.SR]]

Mocák, M., Siess, L. and Müller, E., 2011, "Multidimensional hydrodynamic simulations of the hydrogen injection flash", *Astron. Astrophys.*, **533**, A53. [DOI], [ADS], [arXiv:1106.3260 [astro-ph.SR]]

Monaco, L., Villanova, S., Moni Bidin, C., Carraro, G., Geisler, D., Bonifacio, P., Gonzalez, O. A., Zoccali, M. and Jilkova, L., 2011, "Lithium-rich giants in the Galactic thick disk", *Astron. Astrophys.*, **529**, A90. [DOI], [ADS], [arXiv:1103.1658 [astro-ph.SR]]

Monaco, L., Boffin, H. M. J., Bonifacio, P., Villanova, S., Carraro, G., Caffau, E., Steffen, M., Ahumada, J. A., Beletsky, Y. and Beccari, G., 2014, "A super lithium-rich red-clump star in the open cluster Trumpler 5", *Astron. Astrophys.*, **564**, L6. [DOI], [ADS], [arXiv:1403.6461 [astro-ph.SR]]

Morel, Thierry and Miglio, Andrea, 2012, "Assessing the accuracy of the surface gravity determination in late-type stars with solar-like pulsators", *Mon. Not. Roy. Astron. Soc.*, **419**(1), L34–L38. [DOI], [ADS], [arXiv:1110.2036 [astro-ph.SR]]

Mori, Kanji, Kusakabe, Motohiko, Balantekin, A. Baha, Kajino, Toshitaka and Famiano, Michael A., 2020, "Enhancement of Lithium in Red Clump Stars by the Neutrino Magnetic Moment"

Moshir, M., Kopan, G., Conrow, T., McCallon, H., Hacking, P., Gregorich, D., Rohrbach, G., Melnyk, M., Rice, W., Fullmer, L., White, J. and Chester, T., 1990, "The IRAS Faint Source Catalog, Version 2", in *Bulletin of the American Astronomical Society*, , 22, [ADS]

Mosser, B., Goupil, M. J., Belkacem, K., Michel, E., Stello, D., Marques, J. P., Elsworth, Y., Barban, C., Beck, P. G., Bedding, T. R., De Ridder, J., García, R. A., Hekker, S., Kallinger, T., Samadi, R., Stumpe, M. C., Barclay, T. and Burke, C. J., 2012a, "Probing the core structure and evolution of red giants using gravity-dominated mixed modes observed with Kepler", *Astron. Astrophys.*, **540**, A143. [DOI], [ADS], [arXiv:1203.0689 [astro-ph.SR]]

Mosser, B., Goupil, M. J., Belkacem, K., Michel, E., Stello, D., Marques, J. P., Elsworth, Y., Barban, C., Beck, P. G., Bedding, T. R., De Ridder, J., Garcia, R. A., Hekker, S., Kallinger, T., Samadi, R., Stumpe, M. C., Barclay, T. and Burke, C. J., 2012b, "VizieR Online Data Catalog: Oscillations of red giants observed by Kepler (Mosser+, 2012)", *VizieR Online Data Catalog*, J/A+A/540/A143. [ADS]

Mosser, B., Benomar, O., Belkacem, K., Goupil, M. J., Lagarde, N., Michel, E., Lebreton, Y., Stello, D., Vrard, M., Barban, C., Bedding, T. R., Deheuvels, S., Chaplin, W. J., De Ridder, J., Elsworth, Y., Montalban, J., Noels, A., Ouazzani, R. M., Samadi, R., White, T. R. and Kjeldsen, H., 2014, "Mixed modes in red giants: a window on stellar evolution", *Astron. Astrophys.*, **572**, L5. [DOI], [ADS], [arXiv:1411.1082 [astro-ph.SR]]

Palacios, A., Charbonnel, C. and Forestini, M., 2001, "The Lithium Flash. Thermal instabilities generated by lithium burning in RGB stars", *Astron. Astrophys.*, **375**, L9–L13. [DOI], [ADS], [astro-ph/0106441]

Paxton, B., Bildsten, L., Dotter, A., Herwig, F., Lesaffre, P. and Timmes, F., 2011, "Modules for Experiments in Stellar Astrophysics (MESA)", *Astrophys. J. Suppl.*, **192**, 3. [DOI], [ADS], [arXiv:1009.1622 [astro-ph.SR]]

Paxton, B., Schwab, J., Bauer, E. B., Bildsten, L., Blinnikov, S., Duffell, P., Farmer, R., Goldberg, J. A., Marchant, P., Sorokina, E., Thoul, A., Townsend, R. H. D. and Timmes, F. X., 2018, "Modules for Experiments in Stellar Astrophysics (MESA): Convective Boundaries, Element Diffusion, and Massive

Star Explosions", *Astrophys. J. Suppl.*, **234**, 34. [DOI], [ADS], [arXiv:1710.08424 [astro-ph.SR]]

Paxton, Bill, Smolec, R., Schwab, Josiah, Gautschy, A., Bildsten, Lars, Cantiello, Matteo, Dotter, Aaron, Farmer, R., Goldberg, Jared A., Jermyn, Adam S., Kanbur, S. M., Marchant, Pablo, Thoul, Anne, Townsend, Richard H. D., Wolf, William M., Zhang, Michael and Timmes, F. X., 2019, "Modules for Experiments in Stellar Astrophysics (MESA): Pulsating Variable Stars, Rotation, Convective Boundaries, and Energy Conservation", *Astrophys. J. Suppl.*, **243**(1), 10. [DOI], [ADS], [arXiv:1903.01426 [astro-ph.SR]]

Pinsonneault, M. H., Elsworth, Y., Epstein, C., Hekker, S., Mészáros, S., Chaplin, W. J., Johnson, J. A., García, R. A., Holtzman, J., Mathur, S., García Pérez, A., Silva Aguirre, V., Girardi, L., Basu, S., Shetrone, M., Stello, D., Allende Prieto, C., An, D., Beck, P., Beers, T. C., Bizyaev, D., Bloemen, S., Bovy, J., Cunha, K., De Ridder, J., Frinchaboy, P. M., García-Hernández, D. A., Gilliland, R., Harding, P., Hearty, F. R., Huber, D., Ivans, I., Kallinger, T., Majewski, S. R., Metcalfe, T. S., Miglio, A., Mosser, B., Muna, D., Nidever, D. L., Schneider, D. P., Serenelli, A., Smith, V. V., Tayar, J., Zamora, O. and Zasowski, G., 2014, "The APOKASC Catalog: An Asteroseismic and Spectroscopic Joint Survey of Targets in the Kepler Fields", *Astrophys. J. Suppl.*, **215**, 19. [DOI], [ADS], [arXiv:1410.2503 [astro-ph.SR]]

Placco, Vinicius M., Sneden, Christopher, Roederer, Ian U., Lawler, James E., Den Hartog, Elizabeth A., Hejazi, Neda, Maas, Zachary and Bernath, Peter, 2021, "Linemake: An Atomic and Molecular Line List Generator", *Research Notes of the American Astronomical Society*, **5**(4), 92. [DOI], [ADS], [arXiv:2104.08286 [astro-ph.IM]]

Plets, H., Waelkens, C., Oudmaijer, R. D. and Waters, L. B. F. M., 1997, "Giants with infrared excess.", *Astron. Astrophys.*, **323**, 513–523. [ADS]

Ramírez, I. and Allende Prieto, C., 2011, "Fundamental Parameters and Chemical Composition of Arcturus", *Astrophys. J.*, **743**, 135. [DOI], [ADS], [arXiv:1109.4425 [astro-ph.SR]]

Rebull, L. M., Carlberg, J. K., Gibbs, J. C., Deeb, J. E., Larsen, E., Black, D. V., Altepeter, S., Bucksbee, E., Cashen, S., Clarke, M., Datta, A., Hodgson, E. and Lince, M., 2015, "On Infrared Excesses Associated with Li-rich K Giants", *Astron. J.*, **150**, 123. [DOI], [ADS], [arXiv:1507.00708 [astro-ph.SR]]

Reddy, B. E., Lambert, D. L., Laws, C., Gonzalez, G. and Covey, K., 2002, "A search for ^{6}Li in stars with planets", *Mon. Not. Roy. Astron. Soc.*, **335**, 1005–1016. [DOI], [ADS], [astro-ph/0205268]

Reddy, B. E., Tomkin, J., Lambert, D. L. and Allende Prieto, C., 2003, "The chemical compositions of Galactic disc F and G dwarfs", *Mon. Not. Roy. Astron. Soc.*, **340**, 304–340. [DOI], [ADS], [astro-ph/0211551]

Reddy, Bacham E., Lambert, David L. and Allende Prieto, Carlos, 2006, "Elemental abundance survey of the Galactic thick disc", *Mon. Not. Roy. Astron. Soc.*, **367**(4), 1329–1366. [DOI], [ADS], [arXiv:astro-ph/0512505 [astro-ph]]

Reeves, H., Fowler, W. A. and Hoyle, F., 1970, "Galactic Cosmic Ray Origin of Li, Be and B in Stars", *Nature*, **226**(5247), 727–729. [DOI], [ADS]

Reimers, D., 1975, "Circumstellar envelopes and mass loss of red giant stars.", in *Problems in stellar atmospheres and envelopes.*, [ADS]

Renzini, Alvio and Fusi Pecci, Flavio, 1988, "Tests of evolutionary sequences using color-magnitude diagrams of globular clusters.", *Ann. Rev. Astron. Astrophys.*, **26**, 199–244. [DOI], [ADS]

Ruchti, G. R., Fulbright, J. P., Wyse, R. F. G., Gilmore, G. F., Grebel, E. K., Bienaymé, O., Bland-Hawthorn, J., Freeman, K. C., Gibson, B. K., Munari, U., Navarro, J. F., Parker, Q. A., Reid, W., Seabroke, G. M., Siebert, A., Siviero, A., Steinmetz, M., Watson, F. G., Williams, M. and Zwitter, T., 2011, "Metal-poor

Lithium-rich Giants in the Radial Velocity Experiment Survey", *Astrophys. J.*, **743**, 107. [DOI], [ADS], [arXiv:1111.1623 [astro-ph.SR]]

Salaris, Maurizio, Cassisi, Santi and Weiss, Achim, 2002, "Red Giant Branch Stars: The Theoretical Framework", *Publications of the Astronomical Society of the Pacific*, **114**(794), 375–402. [DOI]URL: http://dx.doi.org/10.1086/342498

Scalo, J. M., Despain, K. H. and Ulrich, R. K., 1975, "Studies of evolved stars. V - Nucleosynthesis in hot-bottom convective envelopes", *Astrophys. J.*, **196**, 805–817. [DOI], [ADS]

Schwab, Josiah, 2020, "A helium-flash-induced mixing event can explain the lithium abundances of red clump stars", *arXiv e-prints*, arXiv:2009.01248. [ADS], [arXiv:2009.01248 [astro-ph.SR]]

Schwarzschild, M. and Härm, R., 1962a, "Red Giants of Population II. II.", *Astrophys. J.*, **136**, 158. [DOI], [ADS]

Schwarzschild, M. and Härm, R., 1962b, "Red Giants of Population II. II.", *Astrophys. J.*, **136**, 158. [DOI], [ADS]

Siess, Lionel and Livio, Mario, 1999, "The accretion of brown dwarfs and planets by giant stars - II. Solar-mass stars on the red giant branch", *Mon. Not. Roy. Astron. Soc.*, **308**(4), 1133–1149. [DOI], [ADS], [arXiv:astro-ph/9905235 [astro-ph]]

Silva Aguirre, V., Ruchti, G. R., Hekker, S., Cassisi, S., Christensen-Dalsgaard, J., Datta, A., Jendreieck, A., Jessen-Hansen, J., Mazumdar, A., Mosser, B., Stello, D., Beck, P. G. and de Ridder, J., 2014, "Old Puzzle, New Insights: A Lithium-rich Giant Quietly Burning Helium in Its Core", *Astrophys. J. Lett.*, **784**, L16. [DOI], [ADS], [arXiv:1402.6339 [astro-ph.SR]]

Singh, Raghubar, Reddy, Bacham E., Bharat Kumar, Yerra and Antia, H. M., 2019a, "Survey of Li-rich Giants among Kepler and LAMOST Fields: Determination of Li-rich Giants' Evolutionary Phase", *Astrophys. J. Lett.*, **878**(1), L21. [DOI], [ADS], [arXiv:1906.03198 [astro-ph.SR]]

Singh, Raghubar, Reddy, Bacham E. and Kumar, Yerra Bharat, 2019b, "Spectroscopic study of two new super Li-rich red clump K giants", *Mon. Not. Roy. Astron. Soc.*, **482**(3), 3822–3830. [DOI], [ADS], [arXiv:1810.12509 [astro-ph.SR]]

Singh, Raghubar, Bharat Kumar, Yerra, Reddy, Bacham E. and Aoki, Wako, 2020, "Concerning the Li-rich status of KIC 9821622: a Kepler field RGB star reported as a Li-rich giant", *Mon. Not. Roy. Astron. Soc.*, **491**(3), 3838–3843. [DOI], [ADS], [arXiv:1911.05243 [astro-ph.SR]]

Skrutskie, M. F., Cutri, R. M., Stiening, R., Weinberg, M. D., Schneider, S., Carpenter, J. M., Beichman, C., Capps, R., Chester, T., Elias, J., Huchra, J., Liebert, J., Lonsdale, C., Monet, D. G., Price, S., Seitzer, P., Jarrett, T., Kirkpatrick, J. D., Gizis, J. E., Howard, E., Evans, T., Fowler, J., Fullmer, L., Hurt, R., Light, R., Kopan, E. L., Marsh, K. A., McCallon, H. L., Tam, R., Van Dyk, S. and Wheelock, S., 2006, "The Two Micron All Sky Survey (2MASS)", *Astron. J.*, **131**, 1163–1183. [DOI], [ADS]

Smiljanic, R., Franciosini, E., Bragaglia, A., Tautvaisiene, G., Fu, X., Pancino, E., Adibekyan, V., Sousa, S. G., Randich, S., Montalban, J., Pasquini, L., Magrini, L., Drazdauskas, A., Garcia, R. A., Mathur, S., Mosser, B., Regulo, C., de Assis Peralta, R., Hekker, S., Feuillet, D., Valentini, M., Morel, T., Martell, S., Gilmore, G., Feltzing, S., Vallenari, A., Bensby, T., Korn, A. J., Lanzafame, A. C., Recio-Blanco, A., Bayo, A., Carraro, G., Costado, M. T., Frasca, A., Jofre, P., Lardo, C., de Laverny, P., Lind, K., Masseron, T., Monaco, L., Morbidelli, L., Prisinzano, L., Sbordone, L. and Zaggia, S., 2018, "The Gaia-ESO Survey: properties of newly discovered Li-rich giants", *ArXiv e-prints*. [ADS], [arXiv:1805.07077 [astro-ph.SR]]

Smith, V. V. and Lambert, D. L., 1989, "Synthesis of lithium and s-process elements in Small Magellanic Cloud asymptotic giant branch stars", *Astrophys. J. Lett.*, **345**, L75–L78. [DOI], [ADS]

Sneden, C., Lucatello, S., Ram, R. S., Brooke, J. S. A. and Bernath, P., 2014, "Line Lists for the A $^2\Pi$-X $^2\Sigma^+$ (Red) and B $^2\Sigma^+$-X $^2\Sigma^+$ (Violet) Systems of CN, $^{13}C^{14}N$, and $^{12}C^{15}N$, and Application to Astronomical Spectra", *Astrophys. J. Suppl.*, **214**, 26. [DOI], [ADS], [arXiv:1408.3828 [astro-ph.SR]]

Sneden, Christopher Alan, 1973, *Carbon and Nitrogen Abundances in Metal-Poor Stars.*, Ph.D. thesis, THE UNIVERSITY OF TEXAS AT AUSTIN. [ADS]

Spite, F. and Spite, M., 1982, "Abundance of lithium in unevolved stars and old disk stars : Interpretation and consequences.", *Astronomy and Astrophysics*, **115**, 357–366. [ADS]

Stanek, K. Z., Zaritsky, D. and Harris, J., 1998, "A "Short" Distance to the Large Magellanic Cloud With the Hipparcos Calibrated Red Clump Stars", *Astrophys. J. Lett.*, **500**(2), L141–L144. [DOI], [ADS], [arXiv:astro-ph/9803181 [astro-ph]]

Starrfield, S., Truran, J. W., Sparks, W. M. and Arnould, M., 1978, "On Li-7 production in nova explosions", *Astrophys. J.*, **222**, 600–603. [DOI], [ADS]

Stello, D., Bruntt, H., Kjeldsen, H., Bedding, T. R., Arentoft, T., Gilliland, R. L., Nuspl, J., Kim, S. L., Kang, Y. B., Koo, J. R., Lee, J. A., Sterken, C., Lee, C. U., Jensen, H. R., Jacob, A. P., Szabó, R., Frandsen, S., Csubry, Z., Dind, Z. E., Bouzid, M. Y., Dall, T. H. and Kiss, L. L., 2007, "Multisite campaign on the open cluster M67 - II. Evidence for solar-like oscillations in red giant stars", *Mon. Not. Roy. Astron. Soc.*, **377**(2), 584–594. [DOI], [ADS], [arXiv:astro-ph/0702092 [astro-ph]]

Stello, Dennis, Huber, Daniel, Bedding, Timothy R., Benomar, Othman, Bildsten, Lars, Elsworth, Yvonne P., Gilliland, Ronald L., Mosser, Benoît, Paxton, Bill

and White, Timothy R., 2013, "Asteroseismic Classification of Stellar Populations among 13,000 Red Giants Observed by Kepler", *Astrophys. J.*, **765**, L41. [DOI], [ADS], [arXiv:1302.0858 [astro-ph.SR]]

Sweigart, A. V. and Mengel, J. G., 1979, "Meridional circulation and CNO anomalies in red giant stars", *Astrophys. J.*, **229**, 624–641. [DOI], [ADS]

Szigeti, L., Mészáros, S., Smith, V. V., Cunha, K., Lagarde, N., Charbonnel, C., García-Hernández, D. A., Shetrone, M., Pinsonneault, M., Allende Prieto, C., Fernández-Trincado, J. G., Kovács, J. and Villanova, S., 2018, "$^{12}C/^{13}C$ isotopic ratios in red-giant stars of the open cluster NGC 6791", *Mon. Not. Roy. Astron. Soc.*, **474**, 4810–4817. [DOI], [ADS], [arXiv:1711.08183 [astro-ph.SR]]

Tajitsu, Akito, Sadakane, Kozo, Naito, Hiroyuki, Arai, Akira and Aoki, Wako, 2015, "Explosive lithium production in the classical nova V339 Del (Nova Delphini 2013)", *Nature*, **518**(7539), 381–384. [DOI], [ADS], [arXiv:1502.05598 [astro-ph.SR]]

Takeda, Y. and Tajitsu, A., 2017, "On the observational characteristics of lithium-enhanced giant stars in comparison with normal red giants", *Pub. Astron. Soc. Japan*, **69**, 74. [DOI], [ADS], [arXiv:1706.02273 [astro-ph.SR]]

Takeda, Yoichi and Tajitsu, Akito, 2014, "Spectroscopic study on the beryllium abundances of red giant stars*", *Pub. Astron. Soc. Japan*, **66**(5), 91. [DOI], [ADS], [arXiv:1406.7066 [astro-ph.SR]]

Takeda, Yoichi and Tajitsu, Akito, 2017, "On the observational characteristics of lithium-enhanced giant stars in comparison with normal red giants†", *Publications of the Astronomical Society of Japan*, **69**(4). [DOI], [https://academic.oup.com/pasj/article-pdf/69/4/74/19489315/psx057.pdf]URL: https://doi.org/10.1093/pasj/psx057. 74

Talon, Suzanne and Charbonnel, Corinne, 1998, "The Li dip: a probe of angular momentum transport in low mass stars", *Astron. Astrophys.*, **335**, 959–968. [ADS], [arXiv:astro-ph/9804211 [astro-ph]]

Tarrant, N. J., Chaplin, W. J., Elsworth, Y., Spreckley, S. A. and Stevens, I. R., 2007, "Asteroseismology of red giants: photometric observations of Arcturus by SMEI", *Mon. Not. Roy. Astron. Soc.*, **382**(1), L48–L52. [DOI], [ADS], [arXiv:0706.3346 [astro-ph]]

Tayar, Jamie, Somers, Garrett, Pinsonneault, Marc H., Stello, Dennis, Mints, Alexey, Johnson, Jennifer A., Zamora, O., García-Hernández, D. A., Maraston, Claudia, Serenelli, Aldo, Allende Prieto, Carlos, Bastien, Fabienne A., Basu, Sarbani, Bird, J. C., Cohen, R. E., Cunha, Katia, Elsworth, Yvonne, García, Rafael A., Girardi, Leo, Hekker, Saskia, Holtzman, Jon, Huber, Daniel, Mathur, Savita, Mészáros, Szabolcs, Mosser, B., Shetrone, Matthew, Silva Aguirre, Victor, Stassun, Keivan, Stringfellow, Guy S., Zasowski, Gail and Roman-Lopes, A., 2017, "The Correlation between Mixing Length and Metallicity on the Giant Branch: Implications for Ages in the Gaia Era", *Astrophys. J.*, **840**(1), 17. [DOI], [ADS], [arXiv:1704.01164 [astro-ph.SR]]

Thomas, H.-C., 1967, "Sternentwicklung VIII. Der Helium-Flash bei einem Stern von 1. 3 Sonnenmassen", *Z. Astrophys.*, **67**, 420–+. [ADS]

Ting, Y.-S., Hawkins, K. and Rix, H.-W., 2018, "A Large and Pristine Sample of Standard Candles across the Milky Way: $\sim 100,000 Red Clump Stars with 3\% Contamination''$, *Astrophys. J. Lett.*, **858**, L7. [*DOI*], [*ADS*], [

Ulrich, R. K., 1986, "Determination of Stellar Ages from Asteroseismology", *Astrophys. J. Lett.*, **306**, L37. [DOI], [ADS]

Villaver, Eva, Livio, Mario, Mustill, Alexander J. and Siess, Lionel, 2014, "Hot Jupiters and Cool Stars", *Astrophys. J.*, **794**(1), 3. [DOI], [ADS], [arXiv:1407.7879 [astro-ph.EP]]

Vrard, M., Mosser, B. and Samadi, R., 2016, "Period spacings in red giants. II. Automated measurement", *Astron. Astrophys.*, **588**, A87. [DOI], [ADS], [arXiv:1602.04940 [astro-ph.SR]]

Wallerstein, G. and Sneden, C., 1982, "A K giant with an unusually high abundance of lithium : HD 112127.", *Astrophys. J.*, **255**, 577–584. [DOI], [ADS]

Wang, R., Luo, A. L., Chen, J. J., Bai, Z. R., Chen, L., Chen, X. F., Dong, S. B., Du, B., Fu, J. N., Han, Z. W., Hou, J. L., Hou, Y. H., Hou, W., Jiang, D. K., Kong, X., Li, L. F., Liu, C., Liu, J. M., Qin, L., Shi, J. R., Tian, H., Wu, H., Wu, C. J., Xie, J. W., Zhang, H. T., Zhang, S., Zhao, G., Zhao, Y. H., Zhong, J., Zong, W. K. and Zuo, F., 2019, "Properties of Radial Velocities Measurement Based on LAMOST-II Medium-resolution Spectroscopic Observations", *Astrophys. J. Suppl.*, **244**(2), 27. [DOI], [ADS], [arXiv:1908.04773 [astro-ph.SR]]

Wenger, M., Ochsenbein, F., Egret, D., Dubois, P., Bonnarel, F., Borde, S., Genova, F., Jasniewicz, G., Laloë, S., Lesteven, S. and Monier, R., 2000, "The SIMBAD astronomical database. The CDS reference database for astronomical objects", *Astron. Astrophys. Suppl.*, **143**, 9–22. [DOI], [ADS], [arXiv:astro-ph/0002110 [astro-ph]]

Wiese, W. L., Fuhr, J. R. and Deters, T. M., 1996, *Atomic transition probabilities of carbon, nitrogen, and oxygen : a critical data compilation*. [ADS]

Wilhelm, Ronald, Beers, Timothy C. and Gray, Richard O., 1999, "Spectroscopy of Hot Stars in the Galactic Halo. II. The Identification and Classification of Horizontal-Branch and Other A-Type Stars", *Astron. J.*, **117**(5), 2308–2328. [DOI], [ADS]

Wright, Edward L., Eisenhardt, Peter R. M., Mainzer, Amy K., Ressler, Michael E., Cutri, Roc M., Jarrett, Thomas, Kirkpatrick, J. Davy, Padgett, Deborah, McMillan, Robert S., Skrutskie, Michael, Stanford, S. A., Cohen, Martin, Walker, Russell G., Mather, John C., Leisawitz, David, Gautier, Thomas N., III, McLean, Ian, Benford, Dominic, Lonsdale, Carol J., Blain, Andrew, Mendez, Bryan, Irace, William R., Duval, Valerie, Liu, Fengchuan, Royer, Don, Heinrichsen, Ingolf, Howard, Joan, Shannon, Mark, Kendall, Martha, Walsh, Amy L., Larsen, Mark, Cardon, Joel G., Schick, Scott, Schwalm, Mark, Abid, Mohamed,

Fabinsky, Beth, Naes, Larry and Tsai, Chao-Wei, 2010, "The Wide-field Infrared Survey Explorer (WISE): Mission Description and Initial On-orbit Performance", *Astron. J.*, **140**(6), 1868–1881. [DOI], [ADS], [arXiv:1008.0031 [astro-ph.IM]]

Yan, Hong-Liang, Shi, Jian-Rong, Zhou, Yu-Tao, Chen, Yong-Shou, Li, Er-Tao, Zhang, Suyalatu, Bi, Shao-Lan, Wu, Ya-Qian, Li, Zhi-Hong, Guo, Bing, Liu, Wei-Ping, Gao, Qi, Zhang, Jun-Bo, Zhou, Ze-Ming, Li, Hai-Ning and Zhao, Gang, 2018, "The nature of the lithium enrichment in the most Li-rich giant star", *Nature Astronomy*, **2**, 790–795. [DOI], [ADS], [arXiv:1809.00187 [astro-ph.SR]]

Yan, Hong-Liang, Zhou, Yu-Tao, Zhang, Xianfei, Li, Yaguang, Gao, Qi, Shi, Jian-Rong, Zhao, Gang, Aoki, Wako, Matsuno, Tadafumi, Li, Yan, Xu, Xiao-Dong, Li, Haining, Wu, Ya-Qian, Jin, Meng-Qi, Mosser, Benoit, Bi, Shao-Lan, Fu, Jian-Ning, Pan, Kaike, Suda, Takuma, Liu, Yu-Juan, Zhao, Jing-Kun and Liang, Xi-Long, 2020, "Most lithium-rich low-mass evolved stars revealed as red clump stars by asteroseismology and spectroscopy", *Nature Astronomy*. [DOI], [ADS], [arXiv:2010.02106 [astro-ph.SR]]

Yong, David, Casagrande, Luca, Venn, Kim A., Chené, André-Nicolas, Keown, Jared, Malo, Lison, Martioli, Eder, Alves-Brito, Alan, Asplund, Martin, Dotter, Aaron, Martell, Sarah L., Meléndez, Jorge and Schlesinger, Katharine J., 2016, "GRACES observations of young [/Fe]-rich stars", *Mon. Not. Roy. Astron. Soc.*, **459**(1), 487–495. [DOI], [http://oup.prod.sis.lan/mnras/article-pdf/459/1/487/13773466/stw676.pdf]URL: https://doi.org/10.1093/mnras/stw676

Yu, Jie, Huber, Daniel, Bedding, Timothy R., Stello, Dennis, Hon, Marc, Murphy, Simon J. and Khanna, Shourya, 2018, "Asteroseismology of 16,000 Kepler Red Giants: Global Oscillation Parameters, Masses, and Radii", *The Astrophysical Journal Supplement Series*, **236**, 42. [DOI], [ADS], [arXiv:1802.04455 [astro-ph.SR]]

Zhang, Xianfei and Jeffery, C. Simon, 2013, "White dwarf–red giant mergers, early-type R stars, J stars and lithium", *Monthly Notices of the Royal Astronomical Society*, **430**(3), 2113–2120. [DOI]URL: http://dx.doi.org/10.1093/mnras/stt035

Zhang, Xianfei, Jeffery, C. Simon, Li, Yaguang and Bi, Shaolan, 2020, "Population synthesis of helium white dwarf–red giant star mergers and the formation of lithium-rich giants and carbon stars", *arXiv e-prints*, arXiv:2001.05600. [ADS], [arXiv:2001.05600 [astro-ph.SR]]

Zhao, G., Zhao, Y.-H., Chu, Y.-Q., Jing, Y.-P. and Deng, L.-C., 2012, "LAMOST spectral survey An overview", *Research in Astronomy and Astrophysics*, **12**, 723–734. [DOI], [ADS]

Zuckerman, B., Kim, S. S. and Liu, T., 1995, "Luminosity Class III Stars with Excess Far-Infrared Emission", *Astrophys. J. Lett.*, **446**, L79+. [DOI], [ADS]